
Report No. FHWA-KS-09-3
FINAL REPORT

FINITE ELEMENT MODELING APPROACH AND PERFORMANCE EVALUATION OF FIBER REINFORCED POLYMER SANDWICH BRIDGE PANELS

Stanley Onyema Oghumu
Louisiana State University
Baton Rouge, Louisiana

August 2009

KANSAS DEPARTMENT OF TRANSPORTATION

**Division of Operations
Bureau of Materials and Research**



1 Report No. FHWA-KS-09-3	2 Government Accession No.	3 Recipient Catalog No.	
4 Title and Subtitle Finite Element Modeling Approach and Performance Evaluation of Fiber Reinforced Polymer Sandwich Bridge Panels		5 Report Date August 2009	
		6 Performing Organization Code	
7 Author(s) Stanley Onyema Oghumu		8 Performing Organization Report No.	
9 Performing Organization Name and Address Kansas Department of Transportation Bureau of Materials and Research 700 SW Harrison Street Topeka, Kansas 66603-3745		10 Work Unit No. (TRAIS)	
		11 Contract or Grant No. C1607	
12 Sponsoring Agency Name and Address Kansas Department of Transportation Bureau of Materials and Research 700 SW Harrison Street Topeka, Kansas 66603-3745		13 Type of Report and Period Covered Final Report May 2006 - June 2009	
		14 Sponsoring Agency Code RE-0330-01	
15 Supplementary Notes For more information write to address in block 9.			
16 Abstract <p>In the United States, about 27% of the bridges are classified as structurally deficient or functionally obsolete. Bridge owners are continually investigating methods to effectively retrofit existing bridges, or to economically replace them with new ones. Modern composite materials for structural applications, at one time only in the domain of aerospace engineering, are increasingly making their way into civil engineering applications. In addition to retrofitting current concrete and steel structures using FRP sheets or plates, a great deal of work is being conducted to develop versatile, fully-composite structural bridge systems.</p> <p>To reduce the self-weight and also achieve the necessary stiffness, sandwich panels are usually used for bridge decks. However, due to the geometric complexity of the FRP sandwich, convenient methods for bridge design have not been developed. The present study aims at developing finite element modeling techniques for sandwich structures. Parametric studies are carried out with the objective of developing equivalent elastic properties, which would be useful parameters in design. A distinction is made between in-plane and out-of-plane behavior, and properties are derived accordingly. The performance of the sandwich, such as the interface stress between the flange and wearing surface can be evaluated. Therefore, through finite element modeling, optimization can be achieved in order to minimize the interface stress. The contribution of stiffness of the wearing surface to structural performance, a factor which is not usually accounted for in typical design procedures, is also examined. An effort is also made to analyze the temperature effects on the structure's performance. A conceptual approach aimed at studying the thermal performance of the panel due to both uniform and gradient temperature variations is presented.</p>			
17 Key Words IBRC, finite element, FRP, Bridge, sandwich panel		18 Distribution Statement No restrictions. This document is available to the public through the National Technical Information Service, Springfield, Virginia 22161	
19 Security Classification (of this report) Unclassified	20 Security Classification (of this page) Unclassified	21 No. of pages 286	22 Price

FINITE ELEMENT MODELING APPROACH AND PERFORMANCE EVALUATION OF FIBER REINFORCED POLYMER SANDWICH BRIDGE PANELS

Final Report

Prepared by

Stanley Onyema Oghumu
Louisiana State University
Baton Rouge, Louisiana

A Report on Research Sponsored By

THE KANSAS DEPARTMENT OF TRANSPORTATION
TOPEKA, KANSAS

August 2009

© Copyright 2009, **Kansas Department of Transportation**

NOTICE

The authors and the state of Kansas do not endorse products or manufacturers. Trade and manufacturers' names appear herein solely because they are considered essential to the object of this report.

This information is available in alternative accessible formats. To obtain an alternative format, contact the Office of Transportation Information, Kansas Department of Transportation, 700 SW Harrison Street, Topeka, Kansas 66603-3745 or phone (785) 296-3585 (Voice) (TDD).

DISCLAIMER

The contents of this report reflect the views of the authors who are responsible for the facts and accuracy of the data presented herein. The contents do not necessarily reflect the views or the policies of the state of Kansas. This report does not constitute a standard, specification or regulation.

ABSTRACT

In the United States, about 27% of the bridges are classified as structurally deficient or functionally obsolete. Bridge owners are continually investigating methods to effectively retrofit existing bridges, or to economically replace them with new ones. Modern composite materials for structural applications, at one time only in the domain of aerospace engineering, are increasingly making their way into civil engineering applications. In addition to retrofitting current concrete and steel structures using FRP sheets or plates, a great deal of work is being conducted to develop versatile, fully-composite structural bridge systems.

To reduce the self-weight and also achieve the necessary stiffness, sandwich panels are usually used for bridge decks. However, due to the geometric complexity of the FRP sandwich, convenient methods for bridge design have not been developed. The present study aims at developing finite element modeling techniques for sandwich structures. Parametric studies are carried out with the objective of developing equivalent elastic properties, which would be useful parameters in design. A distinction is made between in-plane and out-of-plane behavior, and properties are derived accordingly. The performance of the sandwich, such as the interface stress between the flange and wearing surface can be evaluated. Therefore, through finite element modeling, optimization can be achieved in order to minimize the interface stress. The contribution of stiffness of the wearing surface to structural performance, a factor which is not usually accounted for in typical design procedures, is also examined. An effort is also made to analyze the temperature effects on the structure's performance. A conceptual

approach aimed at studying the thermal performance of the panel due to both uniform and gradient temperature variations is presented.

ACKNOWLEDGEMENTS

To Dr. Steve Cai, my major professor and chairman of my advisory committee, I wish to express my sincere thanks for patiently and encouragingly guiding me toward a successful completion of this research. The authors would also like to acknowledge the financial support from the Innovative Bridge Research and Construction Program, Federal Highway Administration through the Kansas Department of Transportation, and Louisiana State University.

TABLE OF CONTENTS

ABSTRACT	iii
ACKNOWLEDGEMENTS	v
TABLE OF CONTENTS	vi
List of Tables	x
List of Figures	xi
Chapter 1 - INTRODUCTION	1
1.1 General Background	1
1.2 Aim and Objectives	4
1.3 Scope and Limitations of Study	6
1.4 Chapter Layout	7
Chapter 2 - LITERATURE REVIEW	8
2.1 Introduction	8
2.2 State-of-the-Art Review	8
2.3 Types of FRP Panels	9
2.3.1 Sandwich Construction	10
2.3.2 Adhesively Bonded Pultruded Shapes	10
2.4 Analysis of Sinusoidal Wave Core Sandwich Panel	13
2.5 Construction Details	18
2.5.1 Deck Details	19
2.5.2 Shipping and Handling	19
2.5.3 Surface Preparation	19
2.5.4 Assembly and Connections	20
2.5.5 Wearing Surface	20
2.6 Manufacturing Processes	20
2.6.1 Hand Lay-Up	21
2.6.2 Vacuum-Assisted Resin Transfer Molding (VARTM)	21
2.6.3 Pultrusion	22
2.6.4 Vacuum Bag Molding	22
2.6.5 Press Molding	22
2.6.6 Autoclave Molding	23
2.7 Bridge Applications of FRP	23
2.7.1 Aberfeldy Footbridge	23
2.7.2 Bonds Mill Lift Bridge	24
2.7.3 Troutville Weigh Station	25
2.7.4 Laurel Run Road Bridge	25
2.7.5 Laurel Lick Bridge	26
2.7.6 Tech 21 (Smith Road) Bridge	26
2.7.7 Miyun Bridge, Beijing	27
2.7.8 Ulenbergstrasse Bridge, Düsseldorf	27
2.7.9 Salem Avenue Bridge, Dayton	28
2.7.10 No-Name Creek Bridge, Kansas	29

Chapter 3 - DERIVATION OF PROPERTIES FOR IN-PLANE BEHAVIOR	31
3.1 Introduction	31
3.2 Micromechanical Analysis	32
3.3 Macromechanical Analysis	40
3.4 Derivation of Equivalent Properties of Core	43
3.4.1 Finite Element Modeling	43
3.4.2 Core Properties	45
3.4.2.1 Equivalent Elastic Modulus in the Vertical Direction, E_z	46
3.4.2.2 Equivalent Elastic Modulus in the Longitudinal Direction, E_x	47
3.4.2.3 Equivalent Elastic Modulus in the Lateral Direction, E_y	47
3.4.2.4 Equivalent Shear Moduli (G_{xy} , G_{yz} and G_{xz}).....	47
3.4.2.5 Shear Modulus, G_{xy} and G_{xz}	48
3.4.2.6 Shear Modulus, G_{yz} and G_{yx}	52
3.4.2.7 Shear Modulus, G_{zx} and G_{zy}	55
3.5 Comparison of Results	59
3.6 Discussion of the Results	61
3.6.1 Case 1: Beam Model	62
3.6.2 Case 2: Panel Model	65
Chapter 4 - PARAMETRIC STUDIES FOR IN-PLANE BEHAVIOR	69
4.1 Introduction.....	69
4.2 Determining Equivalent Properties	69
4.3 Finite Element Modeling	72
4.4 Parameters Affecting the Young's Modulus in the Longitudinal Direction.....	72
4.4.1 Modification Factors	80
4.4.1.1 Half-wavelength Modification Factor, K_1	80
4.4.1.2 Panel Depth Modification Factor, K_2	81
4.4.1.3 Flat/Flute Thickness Modification Factor, K_3	82
4.4.1.4 Flat/Flute Young's Modulus Modification Factor, K_4	84
4.4.2 Formula for Predicting Longitudinal Young's Modulus of the Core	85
4.5 Parameters Affecting the Young's Modulus in the Transverse Direction	86
4.5.1 Modification Factors	92
4.5.1.1 Flute-width Modification Factor, S_1	93
4.5.1.2 Panel Depth Modification Factor, S_2	94
4.5.1.3 Flat/Flute Thickness Modification Factor, S_3	95
4.5.1.4 Flat/Flute Young's Modulus Modification Factor, S_4	96
4.6 Parameters Affecting the Young's Modulus in the Vertical Direction	97
4.6.1 Modification Factors	103
4.6.1.1 Half-wavelength Modification Factor, D_1	104
4.6.1.2 Panel Depth Modification Factor, D_2	105
4.6.1.3 Flat/Flute Thickness Modification Factor, D_3	106
4.6.1.4 Flat/Flute Young's Modulus Modification Factor, D_4	107
4.6.2 Formula for Predicting Vertical Young's Modulus of the Core	108
4.7 Verification of Results.....	108

Chapter 5 - DERIVATION OF PROPERTIES FOR OUT-OF-PLANE BEHAVIOR..	112
5.1 Introduction.....	112
5.2 Beam Analysis.....	113
5.2.1 Modulus of Elasticity in Longitudinal Direction, E_x	114
5.2.2 Modulus of Elasticity in Lateral Direction, E_y	114
5.2.3 Shear Modulus, G	115
5.2.3.1 Equivalent Shear Modulus, G_{xy}	116
5.2.3.2 Equivalent Shear Modulus, G_{yx}	118
5.3 Verification of Elastic Constants	121
5.3.1 FEM of Actual Configuration Beam	121
5.3.2 FEM of Equivalent Beam	121
5.3.3 Hand-Calculation	121
5.3.3.1 Case 1 (flange-web configuration).....	122
5.3.3.2 Case 2 (3-layered).....	123
5.3.3.3 Case 3 (1-layered).....	123
5.3.4 Comparison of Results	124
5.4 Application to FRP Panel.....	125
5.5 Summary	127
Chapter 6 - PARAMETRIC STUDIES FOR OUT-OF-PLANE BEHAVIOR.....	128
6.1 Introduction.....	128
6.2 Flexural Stiffness E_{xlyy}	129
6.2.1 Variation of Stiffness with Core Height, H	130
6.2.2 Variation of Stiffness with Face Parameters	131
6.2.3 Variation of Stiffness with Core Parameters	136
6.2.4 Modification Factors	141
6.2.4.1 Face Longitudinal Elastic Modulus Modification Factor, B_1	142
6.2.4.2 Face Lateral Elastic Modulus Modification Factor, B_2	143
6.2.4.3 Face Thickness Modification Factor, B_3	144
6.2.4.4 Core Mat Elastic Modulus Modification Factor, B_4	145
6.2.4.5 Core Flute-Width Modification Factor, B_5	146
6.2.4.6 Core Half-Wavelength Modification Factor, B_6	147
6.2.4.7 Core Material Thickness Modification Factor, B_7	148
6.2.5 Formula for Predicting Flexural Stiffness E_{xlyy}	149
6.3 Flexural Stiffness E_{ylxx}	150
6.3.1 Variation of Stiffness with Core Height, H	151
6.3.2 Variation of Stiffness with Face Parameters	152
6.3.3 Variation of Stiffness with Core Parameters	156
6.3.4 Modification Factors	162
6.3.4.1 Face Lateral Elastic Modulus Modification Factor, C_1	162
6.3.4.2 Face Longitudinal Elastic Modulus Modification Factor, C_2	163
6.3.4.3 Face Thickness Modification Factor, C_3	164
6.3.4.4 Core Mat Elastic Modulus Modification Factor, C_4	165
6.3.4.5 Core Flute-Width Modification Factor, C_5	167
6.3.4.6 Core Half-Wavelength Modification Factor, C_6	168
6.3.4.7 Core Material Thickness Modification Factor, C_7	169
6.3.5 Formula for Predicting Flexural Stiffness E_{ylxx}	170

6.4	Equivalent Shear Stiffness $G_{xy}A_s$	171
6.4.1	Variation with Parameters	172
6.4.2	Modification Factors	177
6.4.2.1	Face Shear Modulus Modification Factor, D_1	177
6.4.2.2	Face Thickness Modification Factor, D_2	178
6.4.2.3	Core Height Modification Factor, D_3	180
6.4.3	Formula for Predicting Shear Stiffness $G_{xy}A_s$	181
6.5	Application of Stiffness Properties to Deck Model	181
6.5.1	Verification Phases	183
6.5.1.1	Phase I	183
6.5.1.2	Phase II	185
Chapter 7	- STRUCTURAL ANALYSIS WITH WEARING SURFACE	192
7.1	Introduction	192
7.1.1	Bond	192
7.1.2	Durability	193
7.1.3	Fatigue Strength and Flexibility	193
7.1.4	Weight	193
7.1.5	Rideability	193
7.2	Stiffness Contribution of Wearing Surface	193
7.3	Finite Element Modeling	194
7.4	Derivation of Stiffness	197
7.4.1	Hand Calculation Based on Equivalent Beam – Method 1	197
7.4.3	Hand Calculation Based on Simplified Actual Beam Configuration – Method 2	199
7.5	Method Verification	201
Chapter 8	- THERMAL ANALYSIS	206
8.1	Introduction	206
8.2	Determination of Lamina Thermal Expansion Coefficients	207
8.3	Determination of Laminate Thermal Expansion Coefficients	210
8.4	Case Study – Crawford County Bridge	211
8.5	Finite Element Modeling	215
8.6	Structural Behavior due to Gradient Temperature Change	216
8.6.1	Case 1 – Modeling and Analysis of Simply Supported Panel	217
8.6.2	Case 2 – Modeling and Analysis of Continuously Supported Panel	221
8.6.3	Comparison between Results of Simple and Continuous Supports	223
8.7	Structural Behavior due to Uniform Temperature Change	229
Chapter 9	- CONCLUSIONS AND RECOMMENDATIONS	233
9.1	Summary	233
9.2	Conclusions	234
9.3	Recommendations for Further Research	238
REFERENCES	240
APPENDIX A: MICROSOFT C++ PROGRAM FOR GENERATION OF MACRO FILES	244
APPENDIX B: MATLAB PROGRAM SCRIPT FOR GENERATION OF INPUT FILE..	265
APPENDIX C: THERMAL COEFFICIENT OF EXPANSION COMPUTATION	268

LIST OF TABLES

Table 3.1: Individual layer stiffness properties' comparison with Davalos et al.	39
Table 3.2: Elastic equivalent properties of face laminates compared with Davalos et al. (2001) results.....	43
Table 3.3: Equivalent elastic properties (psi) derived from finite element modeling	59
Table 3.4: Comparison of results with work of Davalos et al. (2001).....	60
Table 3.5a: Comparison with analytical results of Qiao et al. (2003).....	61
Table 3.5b: Comparison with experimental results of Qiao et al. (2003)	61
Table 3.6a: Comparison of deflection results (in.). Points in the longitudinal direction along the central line (in.).....	68
Table 3.6b: Comparison of deflection results (in.). Points in the lateral direction along the midspan (in.)	68
Table 4.1: Comparison of results for E_x	110
Table 5.1: Single-layer equivalent properties of sandwich beam	120
Table 5.2: Comparison of Deflection Results (in.)	125
Table 5.3: Comparison of Deflection Results between Actual Configuration and Equivalent Models	127
Table 6.1: Face parameters used for stiffness equations.....	128
Table 6.2: Core parameters used for stiffness equations	128
Table 6.3: Basic Properties	129
Table 6.4: Average difference between equation and actual data for Flexural Stiffness $E_x I_{yy}$	182
Table 6.5: Average difference between equation and actual data for Flexural Stiffness $E_y I_{xx}$	183
Table 6.6: Average difference between equation and actual data for Flexural Stiffness $G_{xy} A_s$	183
Table 6.7: Equivalent stiffness values and corresponding moduli	184
Table 6.8a: Comparison of deflection results. Points in the longitudinal direction along the central line.	184
Table 6.8b: Comparison of deflection results. Points in the lateral direction along the midspan	185
Table 6.9: Panel properties	185
Table 6.10: Sandwich parameters.....	186
Table 6.11: Equivalent stiffness values and corresponding moduli	186
Table 6.12a: Comparison of deflection results (in.). Points in the longitudinal direction along the central line (in.).....	189
Table 6.12b: Comparison of deflection results (in.). Points in the lateral direction along the midspan (in.)	189
Table 8.1: Properties of constituent materials	209
Table 8.2: Laminae thermal coefficients of expansion	209
Table 8.3: Thermal expansion coefficients of face laminates and core	211
Table 8.4: Thermal stresses (psi) for uniform temperature change of panel	232

LIST OF FIGURES

Figure 1.1: Sandwich panel configuration for this study.	4
Figure 1.2: Core component definitions.....	5
Figure 2.1: Fiber reinforced polymer honeycomb (FRPH) sandwich panel.	11
Figure 2.2: Web core sandwich bridge deck system.	12
Figure 2.3: DuraSpan® deck system by Martin Marietta Composites, Inc.	12
Figure 2.4: Representative Volume Element (RVE).	15
Figure 2.5: Coordinate and equilibrium condition for computation of E_y^e	16
Figure 2.6: Installation of No-Name Creek Bridge, Russell, Kansas.	30
Figure 3.1: Principal Material Coordinate System	35
Figure 3.2: Face laminate lay-up (Davalos et al. 2001).....	37
Figure 3.3: Laminate lay-up nomenclature	41
Figure 3.4a: Representative Volume Element (RVE) for this study (Davalos 2001).....	44
Figure 3.4b: ANSYS model of RVE	45
Figure 3.5a: Model for deriving G_{xy}	50
Figure 3.5b: Coordinate system	50
Figure 3.5c: ANSYS model for deriving G_{xy}	50
Figure 3.6b: Coordinate system	51
Figure 3.6a: Model for deriving G_{xz}	51
Figure 3.6c: ANSYS model for deriving G_{xz}	51
Figure 3.7b: Coordinate system	53
Figure 3.7a: Model for deriving G_{yz}	53
Figure 3.7c: ANSYS model for deriving G_{yz}	53
Figure 3.8a: Model for deriving G_{yx}	54
Figure 3.8b: Coordinate system	54
Figure 3.8c: ANSYS model for deriving G_{yx}	54
Figure 3.9a: Model for deriving G_{zx}	56
Figure 3.9b: Coordinate system	56
Figure 3.9c: ANSYS model for deriving G_{zx}	56
Figure 3.10b: Coordinate system	58
Figure 3.10a: Model for deriving G_{zy}	58
Figure 3.10c: ANSYS model for deriving G_{zy}	58
Figure 3.11a: ANSYS model of actual FRP sinusoidal core beam.....	63
Figure 3.11b: Deflection contour of actual FRP sinusoidal core beam.....	63
Figure 3.12a: ANSYS model of 3-layered equivalent FRP beam	64
Figure 3.12b: Deflection contour of 3-layered equivalent FRP beam	64
Figure 3.13a: ANSYS model of actual FRP sinusoidal core panel	66
Figure 3.13b: Deflection contour of actual FRP sinusoidal core panel	66
Figure 3.14a: ANSYS model of 3-layered equivalent FRP panel	67
Figure 3.14b: Deflection contour of 3-layered equivalent FRP panel	67
Figure 4.1: Representative Volume Element of Core	71
Figure 4.2: Variation of E_x with panel depth, half-wavelength and flute-width.....	73
Figure 4.3: Comparison of equivalent model with actual configuration model for flute-width W	74

Figure 4.4: Variation of E_x with panel depth H and half-wavelength L	75
Figure 4.5: Comparison of equivalent model with actual configuration model for half-wavelength L	76
Figure 4.6: Comparison of equivalent model with actual configuration model for panel depth H	77
Figure 4.7: Variation of E_x with flute/flat thickness t	78
Figure 4.8: Variation of E_x with material elastic modulus E_{11}	79
Figure 4.9: Variation of modification factor K_1 with half-wavelength ratio R_1	81
Figure 4.10: Variation of modification factor K_2 with panel depth ratio R_2	82
Figure 4.11: Variation of modification factor K_3 with flute/flat thickness ratio R_3	83
Figure 4.12: Variation of modification factor K_4 with material young modulus ratio R_4	85
Figure 4.13: Variation of E_y with panel depth, flute-width and half-wavelength.....	87
Figure 4.14: Variation of E_y with half-wavelength L	88
Figure 4.15: Variation of E_y with flute-width W	89
Figure 4.16: Variation of E_y with panel depth H	90
Figure 4.17: Variation of E_y with flute-thickness t	91
Figure 4.18: Variation of E_y with material Young's modulus E_{11}	92
Figure 4.19: Variation of modification factor S_1 with flute-width ratio R_1	93
Figure 4.20: Variation of modification factor S_2 with panel depth ratio R_2	94
Figure 4.21: Variation of modification factor S_3 with panel depth ratio R_3	95
Figure 4.22: Variation of modification factor S_4 with panel depth ratio R_4	96
Figure 4.23: Variation of E_z with panel depth, flute-width and half-wavelength	98
Figure 4.24: Variation of E_z with flute-width W	99
Figure 4.25: Variation of E_z with half-wavelength L	100
Figure 4.26: Variation of E_z with panel depth H	101
Figure 4.27: Variation of E_z with flute thickness t	102
Figure 4.28: Variation of E_z with core material Young's Modulus E_{11}	103
Figure 4.29: Variation of modification factor D_1 with wave-length ratio R_1	104
Figure 4.30: Variation of modification factor D_2 with panel depth ratio R_2	105
Figure 4.31: Variation of modification factor D_3 with flute/flat thickness ratio R_3	106
Figure 4.32: Variation of modification factor D_4 with material Young's Modulus ratio R_4	107
Figure 4.33: Plots of E_x results for comparison.....	111
Figure 5.1: ANSYS model for deriving equivalent sandwich beam G_{xy}	117
Figure 5.2: Deflection contour for sandwich beam in deriving G_{xy}	118
Figure 5.3: ANSYS model for deriving equivalent sandwich beam G_{yx}	119
Figure 5.4: Deflection contour for sandwich beam in deriving G_{yx}	120
Figure 5.5: Cross-section of sandwich beam for hand calculation – Case 1	122
Figure 6.1: Variation of Stiffness with Core Height H	131
Figure 6.2: Variation of Stiffness with Face Elastic Modulus E_{x1}	134
Figure 6.3: Variation of Stiffness with Face Elastic Modulus E_{y1}	134
Figure 6.4: Variation of Stiffness with Face Thickness t_1	136
Figure 6.5: Variation of Stiffness with Core Mat Elastic Modulus E	138
Figure 6.6: Variation of Stiffness with Flute-Width W	138
Figure 6.7: Variation of Stiffness with Half-Wavelength L	140

Figure 6.8: Variation of Stiffness with Flat/Flute Thickness t	141
Figure 6.9: Modification Factor by Face Elastic Modulus (1-direction)	143
Figure 6.10: Modification Factor by Face Elastic Modulus (2-direction)	144
Figure 6.11: Modification Factor by Face Thickness	145
Figure 6.12: Modification Factor by Core Mat Elastic Modulus	146
Figure 6.13: Modification Factor by Flute Width	147
Figure 6.14: Modification Factor by Half-Wavelength.....	148
Figure 6.15: Modification Factor by Flat/Flute Thickness	149
Figure 6.16: Variation of Stiffness with Core Height H	152
Figure 6.17: Variation of Stiffness with Face Elastic Modulus E_{y1}	153
Figure 6.18: Variation of Stiffness with Face Elastic Modulus E_{x1}	155
Figure 6.19: Variation of Stiffness with Face Thickness t_1	156
Figure 6.20: Variation of Stiffness with Core Mat Elastic Modulus E	158
Figure 6.21: Variation of Stiffness with Flute-Width W	159
Figure 6.22: Variation of Stiffness with Half-Wavelength L	160
Figure 6.23: Variation of Stiffness with Flat/Flute Thickness t	161
Figure 6.24: Modification Factor by Face Elastic Modulus (2-direction)	163
Figure 6.25: Modification Factor by Face Elastic Modulus (1-direction)	164
Figure 6.26: Modification Factor by Face Thickness	165
Figure 6.27: Modification Factor by Core Mat Elastic Modulus	166
Figure 6.28: Modification Factor by Flute Width	167
Figure 6.29: Modification Factor by Half-Wavelength.....	168
Figure 6.30: Modification Factor by Flat/Flute Thickness	169
Figure 6.31: Variation of Stiffness with Face Elastic Modulus E_{x1}	173
Figure 6.32: Variation of Stiffness with Face Shear Modulus G_{xy1}	174
Figure 6.33: Variation of Stiffness with Face Thickness t_1	175
Figure 6.34: Variation of Stiffness with Core Height H	176
Figure 6.35: Modification Factor by Face Shear Modulus	179
Figure 6.36: Modification Factor by Face Thickness	179
Figure 6.37: Modification Factor by Core Height	180
Figure 6.38: Model of actual FRP sinusoidal core panel – Phase II loading.....	187
Figure 6.39: Model of actual FRP sinusoidal core panel – Phase II boundary conditions	187
Figure 6.40: Model of equivalent FRP panel – Phase II loading.....	188
Figure 6.41: Model of equivalent FRP panel – Phase II boundary conditions	188
Figure 6.42: Deflection contour of actual FRP sinusoidal core panel	190
Figure 6.43: Deflection contour of equivalent FRP panel	190
Figure 7.1: Stiffness contribution of wearing surface.....	196
Figure 7.2: Transformation of two-layered section	197
Figure 7.3: Transformation of sinusoidal wave core sandwich section.....	200
Figure 7.4: Variation of EI with E_{ws} at $t_{ws} = 0.25$ in.	202
Figure 7.5: Variation of EI with E_{ws} at $t_{ws} = 0.5$ in.	202
Figure 7.6: Variation of EI with E_{ws} at $t_{ws} = 0.75$ in.	203
Figure 7.7: Variation of EI with E_{ws} at $t_{ws} = 1.0$ in.	203
Figure 7.8: Variation of EI with E_{ws} at $t_{ws} = 2.0$ in.	204

Figure 8.1: Construction of Crawford County Bridge showing FRP panels and Saddle Beams	212
Figure 8.2: Crawford County bridge temperature measurements by Kansas DOT for Feb. 7-13, 2004	214
Figure 8.3: Crawford County bridge temperature measurements by Kansas DOT for June 21-27, 2004	214
Figure 8.4: ANSYS model showing simple support conditions.....	218
Figure 8.5: Thermal stresses due to gradient temperature changes of Case 1 (Feb. 7-13, 2004)	219
Figure 8.6: Thermal stresses due to gradient temperature changes of Case 1 (June 21-27, 2004)	219
Figure 8.7: ANSYS model showing continuous support conditions.....	221
Figure 8.8: Thermal stresses due to differential temperature changes of Case 2 (Feb. 7-13, 2004).....	222
Figure 8.9: Thermal stresses due to differential temperature changes of Case 2 (June 21-27, 2004)	222
Figure 8.10: Comparison of σ_x (psi) for Simply and Continuously Supported Panels (Feb.)	225
Figure 8.11: Comparison of σ_x (psi) for Simply and Continuously Supported Panels (June)	225
Figure 8.12: Comparison of σ_z (psi) for Simply and Continuously Supported Panels (Feb.)	226
Figure 8.13: Comparison of σ_z (psi) for Simply and Continuously Supported Panels (June)	226
Figure 8.14: Comparison of τ_{xz} (psi) for Simply and Continuously Supported Panels (Feb.)	227
Figure 8.15: Comparison of τ_{xz} (psi) for Simply and Continuously Supported Panels (June)	227
Figure 8.16: Comparison of τ_{yz} (psi) for Simply and Continuously Supported Panels (Feb.)	228
Figure 8.17: Comparison of τ_{yz} (psi) for Simply and Continuously Supported Panels (June)	228

CHAPTER 1 - INTRODUCTION

1.1 General Background

Highway bridge decks in the US are constructed predominantly with steel-reinforced concrete. However, costs of repair and maintenance of these bridges incurred at the federal and state levels are overwhelming. As a result, for many years there has been pressure on transportation agencies to find new cost-effective and reliable construction materials (Ehlen 1999). A very promising alternative is the fully-composite Fiber Reinforced Polymer (FRP) structural bridge system. FRP composites have found increasing applications in bridge design and construction. To improve its structural performance, honeycomb core sandwich panels are used. A special configuration of this panel type is the sinusoidal core geometry which extends vertically between face laminates. This research work focuses on this novel technology developed by Kansas Structural Composites, Inc.

It is well known that FRP possesses significant advantages, which might in the future present a very good challenge to the more ubiquitous steel, reinforced concrete and others in the construction field. One main driving force in the use of FRP has been its high strength and stiffness when determined on a weight basis. One source shows that a FRP bridge deck weighs about 20 percent as much as a structurally equivalent reinforced concrete deck (Murton 2001). The light weight of FRP makes it possible for smaller scale foundations and other supports to be used. Since many bridges in the US are categorized as deficient because of substructure problems or inadequate live load capacity, FRP bridge decks may be a good substitute (Zureick et al. 1995).

Among FRP's high strength properties, the most relevant include durability and corrosion resistance. It is also resistant to chemical attack; hence, it has been suggested that little maintenance may be needed other than periodic wearing surface renewal.

Because deck panels are manufactured in the factory and transported to the construction site, the production process can be closely monitored under a controlled environment. This leads to higher quality products. Potential weather delays can also be greatly reduced as is sometimes a problem with cast-in-place structures. There is also the merit of ease of manufacturing, fabrication, handling and erection, with the project delivery and installation time being greatly reduced.

Other benefits of the use of FRP include electromagnetic neutrality, anti-seismic behavior, versatility and fatigue endurance. It also possesses very high material toughness and resistance to abrasion. Additionally, it has aesthetic benefits. The bridge system can be specified in any color, since this can be pigmented into the resin. This therefore might make painting unnecessary, and gives the structure an attractive appearance.

Like most structural materials, however, FRP has a few drawbacks. One noteworthy disadvantage is the high initial cost. It is interesting though, that this high cost can be economically justified as the life cycle cost may be reduced over the life time of the bridge (Ehlen 1999). This is so because as was noted above, maintenance cost of an FRP bridge could be relatively low due to high durability of the structure. This is of interest because rehabilitation and maintenance of reinforced concrete bridges has been an issue in the US in recent years. More than 200,000 bridges worth \$78 billion

are in need of repair (Klaiber et al. 1987, Munley 1994). Over \$5 billion per year in maintenance would merely maintain the status quo. A similar condition exists in Canada where, according to one report, over 40% of the bridges were built in the fifties and sixties, and most of these are in urgent need of rehabilitation (Nearle 1997).

A concern for FRP bridge design is the lack of design guidance and/or standards. The design and manufacture also require highly trained specialists from many engineering and material science disciplines, and some manufacturing processes may not produce consistent material or structural properties.

A Load and Resistance Factor Design (LRFD) code for structures using FRP is being developed in the US. It will be based on a probability-based limit state design criteria. In addition, the American Society of Civil Engineers (ASCE) is currently engaged in research work for the purpose of developing a standard for the design of pultruded FRP composite structures. It is expected that when completed, this document will serve as the basis for the American Association of State Highway and Transportation Officials (AASHTO) design code for FRP structures (Scott and Wheeler 2001). The results from this research work would no doubt provide valuable contributions.

Although FRP structures have the advantage of being light in weight, this could render the structure aerodynamically unstable. Other demerits include ultraviolet radiation degradation, photo-degradation and a lack of awareness.

Researchers over the last decade are addressing these issues, and the information is being disseminated in the wider engineering community. As part of this

ongoing research, this investigation addresses a special kind of bridge deck configuration – sandwich panels with honeycomb sinusoidal wave core.

1.2 Aim and Objectives

This report is aimed at utilizing finite element modeling techniques to evaluate the performance of fiber reinforced polymer sandwich bridge panels. It focuses specifically on a sinusoidal wave honeycomb core configuration sandwiched by face laminates, which was developed by Kansas Structural Composites, Inc. and proven to be stiffer than other configurations (Plunkett 1997). This panel geometry is shown in Fig. 1.1. The terms which will be used to refer to the panel components are defined in Fig. 1.2. The flats refer to the straight parallel components of the core, while the flutes represent the sinusoidal components.

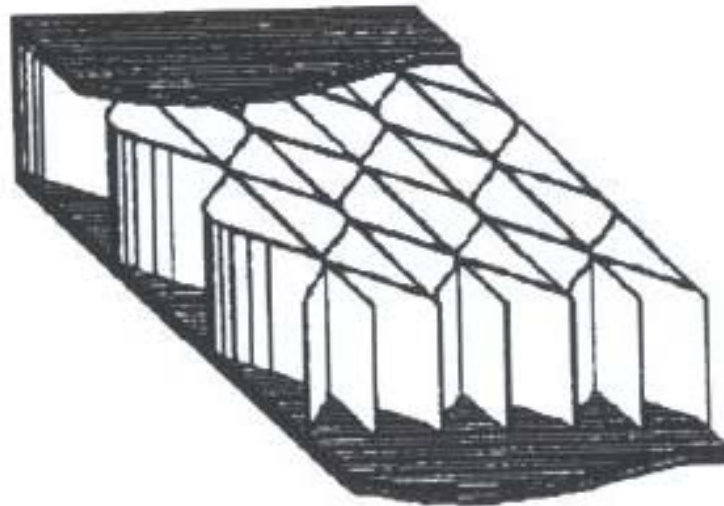


Figure 1.1: Sandwich panel configuration for this study.

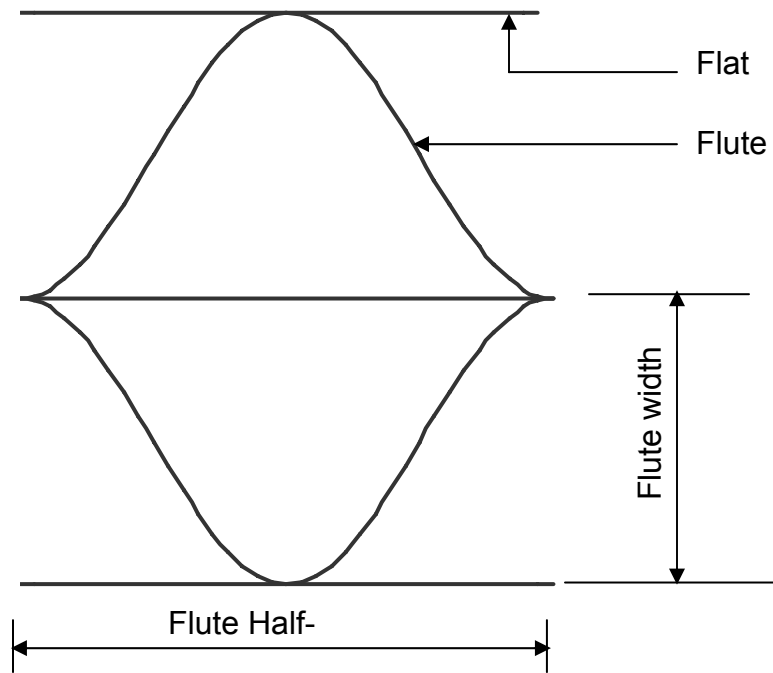


Figure 1.2: Core component definitions.

To achieve the aim of this study, the following objectives are fulfilled:

- Perform a comprehensive review on the development of various FRP panel types
- Compute equivalent laminae stiffness properties from micromechanics
- Compute equivalent stiffness properties for face laminates
- Derive core equivalent stiffness properties for a specific sinusoidal core configuration using FEM (ANSYS 9.0), elasticity and plate theory
- Perform parametric studies to derive equations for elastic moduli as functions of depth, flute-width, flute-wavelength, flat/flute thickness and core laminae Young's Modulus
- Derive equivalent stiffness properties of the entire deck system as a single layer

- Perform parametric studies to derive equations for elastic moduli as functions of parameters of core and face laminates
- Investigate behavior of panels with wearing surface
- Perform temperature analysis
- Draw conclusions and make recommendations based on the analytical results obtained

1.3 Scope and Limitations of Study

Using micromechanics and laminate theory, laminae stiffness and equivalent laminate properties will be computed. Core equivalent stiffness properties for the sinusoidal core configuration will be derived using finite element modeling, elasticity and plate theory. Equivalent properties of the entire sandwich panel as a single layer of plate will also be formulated. These properties will be verified by comparing results of the actual panel configuration with the equivalent model. Parametric studies to derive equations for equivalent elastic properties as functions of parameters of the core and face laminates will then be conducted.

The panel with a layer of wearing surface will also be analyzed, with the intention of investigating the level of stress between the face laminate and the wearing surface as well as the contribution of stiffness of the overlay material. The behavior of different overlay materials will be studied.

Temperature effects could be of significant importance in the behavior of FRP structures. Changes in temperature can cause high levels of stresses and deformations which could become significant when combined with truck loads. Hence, the effects of temperature on the bridge panel will also be investigated.

One of the major limitations in this research is linked to the complexity of the sinusoidal core model configuration. The finite element software used for this research (ANSYS 9.0 University Advanced version) lacks the processing capacity to handle an actual full bridge model. For instance, to build a very small model of 15 ft x 7.5 ft x 5 in. would require about 133,200 elements since a minimum of 4 elements are required to model a sine wave, whereas the element capacity of our available software is 128,000. As a result, a complete modeling of a full bridge is not possible for this deck configuration.

1.4 Chapter Layout

After the brief introduction in this chapter, a detailed literature review which includes a State-of-the-Art review is presented in Chapter 2. A discussion on an approach to deriving equivalent properties due to in-plane behavior follows in Chapter 3. Based on this approach, parametric studies for the core are conducted in Chapter 4 with a view to formulating equations for equivalent elastic properties. Attention is then turned to out-of-plane behavior in Chapter 5 where an approach of predicting equivalent stiffness properties is established. Correspondingly, equations to obtain these properties for varying panel parameters are derived in Chapter 6. A study of the stiffness contribution of a layer of wearing surface to the FRP panel of this work is next carried out in Chapter 7. Chapter 8 focuses on thermal analysis to present the reader with a broad view of the distribution of thermal stresses in the panel. Finally, conclusions are drawn and recommendations made for further research in Chapter 9.

CHAPTER 2 - LITERATURE REVIEW

2.1 Introduction

Fiber Reinforced Polymers have been in use since the 1940's. Due to heavy financial costs, however, the application of FRP was limited to the aerospace and defense industries. To meet the higher performance challenges of space exploration and air travel in the 60's and 70's, fiber materials with higher strength, higher stiffness and lower density (such as boron, aramid and carbon) were commercialized. During the 1970's, research was channeled to developing ways to improve the cost of high performance FRP's. By the late 1980's and early 1990's, the defense industry waned and emphasis was now placed on cost reduction and the continued growth of the FRP industry (Bakis et al. 2002).

Although Fiber Reinforced Polymers have had a long history, it is only in recent years that it has won the attention of Civil Engineers as a potential alternative to more conventional structural materials. Throughout the 1990's, various industries have financed demonstration projects and sponsored research programs on this burgeoning field. As research continues, FRP materials are now finding wider acceptance in the construction industry.

2.2 State-of-the-Art Review

Prior to the 1970's, pultruded FRP structural shapes were developed but limited to small sized commodity products for non-structural applications. In the 1970's and 1980's, larger pultruded shapes for structural purposes and load-bearing elements were produced largely as a result of the advancement in pultrusion technology. Pultrusion companies in the United States began to produce "standard" I-shaped beams for

construction purposes. A customized building system of pultruded components for the construction of industrial cooling towers was developed in the late 1980's and 1990's. Small pultruded FRP structural shapes for the construction of walkways and short-span pedestrian bridges have increased in use since the early 1990's (Bakis et al. 2002).

Several bridges have been constructed in various parts of the world using FRP. These include both pedestrian and vehicular bridges. One example is Aberfeldy Footbridge which crosses the River Tay in Scotland erected in 1992 and is the world's first and longest advanced composite footbridge. Another example is the Bonds Mill lift bridge (completed in 1994) which is an electrically operated lift bridge. It was the first bridge in England to be constructed from plastic. Tech 21 (Smith Road) Bridge is Ohio's first all-composite bridge. The Butler County Engineer's Office installed this structure built entirely of advanced composite materials.

Some of the first applications of fiber-reinforced plastics for complete bridge structures were in China. A number of pedestrian bridges have been built, but the first all composite bridge deck was the Miyun Bridge completed in September 1982 near Beijing, which carries full highway traffic. Ulenbergstrasse Bridge in Germany was the world's first in the use of high tensile strength glass fiber prestressing tendons. More details about these bridges are considered in Section 2.7.

2.3 Types of FRP Panels

FRP decks can be grouped into two categories based on the type of construction – sandwich and adhesively bonded pultruded shapes. In this research work, focus is directed on a honeycomb core sandwich deck. However, an overview of both types is first given.

2.3.1 Sandwich Construction

This type of construction meets the requirement of high strength and stiffness at a minimum unit weight. Use is made of bonded core materials, separating strong, stiff and low density face sheets. The entire deck is made to act compositely. A great advantage this type of construction has is its flexibility in designing structures for varied depths and deflection requirements. This is so since the manufacturing of face and core components can be controlled by the producer. The most efficient core materials are cellular materials (Bakis et al. 2002).

The connection between sandwich deck panels is usually by tongue and groove ends. A clamp mechanism is used to join the panels with the underlying structure. A major problem experienced by this mode of construction is delamination and this may be due to some manufacturing defects. Hence, special focus must be given to the connection details during the design and production stages.

One example of this panel type is the sinusoidal wave core configuration in the plane extending vertically between face laminates. The geometry of this panel can be seen in Fig. 2.1. Another example is the web core geometry with a two-way vertical interior core. It has transverse and longitudinal web configuration making it look like a box, as can be seen from Fig. 2.2.

2.3.2 Adhesively Bonded Pultruded Shapes

Pultruded shapes are produced by manufacturers using well-established processing techniques. These shapes can be grouped into two – standard and custom. The term “standard” implies that the FRP part are produced on a regular basis by the company, are usually available off-the-shelf, have published dimensions and meet

minimum manufacturing-provided property values (Bakis et al. 2002). Examples include “standard” angles, tubes, channels and I-shaped sections. Nonstandard shapes are called “custom” shapes.

FRP decks produced by adhesively bonded pultruded shapes include EZSpan (Atlantic Research), Superdeck (Creative Pultrusions), DuraSpan (Martin Marietta Materials) and Strongwell. The pultruded shapes are typically aligned transverse to the direction of traffic flow. Fig. 2.3 shows a schematic diagram of the DuraSpan pultruded deck system.

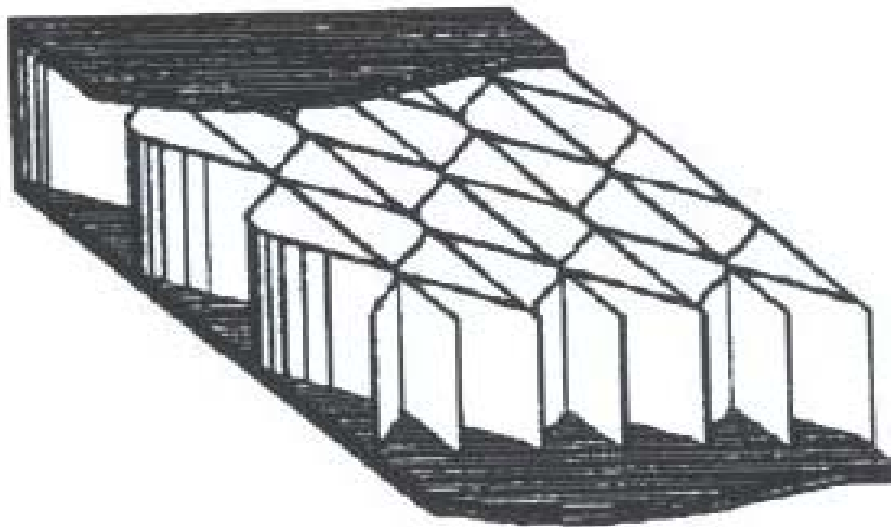


Figure 2.1: Fiber reinforced polymer honeycomb (FRPH) sandwich panel.

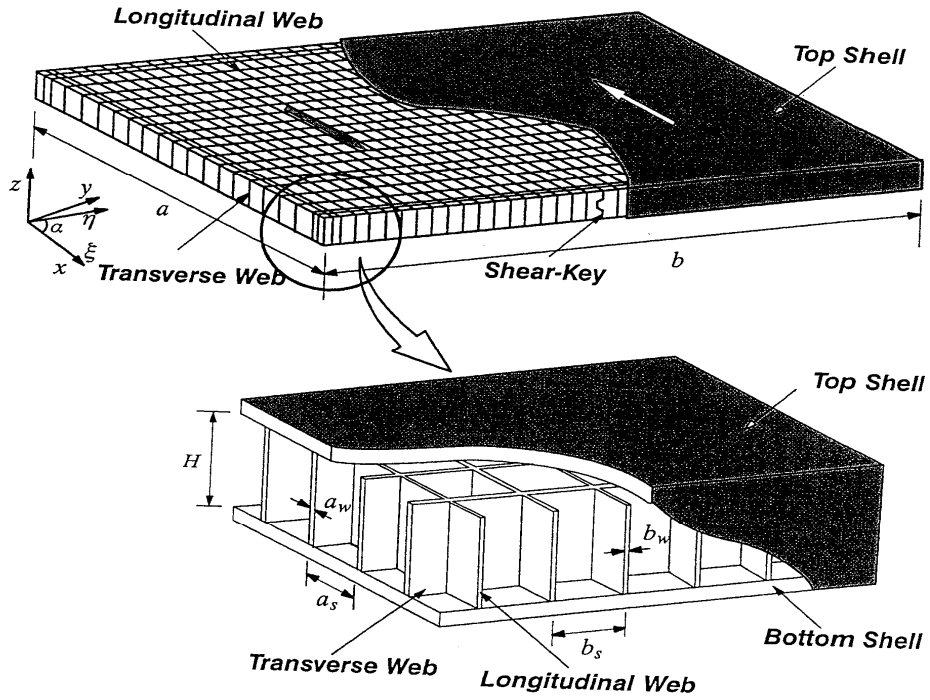


Figure 2.2: Web core sandwich bridge deck system.

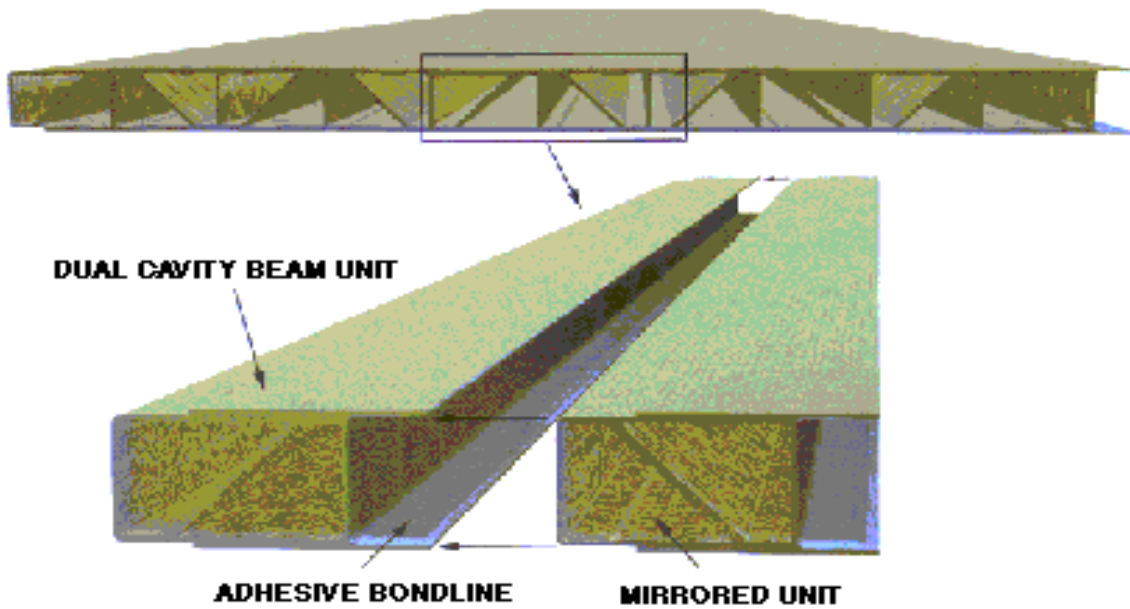


Figure 2.3: DuraSpan® deck system by Martin Marietta Composites, Inc.

2.4 Analysis of Sinusoidal Wave Core Sandwich Panel

The introduction of FRP honeycomb sandwich panels with sinusoidal wave core configuration in the vertical plane between face laminates was done by Plunkett (1997). He investigated the potential of this kind of configuration through a series of studies for testing and field installations. The geometry of this sandwich structure is designed to improve stiffness and buckling response by the continuous support of core elements with the face laminates.

A study by Davalos et al. (2001) went further in design modeling and experimental characterization, and obtained an approximate analytical solution through a homogenization process. To verify the results, experiments were performed and finite element analysis (numerical verification) was carried out. The goal of that study was to develop equivalent elastic properties for the core structure. To achieve this, an energy method combined with mechanics of materials approach was used.

In performing elastic equivalence analysis of the sinusoidal waved honeycomb core structure, Davalos et al. (2001) utilized energy concepts. He assumed that the structure of the sandwich core could be separated into a number of substructures of flat and curved walls, which could be simplified as a series of simply supported elements. Using the theory of minimum energy, the strain energy computed from the exact displacement distribution was minimized. The strain energy of a Representative Volume Element (See Fig. 2.4) – a unit cell of the core – of the structure was computed from the Voigt and Reuss model for upper and lower bounds as below:

$$\frac{\sigma_{ij}^2}{2C_{ij}} V \leq \sum_{k=1}^n (U_b + U_s + U_a)_k \quad \text{Equation 2.1}$$

$$\frac{C_{ij}\varepsilon_{ij}^2}{2} V \leq \sum_{k=1}^n (U_b + U_s + U_a)_k \quad \text{Equation 2.2}$$

where k takes into account individual substructures, U_b is the strain energy due to bending response, U_s represents the strain energy due to shear response and U_a refers to the strain energy due to axial response. In Fig. 2.4, the amplitude of the sinusoidal wave core is $2h$.

The loading arrangement used to obtain the elastic constants involved applying each single principal stress or strain to obtain the corresponding stiffness without other types of strain energy involved. When this load is applied, the strain energy in Equations 2.1 and 2.2 becomes:

$$U = \sum_{k=1}^n \left\{ \int_0^s \left(\frac{\delta_{11} M_{11}^2}{2} + \frac{\alpha_{11} N_{11}^2}{2} + \frac{h_{44} V_{12}^2}{2} \right) ds \right\}_k \quad \text{Equation 2.3}$$

where M_{11} , N_{11} , V_{12} refer to the bending moment, axial force and transverse shear force acting on the core wall, and δ_{11} , α_{11} and h_{44} are the corresponding compliance coefficients.

To compute the modulus of elasticity in the lateral (y) direction, a uniform stress q was applied in that direction. Using Equation 2.3, the internal strain energy U was calculated. The bending moment M_{11} , axial force N_{11} and shear force V_{12} were obtained from equilibrium and geometric considerations of Fig. 2.5. Thus, the compliance coefficients δ_{11} , α_{11} and h_{44} could be calculated. The results obtained for these coefficients are shown in Equation 2.4.

$$\delta_{11} = \frac{12}{E_1 t_2^3}, \quad \alpha_{11} = \frac{1}{E_1 t_2}, \quad h_{44} = \frac{1}{\kappa G_{13} t_2}, \quad \alpha'_{11} = \frac{1}{E_1 t_1} \quad \text{Equation 2.4}$$

where, t_1 and t_2 are the thicknesses of the flat and corrugated core wall respectively (Fig. 2.4) and κ is the shear correction factor.

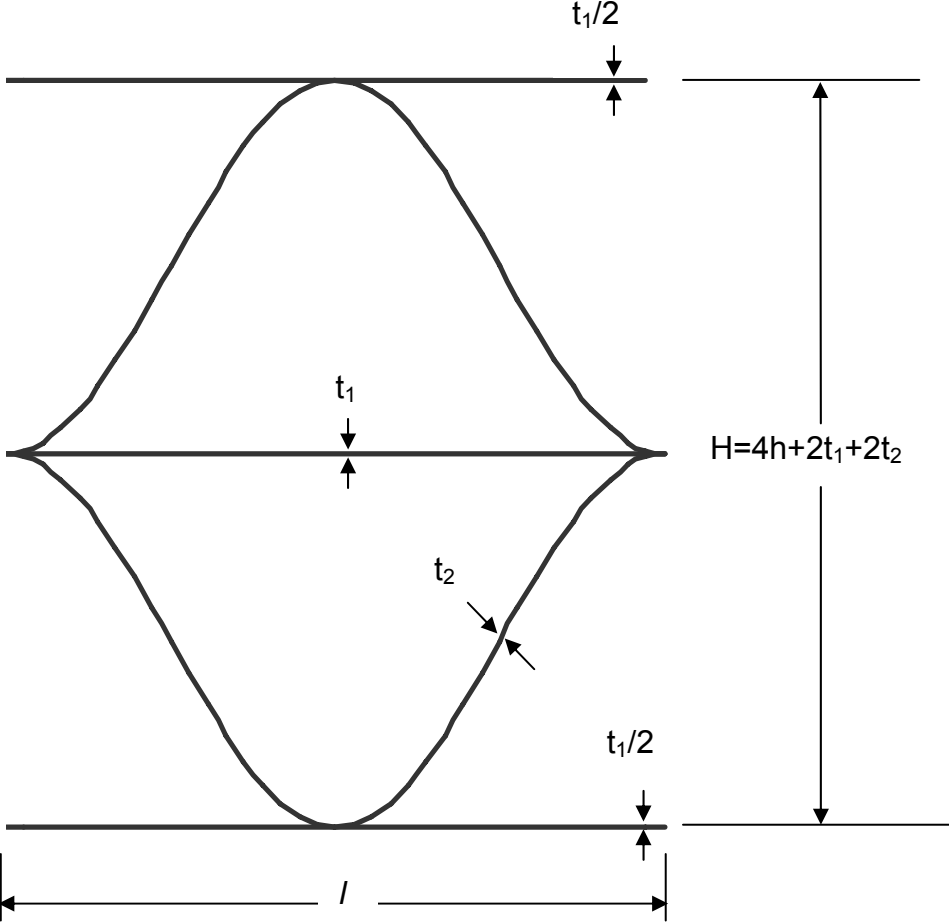


Figure 2.4: Representative Volume Element (RVE).

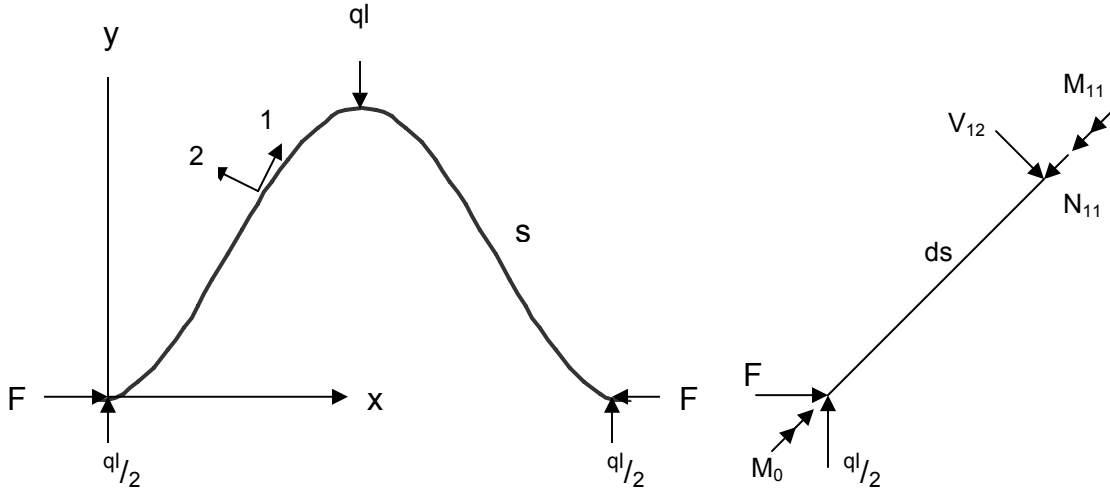


Figure 2.5: Coordinate and equilibrium condition for computation of E_y^e .

The apparent strain of the RVE ε_y was then computed using Castigliano's second theorem which states that the partial derivative of the strain energy with respect to the external force gives the displacement corresponding to that force. Therefore,

$$\Delta_y = H\varepsilon_y = \frac{\partial U}{\partial (ql)} \quad \text{Equation 2.5}$$

Similarly,

$$\Delta_x = l\varepsilon_x = \frac{\partial U'}{\partial (F)} = \frac{Fl}{E_1 t_1} \quad \text{Equation 2.6}$$

The equivalent modulus of elasticity E_y^e and the Poisson's ratio ν_{yx}^e for the RVE could then be calculated using the relation in Equation 2.7:

$$E_y^e = \frac{q}{\varepsilon_y}, \quad \nu_{yx}^e = -\frac{\varepsilon_x}{\varepsilon_y} = \frac{\Delta_x H}{\Delta_y l} \quad \text{Equation 2.7}$$

where q is the applied stress (Fig. 2.5) and ε_y and ε_x are the computed strain from Equations 2.5 and 2.6.

To obtain the equivalent stiffness in the longitudinal (x) direction, the same approach was followed, applying a uniform stress in the x-direction. However, Davalos et al. (2001) assumed that the stiffness contribution in the curved substructure is negligible, leading to an approximate solution for E_x^e as shown in Equation 2.8.

$$E_x^e = \frac{2t_1}{H} E_1 \quad \text{Equation 2.8}$$

Another research project carried out by Qiao et al. (2003) went further to evaluate the core effective in-plane shear modulus of the sinusoidal core configuration G_{xy}^e using energy methods and mechanics of materials approach. He applied a macroscopic shear deformation on the same unit cell shown in Fig. 2.4. The strain energy in a quarter of the unit cell (Fig. 2.6) was given as:

$$U = \int_0^s \left(\frac{\alpha_M M^2}{2} + \frac{\alpha_N N^2}{2} + \frac{\alpha_V V^2}{2} \right) ds + \frac{2F^2 b}{E_1 t_1} \quad \text{Equation 2.9}$$

where, M, N and V represent bending moment, axial force and transverse shear force acting on the core, α_M , α_N and α_V are the corresponding compliance coefficients and b is the quarter wave-length. From Castigliano's theorem,

$$\frac{\partial U}{\partial M_0} = 0, \quad \frac{\partial U}{\partial P} = 0, \quad \frac{\partial U}{\partial F} = \Delta_x \quad \text{Equation 2.10}$$

From these formulations, Qiao et al. (2003) came up with the solution for the core effective in-plane shear modulus as seen in Equation 2.11 below:

$$G_{xy}^e = \frac{\tau}{\gamma} = \frac{2Fh}{b\Delta_x} \quad \text{Equation 2.11}$$

They further verified their analytical formulation using experimental testing. The transverse and vertical moduli of elasticity (E_y and E_z) were evaluated using axial

compression tests, while the effective longitudinal elastic modulus (E_x) was obtained by a three point-bending test. The out-of-plane shear moduli (G_{xz} and G_{yz}) were derived from dynamic tests using piezoelectric sensors.

In his master's thesis, Kalny (2003) verified the equivalent elastic properties predicted by Davalos et al. (2001). He performed coupon tests on the actual manufactured core and face laminates from the same manufacturer (KSCI). From his results, he found that the predicted properties were all within 30% of those determined from actual coupon tests.

In this present study, a verification of the equivalent properties of the face laminates is done using micromechanics, and the core equivalent properties are determined by means of a numerical approach. The properties are then utilized as input into a full-sized panel finite element analysis for verification purposes. A difference between in-plane and out-of-plane behavior is noted in this study. Parametric studies are also performed. The information obtained can be vital in design and optimization procedures. The effects of wearing surface and temperature on the panel are also examined.

2.5 Construction Details

The construction of four different FRP bridges is discussed in connection with details in construction issues. The four bridges are the Laurel Lick, Laurel Hill Creek, Wickwire Run and Market Street bridges. These bridges were among the some 20 highway bridges which the Constructed Facilities Center at West Virginia University, in cooperation with FHWA and the West Virginia DOT-DOH were involved in rehabilitating (Shekar et al. 2002, GangaRao et al. 2001).

2.5.1 Deck Details

The decks for the four bridges were fabricated by Creative Pultrusion Inc. under the trade name of Superdeck. They were all designed to AASHTO HS25-44 standard for live loading. The weight of the decks was about 20% of that of a reinforced concrete deck. The cross sections were made of hexagon and double trapezoids. The fibers used were E-glass multiaxial stitched fabrics with a chopped strand mat and continuous rovings. Vinylester resin was used as the matrix phase.

2.5.2 Shipping and Handling

Special hooks were provided by the manufacturer for the purpose of lifting up the deck modules. Care was taken to prevent any damage of the flanges. To accomplish this, nylon straps were utilized, and the lifting was done in such a way as to transfer the lifting load across the width of the module. To erect the superstructure, a crane was used, whose capacity depended on the size of the deck module.

2.5.3 Surface Preparation

The surfaces of the stringers and the modules were prepared prior to connecting both members. This preparation included sandblasting so as to remove dirt and grease from the surfaces. According to the Market Development Alliance of the FRP Composite Industry (quoted by Shekar et al. 2002), the edges of the modules have to be wiped clean with a cloth dipped in methyl ethyl ketone. As a precautionary measure, the surfaces of the modules and stringers were then covered with blankets until it was time for the bonding operation.

2.5.4 Assembly and Connections

The assembled structure of all four bridges composed of the FRP deck modules aligned transversely to traffic flow and supported by girders. For three of the bridges (Laurel Lick, Laurel Hill Creek and Wickwire Run bridges), the connections of deck-to-deck and deck-to-stringer were by means of both adhesive bonding and mechanical fasteners. The mechanical fasteners were in the form of shear keys which provided adequate shear transfer between modules. In the Market Street Bridge, the interconnection of deck-to-deck was done using adhesive bonding only. The modules were connected to steel plate girders by field welding. A steel washer plate was then used to tie the deck down to the girder.

2.5.5 Wearing Surface

For all four bridges, thin polymer concrete (PC) was used as the overlay material. First, surface preparation was carried out. This included sandblasting the deck to get rid of impurities on the surface and improve the bonding. Vacuum cleaning was done to eliminate polymer powder produced during surface preparation. A urethane-based primer was applied. Care was taken to deal with effects in temperature variations during the curing phase of the overlay. The laying of the wearing surface was done “when the temperature was above 50°F and below 80°F”. This was done to prevent the PC from curing faster or slower than needed (Shekar et al. 2002).

2.6 Manufacturing Processes

There are different manufacturing methods used in the production of structural composites. Examples include hand lay-up, Vacuum-Assisted Resin Transfer Molding

(VARTM), pultrusion, vacuum bag molding, press molding and autoclave molding (Zureick et al. 1995).

2.6.1 Hand Lay-Up

This is a manual approach in which layers of fabric and resin are successively applied onto a mold. The mold is first designed to the shape of the final composite structure. This method is perhaps the simplest, oldest and least complicated. The fiber layers are oriented in such a way as to develop the desired strength and stiffness. After each layer of fabric is placed, a roller is used on the composite so that a strong bond results and excess resin is squeezed out. The stacking of fabric materials and resin is done until the required thickness is achieved.

This method is labor intensive and only suitable for production in low volume. It can have a disadvantage of low quality control and inconsistency in properties of various parts of the finished product. However, with this method, complicated shaped composites can be manufactured, such as the complex core configuration of the sinusoidal honeycomb panel.

In recent years, the advances in manufacturing technology have resulted in some improvement in this manual process. Today, the hand lay-up has become automated in several applications.

2.6.2 Vacuum-Assisted Resin Transfer Molding (VARTM)

In this process, dry fabrics needed to produce the structural component are stacked together successively. The fabric is placed in an open mold surface without a top. When the lay-up operation is completed, the mold is covered, and a vacuum is applied to consolidate the material. Resin is then allowed to flow and disperse through

the entire structural network, with the mold kept under vacuum. The resin is cured under ambient conditions.

This process has a great advantage of comparatively low cost of production, since the materials, molds, equipments are inexpensive. It is also advantageous over many other methods because of minimized environmental hazards from toxins associated with the process. The mold is sealed during the resin application, thus controlling environmental threats and reducing health risks of workers.

2.6.3 Pultrusion

This method is used primarily to produce prismatic structural members. Fibers are passed through a resin bath to coat them. The coated fibers are then formed into the desired shapes and passed through a die that helps to consolidate the fibers and produce a composite with a high fiber volume fraction. Then the full section emerges. The resulting shape of the final section depends on the way the die is fabricated.

2.6.4 Vacuum Bag Molding

The purpose of this process is to create a very good bond for the individual plies. The entire composite is placed into a flexible bag and a vacuum is applied. This helps to push together the plies, thus developing a good bond. Volatiles that form during the curing process are also removed.

2.6.5 Press Molding

Here, high pressure and temperature are the catalysts to developing strong chemical bonds between layers. The composite material is placed into the press, where external pressure and elevated temperature are applied. Components of simple shape configurations are usually produced by this method.

2.6.6 Autoclave Molding

The autoclave molding process allows for more complex shapes to be manufactured than does the press molding. A furnace is used to cure the composite at very high temperatures and pressure. The high pressures can force voids and excess resin out of the composite and increase the fiber volume fraction. Also, because the resin is cured at elevated temperatures, properties superior to those resulting from curing at ambient temperatures are developed.

2.7 Bridge Applications of FRP

The applications of FRP in civil engineering can be classified into three broad areas. First: in new construction. New structures such as bridges and columns built exclusively out of FRP have proved durable and very resistant to environmental hazards. A second, and more common application, is in the repair and rehabilitation of damaged or deteriorating structures. Third, FRP have been used in architectural or aesthetic applications such as in cladding, roofing, flooring and partitions. FRP can be used for barriers, docks, marinas, covers, blast shields, vehicle platforms for unstable ground, rapid construction, bridges, bridge decks, etc.

FRP bridges (both pedestrian and vehicular) have been constructed in Asia/Far East, Europe, North America and the Caribbean. In this section, we highlight some noteworthy examples of the considerable recent developments in the diverse use of FRP in pedestrian and highway bridges in the world.

2.7.1 Aberfeldy Footbridge

This bridge, which crosses the River Tay in Scotland, was erected in 1992. It is the world's first and also longest advanced composite footbridge (Scott and Wheeler

2001, Khalifa 1993). The bridge is a cable-stayed structure with a main span of 63 m (207 ft) and two back spans of 25 m (82 ft). The two pylons are each made of Glass FRP, are 'A' shaped and have a height of 18 m (59 ft). The cables are Parafil (Kevlar aramid fibers sheathed in a protective low density polyethylene). The fabrication of the bridge deck was from the Advanced Composite Construction System (ACCS). A unique method of erection of the towers, cables and deck was employed which needed no site crane. This was made possible due to the lightweight components.

Glass reinforced polyester (GRP) handrailing and a wear-resistant deck finish were used to complete the bridge. Minimal foundations and rapid site assembly made this solution very cost-effective. It was originally designed with a live load capacity of 3.5 kN/m² (0.5 psi), but has been strengthened since then to accommodate golf carts and had ballast added to improve its performance.

2.7.2 Bonds Mill Lift Bridge

Bonds Mill Bridge is an electrically operated lift bridge. It was the first bridge in England to be constructed from plastic (Hayes 1998). Its construction was completed in 1994. It is also the world's first advanced composite road bridge. It is 27 ft long, 14 ft wide and 2.8 ft deep and was manufactured from Maunsell Structural Plastics' Advanced Composites Construction System (ACCS). It was constructed utilizing a series of pultruded GRP sections running longitudinally and are bonded together using an epoxy resin to form a cellular box girder with six main cells which are filled with epoxy foam. The deck is a 'double ply' of ACCS skins with cells running in two orthogonal directions. The total weight of the entire system is 4.5 tons (10 kip) for 35 m² (377 ft²) of deck area, which gives a live to dead load ratio of 13.5. Composite materials

were used because lighter weight structure made it possible to use a smaller lift mechanism.

2.7.3 Troutville Weigh Station

This bridge, located in Troutville, Virginia, was constructed in 1999 and is a 3.05 meters (10 feet) by 4.65 meters (15 feet) composite deck section (Scott and Wheeler 2001). Standard EXTREN® structural shapes and plate of 4.65 m (15 ft) width were used in the construction of the bridge deck. (EXTREN® is a proprietary combination of fiberglass reinforcements and thermosetting polyester or vinyl ester resin systems. It is produced in more than 100 standard shapes and all shapes have a surface veil to protect against glass fibers penetrating the resin surface in service and to increase corrosion and UV resistance). The deck has as support steel I-girders and experiences traffic of over 13,000 fully loaded trucks per day.

Some other features of the bridge include routine inspection capability installed into the system and flexible foundation for the purpose of future experimental bridge decks. A data acquisition monitoring system to collect and report real data has been installed by Virginia Tech.

2.7.4 Laurel Run Road Bridge

This bridge was constructed in Somerset County, Pennsylvania, and was open to traffic in October 1998. (Scott and Wheeler 2001) It is a short span composite deck with steel stringers, and has a dimension of 8.66 m (28 ft) by 10.04 m (33 ft). It consists of the Superdeck™ (modular FRP composite deck) supported on a W14 x 68 galvanized steel I-girders at a spacing of 0.9 m (3 ft) centers and a substructure of steel-reinforced concrete. The modular deck design is one featuring trapezoids connected with

hexagon-shaped pins. Epoxy polymer concrete was overlaid as the wearing surface. FRP square tubes were used for the kerbs. The bridge has been designed for AASHTO HS25-44 live loading.

2.7.5 Laurel Lick Bridge

The construction of this short-span bridge was completed in May 1997 in Lewis County, West Virginia (Shekar et al. 2002, Hayes 1998). It spans 6.10 m (20 ft) and has a width of 4.88 m (16 ft). It consists of modular FRP composite deck supported by pultruded FRP piles and I-beams. Hollow glass fabric shapes were pultruded and combined to obtain an H-deck. This is composed of E-glass fibers in the form of triaxial stitched fabrics, continuous rovings and chopped strand mats.

Sandstone foundation supported the piles for the bridge and was also filled with polymer concrete. The wide-flange pultruded I-beams were attached to the reinforced concrete cap pilings with steel clip plates. These I-beams were spaced at 0.76 m (2.5 ft) centers. The FRP deck modules were connected to these I-beams with 0.5-in. blind fasteners. Polyester Polymer concrete overlay of 1.0 cm (0.4 in.) thick was used as the wearing surface. The kerbs were made of FRP square tubes and a live loading based on AASHTO HS25-44 was the design standard.

2.7.6 Tech 21 (Smith Road) Bridge

This is Ohio's first all-composite bridge. The Butler County Engineer's Office installed this structure built entirely of advanced composite materials in 1997. (Foster et al. 2000) Structural Polymer Matrix Composites (PMC) such as glass fibers in thermosetting resins were used in the construction of the bridge, providing high specific strength, specific stiffness, and corrosion resistance. This bridge (also known as the

'smart bridge') is also the nation's first fully instrumented bridge. Health monitoring instrumentation was installed for the purpose of providing information on the performance under field conditions. Special sensors have been embedded and linked to special computers designed for continuous monitoring. The bridge has a span of 10.06 m (33 ft), a width of 7.3 m (24 ft) and a depth of about 0.85 m (2.8 ft). It has a weight of less than 22,000 lbs. It consists of a DuraSpan™ deck bonded compositely with three U-shaped FRP girders which serve as supports, and has a reinforced concrete substructure. The deck is a sandwich FRP construction consisting of pultruded tubes between two face sheets. The tubes run parallel with the traffic direction. The bridge was designed with the AASHTO HS25-44 standard for live loading (Scott and Wheeler 2001).

2.7.7 Miyun Bridge, Beijing

Some of the first applications of fiber-reinforced plastics for complete bridge structures were in China. A number of pedestrian bridges have been built but the first all composite bridge deck was the Miyun Bridge completed in September 1982 near Beijing, which carries full highway traffic (Scott and Wheeler 2001, Khalifa et al. 1993).

2.7.8 Ulenbergstrasse Bridge, Düsseldorf

Ulenbergstrasse Bridge, Düsseldorf, Germany was the world's first in the use of high tensile strength glass fiber prestressing tendons (Khalifa et al. 1993). The bridge cross section has been monitored since its completion in July 1986 with four fiber optic sensors. The results obtained show the effects of temperature variation on strain and also detect any cracking of the concrete structure. This type of monitoring program has thereby proved a cost effective way of introducing a new structural material without

lengthy proving trials. Any degradation in structural performance will be indicated by the sensor and the exact location of the defect will be known. Any remedial steps that must be taken will therefore be directed to solving problems as they arise.

2.7.9 Salem Avenue Bridge, Dayton

The design, construction and long-term observation of this bridge illustrate some difficulties encountered in the use of FRP in bridge construction (Scott and Wheeler 2001). It was originally built in 1951 with steel and consisted of twin structures with a longitudinal joint and a four-foot raised concrete median down the centre. After many decades, it was observed that the bridge needed replacement; it had developed numerous potholes and cracks. Therefore, in 1999, ODOT began an experiment to rebuild the 679-ft bridge with light-weight, high-strength FRP panels as part of a project to test this space-age material for various bridge applications. The construction was done in 2000 and was designed based on AASHTO HS25-44 code for live loading.

Unfortunately, though, this new material presented some new problems for construction crews and engineers. The bridge was constructed with four FRP composite deck systems each from a different manufacturer. These FRP panels for the span did not fit together smoothly and didn't bond correctly to the bridge's beams. Additionally, after a few months of the completion of the project, some complications with some of the panels were noticed leading to a closure of the north side of the bridge in September 2000. Composite deck cracking and blistering were observed. Sometime later, two of the panels were observed to have experienced delamination.

This led to investigations which revealed that the delaminations were due to defects in manufacturing. It was also found that the haunch of the steel girders did not

have a uniform contact bearing area under the FRP decks. The joints between different deck systems were also observed to be open because of the variations in the stiffnesses. Thus, variable deflection could result in damage. This shows the need for more careful procedures in the design of connections and other details, as well as proper material selection.

2.7.10 No-Name Creek Bridge, Kansas

On November 8, 1996, the nation's first all composite FRP bridge on a public road was installed over No-Name Creek, just three miles west of Russell, Kansas and this was done by Kansas Structural Composites, Inc. (KSCI) of Russell, Kansas (Davalos et al. 2001, Plunkett 1997). It is a short-span, self-supporting bridge of 23 ft in length and 27 ft in width and demonstrates the viability of the structural panel concept. It was built with the capability of supporting an AASHTO HS-25 load in both lanes. The bridge was constructed of three adjoining longitudinal sandwich panels with a depth of 22.5 in. The sandwich structure composed of 20.5-in. thick core with a 0.75-in. lower face, and a 0.5-in. upper face. The core has a sinusoidal wave configuration in the plane extending vertically between the faces as seen in Fig. 2.1. Demonstrating the simplicity of the project, the whole installation process required just one and a half days. Part of the construction is shown in Fig. 2.6.



Figure 2.6: Installation of No-Name Creek Bridge, Russell, Kansas.

Further research continues on FRP. This includes concrete repair and reinforcement, bridge deck repair and new installation, composite-hybrid technology (the marriage of composites with concrete, wood and steel), marine piling and pier upgrade programs.

CHAPTER 3 - DERIVATION OF PROPERTIES FOR IN-PLANE BEHAVIOR

3.1 Introduction

Micro- and macro- mechanical analyses are two points of view that have long been used to examine composite materials. In the micro-mechanical approach, consideration is given to the basic constituents of the composite material – the fibers and matrix. The behavior of the material is therefore a function of the individual elements. Thus, a lamina (or ply) is viewed as heterogeneous. Macro-mechanics, on the other hand, considers the lamina as having averaged properties, and is useful in analyzing a stack of laminae – a laminate. The assumptions, approximations and equations used in these two analyses have been well documented in literature. In the next two sections (Sections 3.2 and 3.3) therefore, the equations shown are from previous work, such as those of Vinson and Sierakowski (1986). They are reproduced here to show their application to the present study. The information is needed to analyze the component materials of the structure under consideration in this work – FRP sinusoidal wave-core sandwich panel. First, individual laminae are studied using micro-mechanics. These plies include those of the faces and the core mat. Then, using macro-mechanics, the face laminates can be analyzed.

After the lamina and laminate properties have been computed, an approach is next developed in this work (Section 3.4) to derive the properties for in-plane behavior of the core using finite element modeling.

3.2 Micromechanical Analysis

To determine the properties of a lamina, the basic components of the composite – the fiber and matrix element – are considered. It is noteworthy at this point that the fibers and matrix are assumed to be homogeneous, isotropic and linearly elastic (Vinson and Sierakowski 1986). One of the most crucial factors which determine the properties of composites is the relative proportions of the matrix and reinforcing fibers. These relative proportions are indicated as volume or weight fractions. These parameters are defined thus (Agarwal and Broutman 1980):

$$V_f = \frac{V_f}{V_c}, \quad V_m = \frac{V_m}{V_c} \quad \text{Equation 3.1}$$

$$W_f = \frac{W_f}{W_c}, \quad W_m = \frac{W_m}{W_c} \quad \text{Equation 3.2}$$

where $w_c = w_f + w_m$ and $v_c = v_f + v_m$, V_f and V_m represent the fiber and matrix volume fractions, W_f and W_m refer to the fiber and matrix weight fractions, v_f and v_m symbolize the fiber and matrix volumes, w_f and w_m are the weights of the fiber and matrix.

Apart from the volume and weight fractions, the properties of the constituent materials are also determining factors for the properties of the laminates. In the unidirectional composite, the assumptions that the fibers have uniform properties and diameter, and are parallel throughout the composite are made. Also assumed is that perfect bonding exists between fibers and matrix, and that these constituents both behave elastically.

In the longitudinal direction of the composite (with the assumption stated above), the strains in the fiber ε_f , matrix ε_m and composite ε_c are all equal. Therefore,

$$\varepsilon_f = \varepsilon_m = \varepsilon_c \quad \text{Equation 3.3a}$$

Also, the stresses in the fiber σ_f and the matrix σ_m are:

$$\sigma_f = E_f \varepsilon_f \quad \text{Equation 3.3b}$$

$$\sigma_m = E_m \varepsilon_m \quad \text{Equation 3.3c}$$

where E_f and E_m represent the modulus of elasticity of the fiber and matrix respectively.

The average stress in the composite (for composites with parallel fibers) becomes,

$$\sigma_c = \sigma_f V_f + \sigma_m V_m \quad \text{Equation 3.4}$$

From Equation 3.4, the following formula for the elastic modulus of the composite is obtained:

$$\frac{d\sigma_c}{d\varepsilon} = \frac{d\sigma_f}{d\varepsilon} V_f + \frac{d\sigma_m}{d\varepsilon} V_m \quad \text{Equation 3.5}$$

For a linear stress-strain curve,

$$E_c = E_f V_f + E_m V_m \quad \text{Equation 3.6}$$

This above relationship is known as Rule of Mixtures, and shows that the contributions of the fibers and matrix to the average composite properties are proportional to their volume fractions. Each lamina in the two face laminates is treated as an orthotropic material, requiring twelve physical quantities. These quantities are E_1 , E_2 , E_3 , G_{12} , G_{23} , G_{31} , ν_{12} , ν_{13} , ν_{21} , ν_{23} , ν_{31} and ν_{32} . It has been proved that (Vinson and Sierakowski 1986):

$$\nu_{ij} = \frac{E_i}{E_j} \nu_{ji}, \quad (i, j=1, 2, 3) \quad \text{Equation 3.7}$$

where E , G and ν represent elastic modulus, shear modulus and Poisson's ratio of the lamina.

By assuming that the composite is macroscopically transversely isotropic, $(E, G \text{ or } \nu)_{12} = (E, G \text{ or } \nu)_{13}$ and $(E, G \text{ or } \nu)_{22} = (E, G \text{ or } \nu)_{23}$ so that the number of independent constants reduces to five. Each face laminate is composed of distinct layers of unidirectional laminae. The properties of the basic unidirectional composite are first computed, and then properties of the laminate are obtained. Fig. 3.1 below gives a description of the coordinate system. Axes 1 and 2 represent directions parallel and perpendicular to fibers respectively. They form the local coordinate system. Axes X and Y form the global coordinate system.

Several models exist in computing these elastic constants such as Rule of Mixtures (ROM), Cylindrical Assemblage Model (CAM) and Periodic Microstructure Model (PMM) (Barbero 1998). From the Rule of Mixtures discussed above, the modulus of elasticity in the fiber direction can be expressed as (Whitney et. al. 1982):

$$\begin{aligned} E_1 &= E_{1f}V_f + E_{1m}V_m \\ &= E_{1f}V_f + E_{1m}(1 - V_f) \end{aligned} \quad \text{Equation 3.8}$$

For the transverse direction, it is assumed that the total displacement of the composite is the sum of the displacements of the fiber and the matrix components. Hence, unlike the case of the longitudinal (fiber) direction, the strain values for these components in the transverse direction are not necessarily equal. The elastic modulus can be written as shown in Equation 3.9:

$$E_2 = \frac{E_{2m}(1 + \varepsilon\eta_2V_f)}{(1 - \eta_2V_f)} \quad \text{Equation 3.9}$$

where:

$$\eta_2 = \frac{(E_{2f} / E_{2m} - 1)}{(E_{2f} / E_{2m} + \varepsilon)}$$

and,

$\varepsilon = 2$, for square packing of fibers

$= 1$, for hexagonal packing of fibers

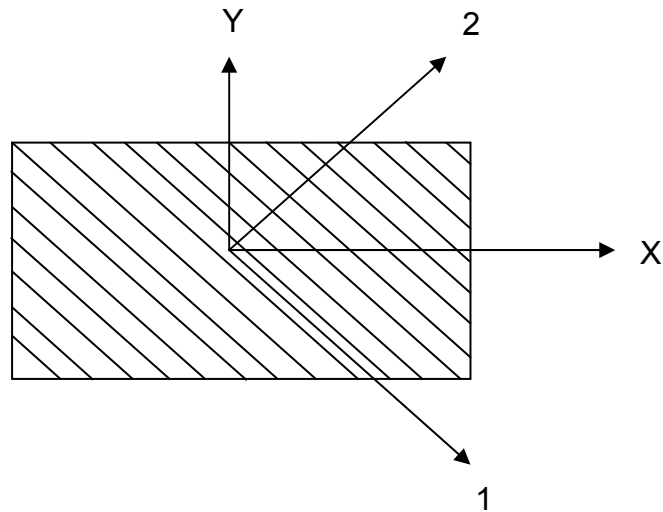


Figure 3.1: Principal Material Coordinate System

The major Poisson's ratio ν_{12} is defined as the negative of the ratio of the strain in direction 2 to that in direction 1 when the stress is applied in direction 1. Minor Poisson's ratio ν_{21} is the negative of the ratio of the strain in direction 1 to that in direction 2 when the stress is applied in direction 2. The major Poisson's ratio can be defined from the simple Rule of Mixtures (Whitney et. al. 1982):

$$\nu_{12} = \nu_{12f} V_f + \nu_{12m} (1 - V_f) \quad \text{Equation 3.10}$$

where, ν_{12f} and ν_{12m} represent major Poisson's ratios for the fiber and matrix respectively.

The minor Poisson's ratio is computed from the interaction below:

$$v_{21} = \frac{E_2}{E_1} v_{12} \quad \text{Equation 3.11}$$

If the unidirectional composite is transversely isotropic, Poisson's ratio v_{23} is further defined as the negative of the ratio of the strain in the 3 direction (vertical) to the strain in the 2 direction when the stress is applied in the 2 direction. This additional quantity is expressed by the following equation (Whitney et al. 1982):

$$v_{23} = \frac{2E_1K_2 - E_1E_2 - 4v_{12}^2K_2E_2}{2E_1K_2} \quad \text{Equation 3.12}$$

where K_2 = plane strain bulk modulus. For a continuous fiber reinforced unidirectional material,

$$K_2 = \frac{(K_{2f} + G_{23m})K_{2m} + (K_{2f} - K_{2m})G_{23m}V_f}{(K_{2f} + G_{23m}) - (K_{2f} - K_{2m})V_f} \quad \text{Equation 3.13}$$

where K_{2f} and K_{2m} = plane strain bulk moduli for fiber and matrix respectively.

From the Rule of Mixtures, the in-plane shear modulus G_{12} is obtained as below:

$$G_{12} = \frac{G_m}{V_m + V_f G_m / G_f} \quad \text{Equation 3.14}$$

where G_f and G_m are the in-plane shear moduli of the fiber and matrix respectively.

The more accurate cylindrical assemblage model (CAM), which is used in this work, predicts the in-plane shear modulus as (Barbero 1998):

$$G_{12} = G_m \left[\frac{(1 + V_f) + (1 - V_f)G_m / G_f}{(1 - V_f) + (1 + V_f)G_m / G_f} \right] \quad \text{Equation 3.15}$$

Finally, the interlaminar shear modulus G_{23} is predicted from the equation below:

$$G_{23} = G_m \frac{V_f + \eta_{23}(1 - V_f)}{\eta_{23}(1 - V_f) + V_f G_m / G_f} \quad \text{Equation 3.16}$$

where,

$$\eta_{23} = \frac{3 - 4\nu_m + G_m / G_f}{4(1 - \nu_m)}$$

To form the laminates, several layers of thin laminae are stacked together with resin serving as the bonding agent. In Fig. 3.2, the lay-up of the face laminates for this study is seen. The lay-up includes the following four types of fiber layers: Chopped Strand Mat (ChopSM), Continuous Strand Mat (ContSM), Bidirectional Stitched Fabrics (SF) and unidirectional layers. The constituent materials were E-glass fibers and polyester resin. The materials were manufactured by Brunswick Technologies, Brunswick, Maine (Davalos et al. 2001).

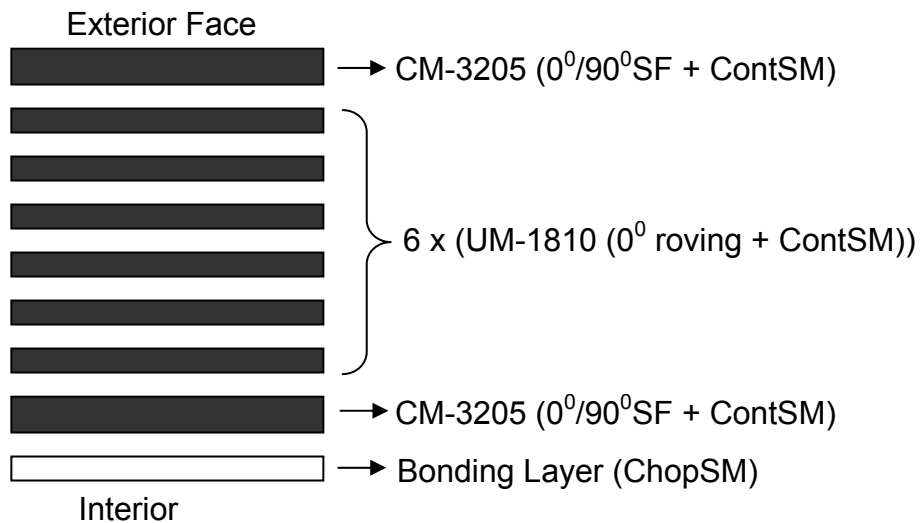


Figure 3.2: Face laminate lay-up (Davalos et al. 2001)

With the formulation discussed above, the elastic constants are derived for each layer of Fig. 3.2. The results are presented in Table 3.1. The table shows a comparison with the results obtained by Davalos et al. (2001). As can be observed from the table, there is very good comparison between both sets of results. Constants for the randomly

oriented core mat used for the core are also computed and shown in the table. More about the core will be discussed later.

Table 3.1: Individual layer stiffness properties' comparison with Davalos et al. (2001)

Ply Name	Orientation	E ₁ (GPa)		E ₂ (GPa)		G ₁₂ (GPa)		G ₂₃ (GPa)		ν ₁₂	
		Davalos	Proposed	Davalos	Proposed	Davalos	Proposed	Davalos	Proposed	Davalos	Proposed
Bond Layer	Random	9.72	10.54	9.72	10.54	3.5	3.798	2.12	2.11	0.394	0.388
CM3205	0 or 90	27.72	28.14	8	9.36	3.08	3.076	2.88	2.8	0.295	0.285
CM3205	Random	11.79	16.4	11.79	16.4	4.21	5.86	2.36	2.33	0.402	0.4
UM1810	0	30.06	30.48	8.55	10	3.3	3.295	3.08	2.97	0.293	0.283
UM1810	Random	15.93	17.68	15.93	17.68	5.65	6.31	2.96	2.87	0.409	0.4
Core Mat	Random	11.79	12.65	11.79	12.65	4.21	4.54	2.97	2.33	0.402	0.393

3.3 Macromechanical Analysis

Having derived the properties of each lamina, the next step is to compute equivalent elastic properties of the laminate. To achieve this, macro-mechanical analysis is employed. To obtain the equivalent elastic constants, stiffness properties of the composite material have to be derived first. Since each lamina has different stacking ply orientation θ , the laminae constants have to be transformed to the global coordinate system. Before that is done, a stiffness matrix $[Q]$ is needed. This matrix relates the stress and strain matrices in the form (Vinson and Sierakowski 1986):

$$\{\sigma\} = [Q]\{\varepsilon\} \quad \text{Equation 3.17}$$

$[Q]$, which is in the local coordinate system of the lamina is then transformed to the global coordinate system using the transformation below:

$$[\bar{Q}] = [T]^{-1}[Q][T] \quad \text{Equation 3.18}$$

where $[T]$ is the transformation matrix between local and global coordinate systems.

A laminate with a thickness of h and mid-plane being $z = 0$ is considered. h_k is the vectorial distance to the upper face of the k th lamina. This nomenclature is described in Fig. 3.3 below.

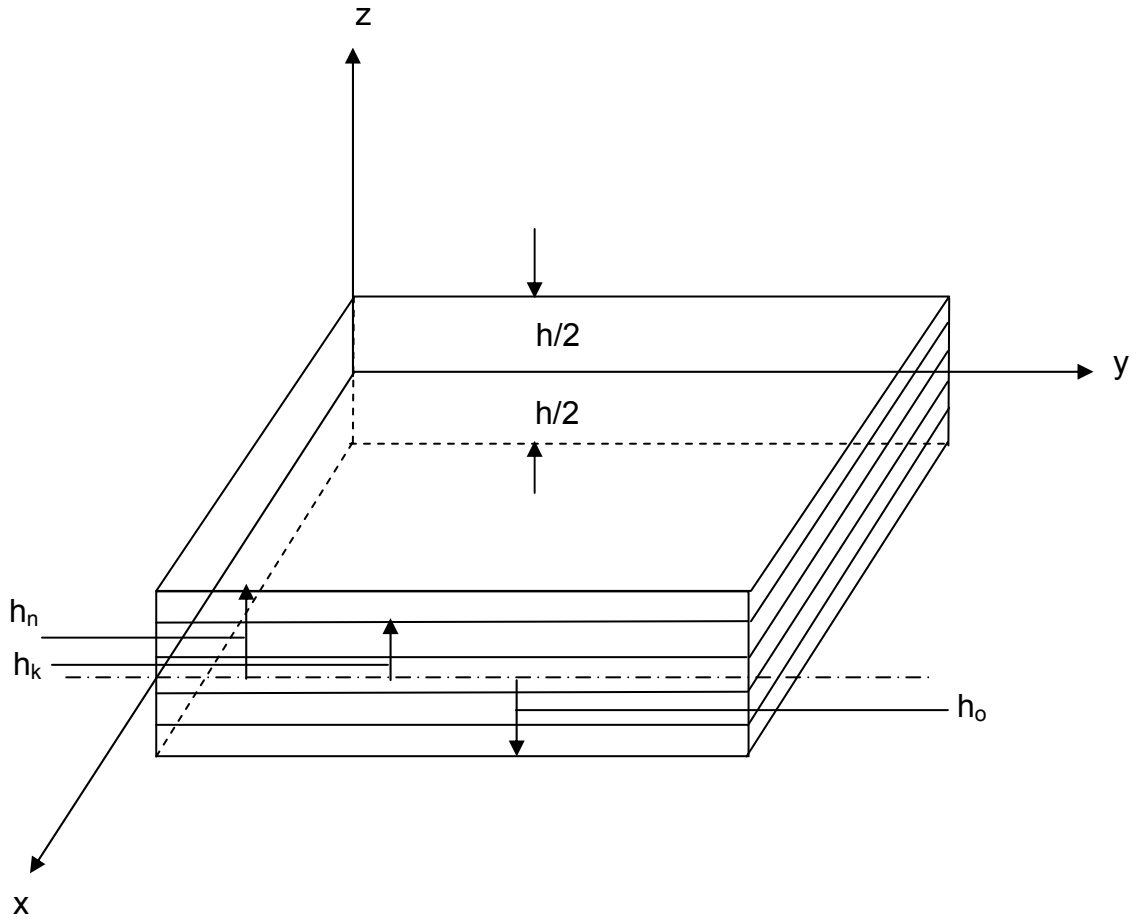


Figure 3.3: Laminate lay-up nomenclature

Using the transformed stiffness matrix $[Q]$ of each lamina and the nomenclature as described in Fig. 3.3, the stiffness matrix of the laminate is then computed. The stiffness matrix of the laminate is expressed in this form:

$$\text{Laminate stiffness} = \begin{bmatrix} [A] \cdots [B] \\ [B] \cdots [D] \end{bmatrix} \quad \text{Equation 3.19}$$

where the $[A]$ matrix is the extensional stiffness matrix, $[B]$ matrix is known as the bending-stretching coupling matrix and $[D]$ is the flexural stiffness matrix. The terms of these matrices can be calculated from the equations below:

$$A_{ij} = \sum_{k=1}^n (\bar{Q}_{ij})_k [h_k - h_{k-1}], \quad \text{Equation 3.20}$$

$$B_{ij} = \frac{1}{2} \sum_{k=1}^n (\overline{Q}_{ij})_k [h_k^2 - h_{k-1}^2], \quad \text{Equation 3.21}$$

$$\text{and } D_{ij} = \frac{1}{3} \sum_{k=1}^n (\overline{Q}_{ij})_k [h_k^3 - h_{k-1}^3] \quad \text{Equation 3.22}$$

For a balanced, symmetric laminate such as the one in this work, the effective elastic constants can be expressed in terms of the laminate thickness h , and terms in the extensional stiffness matrix, A_{ij} . These constants represent the properties of the equivalent orthotropic plate. The moduli of elasticity are given by the following equations (Whitney et. al. 1982):

$$E_x = (A_{11}A_{22} - A_{12}^2) / hA_{22} = \text{equivalent longitudinal modulus of elasticity} \quad \text{Equation 3.23}$$

$$\text{and } E_y = (A_{11}A_{22} - A_{12}^2) / hA_{11} = \text{equivalent lateral modulus of elasticity} \quad \text{Equation 3.24}$$

The Poisson's ratios have the formulae below:

$$v_{xy} = A_{12} / A_{22} = \text{major Poisson's ratio} \quad \text{Equation 3.25}$$

$$\text{and } v_{yx} = A_{12} / A_{11} = \text{minor Poisson's ratio} \quad \text{Equation 3.26}$$

Finally, the shear modulus is given by Equation 3.27:

$$G_{xy} = A_{66} / h \quad \text{Equation 3.27}$$

These constants are computed for the entire laminate lay-up shown in Fig. 3.2 and the results are given in Table 3.2 below. The table also compares the results proposed here with those obtained by Davalos et al. (2001). A very good comparison between both sets of results is noticed, differing by not more than 2%.

Table 3.2: Elastic equivalent properties of face laminates compared with Davalos et al. (2001) results

Property	Proposed	Davalos (2001)
E_x (GPa)	20.15	19.62
E_y (GPa)	12.87	12.76
G_{xy} (GPa)	3.764	3.76
ν_{xy}	0.295	0.302

3.4 Derivation of Equivalent Properties of Core

3.4.1 Finite Element Modeling

In this section, an approach for determining the properties for in-plane behavior of the sinusoidal wave core is developed. The properties of the core material (core mat) have already been computed using the micro-mechanics analysis in the previous section (See Table 3.1). Determining the equivalent properties of the complicated sinusoidal wave core, which is equivalent to a solid core, is done with the aid of finite element modeling by using the core mat properties as inputs. All finite element models created in this work was done using the program ANSYS 9.0. This is powerful computer software for engineering modeling and analysis.

Because of the complexity in modeling a sinusoidal wave core configuration, the models were generated with the aid of the computer software, Microsoft Visual C++ 6.0. A program which was originally developed by Kalny (2003) was further modified here for the purpose of this study (Appendix A). This program is designed to generate macro files for the nodes and elements of the core, by reading an input file. Additionally, because writing an input file for a large core can be quite cumbersome, a program in MATLAB 6.5 was written to generate the entire input file which would be recognized by

the C++ software (Appendix B). This also reduces the probability of errors in the file, which can be a great source of inaccuracy in final results.

First of all, what is known as a Representative Volume Element (RVE) is defined. This is the basic segment or cell unit of the whole structure. The honeycomb panel used in this research was manufactured by Kansas Structural Composites, Inc. (KSCI, Russell, Kansas), and has the following dimensions for the RVE: $h = 1$ in., $l = 4$ in. and $t_1 = t_2 = 0.0898$ in. In studying the in-plane behavior of the core, the top and bottom faces of the panel are not included. However, they can simply be added to the equivalent core in actual application. Fig. 3.4 below describes the RVE. The wave function used to define the core configuration is:

$$y = h \left(1 - \cos \frac{2\pi x}{l} \right) \quad \text{Equation 3.28}$$

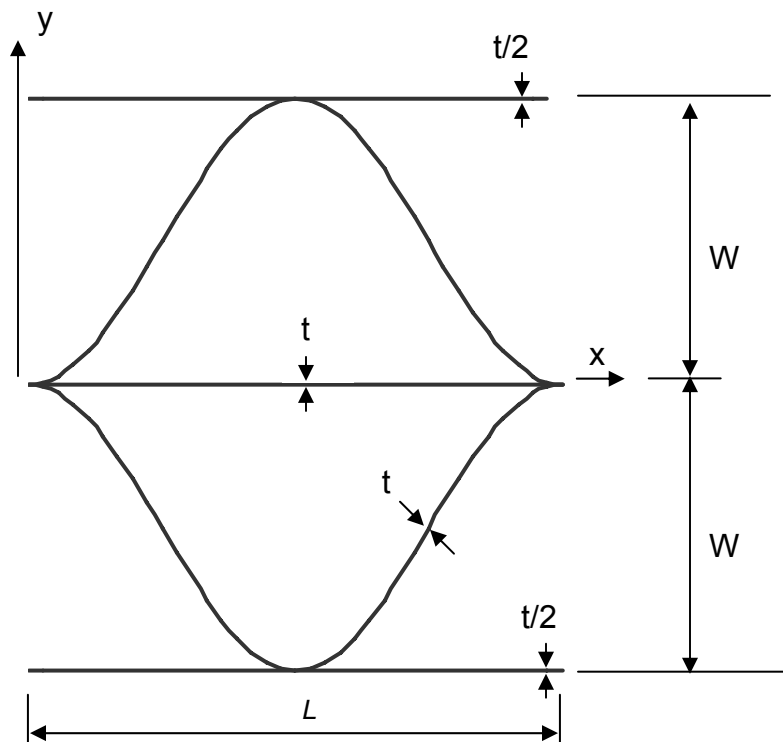


Figure 3.4a: Representative Volume Element (RVE) for this study (Davalos 2001).

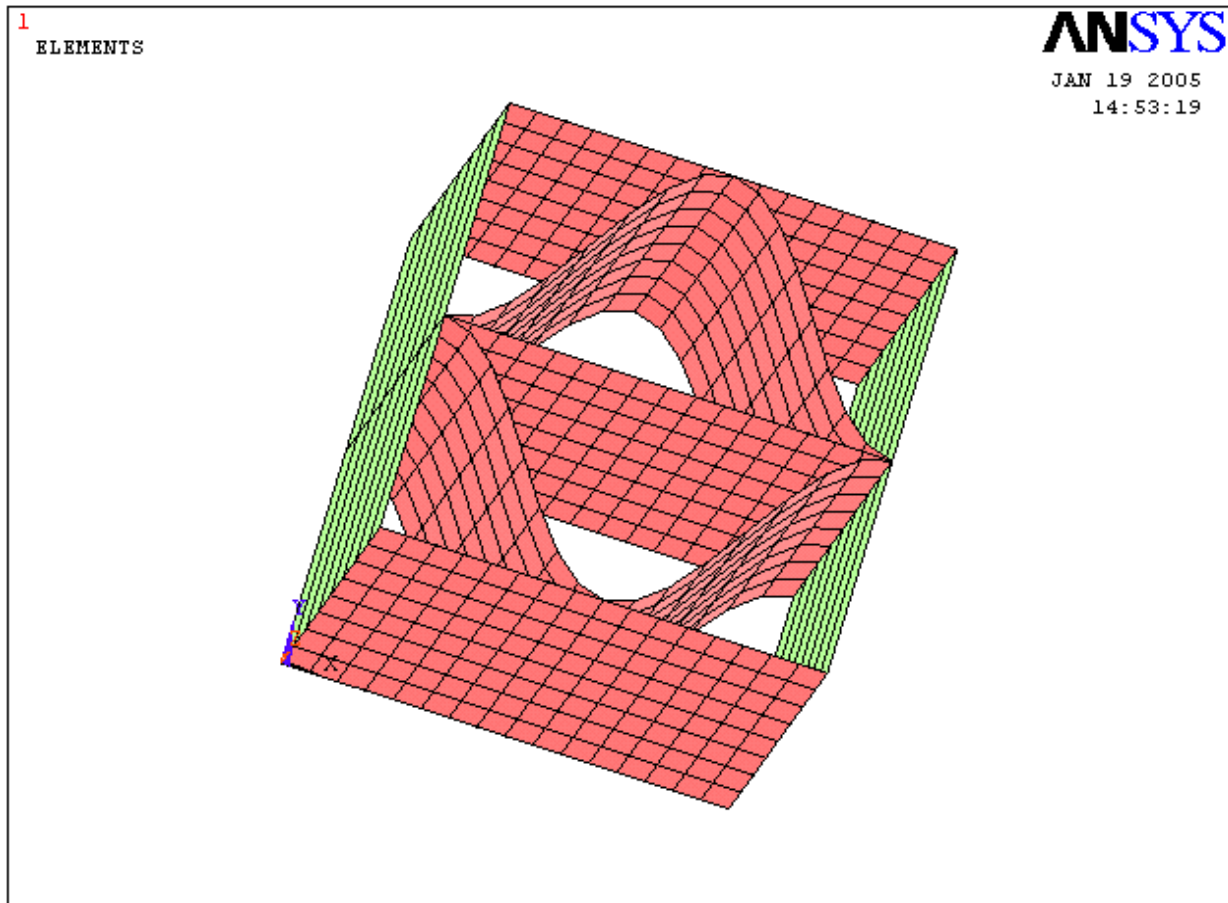


Figure 3.4b: ANSYS model of RVE

The depth of the panel used as the basis of this work is 5 inches. Since the two faces have a total depth of 0.43 inches (as discussed in the previous sections), the core itself has a thickness of 4.14 inches

3.4.2 Core Properties

The core properties verified in this study are elastic and shear moduli. They are discussed in the following sections. The core is treated as an orthotropic material. The equivalent properties of the structure are calculated based on FE modeling using 4-

noded structural elastic shell elements. These elements have six degrees of freedom per node.

In the following sections, attention is given to obtaining the equivalent Young's modulus in the three perpendicular directions, E_x , E_y and E_z .

3.4.2.1 Equivalent Elastic Modulus in the Vertical Direction, E_z

To calculate the equivalent elastic modulus E_z of the core, a normal uniform pressure is applied on the RVE in the vertical direction. To accomplish this, 1-inch thick shell elements are placed on the top and bottom of the core. The top face serves as a medium for load application while the bottom provides the needed support. These elements are made very rigid so that there is no relative deflection within them, and hence, the resulting values of displacements represent core values only. A uniform pressure of 625 psi is applied to the top face, while all bottom nodes are constrained for translation in the three directions, u_x , u_y and u_z . To prevent side-sway of the RVE model, the nodes on the top face are constrained for lateral movement. In this way, the structure can be analyzed as a simplified elastic spring model, once the displacement of the rigid face, δ_z , is obtained.

For linear elastic behavior, displacement,

$$\delta_z = \frac{\sigma_z H}{E_z} \quad \text{Equation 3.29}$$

where σ_z = applied pressure, H = depth of RVE (that is, length of the element in the vertical direction), and E_z = the modulus of elasticity in the vertical direction. The value for E_z is thus obtained from the equation above.

3.4.2.2 Equivalent Elastic Modulus in the Longitudinal Direction, Ex

The same principle is applied in the computation of E_x . Rigid shell elements are placed at the longitudinal ends of the RVE, serving as supports and application area for the pressure. A uniform pressure of 625 psi is again applied to one of the end faces while the nodes of the other end face are constrained for translation in the three directions, u_x , u_y and u_z . Sway is prevented by constraining the nodes of the two faces for lateral movement.

Thus, in the same vein,

$$\text{Displacement, } \delta_x = \frac{\sigma_x L}{E_x} \quad \text{Equation 3.30}$$

where σ_x = applied pressure, L = length of RVE (that is, length of the element in the longitudinal direction), and E_x = the modulus of elasticity in the longitudinal direction

3.4.2.3 Equivalent Elastic Modulus in the Lateral Direction, Ey

Finally, to compute the modulus of elasticity in the width direction, the same operation is performed – placing rigid shell elements at the two ends of the lateral direction and applying a uniform pressure of 625 psi. The same constraints are applied as in the previous two cases.

$$\text{Displacement, } \delta_y = \frac{\sigma_y W}{E_y} \quad \text{Equation 3.31}$$

where σ_y = applied pressure, W = width of RVE (that is, length of the element in the lateral direction), and E_y = the modulus of elasticity in the lateral direction

3.4.2.4 Equivalent Shear Moduli (Gxy, Gyz and Gxz)

The finite element models created for deriving the elastic moduli are also used in evaluating the shear properties. These shear properties of the core are derived based

on beam theory. When a beam deflects, it experiences two modes of deformation. The theory shows that the total deflection of a beam is the sum of the contributions from bending and shear. The bending mode results from the curve due to bending moment distribution. The shear mode is due to shear deformation caused by shear forces at every cross-section of the beam. Therefore:

$$\delta_{\text{total}} = \delta_{\text{bending}} + \delta_{\text{shear}} \quad \text{Equation 3.32}$$

where, δ_{bending} = deflection contribution from bending and, δ_{shear} = deflection contribution from shear. For a cantilever beam, the deflection due to bending δ_{bending} , and that due to shear δ_{shear} , as a result of a concentrated load at the free end can be defined as,

$$\delta_{\text{bending}} = \frac{PL^3}{3EI}, \quad \text{Equation 3.33a}$$

$$\delta_{\text{shear}} = \frac{PL}{GA_s} \quad \text{Equation 3.33b}$$

where P is the value of the concentrated load, L is the span of the beam, E represents the elastic modulus in the span direction, I is the moment of inertia, G is the shear modulus and A_s symbolizes the shear area.

To obtain the shear moduli, the model is analyzed as a cantilever beam. The moduli of elasticity used are those calculated in Sections 3.4.2.1 to 3.4.2.3.

3.4.2.5 Shear Modulus, Gxy and Gxz

To obtain the equivalent shear modulus Gxy, the same kind of model employed in calculating elastic modulus in the longitudinal (x) direction is used – RVE with rigid shell elements placed at the longitudinal ends. One end face is constrained for both translation and rotation in all directions to simulate fixed end condition. On the central

node of the other end face, a concentrated force of 1000 lb is applied in the transverse (y) direction. After the finite element analysis, the uniform transverse displacement δ_{total} is obtained. The bending contribution to the deflection $\delta_{bending}$ is calculated based on E_x and the other cross-sectional parameters. The shear modulus G_{xy} is thus computed from Equations 3.32 and 3.33.

Fig. 3.5 below describes the model, showing the coordinate system, load and constraints.

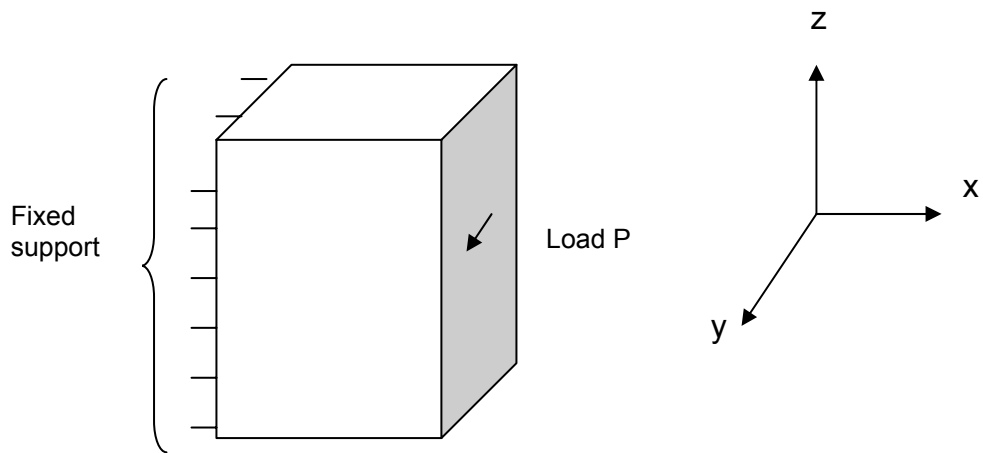


Figure 3.5a: Model for deriving G_{xy}

Figure 3.5b: Coordinate system

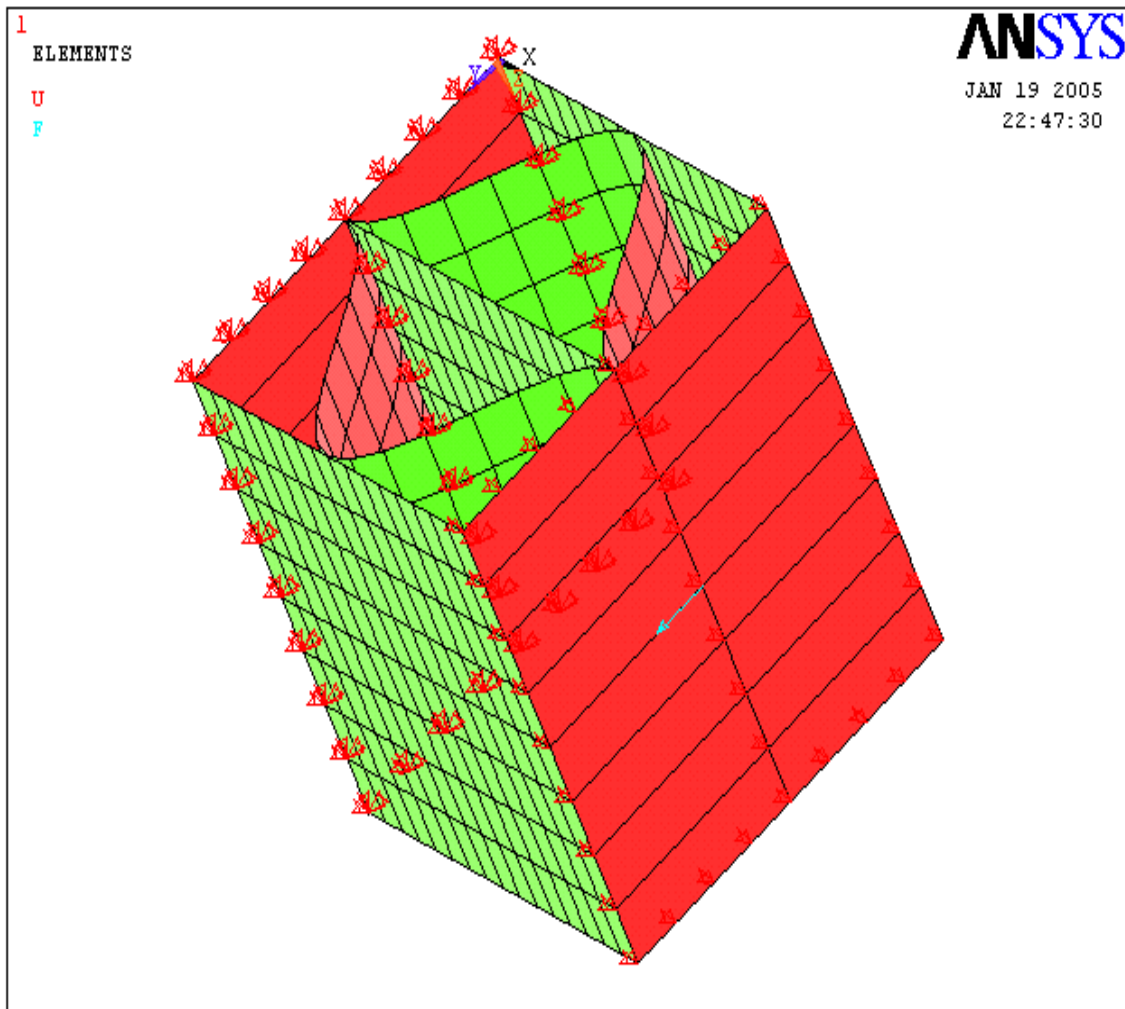


Figure 3.5c: ANSYS model for deriving G_{xy}

The same model is used to compute the shear modulus G_{xz} . The same concentrated force of 1000 lb, boundary conditions and analysis approach are also used. However because the interested is in G_{xz} , the concentrated load is now applied in the vertical (z) direction. This can be visualized from Fig. 3.6.

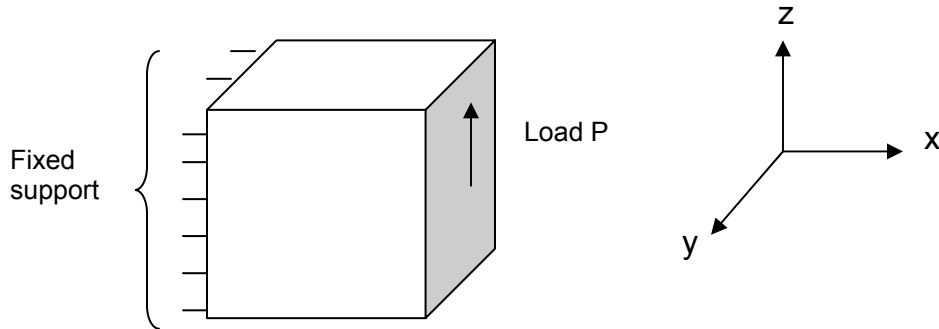


Figure 3.6a: Model for deriving G_{xz}

Figure 3.6b: Coordinate system

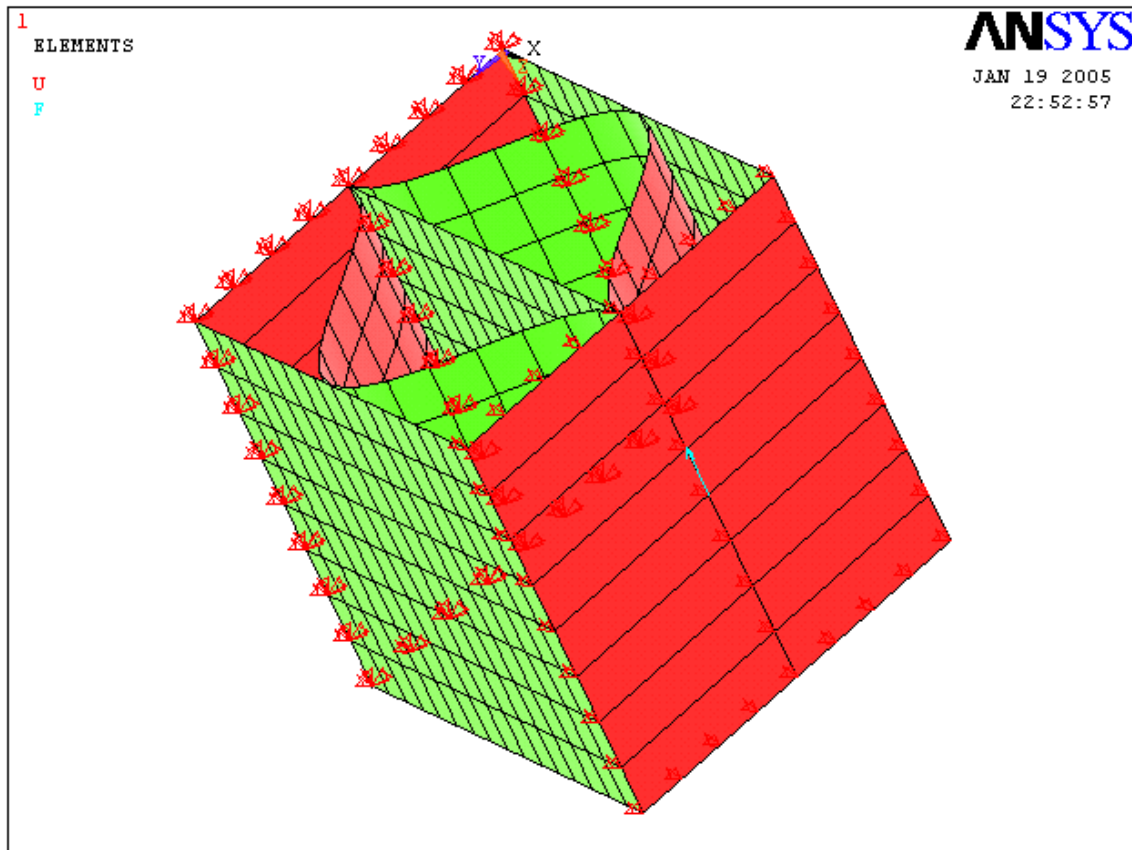


Figure 3.6c: ANSYS model for deriving G_{xz}

3.4.2.6 Shear Modulus, G_{yz} and G_{yx}

Equivalent shear modulus G_{yz} is derived using the same approach. However, the model employed here is the same one used to derive elastic modulus in the lateral (y) direction. This time the rigid shell elements are placed at the two lateral ends of the model. One end face has fixed end conditions while on the central node of the other end face, the 1000 lb concentrated force is applied in the vertical (z) direction. The uniform vertical displacement δ_{total} is obtained. The contribution of bending to the deflection $\delta_{bending}$ is calculated based on E_y and the other cross-sectional parameters. The shear modulus G_{yz} is then obtained from Equations 3.32 and 3.33. In Fig. 3.7, an illustration of this model can be seen.

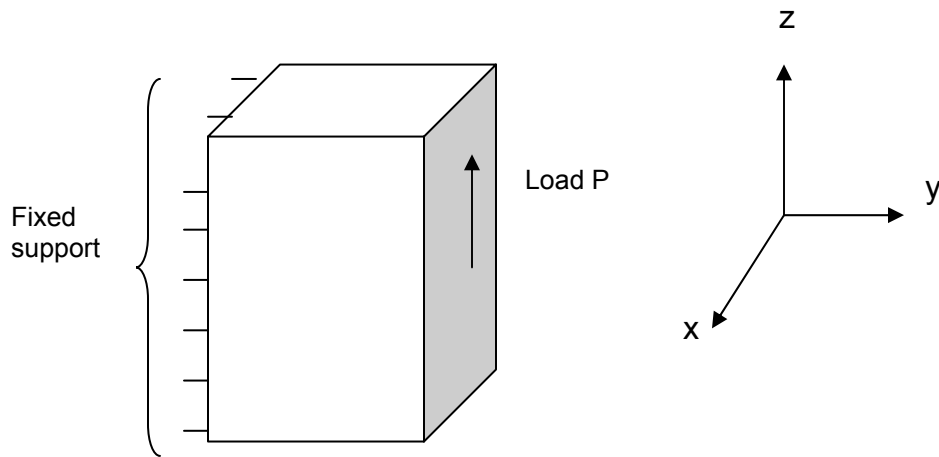


Figure 3.7a: Model for deriving G_{yz}

Figure 3.7b: Coordinate system

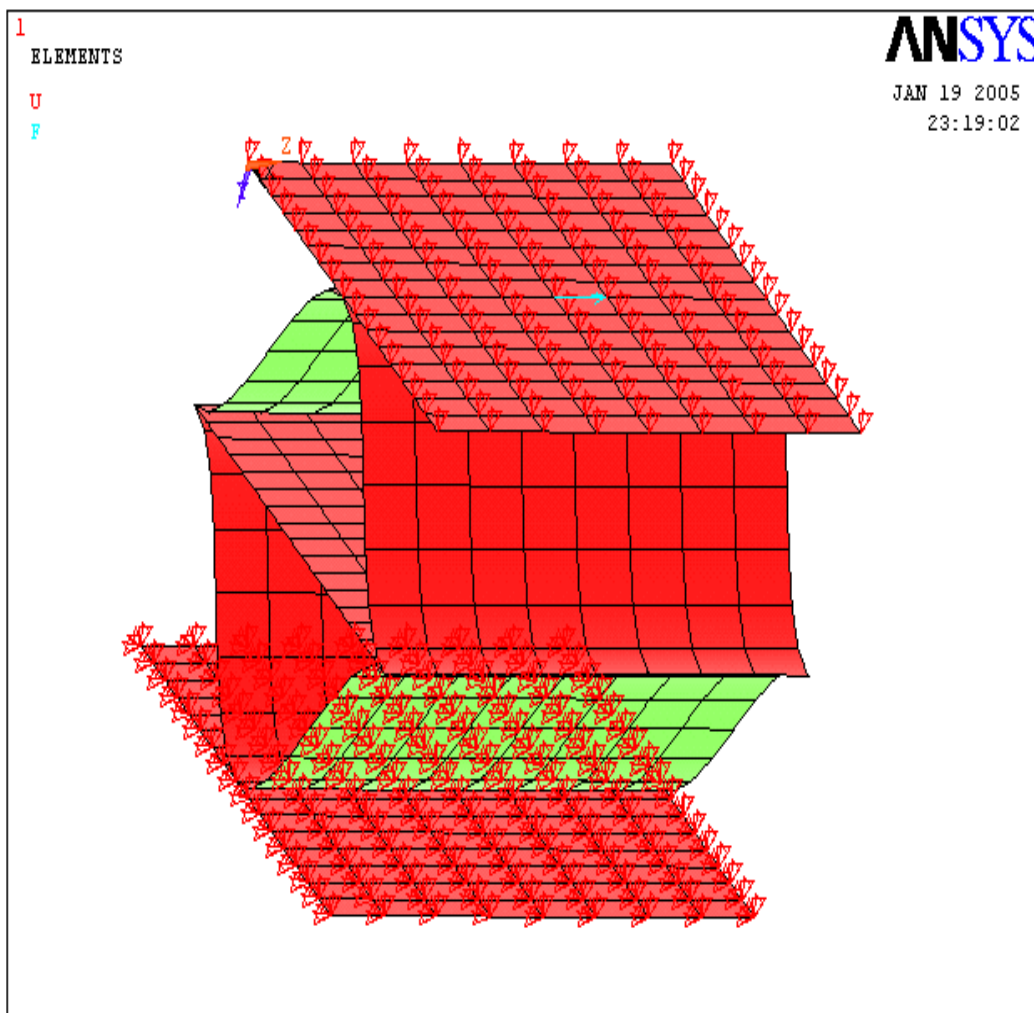


Figure 3.7c: ANSYS model for deriving G_{yz}

Using the same model, G_{yx} is also computed. The loading, boundary conditions and analysis approach remain the same. The only difference is that the 1000 lb force is now applied in the longitudinal (x) direction. Observe this in Fig. 3.8.

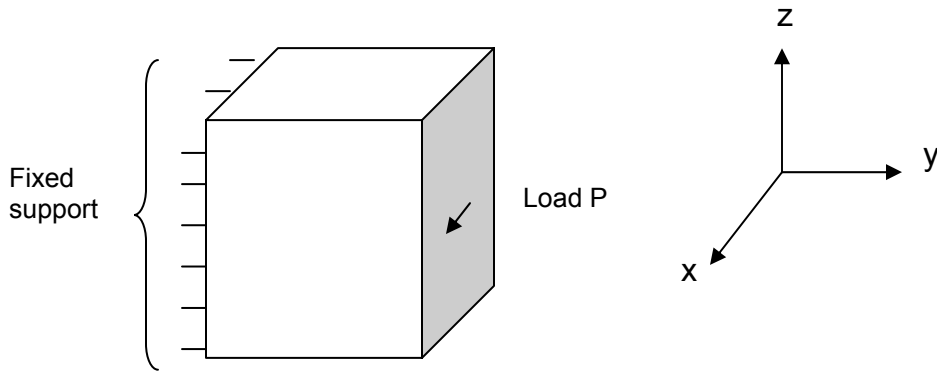


Figure 3.8a: Model for deriving G_{yx}

Figure 3.8b: Coordinate system

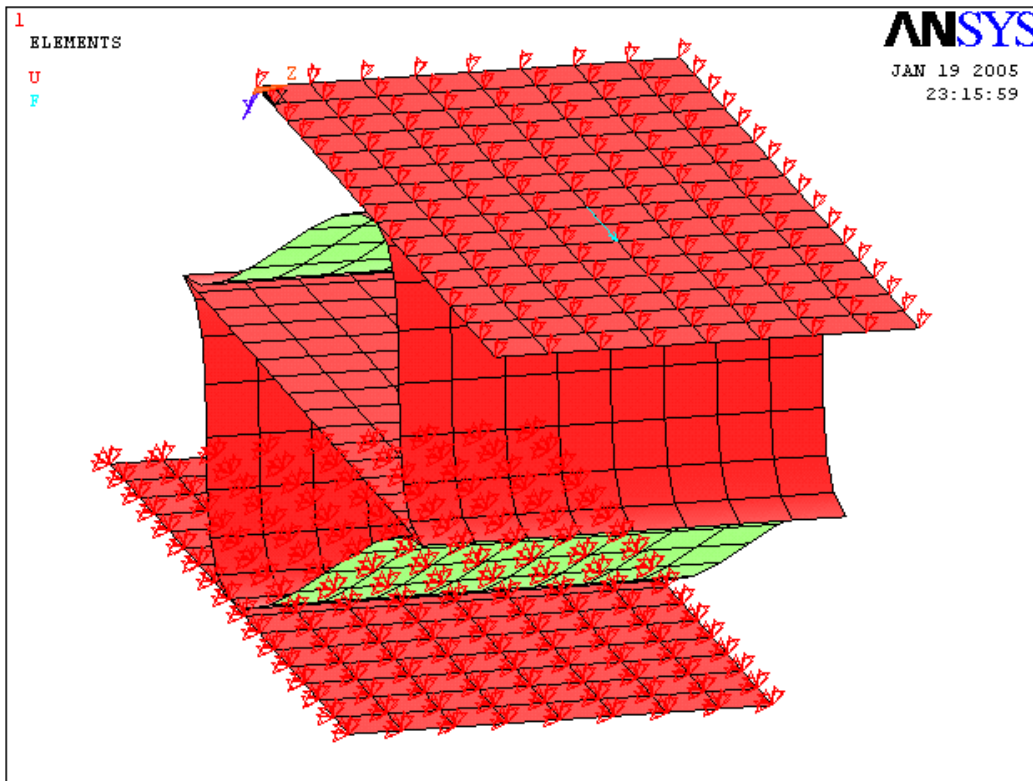


Figure 3.8c: ANSYS model for deriving G_{yx}

3.4.2.7 Shear Modulus, G_{zx} and G_{zy}

The model used here for the calculation of equivalent shear modulus G_{zx} is that used to derive elastic modulus in the vertical (z) direction. The rigid shell elements are placed at the two vertical ends of the model. One end face has fixed end conditions on all its nodes. On the central node of the other end face, 1000 lb concentrated force is applied in the longitudinal (x) direction. The uniform vertical displacement δ_{total} is obtained. The contribution of bending to the deflection $\delta_{bending}$ is calculated based on Ez and the other cross-sectional parameters. The shear modulus G_{zx} is then obtained from Equations 3.32 and 3.33. An illustration of this model is found in Fig. 3.9.

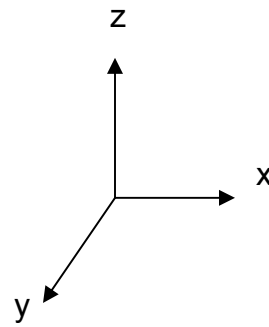
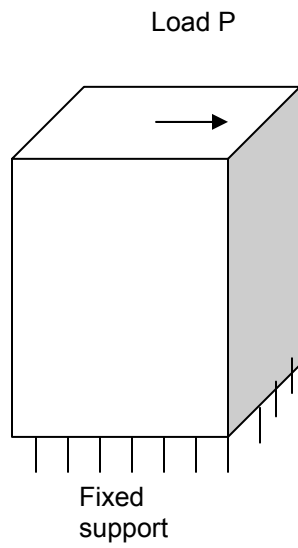


Figure 3.9a: Model for deriving G_{zx}

Figure 3.9b: Coordinate system

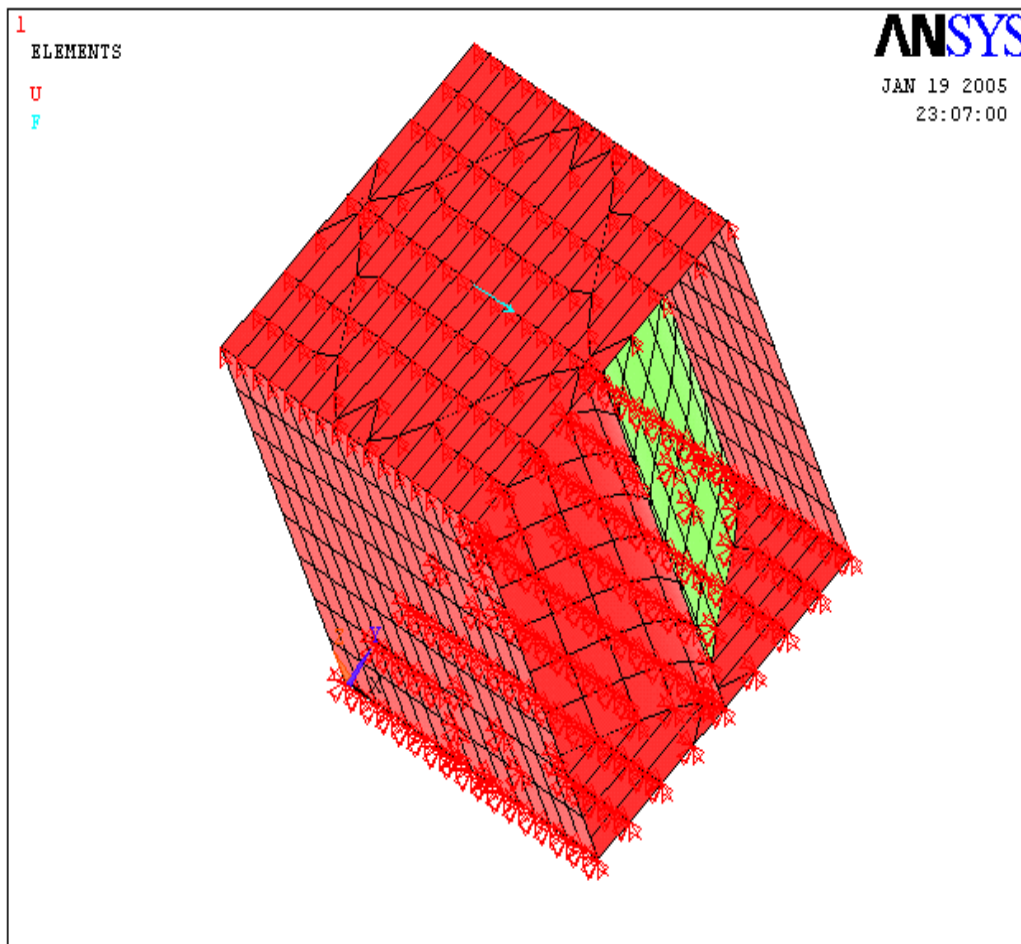


Figure 3.9c: ANSYS model for deriving G_{zx}

Gzy is calculated using the same model, boundary conditions and analysis approach. The 1000 lb concentrated load is also applied in the same position, but in lateral (y) direction. Fig. 3.10 below shows this. A summary of the results obtained from the analysis is presented in Table 3.3.

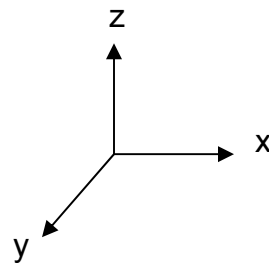
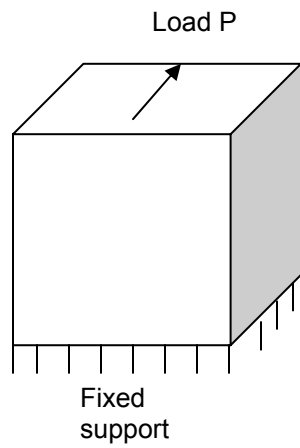


Figure 3.10a: Model for deriving G_{zy}

Figure 3.10b: Coordinate system

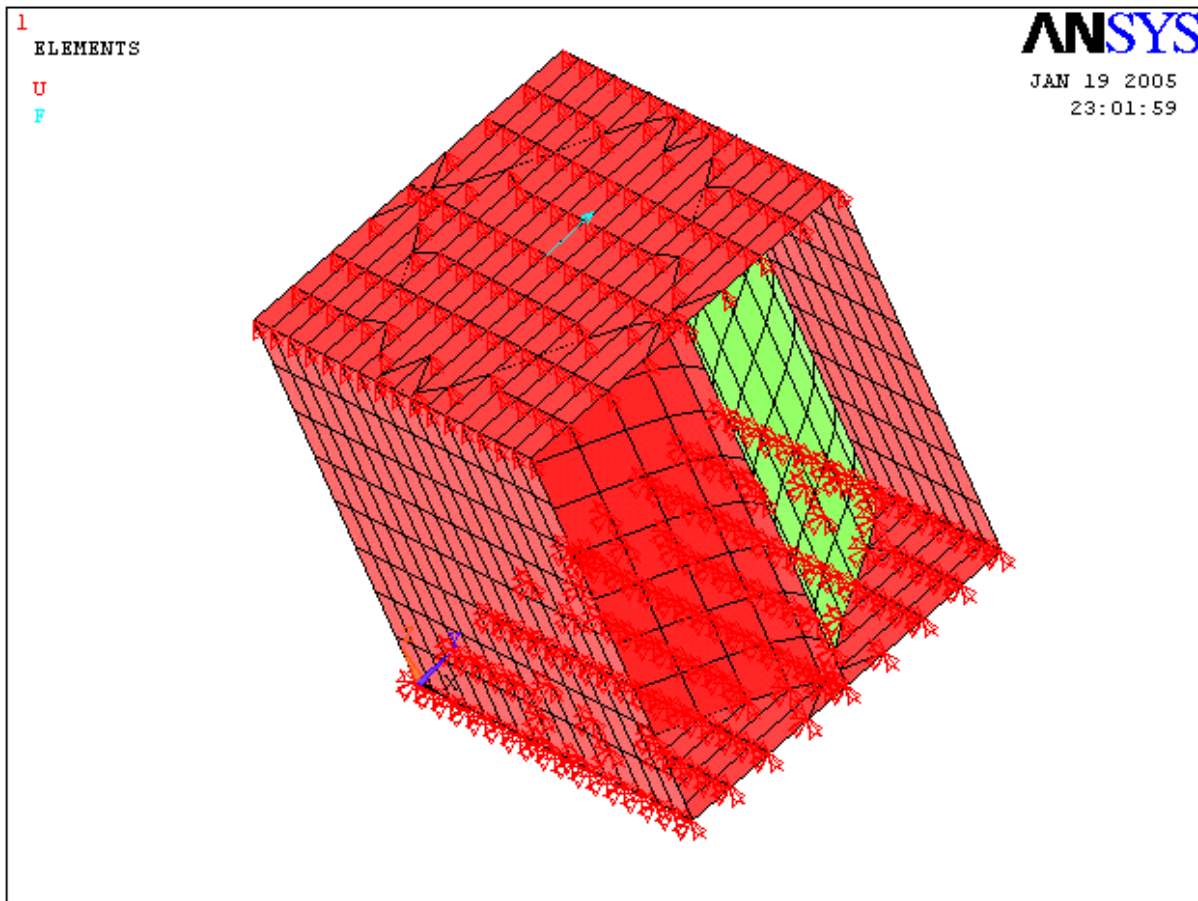


Figure 3.10c: ANSYS model for deriving G_{zy}

Table 3.3: Equivalent elastic properties (psi) derived from finite element modeling

E_x	82350.62
E_y	6440.79
E_z	195192.37
G_{xy}	3210.94
G_{yx}	23.15
G_{xz}	38353.45
G_{zx}	34423.54
G_{yz}	16006.13
G_{zy}	20771.66

As seen from the results, G_{xy} is much greater than G_{yx} . This is because there is more shear stiffness in the core when spanning in the longitudinal direction with an applied force in the lateral direction than there is in the reverse direction. The deflection is less in the former case. This outcome is due to the sinusoidal geometry of the honeycomb core.

3.5 Comparison of Results

The results above are compared with results obtained in experiments and analytical approach by Davalos et al. (2001) and Qiao et al. (2003). In Table 3.4 below, the comparison with the work of Davalos et al. is presented. Then in Table 3.5, the comparison with Qiao et al. can be seen.

From Table 3.4, it can be observed that the results of Davalos et al. compare generally well with those in this present work. The difference between the shear modulus values G_{yz} is about 3%, while the elastic moduli, E_x and E_z compare within 6%. The values of the shear modulus, G_{xz} has a difference of about 20%. On the other hand, there are very large differences between the values for E_y and G_{xy} . However,

these large differences are not of serious concern since E_y and G_{xy} have little importance in application.

Table 3.4: Comparison of results with work of Davalos et al. (2001)

Property	Proposed (psi)	Davalos et al. 2001 (psi)
E_x	82350.62	76779
E_y	6440.79	142.96
E_z	195192.37	182970
G_{xy}	3210.94	102.26
G_{yx}	23.15	
G_{xz}	38353.45	45825
G_{zx}	34423.54	
G_{yz}	16006.13	16497
G_{zy}	20771.66	

Qiao et al. also performed experiments on some specimens and came up with results for the elastic constants in the Table 3.5. He also used analytical approach to derive the constants. As we see in the table, his results compare closely with those of the present work. Qiao's experimental results for E_x , E_y and E_z have differences of less than 13%, 6% and 1% respectively with the results obtained in this research. From his analytical results, the difference in E_x is about 13%, 6% for E_y , 2% for E_z and 6% for G_{xy} . So even though the shear modulus G_{xy} in this work differs greatly from that of Davalos et al., it has a very good comparison with the work of Qiao et al.

From Tables 3.5a and 3.5b, the computed values of E_x and E_y can be observed to differ. This is because in comparing the results with the experiments of Qiao et al. (2003), two different models were used in this work. The experiments performed by Qiao et al. were based on a model which had the full thickness t_1 of the two external

flats. However in his analytical approach, he used a model whose external flats each had half the full thickness ($t/2$). Therefore, for consistency in the comparison, two different finite element models were used. In comparing results with Qiao's experiment, the finite element model had external flats with full thickness. This thickness was reduced by half in the second model to compare with Qiao's analytical method. This accounts for the differences in E_x and E_y in the tables.

Table 3.5a: Comparison with analytical results of Qiao et al. (2003)

Property	Proposed (psi)	Qiao Analysis (psi)
E_x	82350.62	76950.00
E_y	6440.79	6515.10
G_{xy}	3210.94	3437.10

Table 3.5b: Comparison with experimental results of Qiao et al. (2003)

Property	Proposed (psi)	Qiao Experiment (psi)
E_x	123500.00	105507.00
E_y	6528.38	6121.80
E_z	235232.93	234270.00

3.6 Discussion of the Results

It was noted earlier that the approach used in this chapter studies the in-plane behavior of the structure. In this section, an examination is performed to investigate whether these properties developed for in-plane behavior could be applied to bending behavior. This investigation is performed for two cases – a beam and a panel.

3.6.1 Case 1: Beam Model

To test these equivalent elastic properties, an FRP honeycomb sandwich beam with the actual sinusoidal core configuration is analyzed using finite element modeling. The beam is simply supported over a span of 8 ft. The beam cross-section is 8 in. x 5 in. The simple support condition is modeled by constraining the nodes on the left end of the beam from translation in the vertical and longitudinal (u_z and u_x) directions while those on the right end are prevented from vertical (u_z) displacement. To maintain stability of the structure, the nodes at these two ends are also constrained for translation in the transverse direction (u_y). A pressure load of 62.5 psi is applied to mid-span elements within an area of 4 in. x 4 in. The ANSYS actual configuration beam model is shown in Fig. 3.11.

An equivalent beam having the same dimensions, loading and support conditions as the actual beam is also modeled and analyzed. The equivalent beam is modeled using structural-layered shell elements, so that a three layered structure can be modeled. The three layers represent the faces and the equivalent core. The properties developed in the previous section and presented in Table 3.3 are used for the equivalent core layer, while those verified and shown in Table 3.2 are used for the face laminates. Fig. 3.12 shows the ANSYS equivalent model.

After the finite element analysis, the maximum deflections for both models which occur at mid-span are noted. The actual beam recorded a deflection of 0.2272 inches, while the equivalent had a deflection of 0.1878 inches. A comparison shows a difference of about 17%. This difference is relatively significant.

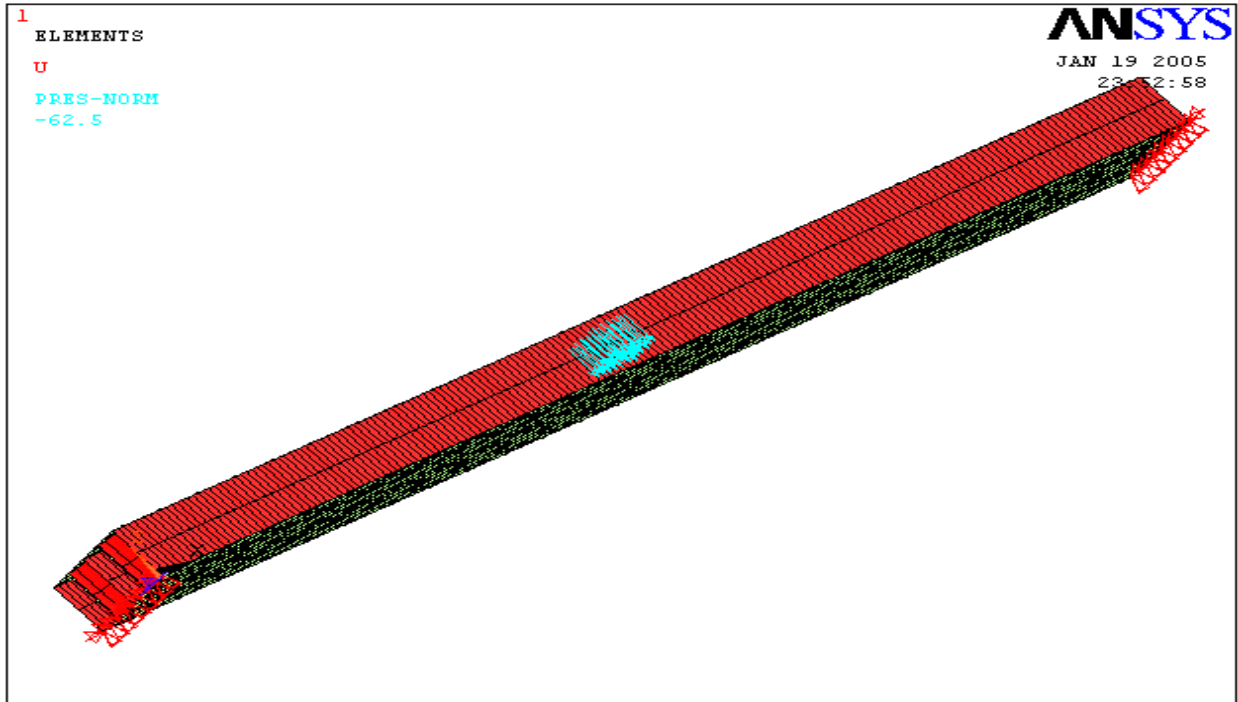


Figure 3.11a: ANSYS model of actual FRP sinusoidal core beam

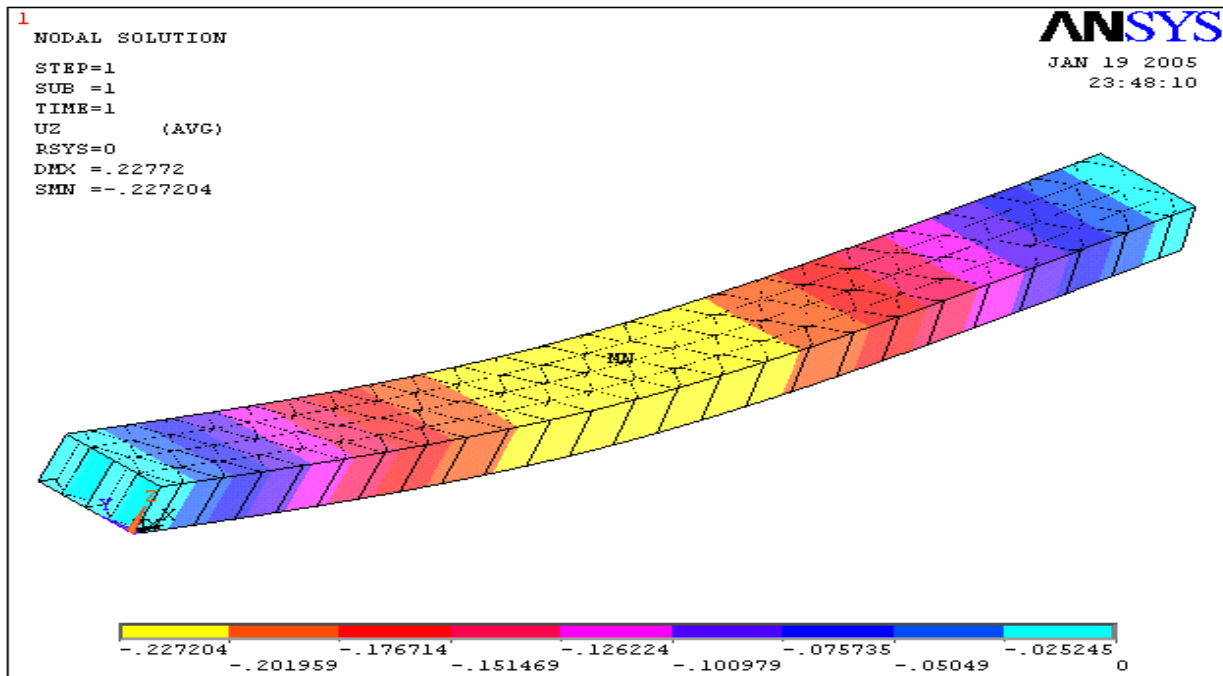


Figure 3.11b: Deflection contour of actual FRP sinusoidal core beam

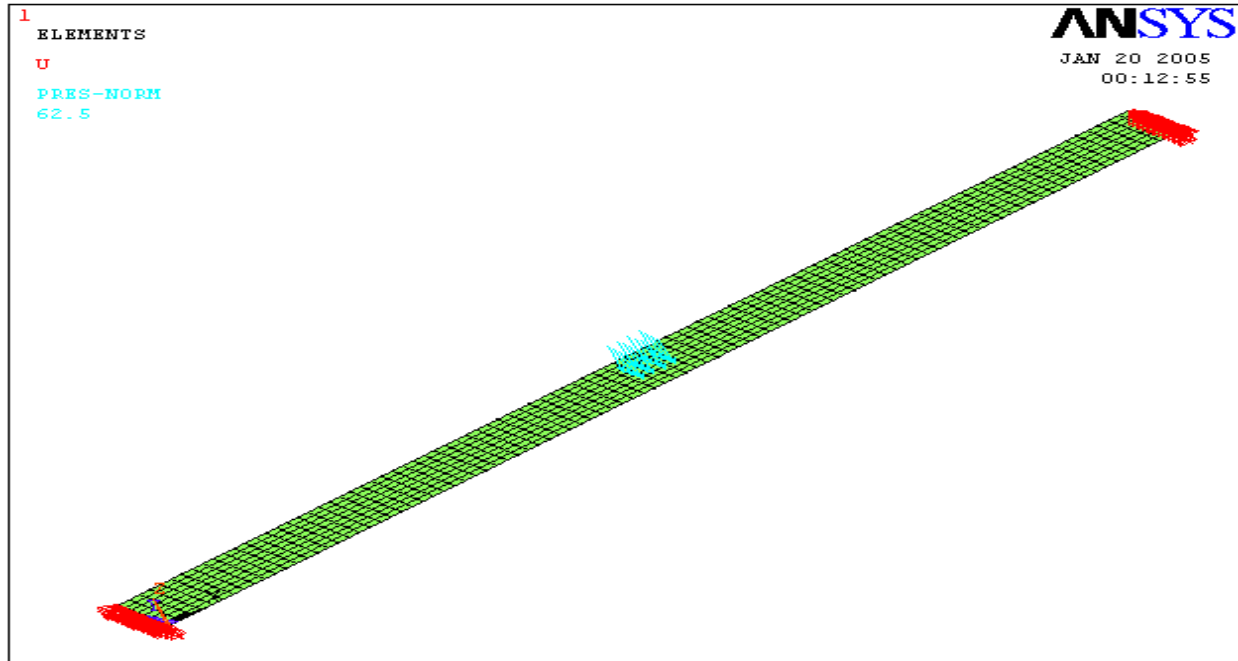


Figure 3.12a: ANSYS model of 3-layered equivalent FRP beam

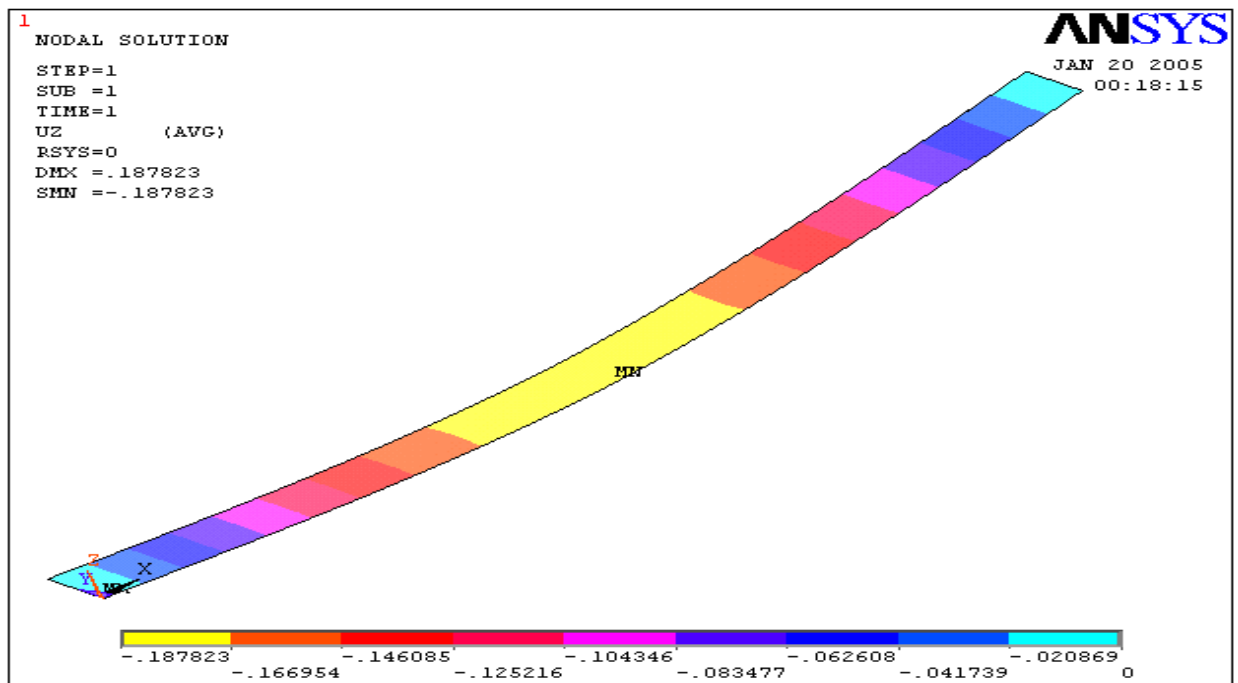


Figure 3.12b: Deflection contour of 3-layered equivalent FRP beam

3.6.2 Case 2: Panel Model

In the second case of this examination, a full-size FRP honeycomb panel is also analyzed by finite element method. The model is 15 feet x 7.75 feet x 5 inches and simply supported over the span. A load equivalent to 10 kips is applied at the center of the deck. This load is distributed over elements within an area of 12 inches x 9 inches.

Since the model is symmetric about its mid-span, half of the bridge is modeled, and the loading and boundary conditions are simulated accordingly. The left support is constrained for displacement in the vertical and lateral (u_z and u_y) directions while rotation about the lateral axis and displacement in longitudinal direction (Rot_y and u_x) are constrained on the right support. Half the total load is used in this model, for symmetry. In Fig. 3.13, the full scale ANSYS model and vertical deflection contour can be seen.

Just as was done in Case 1, an equivalent panel is also modeled and analyzed. The panel has the same dimensions, loading and support conditions as that of the actual configuration model. Structural-layered elastic shell elements are employed to simulate a three-layered equivalent panel structure with two faces and a core. Tables 3.2 and 3.3 were used to input the properties of the panel. Fig. 3.14 illustrates the model by ANSYS as well as the vertical deflection contour.

The results of deflection are recorded for two cases. First, at quarter points along the longitudinal centerline. Then, at quarter points along the lateral direction on the right end of the symmetric model (midspan of full model). These two sets of results are shown in Table 3.6. A comparison shows an approximately consistent difference of

about 19%, which is significant and about the same as that for the beam model in Case 1.

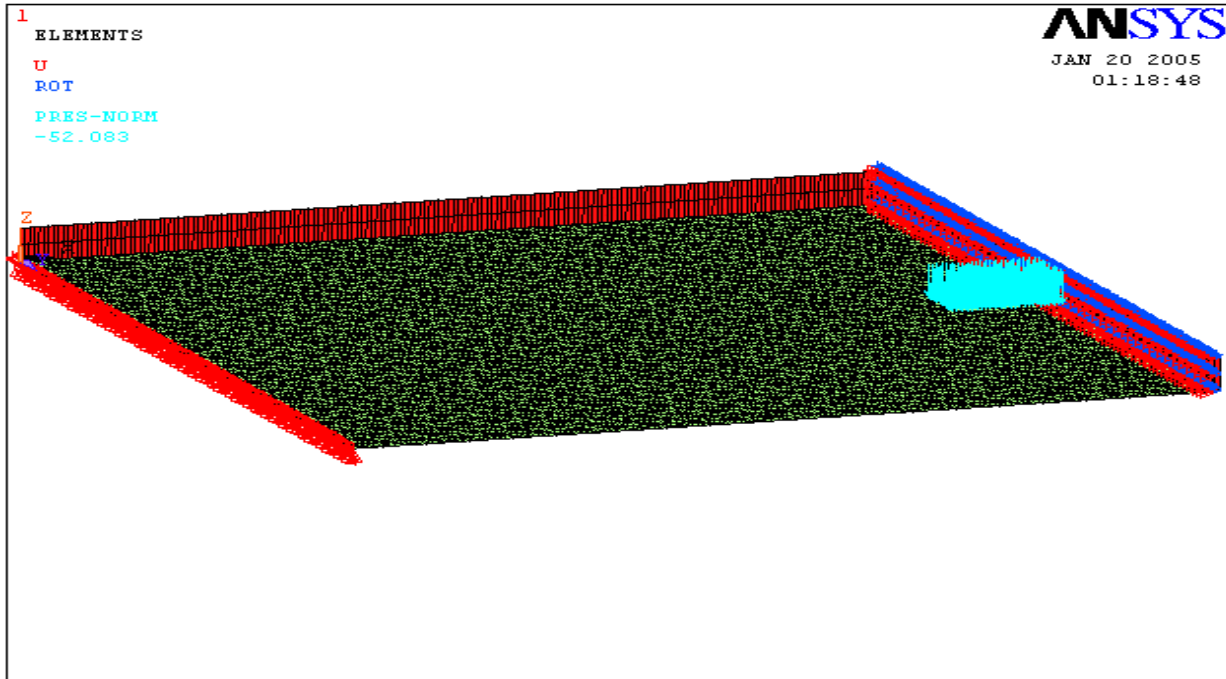


Figure 3.13a: ANSYS model of actual FRP sinusoidal core panel

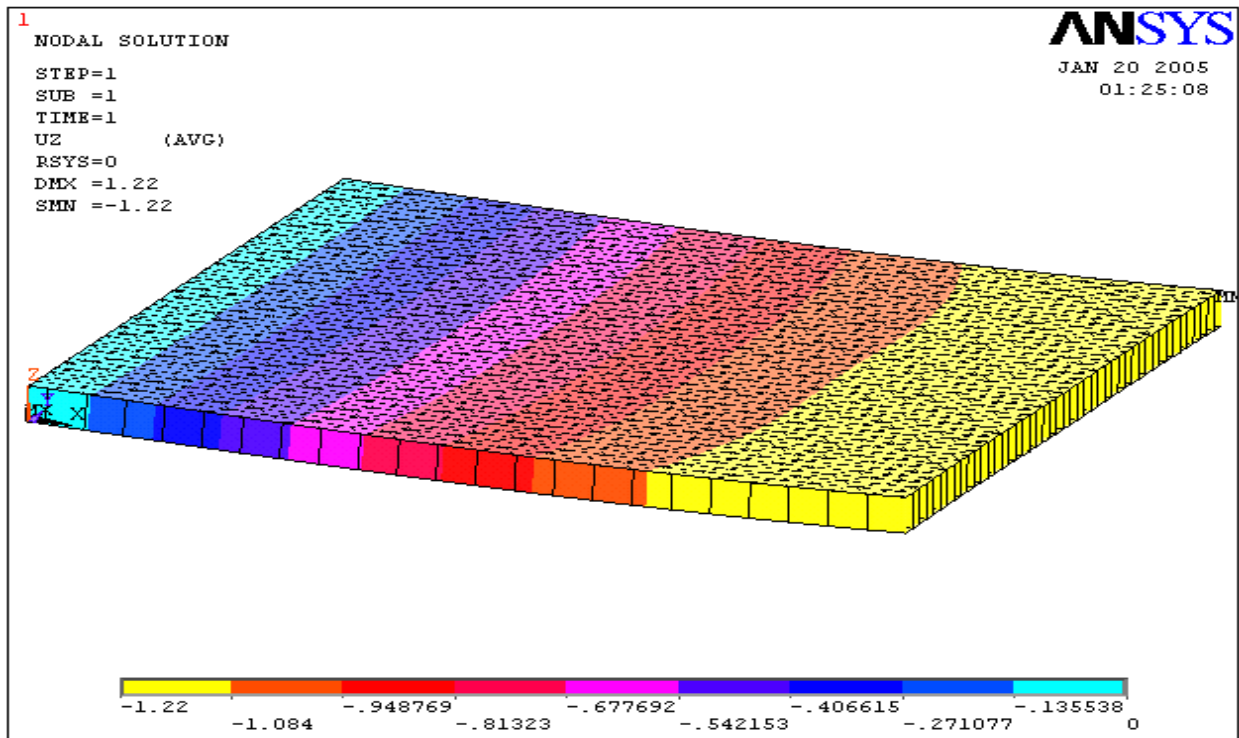


Figure 3.13b: Deflection contour of actual FRP sinusoidal core panel

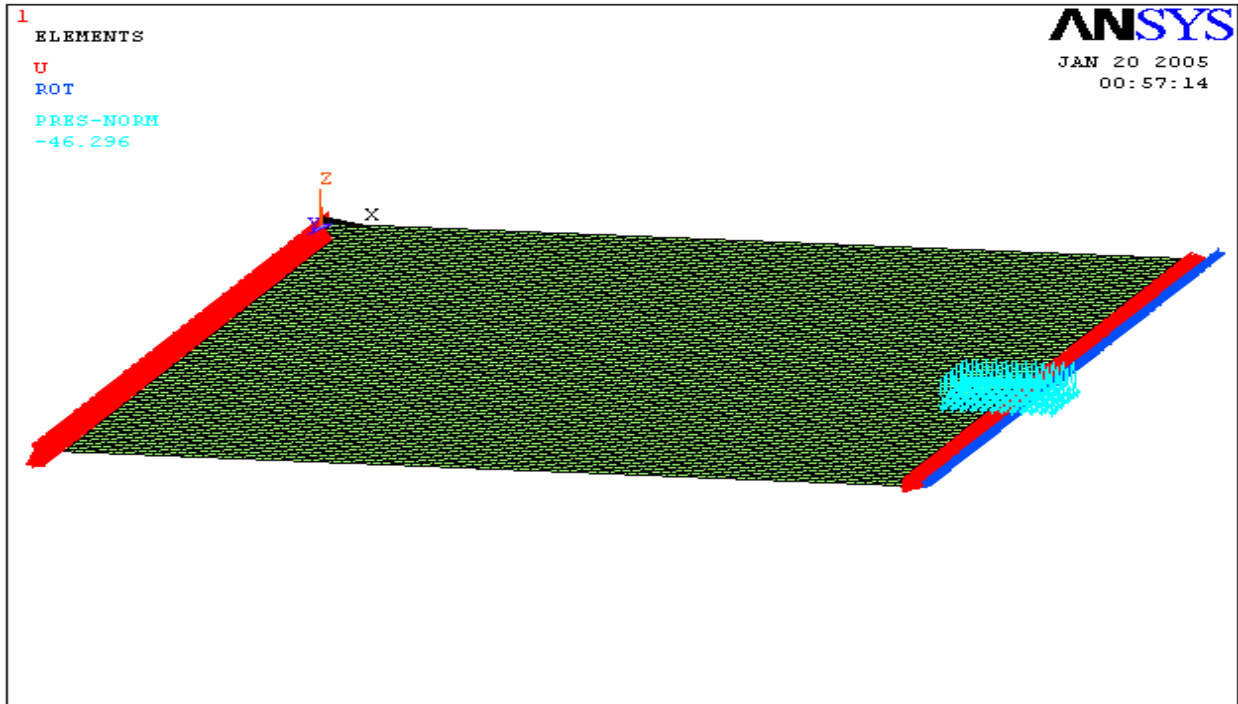


Figure 3.14a: ANSYS model of 3-layered equivalent FRP panel

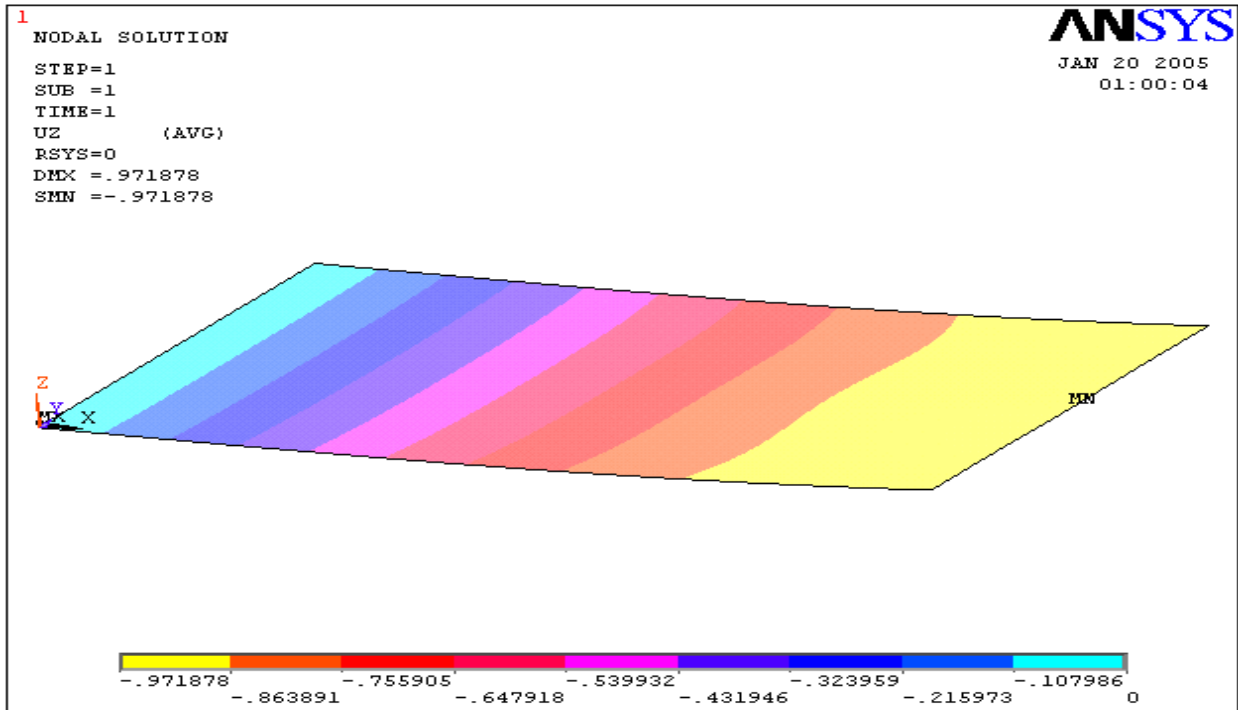


Figure 3.14b: Deflection contour of 3-layered equivalent FRP panel

Table 3.6a: Comparison of deflection results (in.). Points in the longitudinal direction along the central line (in.)

x	Actual Configuration	Equivalent (Equation)	% diff.
0	0	0	
45	0.8073	0.6526	19.1599
90	1.2016	0.9719	19.1145
135	0.8073	0.6526	19.1599
180	0	0	

Table 3.6b: Comparison of deflection results (in.). Points in the lateral direction along the midspan (in.)

y	Actual Configuration	Equivalent (Equation)	% diff.
0	1.2191	0.9586	21.3666
23	1.1798	0.9498	19.4974
46.5	1.2016	0.9719	19.1145
69	1.1801	0.9498	19.5178
93	1.2196	0.9586	21.3988

The fact that the results obtained in the previous analysis do not compare too well might raise some concerns about the validity of the approach. However, a closer examination of the method used in deriving the equivalent panel properties reveals that attention was not given to bending behavior. In other words, the moduli of elasticity in the three orthogonal directions are obtained based on the equivalency of axial stiffness. For this honeycomb sandwich configuration, however, there is obviously a difference in behavior in the equivalence of axial and bending stiffnesses. We will discuss bending behavior further when we analyze the case of a single-layered equivalent model (Chapters 5 and 6).

From the foregoing, we can conclude that the results are useful when we deal with situations relating to in-plane behavior or axial effects. Separate properties will be derived for bending (out-of-plane) behavior.

CHAPTER 4 - PARAMETRIC STUDIES FOR IN-PLANE BEHAVIOR

4.1 Introduction

In the previous chapter (Chapter 3), an approach was developed and verified to derive the properties for in-plane behavior of the sinusoidal wave core. A core geometry with specific properties was considered. In this chapter, we are interested in developing equations relating the core properties for in-plane behavior with the core parameters. This becomes very useful when we have a core section whose parametric values differ from those considered in the previous chapter. Therefore, in this section attention is given to the relationship between core parameters and stiffness properties and equations relating them are derived. With these simplified equations, the equivalent stiffness properties from specific core parametric values can be obtained. This parametric study is performed using as the basis the same RVE described in the preceding sections, and its basic parameters. Just as was done in Chapter 3, the top and bottom faces of the panel are not included in this parametric study but can be conveniently added to the equivalent core in actual application.

4.2 Determining Equivalent Properties

Due to the complex nature of the core configuration, analysis and design can become complicated. In real design situations, it is favorable to deal with complex shapes using their equivalence. Therefore, a study by Davalos et al. (2001) focused on developing equivalent elastic properties for this complex core structure. He performed design modeling and experimental characterization, and obtained an approximate analytical solution through a homogenization process. To verify the results, experiments

were carried out and finite element analysis was performed. To obtain the equivalent properties of the core, an energy method combined with mechanics of materials approach was used.

FRP panels used in this study were developed by Kansas Structural Composites Inc. The production of the panel involves sequentially bonding a flat sheet to a corrugated sheet to form the flat and waved FRP cells. It is then assembled and co-cured with the upper and lower face laminates. The Representative Volume Element (RVE) of the honeycomb core manufactured by KSCI had a 2-in. flute-width and 4-in. half-sine wavelength. The constituent materials were E-glass fibers and polyester resin. The depth of the panel is 5 in. The sinusoidal wave-core is made of mats arranged in the form of flats and flutes each having a thickness of 0.0898 in., and elastic modulus of 1,710 ksi. In this work, we refer to all these parametric values as the basic parameters.

Verification of the results obtained was done by carrying out experimental testing and finite element modeling of FRP honeycomb beams. These were then correlated with analytical solutions based on first-order shear deformation theory. It was observed that the analytical solution correlated well with both the finite element modeling and experimental results.

What Davalos et al. obtained in his work were equivalent properties for a core with fixed dimensions. An optimization research may however reveal a more efficient section. Therefore, in this present work, attention is given to the relationship between core parameters and elastic modulus, and equations relating them are derived. With these simplified equations, the equivalent orthotropic stiffness from specific core dimensions and properties can be obtained. This parametric study is performed using

the RVE, which is the basic segment or cell unit of the whole structure. The RVE is reproduced in Fig. 4.1.

The equivalent orthotropic modulus of elasticity E of the RVE is a function of panel depth H , flute width W , flute half-wavelength L , flat/flute thickness t and elastic properties of the flat/flute materials. (The flat and flute laminae are composed of randomly oriented fibers. Hence the moduli of elasticity of these materials are assumed equal in all directions in the plane).

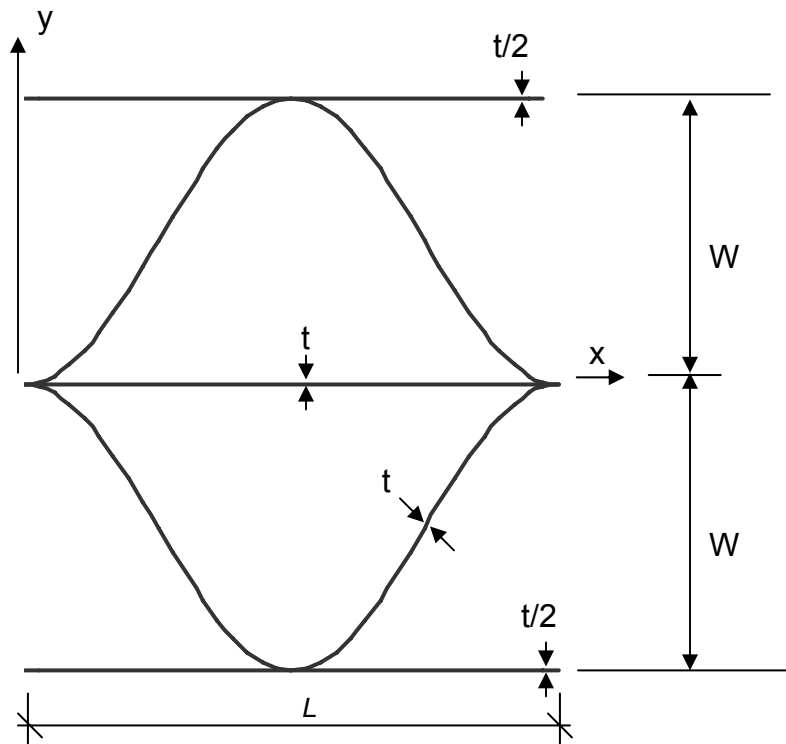


Figure 4.1: Representative Volume Element of Core

4.3 Finite Element Modeling

Determining the equivalent properties of the sinusoidal wave core is done with the aid of finite element modeling. The finite element models created was done using the program ANSYS 9.0 which is powerful computer software for engineering modeling and analysis.

4.4 Parameters Affecting the Young's Modulus in the Longitudinal Direction

First, an effort is made to determine to what degree each parameter influences the Modulus of Elasticity. Each parameter is varied within a reasonable range of dimensions while keeping others constant, each time computing the elastic modulus. The elastic modulus is obtained using the following procedure. First, a uniformly distributed load is applied to the core in the longitudinal direction. To ensure uniform displacement, rigid elements are used at the two ends for load application and support. Boundary conditions are simple supports (like the pin and roller supports of a simple beam). This is done by constraining the nodes at one end for translation in the three directions, u_x , u_y and u_z while the nodes at the other end are constrained for lateral movement only. The longitudinal displacement is obtained, and E_x is calculated using the constitutive stress-strain relationship below:

$$E_x = \frac{\sigma_x L}{\Delta L} \quad \text{Equation 4.1}$$

It is pertinent to note that inherent in this approach is the assumption that the behavior is linearly elastic.

Plots of E_x against flute width, half wavelength and panel depth are represented in Fig. 4.2. The results indicate that the flute width has a more significant effect on the equivalent elastic constant. It is varied within the range of 0.5 inches to 5 inches. While

the flute width is varied, all other parameters are kept constant at their basic parametric values. Regression analyses of the results show that the relationship between the flute width W and the elastic modulus E_x (with other parameters kept constant) can be expressed as follows:

$$E_x = aW^n \tag{Equation 4.2}$$

where $a = 1.6609E + 05$, and $n = 1.0083$.

Fig. 4.3 shows that the proposed equivalent formula in Equation 4.2 provides a very good fit of the finite element analysis performed on the actual configuration model. The difference between both data sets as shown in the figure is about 0.19%.

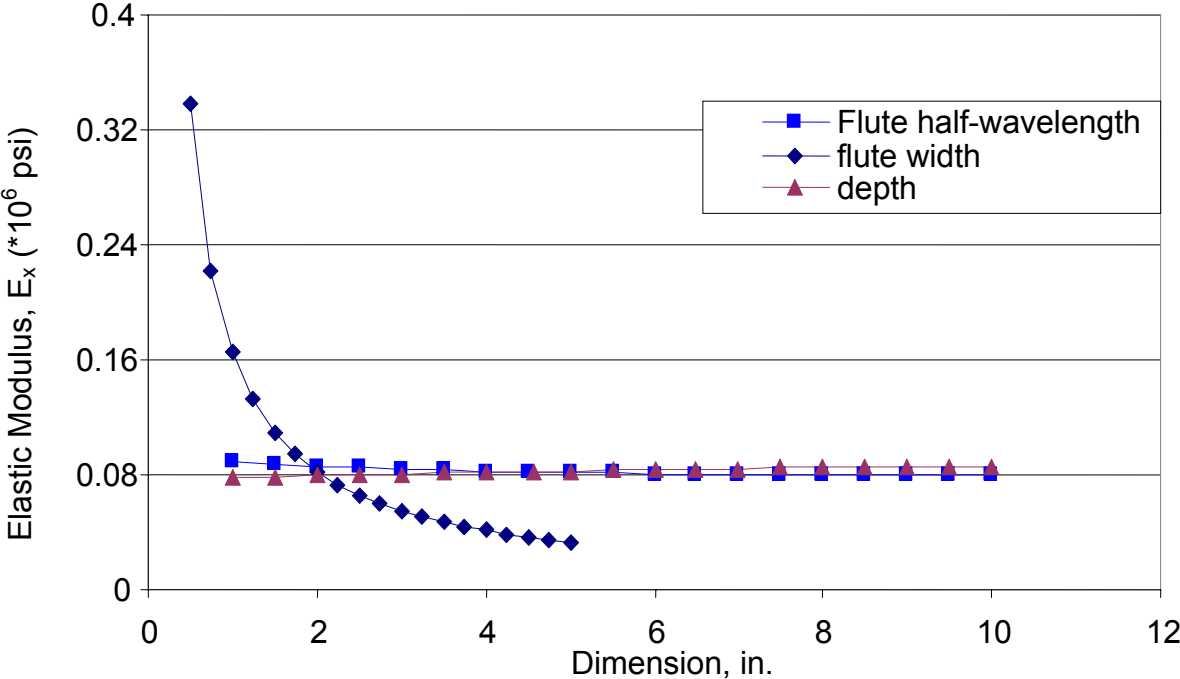


Figure 4.2: Variation of E_x with panel depth, half-wavelength and flute-width

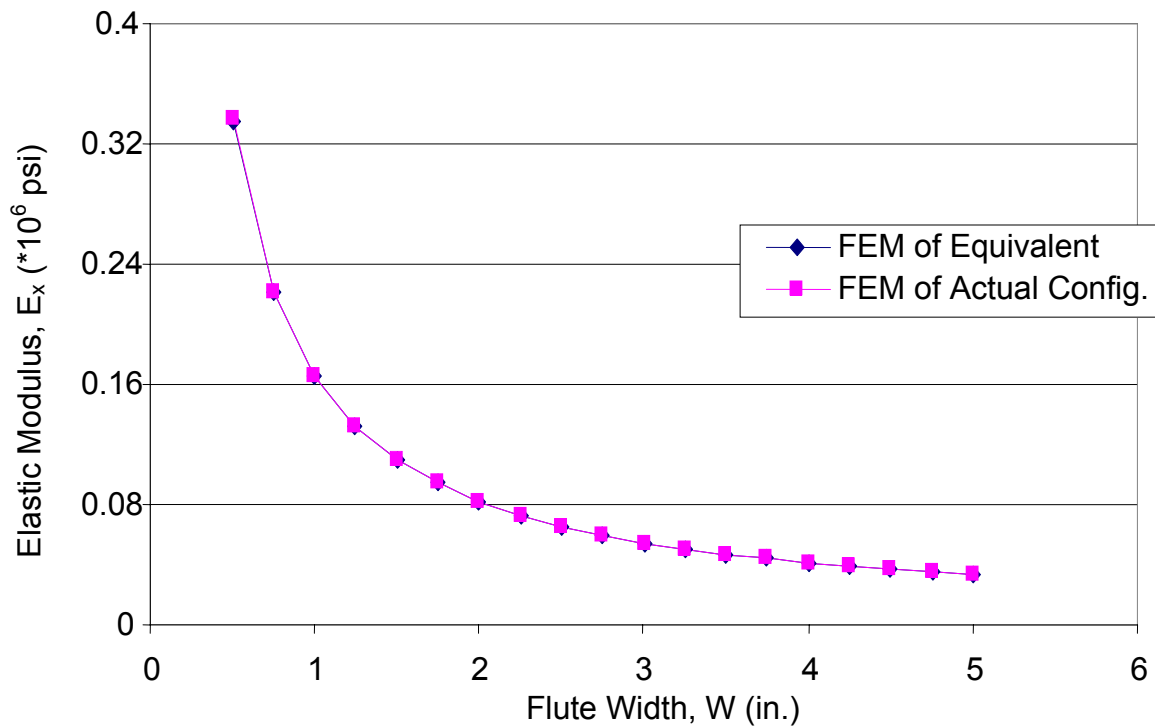


Figure 4.3: Comparison of equivalent model with actual configuration model for flute-width W

The flute half-wavelength L is varied within the range of 1 inch to 10 inches while the other parameters are kept constant at their basic parametric values, and the results can be visualized from the plot in Fig. 4.4. As the half wave-length increases, there is gradual reduction in the elastic constant, and this relationship can be expressed thus:

$$E_x = dL^m \tag{Equation 4.3}$$

where $d = 0.8881E + 05$ and $m = -0.0523$.

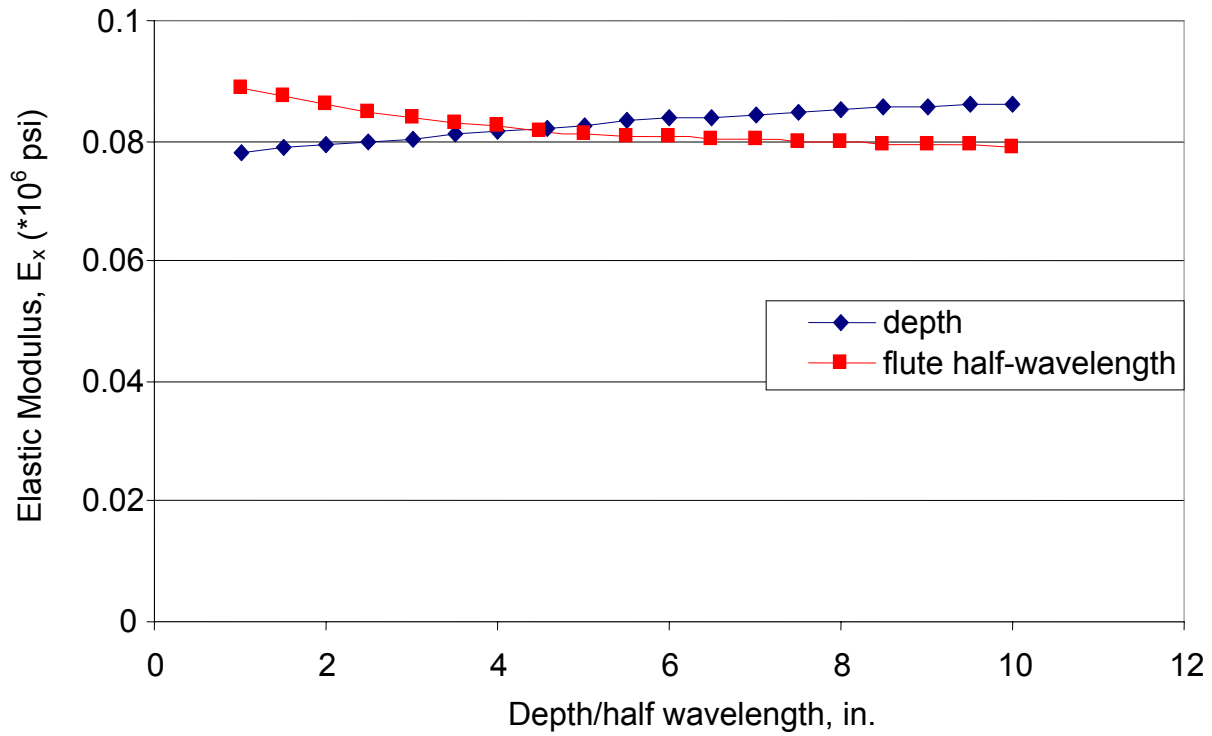


Figure 4.4: Variation of E_x with panel depth H and half-wavelength L

It can be noticed from Fig. 4.5 that the proposed equivalent equation reflects a very good fit of the finite element analysis performed on the actual configuration model. The difference between both results is only about 0.25%.

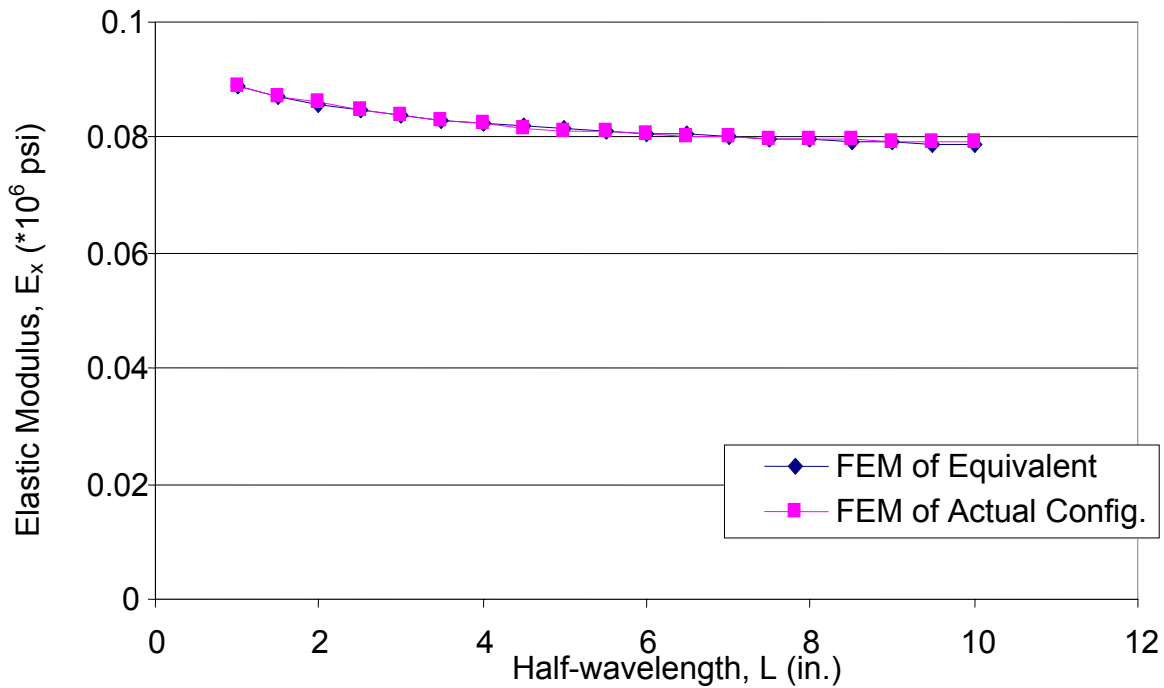


Figure 4.5: Comparison of equivalent model with actual configuration model for half-wavelength L

In contrast to the half-wavelength, there is a gradual rise in the elastic modulus as the panel depth H is increased from 1 inch to 10 inches. Again, other parameters are held constant while H is varied. This variation can also be seen from Fig. 4.4, and can be expressed by the following equation:

$$E_x = fH^r \tag{Equation 4.4}$$

where $f = 0.7585E+05$ and $r = 0.0553$

Once again, a good fit by the proposed equivalent equation of the actual configuration model results from the finite element analysis can be seen. This can be noticed from Fig. 4.6. The difference between the two curves is approximately 0.26%.

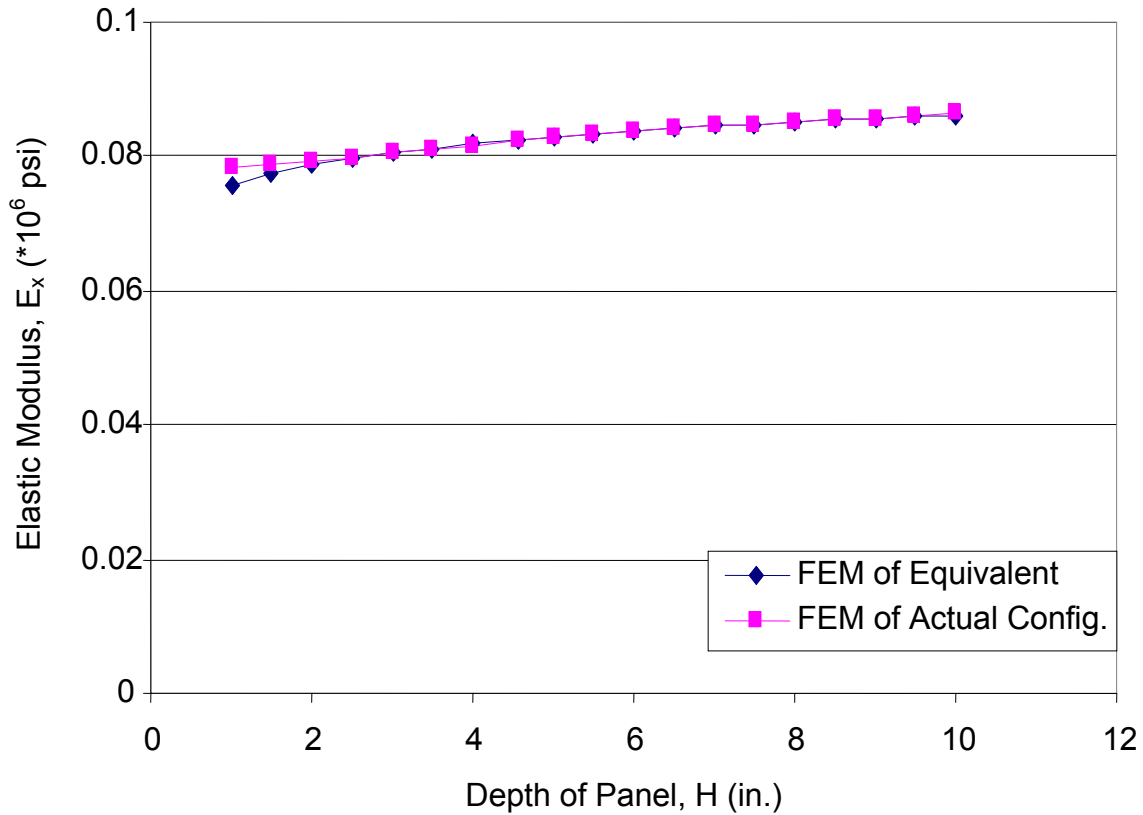


Figure 4.6: Comparison of equivalent model with actual configuration model for panel depth H

There is a more linear relationship between the flat/flute thickness t and the elastic constant as it is varied from 0.01 to 0.2 in. The results for this variation are presented in the plot on Fig. 4.7, and the relationship (with all other parameters kept constant at their basic values) can be expressed by the following equation:

$$E_x = u + vt \tag{Equation 4.5}$$

where $u = -3.6898E + 02$ and $v = 9.2268E + 05$.

Fig. 4.7 also shows how well the proposed equivalent equation (Equation 4.5) fits the results of the actual configuration model obtained from the finite element analysis. A very good fit is noticed, the difference between both curves being only about 0.11%.

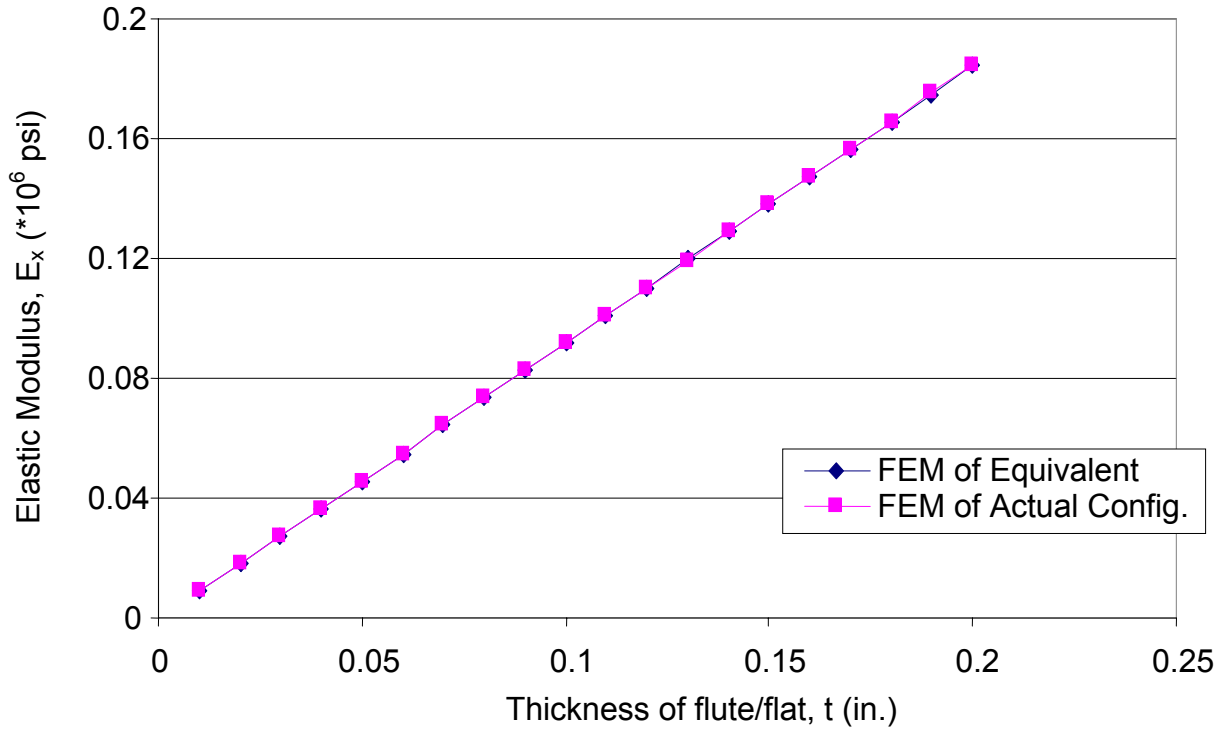


Figure 4.7: Variation of E_x with flute/flat thickness t

The relationship between the modulus of elasticity of the flat/flute E_{11} and the equivalent Young's Modulus E_x is linear and can be visualized in the graph in Fig. 4.8. E_{11} was varied between 500 ksi and 10,000 ksi. This variation can be expressed by the following equation:

$$E_x = z + wE_{11} \quad \text{Equation 4.6}$$

where, $z = 3.1381E - 03$ and $w = 4.6309E - 02$.

From Fig. 4.8, it can be observed that the proposed equivalent equation (Equation 4.6) provides a very good curve fit of the actual configuration model results

obtained from the finite element analysis. The difference between the two plots is only about 0.3%.

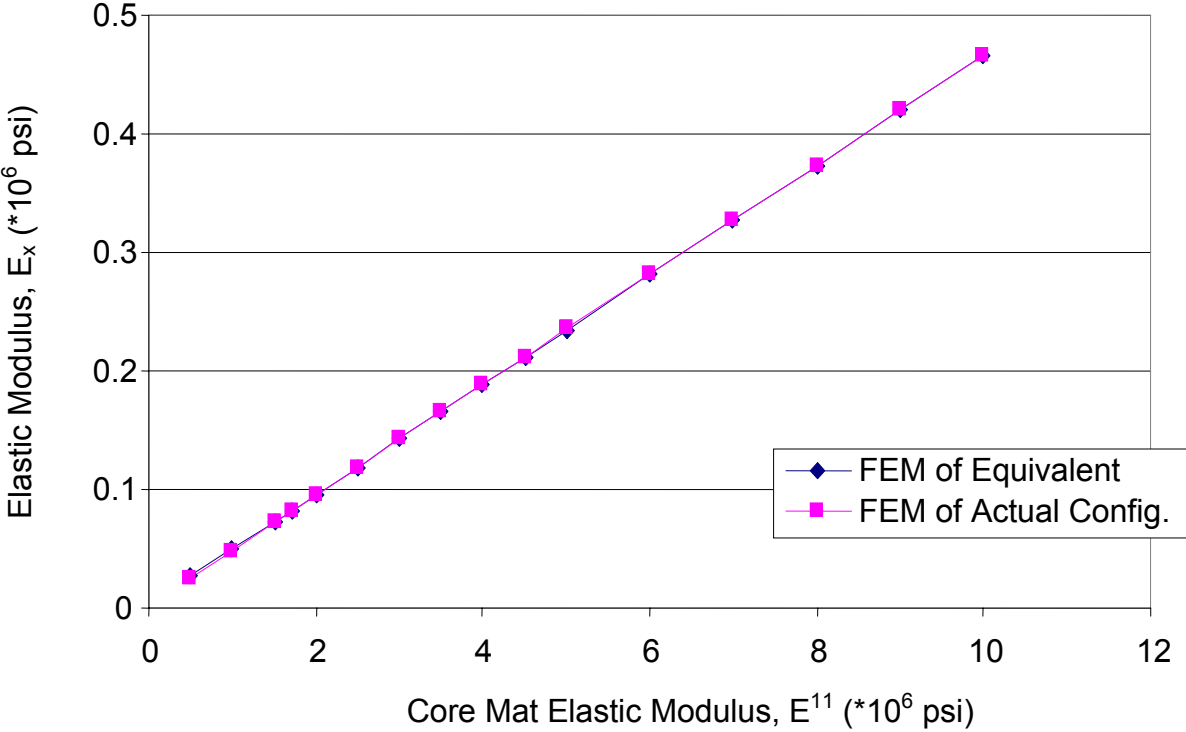


Figure 4.8: Variation of E_x with material elastic modulus E^{11}

Equations 4.2 to 4.6 could be used to compute the elastic modulus in the longitudinal direction of the FRP sinusoidal wave core manufactured by KSCI when only one of its parameters is changed from the original basic value. For example, if for some reason the core mat is changed to a different material, but the flute-width, half-wavelength, core height and core mat thickness remain unchanged, Equation 4.6 could be used to calculate E_x . However, it must be kept in mind that E_x obtained is true only for in-plane (axial) behavior such as when analyzing a column. It must also be noted that this is limited to the linear elastic range.

4.4.1 Modification Factors

The formulations in the previous section are valid only for a single variable. What if more than one of the parameters is altered? Therefore a more general relationship between the elastic modulus and the other aforementioned parameters is sought. Having understood the link between the various parameters, a more general equation for the elastic modulus E_x is now derived. In deriving this formula, a systematic approach that assumes that the parameters are independent variables of E_x is used. This leads us to the concept of modification factors of the equivalent elastic constant for a variation in core parameters. This concept will be better understood as we next consider the modification factor by each parameter. As discussed previously, one of the most important factors influencing the elastic constant is the flute width. The relationship can be seen in Equation 4.2.

4.4.1.1 Half-wavelength Modification Factor, K_1

As was discussed in the previous section, the elastic constant E_x decreases as half-wavelength L increases, and this relation is found in Equation 4.3. A plot of the modification factor for half-wavelength, $K_1(=E_x / E_{x(L=4)})$ against the ratio $R_1(=L / L_4)$ shows a similar behavior. L_4 represents the basic half-wavelength of 4 in. and $E_{x(L=4)}$ is the elastic modulus of the panel when the half-wavelength is 4 in. This relationship can be seen in the graph in Fig. 4.9. Analyzing the results yields an equation for the modification factor K_1 of the form:

$$K_1 = \alpha R_1^m \quad \text{Equation 4.7}$$

where, $\alpha = 1.0029$, $m = -5.2332E - 02$, $R_1 = 0.25L$ and L is in inches.

It can be observed from Fig. 4.9 that the proposed equivalent equation (Equation 4.7) provides a very good curve fit of the actual configuration model results obtained from the finite element analysis. The difference between both curves is approximately 0.25%.

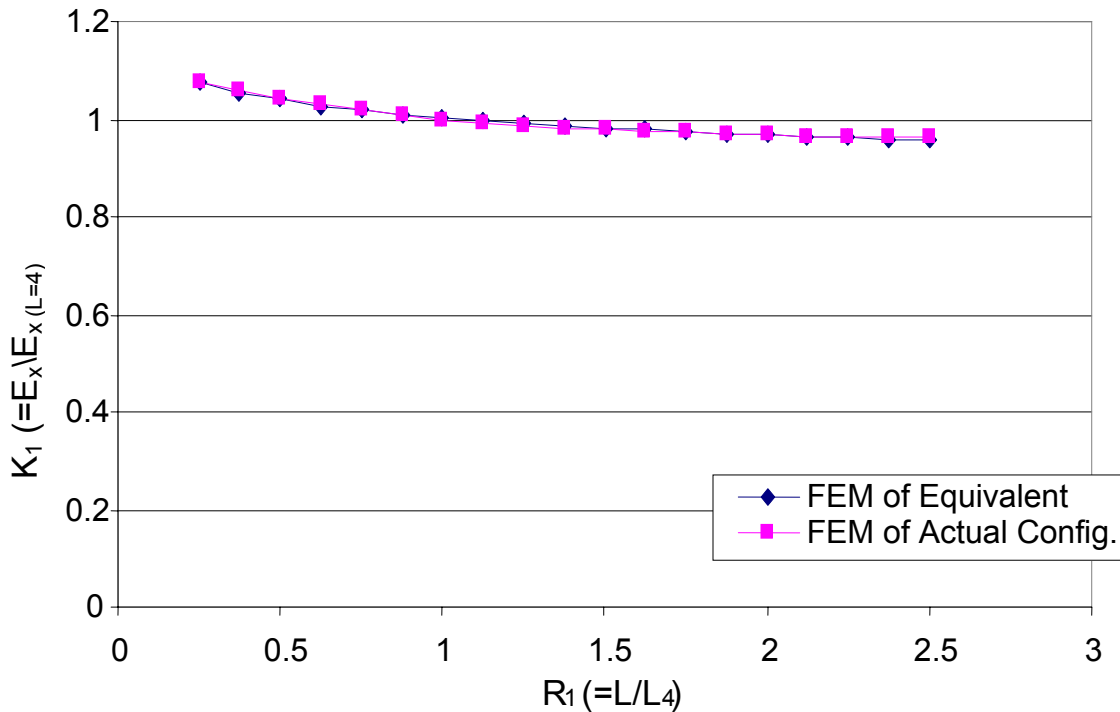


Figure 4.9: Variation of modification factor K1 with half-wavelength ratio R1

4.4.1.2 Panel Depth Modification Factor, K2

Fig. 4.4 showed an increased in the modulus of elasticity with a rise in the panel depth H . A relationship was developed to define this relationship (Equation 4.4). The depth ratio $R_2 (= H/H_{4.57})$ is now varied for a range of depth between 1 inch and 30 inches, where $H_{4.57}$ is the basic panel depth of 4.57 inches. When the ratio $E_x / E_{x(H=4.57)}$ is plotted against R_2 , the graph in Fig. 4.10 results. The ratio $E_x / E_{x(H=4.57)}$ is the panel

depth modification factor K_2 , and $E_{x(H=4.57)}$ represents the elastic modulus at a depth of 4.57 in. The plot in Fig. 4.10 can be represented by the following equation:

$$K_2 = \beta(R_2^p) \quad \text{Equation 4.8}$$

where, $\beta = 1.0062$, $p = 4.7176E - 02$, $R_2 = H / 4.57$ and H is in inches.

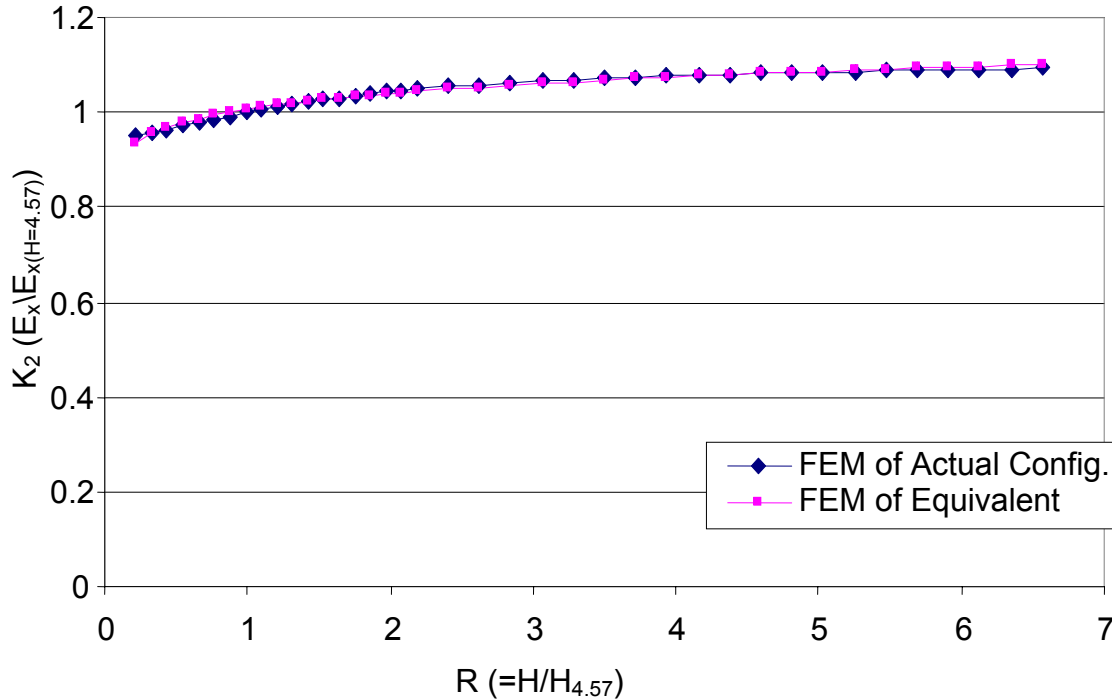


Figure 4.10: Variation of modification factor K2 with panel depth ratio R2

Again, the “FEM of Equivalent” plot fits very well with the “FEM of Actual Config.” from the analysis (Fig. 4.10). A difference of about 0.35% between both curves in the figure is recorded.

4.4.1.3 Flat/Flute Thickness Modification Factor, K3

Next, attention is given to the effect the flute/flute thickness t has on the elastic modulus. A linear relationship of this parameter with the elastic constant was observed in the previous section, and its equation was derived (Equation 4.5). This can also be

visualized in Fig. 4.7. To obtain the modification factor for the flat/flute K_3 , we follow the same procedure as previously described for the other parameters. The thickness ratio $R_3 (= t / t_{0.0898})$ is computed for a range of t between 0.01 inch and 0.2 inch, where $t_{0.0898}$ is the basic flat flute thickness of 0.0898 inch. The modification factor $K_3 (= E_x / E_{x(t=0.0898)})$ is plotted against R_3 and the resulting graph is plotted in Fig. 4.11.

The expression for the flat/flute modification factor can thus be written as:

$$K_3 = b + cR_3 \tag{Equation 4.9}$$

where, $b = -4.4806E - 03$, $c = 1.0061$, $R_3 = t / 0.0898$ and t is in inches.

A very good fit of the two plots in Fig. 4.11 from the analysis can be observed.

The average difference between both curves is 0.17%.

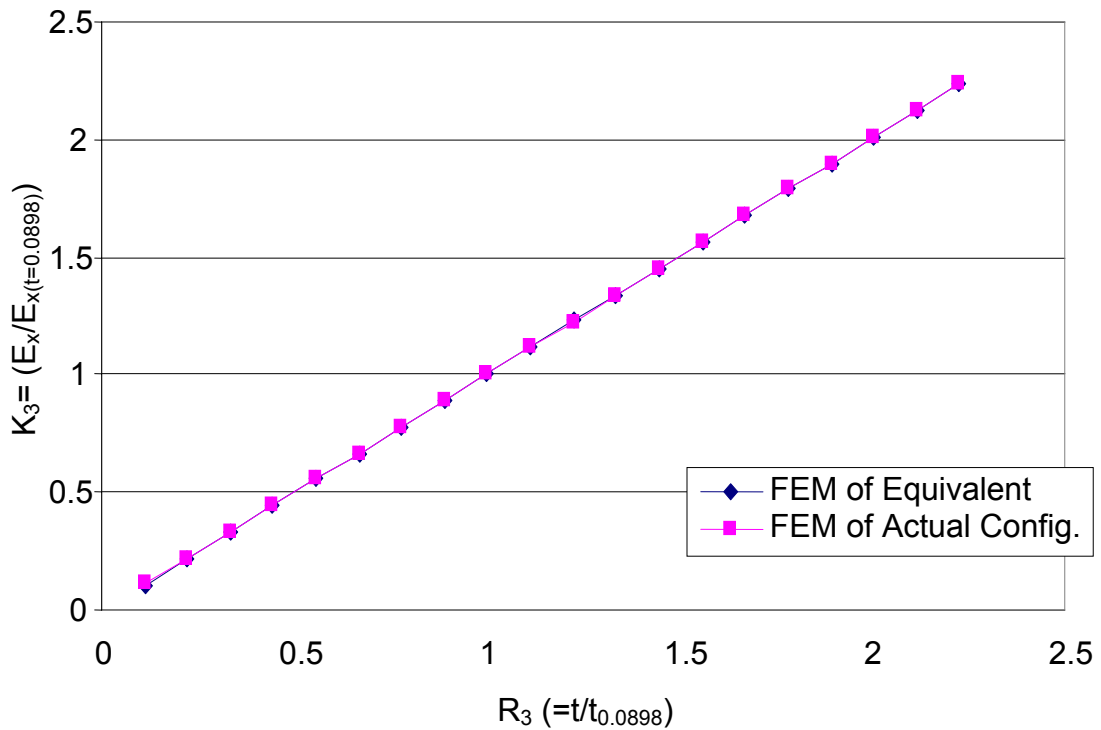


Figure 4.11: Variation of modification factor K3 with flute/flat thickness ratio R3

4.4.1.4 Flat/Flute Young's Modulus Modification Factor, K4

Finally, following the same approach, an equation for the modification factor of core laminate material stiffness and the equivalent modulus of elasticity is derived. In Equation 4.6, it can be recall that E_x and E_{11} have a linear relationship. Fig. 4.12 shows the relationship between elastic modulus ratio $R_4(=E_{11}/E_{11b})$ and modification factor $K_4(=E_x/E_x(E_{11b}))$. This relationship can be expressed by the following equation:

$$K_4 = g + kR_4 \quad \text{Equation 4.10}$$

where $g = 3.8144E - 02$, $k = 0.9625$, $R_4 = E_{11}/(1.71E + 6)$ and E_{11} is in psi.

Just as was done in the previous cases, a very good fit of the two plots from the analysis can be noticed. (Fig. 4.12) The difference computed between both sets of data is about 0.33%.

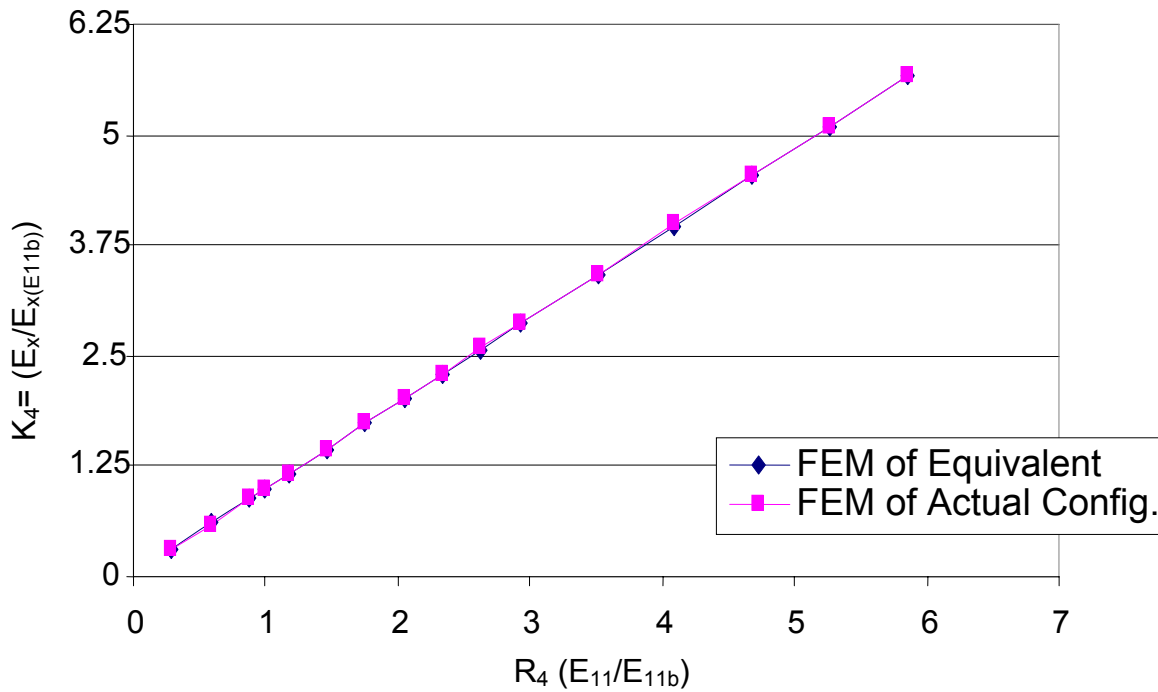


Figure 4.12: Variation of modification factor K4 with material young modulus ratio R4

4.4.2 Formula for Predicting Longitudinal Young's Modulus of the Core

Having derived and discussed the interrelationship between panel parameters, the following formula is now proposed for calculating the modulus of elasticity in the longitudinal direction E_x .

$$E_x = K_1 K_2 K_3 K_4 a W^n \quad \text{Equation 4.11}$$

where $a = 1.6609E + 05$, $n = -1.0083$, W is the flute width (inches), K_1 represents the half-wavelength modification factor from Equation 4.7, K_2 symbolizes the panel depth modification factor from Equation 4.8, K_3 refers to the flat/flute thickness modification factor from Equation 4.9 and K_4 refers to the flat/flute Young's Modulus modification factor from Equation 4.10.

Simplification of the equation by substituting K1 to K4 into Equation 4.11 yields the formula in Equation 4.12:

$$E_x = KL^m H^p W^n t E_{11} \quad \text{Equation 4.12}$$

where $K = 1.0580$, $m = -5.2332E - 02$, $p = 4.7176E - 02$ and $n = -1.0083$.

4.5 Parameters Affecting the Young's Modulus in the Transverse Direction

Here again, a uniformly distributed load is applied to the core, but this time in the transverse direction. Rigid elements are used at the two lateral ends for load application and support to ensure uniform displacement. Simple support boundary conditions are applied just as was done in Section 4.4. The transverse displacement is obtained, and E is calculated using the constitutive stress-strain relationship below:

$$E_y = \frac{\sigma_y W}{\Delta W} \quad \text{Equation 4.13}$$

The equivalent elastic modulus E_y is plotted against flute width, half wavelength and panel depth. This is shown in Fig. 4.13. From the results, the flute half wavelength L is seen to have a more significant effect on the equivalent elastic constant. With other parameters held constant at their basic values, L is varied within the range of 1 inch to 10 inches. The relationship between the half wavelength L and the elastic modulus E_y can be expressed as follows:

$$E_y = aL^n \quad \text{Equation 4.14}$$

where $a = 7.2066E + 05$ and $n = -3.4594$.

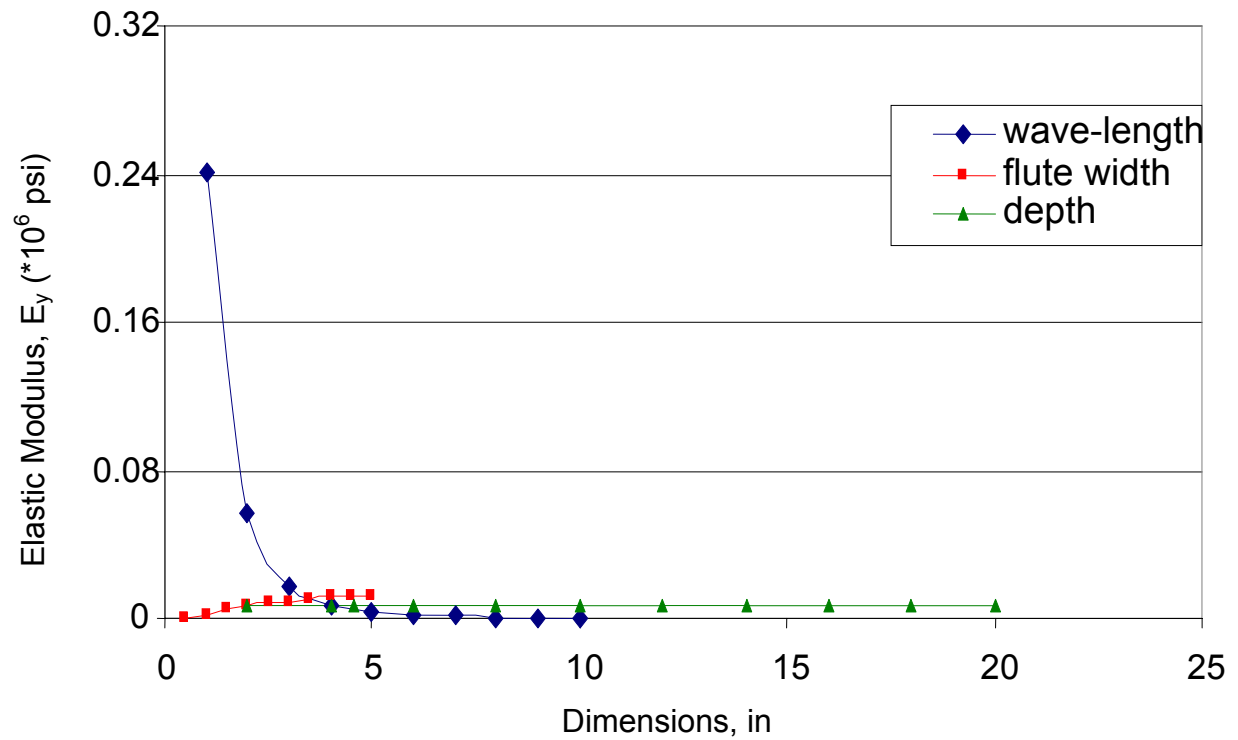


Figure 4.13: Variation of E_y with panel depth, flute-width and half-wavelength

Fig. 4.14 shows that an acceptable fit exists between the proposed equivalent formula in Equation 4.14 and the results of the actual configuration model obtained from the finite element analysis. The difference between both sets of results is about 5%.

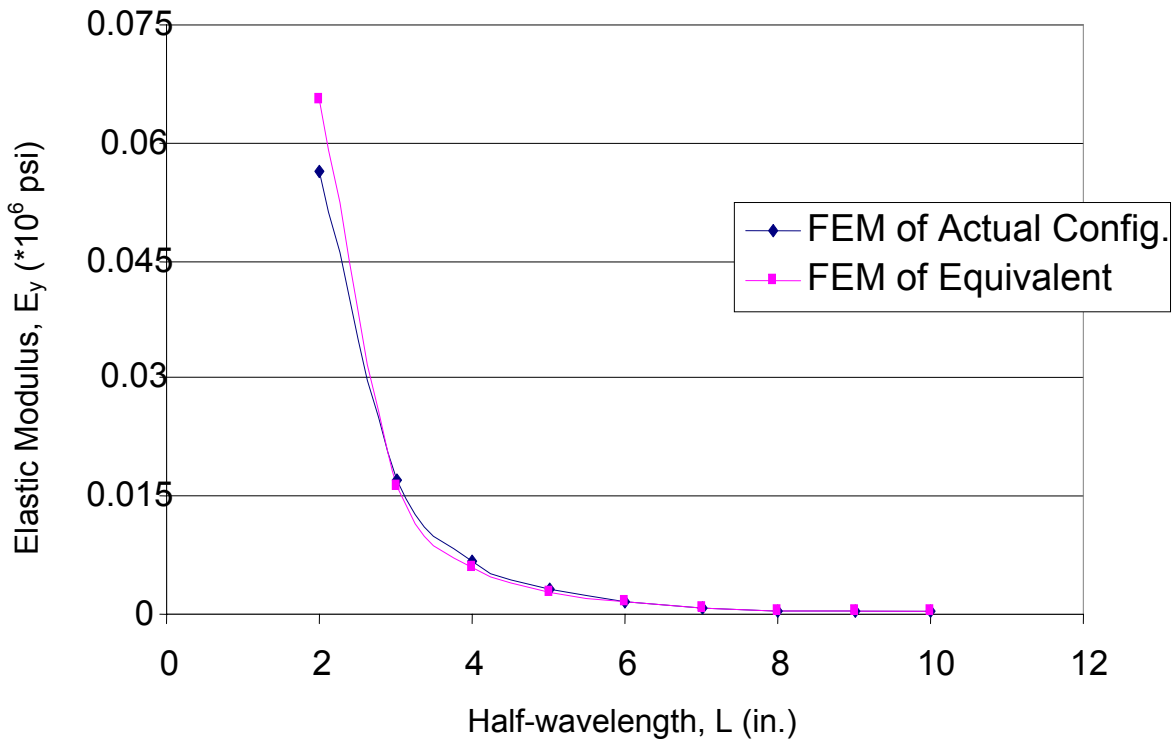


Figure 4.14: Variation of E_y with half-wavelength L

The flute width W is varied within the range of 0.5 in. to 5 in. keeping the other parameters constant. (Fig. 4.15) As the flute width increases, there is a corresponding increase in the elastic constant, and this relationship can be expressed thus:

$$E_y = d + m \ln W \quad \text{Equation 4.15}$$

where $d = 2.184972E - 03$ and $m = 6.5441E - 03$.

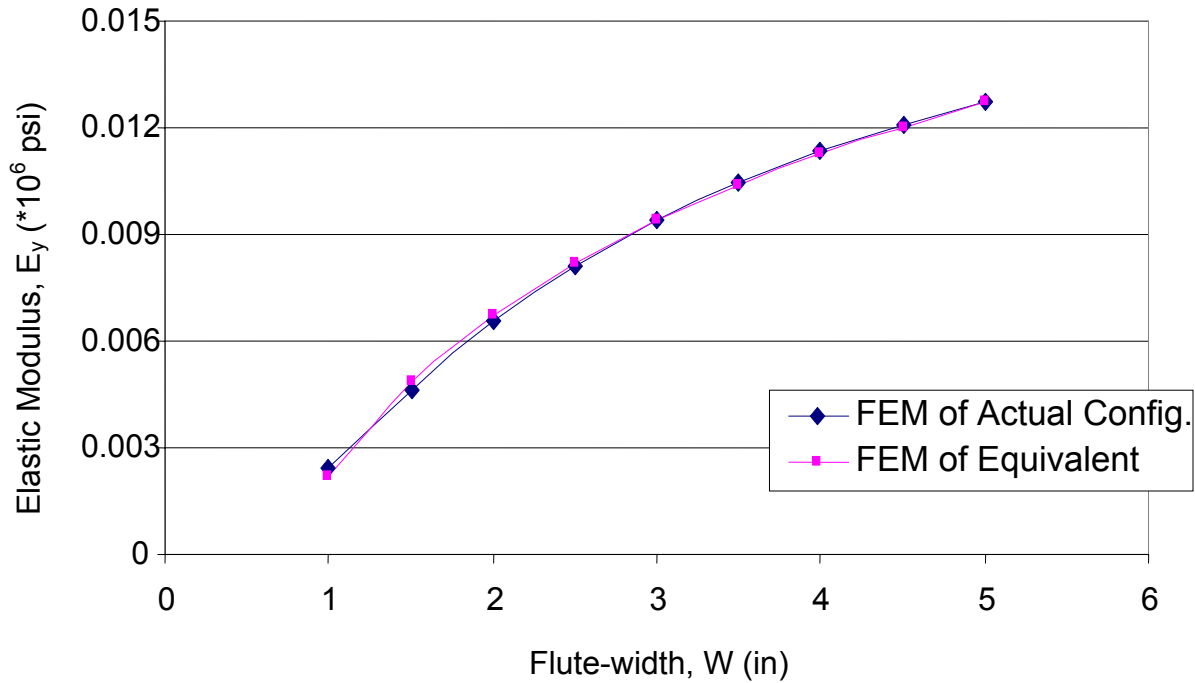


Figure 4.15: Variation of E_y with flute-width W

A good curve fit exists between the graphs for the proposed equivalent equation and the actual configuration model as can be observed from Fig. 4.15. The difference between both curves is approximately 1.2%.

The panel depth H , on the other hand, has only slight effect on the elastic modulus as it is varied from 2 in. to 20 in. (Fig. 4.13) As this parameter is increased, there is a decrease in the equivalent elastic constant. This variation can also be seen from Fig. 4.16, and can be expressed by the following equation:

$$E_y = fH^r \tag{Equation 4.16}$$

where $f = 6.8590E + 03$ and $r = -2.5138E - 02$.

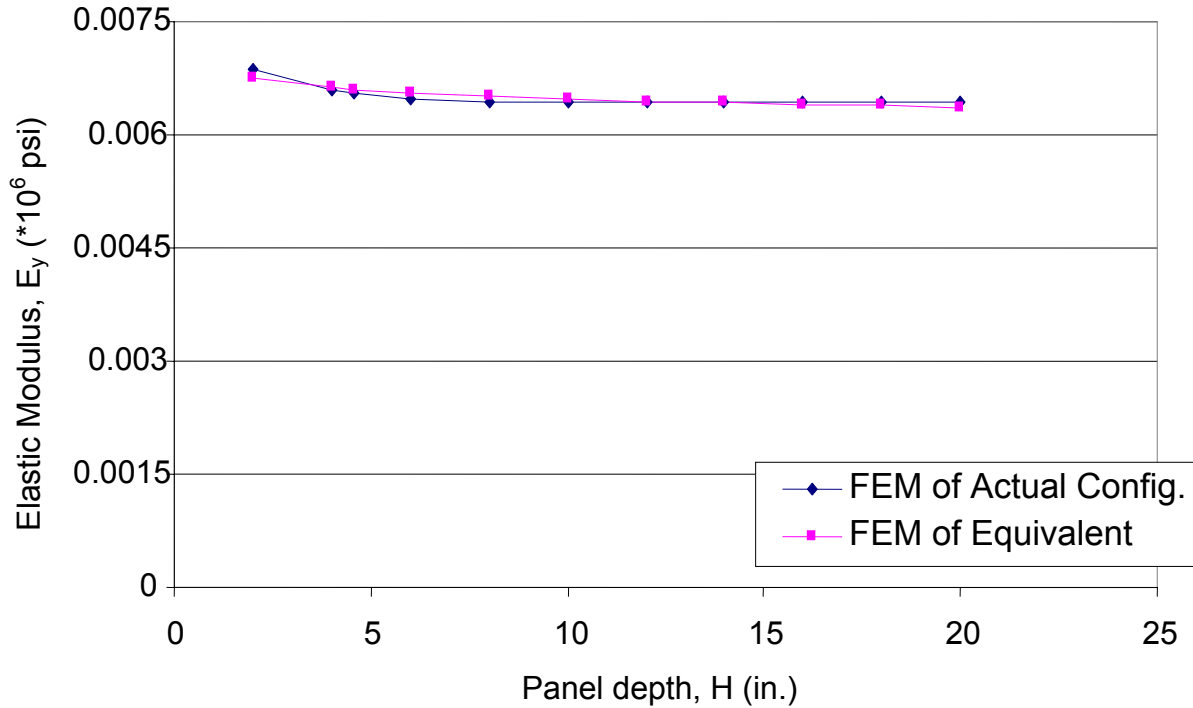


Figure 4.16: Variation of E_y with panel depth H

Fig. 4.16 shows a very good curve fit between the two plots obtained from the analysis. The difference is about 0.6%.

The relationship between the flat/flute thickness t and the elastic constant as it is varied from 0.01 in. to 0.2 in. can be observed from the plot in Fig. 4.17, and the relationship can be expressed by the following equation:

$$E_y = ut^v \quad \text{Equation 4.17}$$

where $u = 1.3490E + 06$ and $v = 2.2267$.

From Fig. 4.17, a good curve fit can be seen of the actual configuration model results by the proposed equivalent equation (Equation 4.17). The difference computed between both sets of data is approximately 5%.

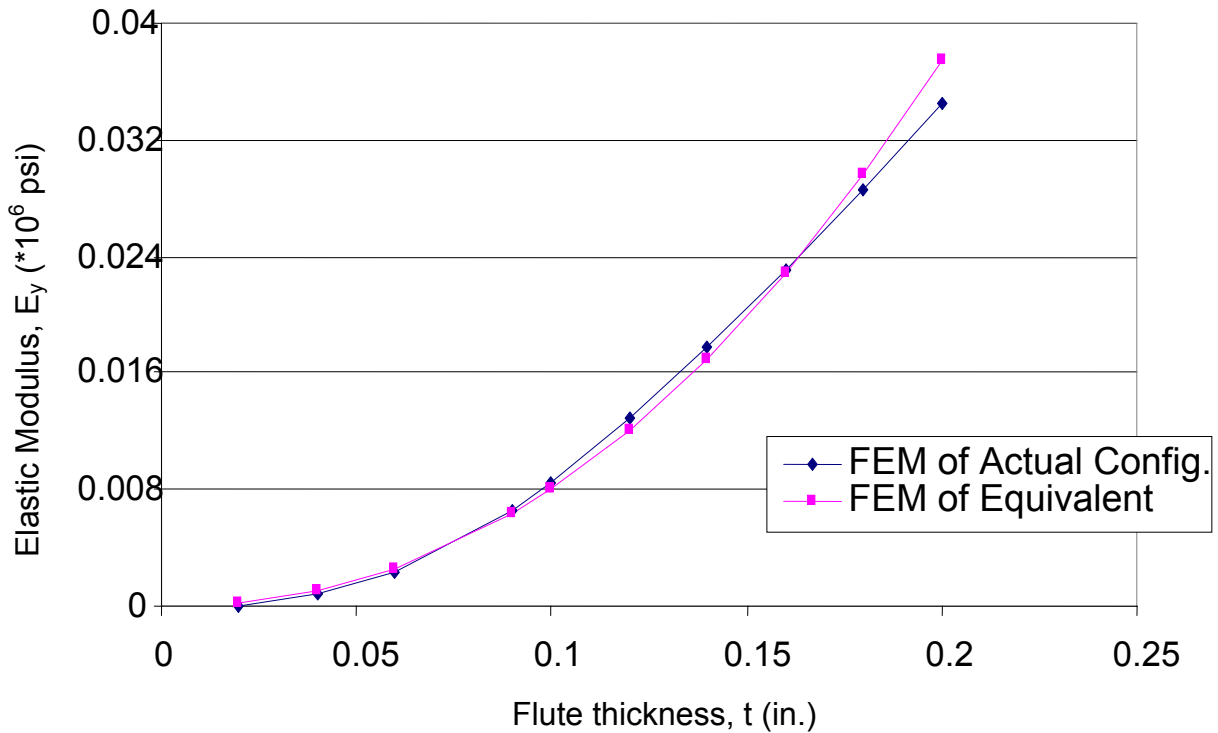


Figure 4.17: Variation of E_y with flute-thickness t

Finally, a linear relationship is observed between the modulus of elasticity of the flat/flute E₁₁ (or E₂₂) and the equivalent Young's Modulus E_y. This linear relationship can be visualized in the graph in Fig. 4.18. E₁₁ was varied between 500 ksi and 6,500 ksi. The variation can be expressed by the following equation:

$$E_y = z + wE_{11} \quad \text{Equation 4.18}$$

where $z = 2.0181E - 04$ and $w = 3.7114E - 03$.

It is noted that in this case also, there is a very good fit between the graphs for the proposed equivalent equation and the actual configuration model as can be observed from Fig. 4.18. The difference between both data sets as computed is about 0.15%.

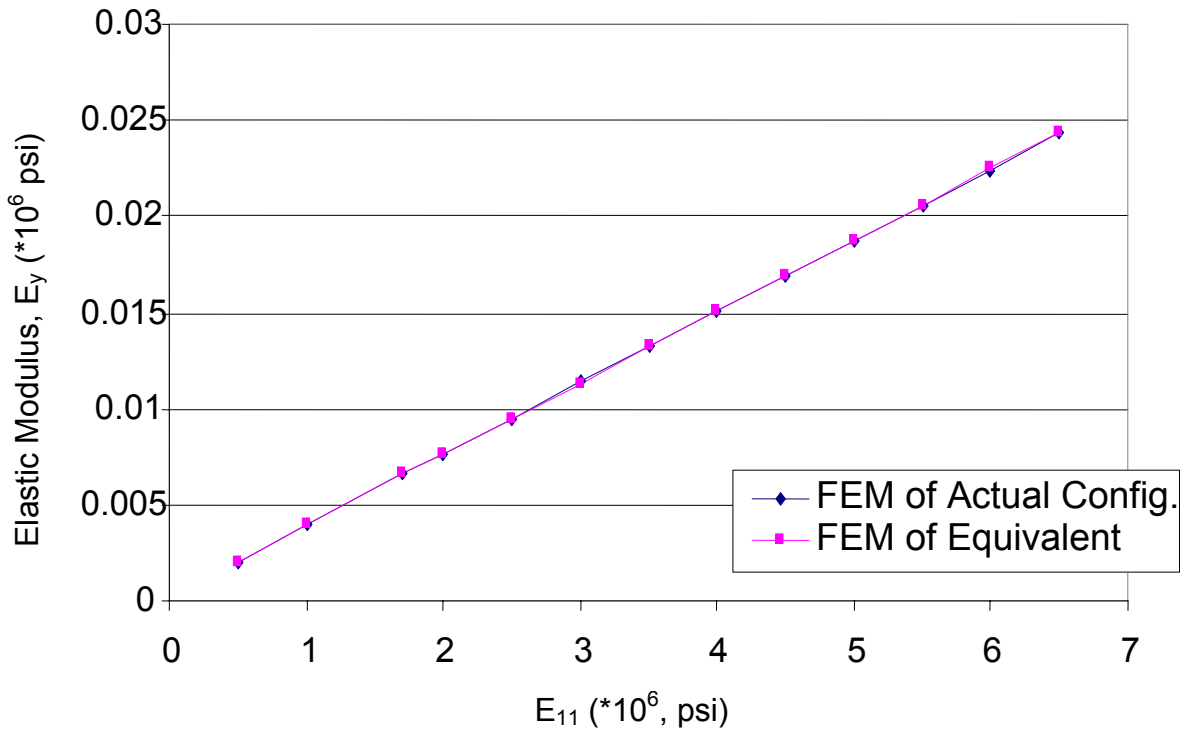


Figure 4.18: Variation of E_y with material Young's modulus E_{11}

Here again, Equations 4.14 to 4.18 could be used to compute the elastic modulus in the lateral direction (E_y) of the FRP sinusoidal wave core manufactured by KSCI when only one of its parameters is changed from the original basic value. However, it must be noted that E_y obtained is true only for in-plane (axial) behavior. Also, this is limited to the linear elastic range.

4.5.1 Modification Factors

To obtain a more general equation relating the elastic modulus E_y and the other parameters, the same systematic approach as used in Section 4.4 is followed. Therefore, a derivation of modification factors is needed. The most sensitive parameter is the half-wavelength, whose relationship with E_y is found in Equation 4.14.

4.5.1.1 Flute-width Modification Factor, S1

It was observed previously that the elastic constant E_y increases as flute-width w increases, and this relation is found in Equation 4.15. This behavior is similar to that of the modification factor. A plot of the modification factor for flute-width, $S_1 (= E_y / E_{y(w=2)})$ against the ratio $R_1 (= W / W_2)$ is seen in Fig. 4.19. W_2 represents the basic flute-width of 2 in. and $E_{y(w=2)}$ is the elastic modulus of the panel when the flute-width is 2 in. The equation representing this relationship is:

$$S_1 = \alpha + m \ln R_1 \quad \text{Equation 4.19}$$

where $\alpha = 1.0246$, $m = 0.9977$, $R_1 = 0.5W$ and W is in inches.

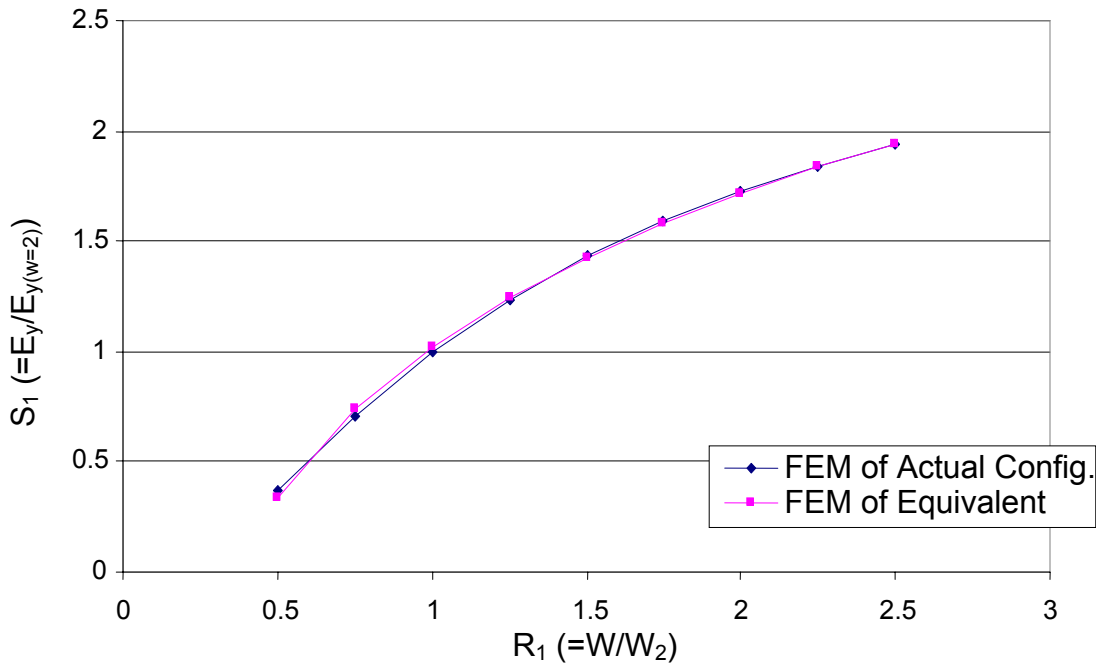


Figure 4.19: Variation of modification factor S1 with flute-width ratio R1

4.5.1.2 Panel Depth Modification Factor, S_2

From Equation 4.16 (or Fig. 4.16), the modulus of elasticity decreases slightly with an increase in panel depth H . To obtain the panel depth modification factor, the depth ratio $R_2 (= H/H_{4.57})$ is varied for a range of depth between 2 in. and 20 in., where $H_{4.57}$ is the basic panel depth of 4.57 in. When the ratio $E_y / E_{y(H=4.57)}$ is plotted against R_2 , the graph in Fig. 4.20 is obtained. The ratio $E_y / E_{y(H=4.57)}$ is the panel depth modification factor S_2 , and $E_{y(H=4.57)}$ represents the transverse elastic modulus at a depth of 4.57 in. The equation defining this relationship can be represented as follows:

$$S_2 = \beta(R_2^p) \quad \text{Equation 4.20}$$

where $\beta = 1.0065$, $p = -2.5138E-02$, $R_2 = H / 4.57$ and H is in inches.

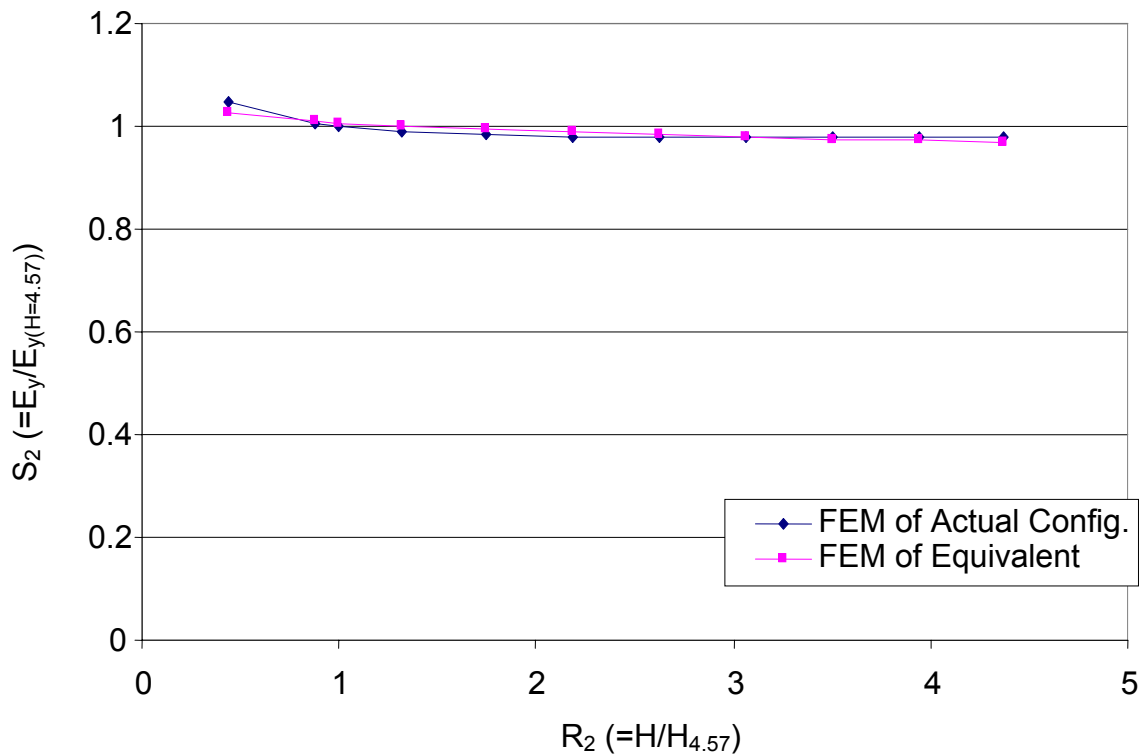


Figure 4.20: Variation of modification factor S_2 with panel depth ratio R_2

4.5.1.3 Flat/Flute Thickness Modification Factor, S_3

The equation showing the relationship between the flat/flute thickness and the elastic constant was derived in the previous section (Equation 4.17). This can also be visualized in Fig. 4.17. To obtain the modification factor for the flat/flute S_3 , the same procedure as previously described for the other parameters is followed. The thickness ratio $R_3 (= t / t_{0.0898})$ for a range of t between 0.02 in. and 0.2 in. is computed, where $t_{0.0898}$ is the basic flat/flute thickness, 0.0898 in. A plot of the modification factor $S_3 (= E_y / E_{y(t=0.0898)})$ against R_3 is made, to obtain the graph in Fig. 4.21. The equation can thus be written as:

$$S_3 = b(R_3^c) \quad \text{Equation 4.21}$$

where $b = 0.9603$, $c = 2.2267$, $R_3 = t / 0.0898$ and t is in inches.

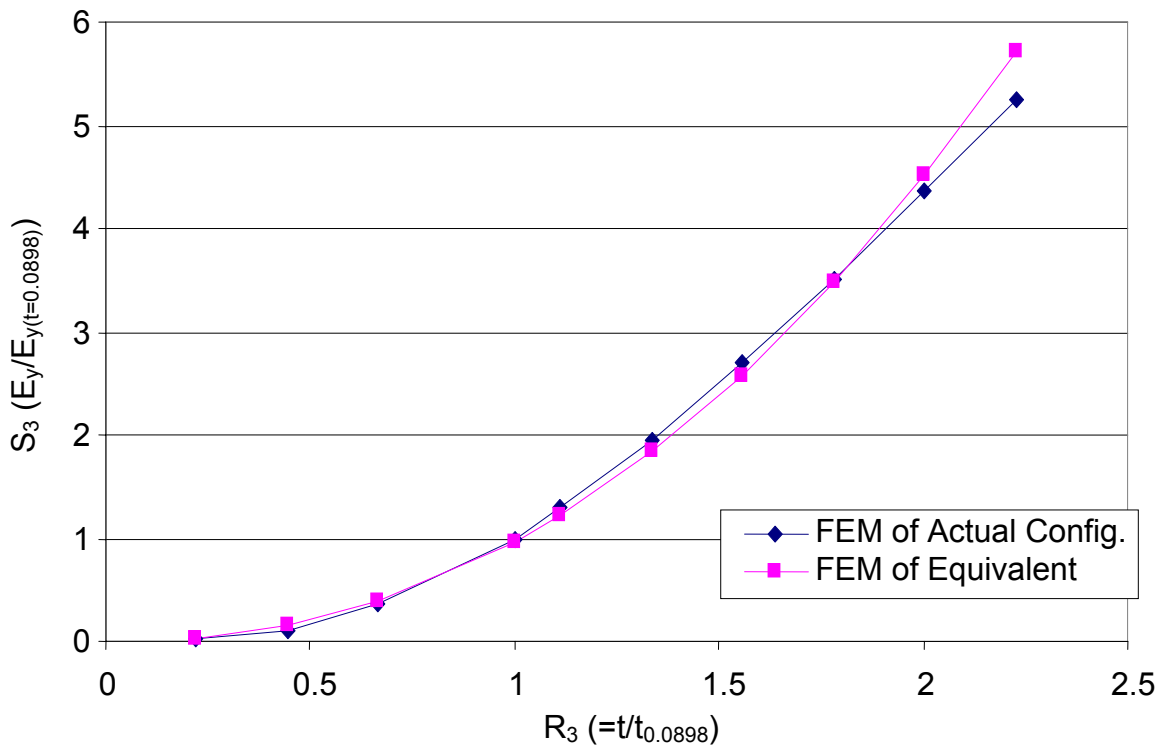


Figure 4.21: Variation of modification factor S_3 with panel depth ratio R_3

4.5.1.4 Flat/Flute Young's Modulus Modification Factor, S_4

Finally, a general equation for the modification factor of core laminate material stiffness and the equivalent modulus of elasticity is derived. The relationship between E_x and E_{11} is linear as can be seen from Equation 4.18. In Fig. 4.22, modification factor $K_4 (= E_x / E_x(E_{11b}))$ is plotted against elastic modulus ratio $R_4 (= E_{11} / E_{11b})$. This relationship can be expressed by the following equation:

$$S_4 = g + kR_4 \quad \text{Equation 4.22}$$

where $g = 3.0766E - 02$, $k = 0.9676$, $R_4 = \frac{E_{11}}{(1.71E + 6)}$ and E_{11} is in psi.

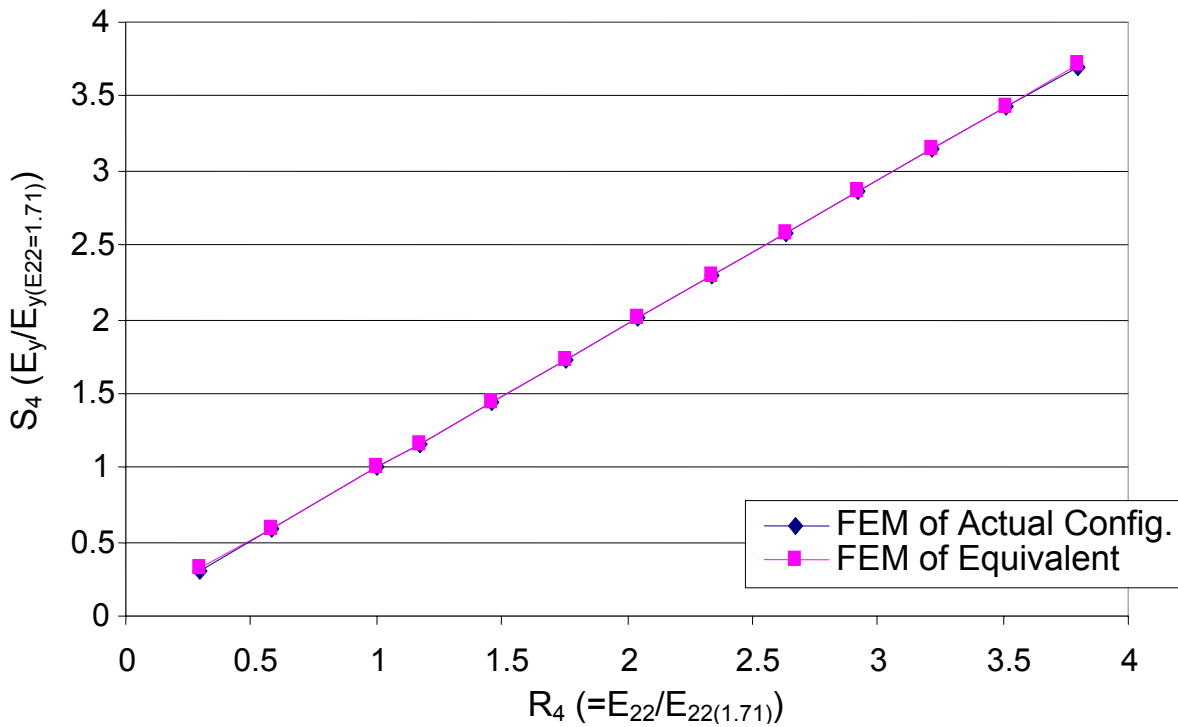


Figure 4.22: Variation of modification factor S_4 with panel depth ratio R_4

4.5.2 Formula for Predicting Transverse Young's Modulus of the Core

From the derivations above, the following formula for calculating the modulus of elasticity in the transverse direction E_y is now proposed:

$$E_y = S_1 S_2 S_3 S_4 a L^n \quad \text{Equation 4.23}$$

where $a = 7.2066E + 05$, $n = -3.4594$, L is the half-wavelength (in.), S_1 represents the flute width modification factor from Equation 4.19, S_2 symbolizes the panel depth modification factor from Equation 4.20, S_3 refers to the flat/flute thickness modification factor from Equation 4.21 and S_4 is the flat/flute Young's Modulus modification factor from Equation 4.22.

From Equations 4.14 to 4.23, the equation below is obtained:

$$E_y = S L^k H^r t^q (C + \ln W) E_{11} \quad \text{Equation 4.24}$$

where $S = 9.3770E + 01$, $k = -3.4594$, $r = -2.5138E - 02$, $q = 2.2267$ and $C = 0.3069$.

4.6 Parameters Affecting the Young's Modulus in the Vertical Direction

Using the same loading and boundary conditions as in the two previous cases, but this time in the vertical direction, the elastic modulus E_z is calculated using the constitutive stress-strain relationship below:

$$E_z = \frac{\sigma_z H}{\Delta H} \quad \text{Equation 4.25}$$

Fig. 4.23 shows plots of equivalent elastic modulus E_z against flute-width, half-wavelength and panel depth. The most sensitive of the three parameters is the flute-width W which results in a decrease in E_z as it is varied within a range of 0.5 in. to 5 in. As has been the practice, the other parameters are kept constant at their basic

parametric values while W is varied. The relationship between the flute-width W and the elastic modulus E_z can be expressed as follows:

$$E_z = aW^n \quad \text{Equation 4.26}$$

where $a = 3.4890E + 05$ and $n = -0.7194$.

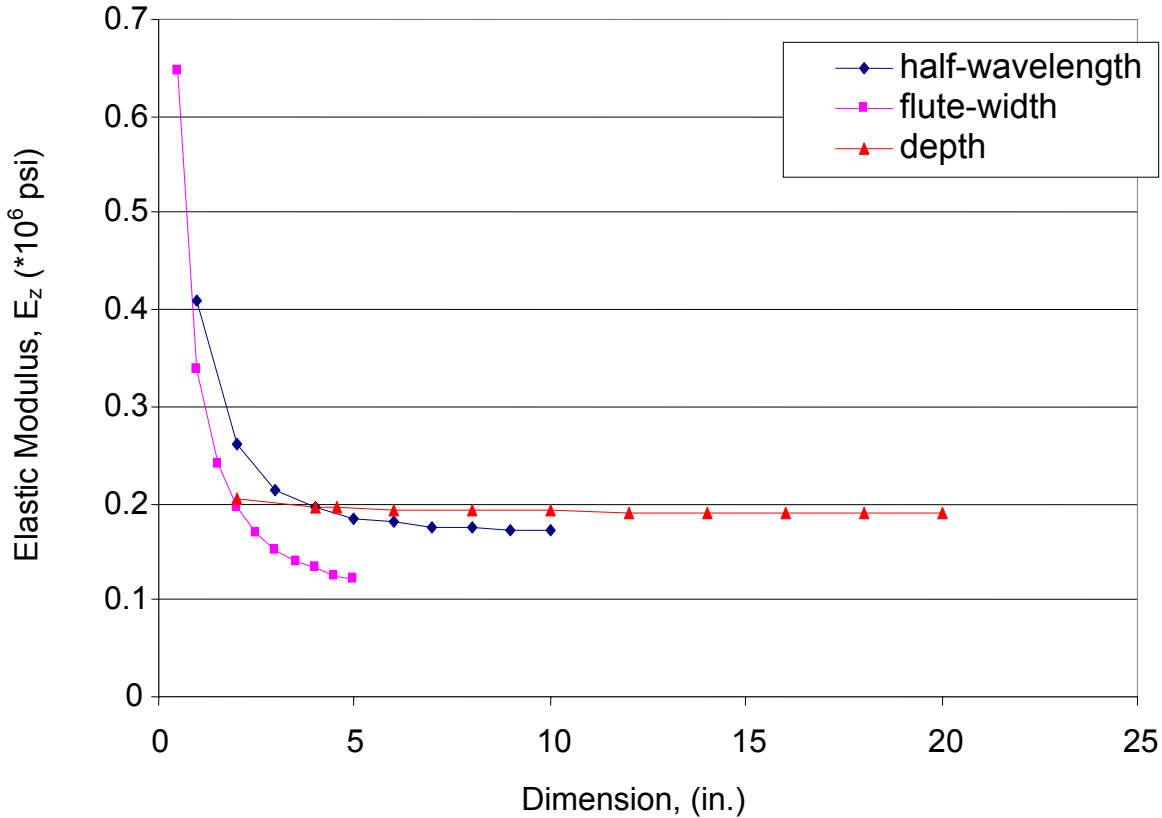


Figure 4.23: Variation of E_z with panel depth, flute-width and half-wavelength

From Fig. 4.24, an acceptable curve fit of the actual configuration model results obtained from the finite element analysis can be observed. The average difference between the curves for the “FEM of Equivalent” and the “FEM for Actual Config.” is computed to be about 5%.

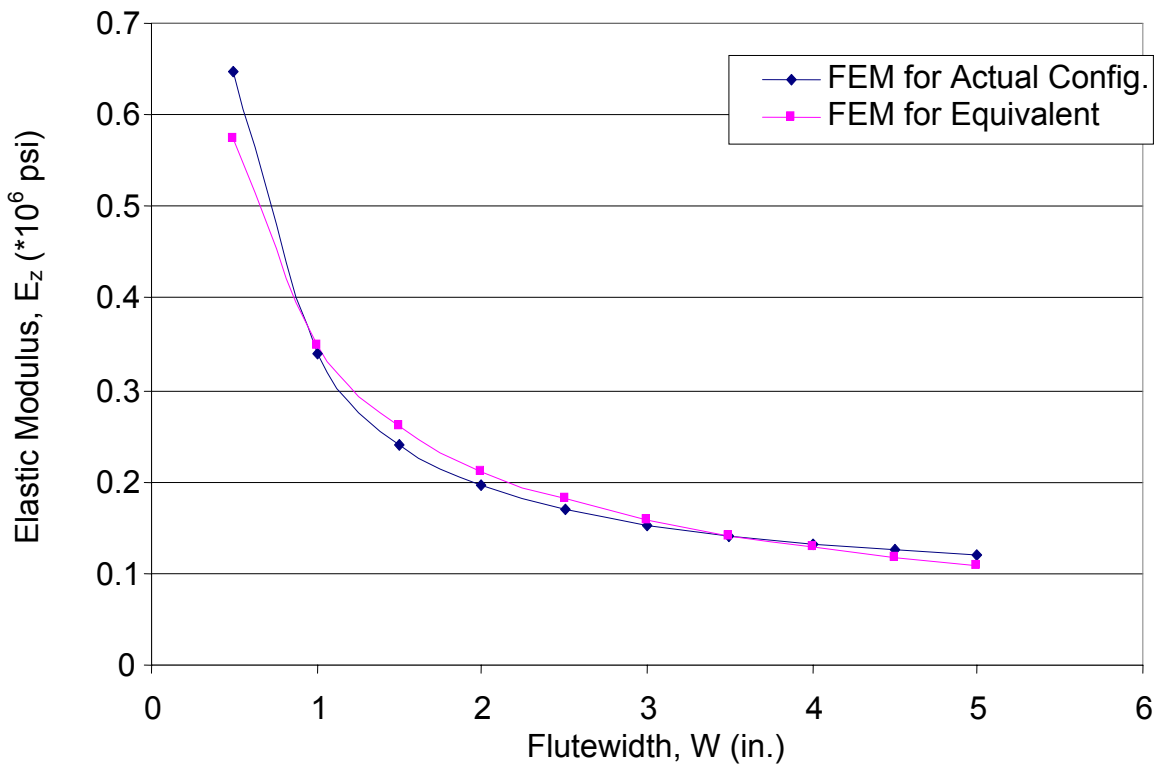


Figure 4.24: Variation of Ez with flute-width W

Similarly, varying the half-wavelength L (and keeping other parameters constant) within a range of 1 in. to 10 in., a decrease in E_z is observed as L increases (Fig. 4.25).

The equation for this variation can be expressed as follows:

$$E_z = dL^m \tag{Equation 4.27}$$

where $d = 3.5107E + 05$ and $m = -0.3538$.

Fig. 4.25 also shows a pretty good curve fit of the actual configuration results obtained from the finite element analysis by the proposed equivalent equation (Equation 4.27). The difference between both curves in the figure is about 6%.

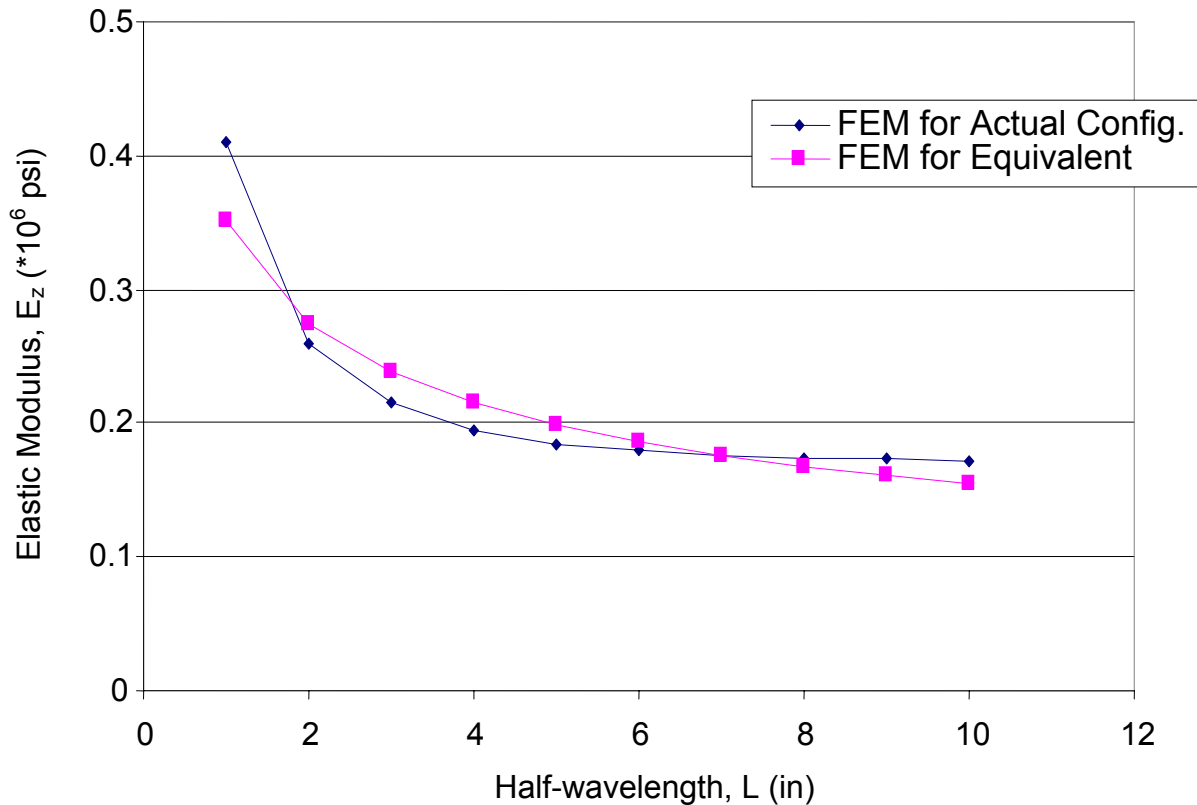


Figure 4.25: Variation of E_z with half-wavelength L

On the other hand, the panel depth H has only slight effect on the elastic modulus as it is varied from 2 in. to 20 in. (Fig. 4.26). There is a decrease in the equivalent elastic constant as this parameter is increased. This decrease in E_z can be expressed by the following equation:

$$E_z = fH^r \quad \text{Equation 4.28}$$

where $f = 2.0394E + 05$ and $r = -2.5096E - 02$.

A close look at Fig. 4.26 reveals a very good curve fit of the actual configuration results from the finite element analysis by the proposed equivalent formula in Equation 4.28. The average difference between both curves is only about 0.5%.

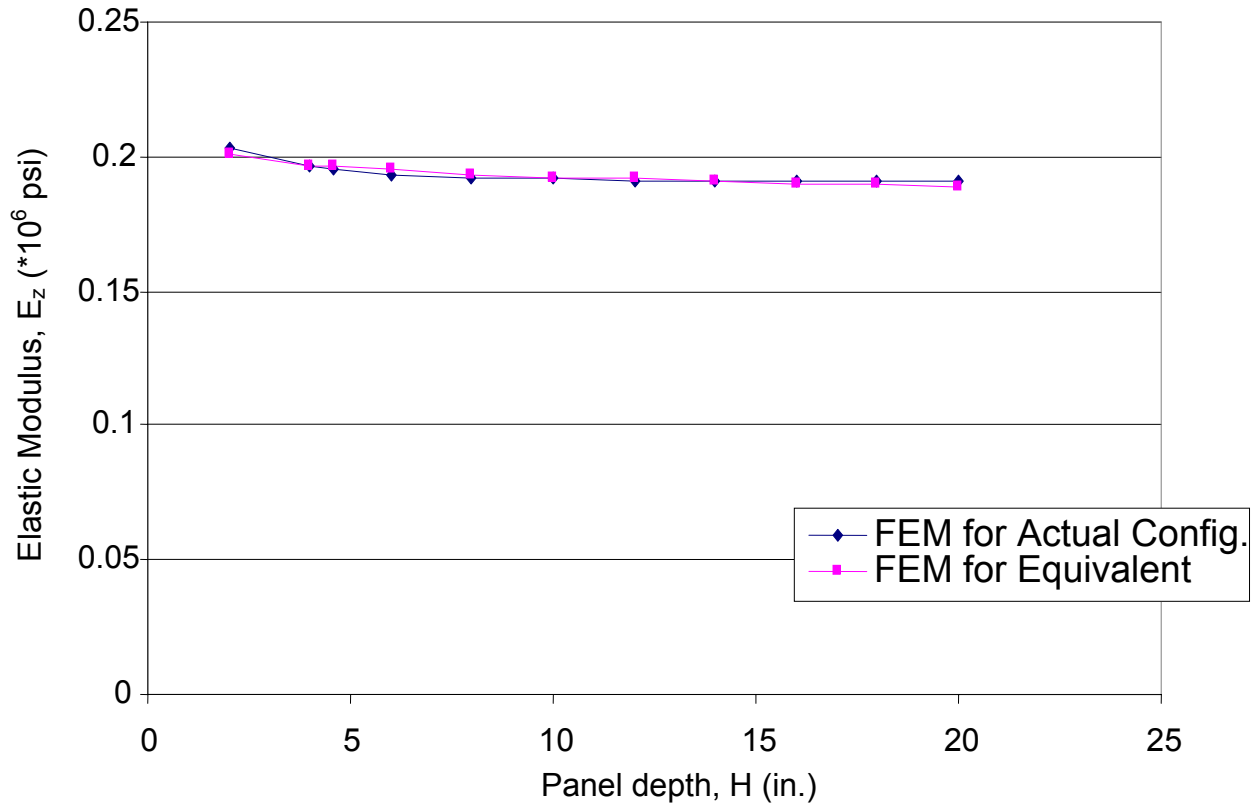


Figure 4.26: Variation of E_z with panel depth H

Fig. 4.27 shows a linear relationship between the flat/flute thickness t and the elastic constant as t is varied from 0.02 in. to 0.2 in. The following equation describes this relationship:

$$E_z = u + vt \tag{Equation 4.29}$$

where $u = -8.1127E - 04$ and $v = 2.1833$.

The curve fit by the proposed equivalent formula in Equation 4.29 of the actual configuration results from the analysis can be seen to be very good. (Fig. 4.27) The difference between the two graphs in the figure is only about 0.1%.

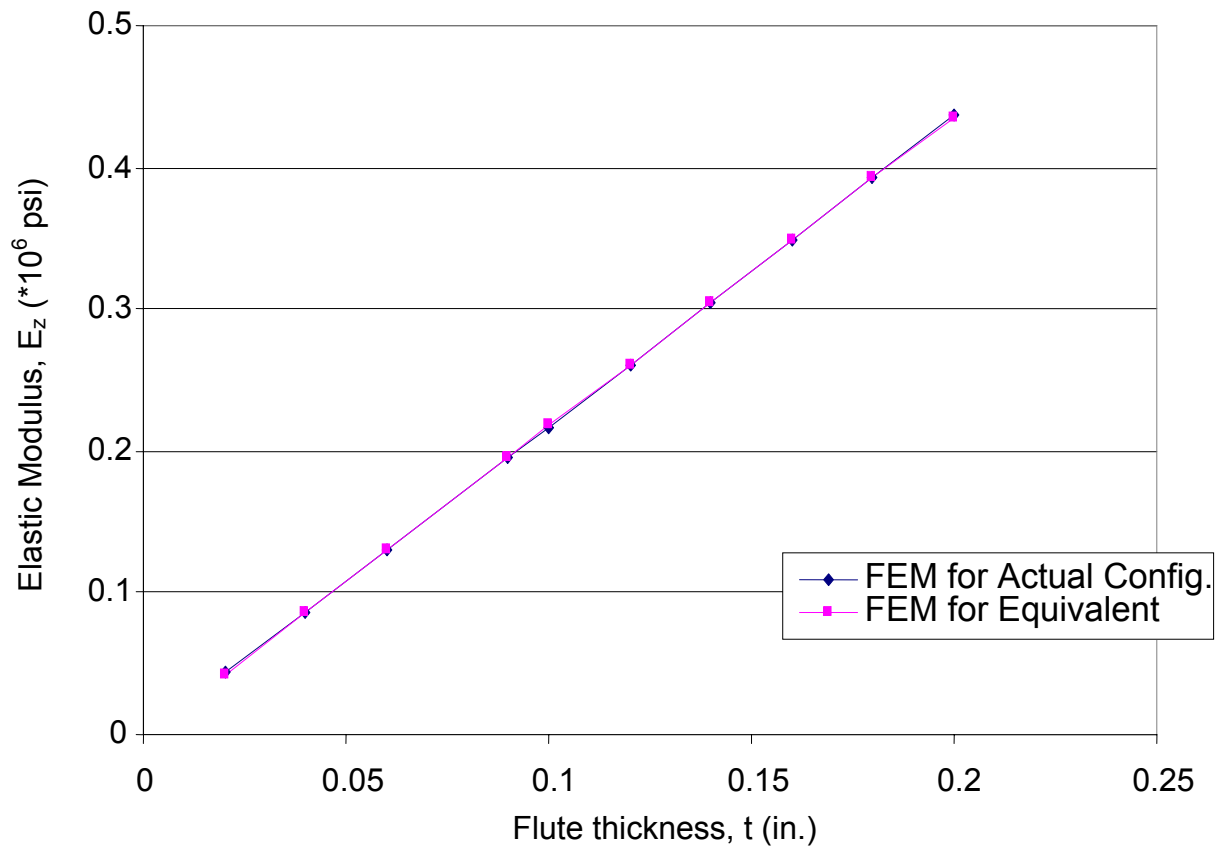


Figure 4.27: Variation of E_z with flute thickness t

Lastly, a linear relationship between the modulus of elasticity of the flat/flute E_{11} (or E_{22}) and the equivalent Young's Modulus E_z is also observed. Fig. 4.28 shows that as E_{11} increases from 500 ksi to 6,500 ksi, E_z rises correspondingly. The formula below defines this variation:

$$E_z = z + wE_{11} \quad \text{Equation 4.30}$$

where $z = 2.5707E - 03$ and $w = 0.1125$.

Once again, from Fig. 4.28 a very good curve fit between both plots can be observed. The average difference is computed to be about 0.2%.

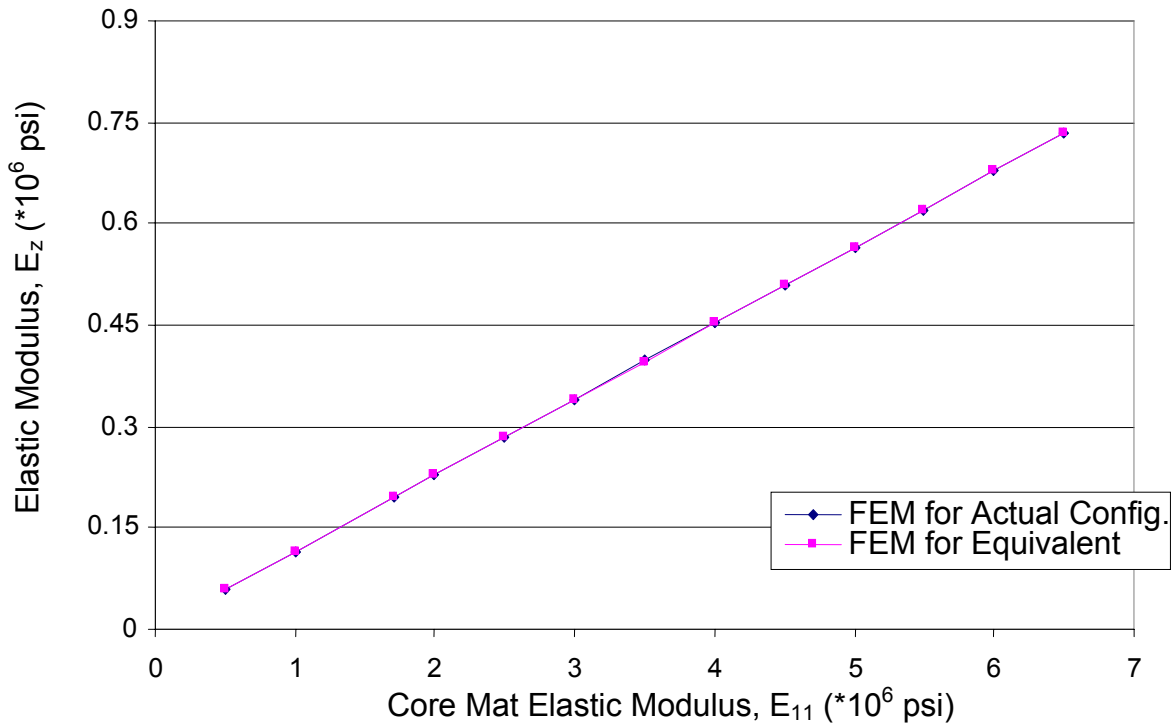


Figure 4.28: Variation of EZ with core material Young's Modulus E11

A similar conclusion can be reached about Equations 4.26 to 4.30 as was done for E_x and E_y . These equations could be used to compute the elastic modulus in the vertical direction (E_z) of the FRP sinusoidal wave core manufactured by KSCI when only one of its parameters is changed from its original basic value. It must be noted though, that E_z obtained is true only for in-plane (axial) behavior and is limited to the linear elastic range.

4.6.1 Modification Factors

Just as was done for the two other directions, modification factors of the equivalent elastic constant in the vertical direction for variation in core parameters is now sought. This will lead to a more general equation relating E_z and core properties.

First of all, it should be noted that the most sensitive parameter is the flute-width. The equation relating E_z and W is found in Equation 4.26.

4.6.1.1 Half-wavelength Modification Factor, D1

From Fig. 4.25, E_z decreases as half-wavelength L increases, and this relation is found in Equation 4.27. Similarly, by plotting the modification factor for half-wavelength, $D_1 (= E_z / E_{z(L=4)})$ against the ratio $R_1 (= L / L_4)$, the graph in Fig. 4.29 is obtained. L_4 represents the basic half-wavelength of 4 in. and $E_{z(L=4)}$ is the elastic modulus of the panel when the half-wavelength is 4 in. The equation can be expressed as follows:

$$D_1 = \alpha R_1^m \quad \text{Equation 4.31}$$

where $\alpha = 1.1021$, $m = -0.3538$, $R_1 = 0.25L$ and L is in inches.

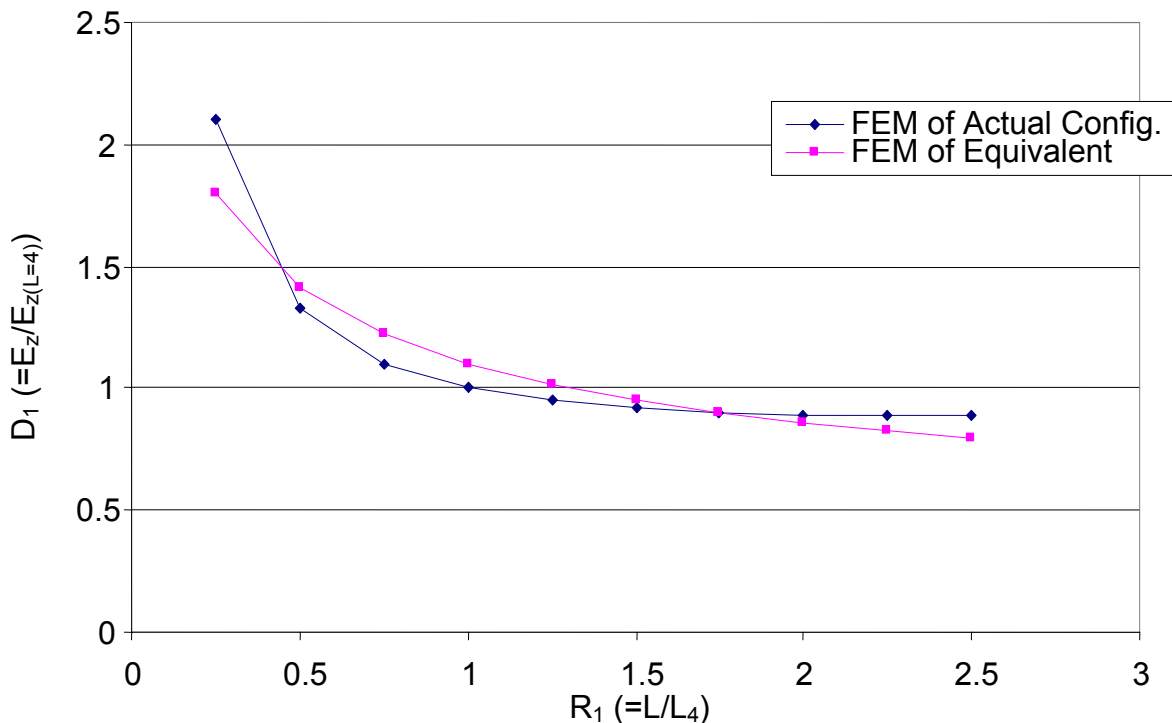


Figure 4.29: Variation of modification factor D1 with wave-length ratio R1

4.6.1.2 Panel Depth Modification Factor, D2

The second modification factor required is that with respect to panel depth H . Notice from Fig. 4.26 that E_z increases slightly as H rises. The panel depth modification factor is obtained by varying the depth ratio $R_2 (= H/H_{4.57})$ for a range of depth between 2 in. and 20 in., where $H_{4.57}$ is the basic panel depth of 4.57 in. By plotting this variation, the graph in Fig. 4.30 is obtained. D_2 represents the panel depth modification factor $E_z / E_{z(H=4.57)}$, where $E_{z(H=4.57)}$ is the transverse elastic modulus at a depth of 4.57 in.

The following equation defines this relationship:

$$D_2 = \beta R_2^p \quad \text{Equation 4.32}$$

where $\beta = 1.0064$, $p = -2.5096E - 02$, $R_2 = H / 4.57$ and H is in inches.

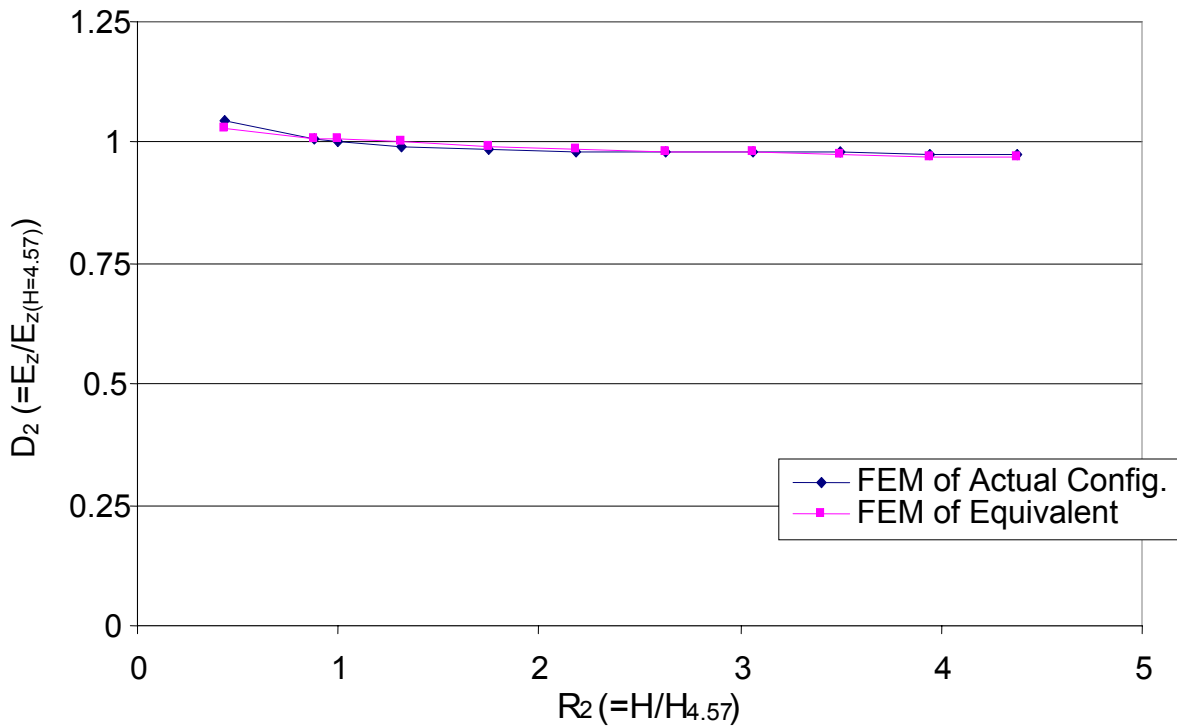


Figure 4.30: Variation of modification factor D2 with panel depth ratio R2

4.6.1.3 Flat/Flute Thickness Modification Factor, D3

The flute/flute thickness t has a linear effect on the elastic modulus E_z . This behavior is found in Fig. 4.27 and Equation 4.29. The thickness ratio, $R_3 (= t / t_{0.0898})$ is computed for a range of t between 0.02 in. and 0.2 in. where $t_{0.0898}$ is the basic flat flute thickness, 0.0898 in. In Fig. 4.31, the modification factor $D_3 (= E_z / E_{z(t=0.0898)})$ is plotted against R_3 . The expression for the flat/flute modification factor can be written as follows:

$$D_3 = b + cR_3 \quad \text{Equation 4.33}$$

where $b = -4.1591E - 03$, $c = 1.0051$, $R_3 = t / 0.0898$ and t is in inches.

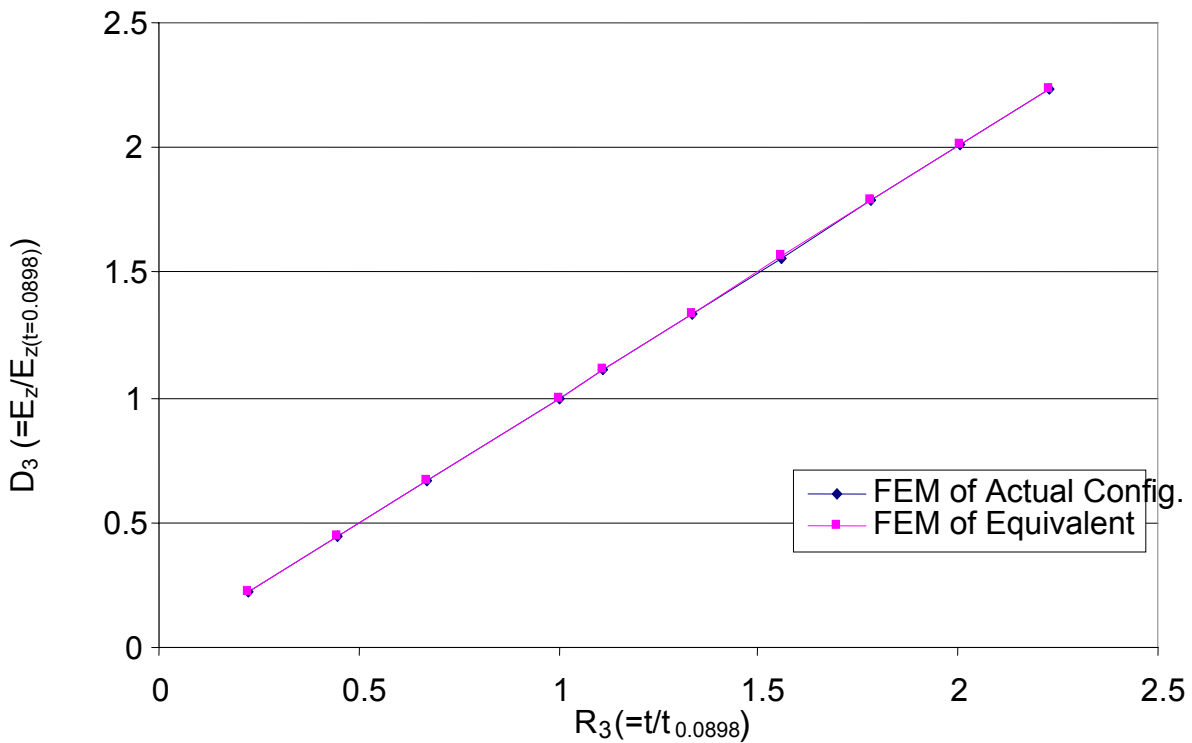


Figure 4.31: Variation of modification factor D3 with flute/flat thickness ratio R3

4.6.1.4 Flat/Flute Young's Modulus Modification Factor, D4

The final parameter to be considered is the core laminate material stiffness E_{11} . An equation for modification factor of the equivalent modulus of elasticity due to E_{11} is sought. It can be recalled from Equation 4.30 that E_x and E_{11} have a linear relationship. Fig. 4.32 shows the relationship between elastic modulus ratio $R_4 (= E_{11} / E_{11b})$ and modification factor $D_4 (= E_z / E_z(E_{11b}))$. From a regression analysis, this relationship can be expressed in the form:

$$D_4 = g + kR_4 \quad \text{Equation 4.34}$$

where $g = 1.3179E - 02$, $k = 0.9859$, $R_4 = \frac{E_{11}}{(1.71E + 6)}$ and E_{11} is in psi.

It is noted that in each case, there is very good curve fit of the “FEM of Actual Config.” plot by the “FEM of Equivalent” plot from the analysis.

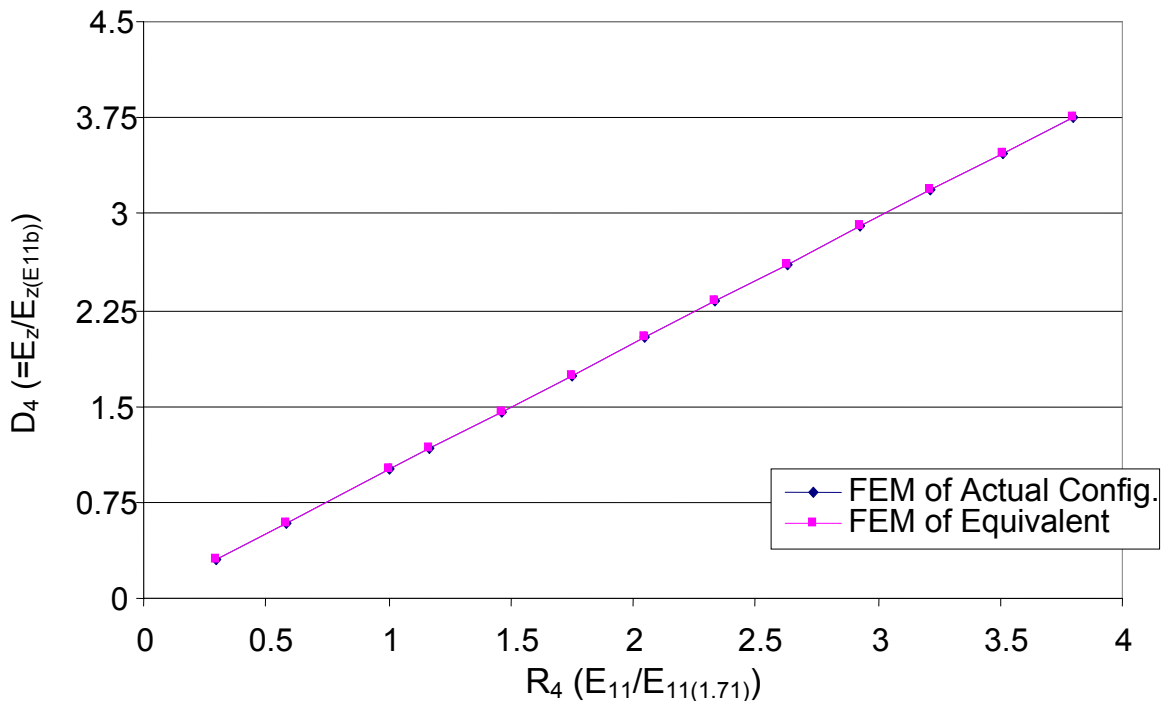


Figure 4.32: Variation of modification factor D4 with material Young's Modulus ratio R4

4.6.2 Formula for Predicting Vertical Young's Modulus of the Core

The following formula for calculating the modulus of elasticity in the vertical direction E_z is now proposed:

$$E_z = D_1 D_2 D_3 D_4 a W^n \quad \text{Equation 4.35}$$

where $a = 3.4890E + 05$, $n = -0.7194$, W = flute width (in.), D_1 represents the half-wavelength modification factor from Equation 4.31, D_2 refers to the panel depth modification factor from Equation 4.32, D_3 symbolizes the flat/flute thickness modification factor from Equation 4.33 and D_4 is the flat/flute Young's Modulus modification factor from Equation 4.34.

From Equations 4.26 to 4.35, the modulus of elasticity becomes:

$$E_z = D W^g L^u H^v t E_{11} \quad \text{Equation 4.36}$$

where $D = 3.8002$, $g = -0.7194$, $u = -0.3538$ and $v = -2.5096E - 02$.

4.7 Verification of Results

The results from the above formulation are compared with those from the work of Davalos et al. (2001). Davalos et al. developed an approximate solution for the equivalent elastic modulus in the longitudinal direction of the core E_x which can be seen in Equation 2.8. Different values for three of the parameters (core height H , flat/flute thickness t and core mat elastic modulus E_{11}) are used in a finite element analysis in this study to compute E_x . With those same parametric values, E_x is calculated using Equation 2.8 as well as the proposed formula in Equation 4.12. A comparison of the results from each of the two equations with the finite element analysis is presented in

Table 4.1 and Fig. 4.33. (There is no available information to compare with the results from the present study of the other two directions E_y and E_z).

Table 4.1: Comparison of results for E_x

Data #	H (in.)	t (in.)	E_{11} ($\times 10^6$ psi)	E_x ($\times 10^6$ psi)			% Diff with Actual Configuration FEM Results	
				Actual Configuration FEM	Equivalent FEM (Present) (Eqn. 4.12)	Davalos et al. (Eqn. 2.8)	Equivalent FEM (Present)	Davalos et al.
1	6	0.04	1	0.0458	0.0469	0.04	2.40	12.71
2	22.5	0.04	1	0.0473	0.0473	0.04	0.04	15.35
3	6	0.15	1	0.1743	0.1774	0.15	1.74	13.92
4	22.5	0.15	1	0.1795	0.1773	0.15	1.26	16.44
5	6	0.04	5	0.2212	0.2221	0.2	0.39	9.58
6	22.5	0.04	5	0.2337	0.2364	0.2	1.13	14.42
7	6	0.15	5	0.8412	0.8418	0.75	0.07	10.84
8	22.5	0.15	5	0.8878	0.8863	0.75	0.17	15.52

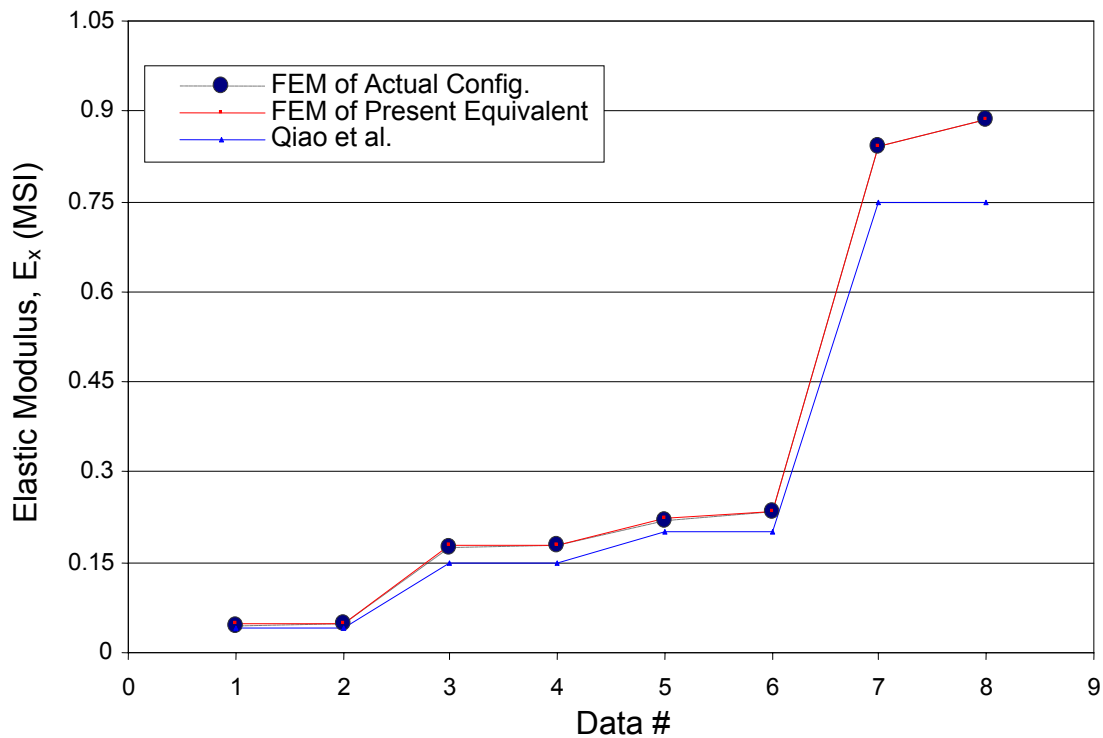


Figure 4.33: Plots of E_x results for comparison

It can be observed from Table 4.1 and Fig. 4.33 that the proposed equation (Equation 4.12) compares very well with the results from finite element analysis (FEM). The average difference between both data sets is about 0.8%. On the other hand, Equation 2.8 (Davalos et al.) does not compare as well with the results from FEM. There is an average difference of about 14% between both results. Equation 2.8 is a much simplified formula which does not take into account the geometric configuration of the core structure. It assumes that the stiffness contribution of the flute is negligible. Thus the proposed formula in Equation 4.12 can be used with a high level of confidence.

Therefore, with the equations derived in this chapter, equivalent elastic constants could be calculated from known geometric parameters and material properties.

CHAPTER 5 - DERIVATION OF PROPERTIES FOR OUT-OF-PLANE BEHAVIOR

5.1 Introduction

In the previous two chapters attention was given to elastic stiffness properties for in-plane behavior of the FRP sinusoidal wave core. As discussed, the application of this study would be in situations where axial effects of a structure are being analyzed. In this chapter, focus is directed to properties related to out-of-plane behavior. This behavior will include the bending of beams and decks. In this chapter, we develop and verify an approach to obtain the flexural and shear stiffness properties of the sinusoidal wave core sandwich panel. Then in chapter 6, following the verified approach, parametric studies will be performed to develop stiffness equations for the out-of-plane behavior.

To achieve our goal in this chapter, we seek to derive a single layered equivalent model of the entire sandwich panel – that is, a single layer whose out-of-plane behavior is the same as the actual sandwich panel including the top and bottom faces (or called skins) and the core. In the case of in-plane behavior, once we know the equivalent core, the faces can be added to the equivalent core and the total in-plane properties can be calculated easily. However, it is not the case for the out-of-plane behavior. Therefore, the faces are added to the finite element model to predict an equivalent layer for the entire section, which makes it more complicated than the case of in-plane behavior. As we will find, this approach yields properties that are more valid for bending deflection purposes than does the three-layered equivalent model formulated in the previous two chapters that should be limited to the applications of in-plane behavior.

First, the equivalent properties in the three orthogonal directions are derived using a beam model with the actual core configuration. Using a beam to represent a deck is by no means a new concept. In bridge design, one of the approaches used is to view the deck as a series of several beams joined together laterally. The beam has either a unit or an equivalent width. Similarly, in the approach proposed here, a beam model with a certain width will be used.

After the properties are derived, they are verified by comparing deflection results from finite element modeling of a sandwich beam and its equivalent model. Once verified, the properties can finally be applied to the equivalent model of a full-scale sinusoidal core sandwich bridge panel. A final verification is done to check if the application to a full scale bridge panel is valid.

5.2 Beam Analysis

To accurately predict the out-of-plane behavior of the sandwich structure, the beam is subjected to bending forces instead of axial loads. With this approach, the effects of the stiffness contribution provided by both the face laminates and the core of the sandwich structure for a single layer equivalent structure are captured.

Two factors contribute to the deflection of beams subjected to vertical loads – shear and bending. The shear contribution, however, becomes less significant as the beam becomes shallower. Therefore, use is made of a beam model with a very high span-to-depth ratio – 15 foot span and only 5 inches deep. The shear contribution to deflection can thus be neglected. This is a safe assumption for a beam whose span to depth ratio is greater than 10.

5.2.1 Modulus of Elasticity in Longitudinal Direction, E_x

The first step in this approach is to derive the equivalent elastic modulus in the longitudinal direction E_x for out-of-plane (bending) behavior. The beam model is subjected to conditions of a cantilever. To obtain E_x , stiff shell elements are placed at the two longitudinal ends of the sandwich beam model. The beam is 15 foot in span (L), 8 inches wide and 5 inches deep. It is cantilevered by constraining the nodes at one end for translational and rotational motions. At the other end, a force of 10,000 lb is applied in the vertical direction, causing the beam to bend about its lateral axis. In this way, the structure can be analyzed as a simple beam using the classic beam theory. From the finite element results for deflection, E_x can be calculated as below:

$$E_x = \frac{P_z L^3}{3\delta_z I_{yy}} \quad \text{Equation 5.1}$$

where P_z is the applied vertical force, L represents the span of the beam, δ_z refers to the vertical end deflection of the beam and I_{yy} symbolizes the moment of inertia about the lateral axis.

5.2.2 Modulus of Elasticity in Lateral Direction, E_y

The same approach is used to derive the equivalent elastic modulus in the lateral direction. However, in this case, the beam is made 15 feet in the lateral direction (W) of the deck and 8 inches in the longitudinal direction of the deck since interest is in the transverse direction. As previously, rigid shell elements are used, but this time placed at the two transverse ends of the beam model. The same constraints are imposed to simulate a cantilever, and a 10,000 lb vertical load is applied at the free end of the cantilever. E_y can thus be computed from the formula below:

$$E_y = \frac{P_z W^3}{3\delta_z I_{xx}} \quad \text{Equation 5.2}$$

where P_z refers to the applied vertical force, W is the span of the beam in the transverse direction, δ_z represents the vertical end deflection of the beam and I_{xx} is the moment of inertia about the longitudinal axis.

5.2.3 Shear Modulus, G

The shear contribution to deflection is sometimes ignored in structural analysis. In the case of a beam, for instance, it is usually assumed that the deflection is mainly due to the bending of the beam. But there is also shear contribution to that deflection. For long beams, this contribution from shear can be neglected since it does not contribute significantly. In other cases such as deep beams and sandwiched structures, however, the shear contribution has to be accounted for, because it can become a major factor in the structure's behavior. A more accurate procedure requires that the deflection in a beam is a summation of the contributions from bending and shear. Thus,

$$\Delta_{\text{total}} = \Delta_{\text{bending}} + \Delta_{\text{shear}} \quad \text{Equation 5.3a}$$

For a cantilever beam with a point load at the free end,

$$\Delta_{\text{bending}} = \frac{PL^3}{3EI} \quad \text{Equation 5.3b}$$

and,

$$\Delta_{\text{shear}} = \frac{PL}{GA_s} \quad \text{Equation 5.3c}$$

Since the shear contribution is not significant in long beams, the beam used is one which has a small span-to-depth ratio. It is also pertinent to note that this ratio is not

made too small, because the beam theory which is used here does not apply to very deep beams.

To obtain the equivalent shear modulus, a point load is applied to the free end of the cantilever beam model. The beam model used is 24 in. long, 8 in. wide and 5 in. deep. The relationship defined in Equation 5.3 above can therefore be applied.

5.2.3.1 Equivalent Shear Modulus, G_{xy}

Rigid shell elements are placed at the longitudinal ends of the model. In this case, the longitudinal direction (x) of the model serves as the span, which is 24 in. long (L). The nodes on one of the ends are fixed by constraining both rotational and translational degrees of freedom. At the other end, the nodes are kept free to simulate a cantilevering beam. At this same free end, a force P_y of 1,000 lb is applied to the central node in the lateral (y) direction. This force causes a displacement in the lateral direction δ_y, which is used to calculate the shear modulus G_{xy} by the following relation:

$$G_{xy} = P_y L / (A_s (\delta_y - (P_y L^3 / 3E_x I_{zz}))) \quad \text{Equation 5.4}$$

where, shear area, A_s is 1.2 times area y-z, E_x is obtained from Equation 5.1 and I_{zz} represents the moment of inertia about the vertical axis.

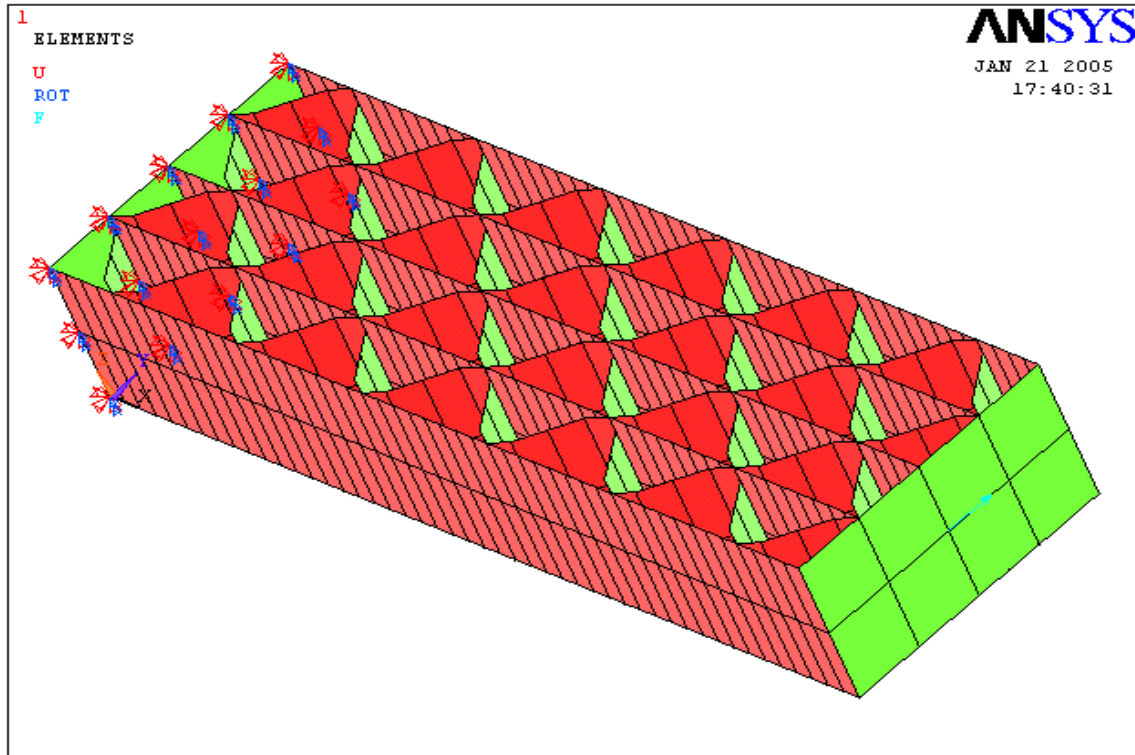


Figure 5.1: ANSYS model for deriving equivalent sandwich beam G_{xy}

In Fig. 5.1, the ANSYS model used to derive the shear modulus G_{xy} can be seen. For clarity, the top face of the model is not shown. Fig. 5.2 shows the deflection contour of the model analysis.

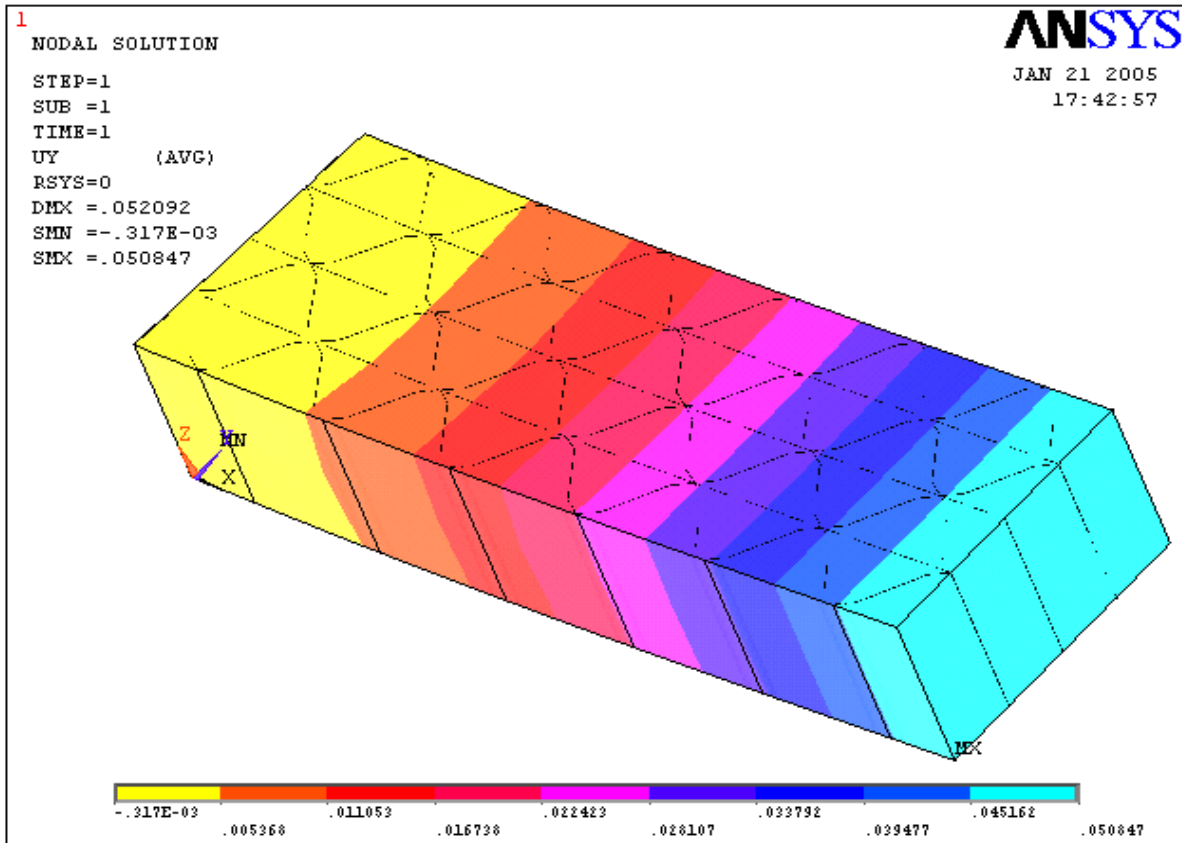


Figure 5.2: Deflection contour for sandwich beam in deriving G_{yx}

5.2.3.2 Equivalent Shear Modulus, G_{yx}

The approach above is further verified by obtaining the shear modulus G_{yx} . It is expected that G_{yx} will compare very closely to G_{xy} . This time the rigid shell elements are placed at the two lateral ends. The beam is modeled as a cantilever in the lateral (y) axis by constraining the nodes at one end from both translational displacement and rotation, while those of the other end are kept free. At the free end, a point load of 1,000 lb (P_x) is applied to the central node in the longitudinal (x) direction. Similarly, the shear modulus can be calculated from the relation below:

$$G_{yx} = P_x W / (A_s (\delta_x - (P_x W^3 / 3E_y I_{zz}))) \quad \text{Equation 5.5}$$

where W represents the span of the model (in the lateral direction), E_y is obtained from Equation 5.2, shear area, A_s is 1.2 times area x - z and I_{zz} symbolizes the moment of inertia about the vertical axis.

Fig. 5.3 shows the ANSYS model used to derive the shear modulus G_{yx} . The top face of the model is not shown for clarity purposes. Fig. 5.4 shows the deflection contour of the model.

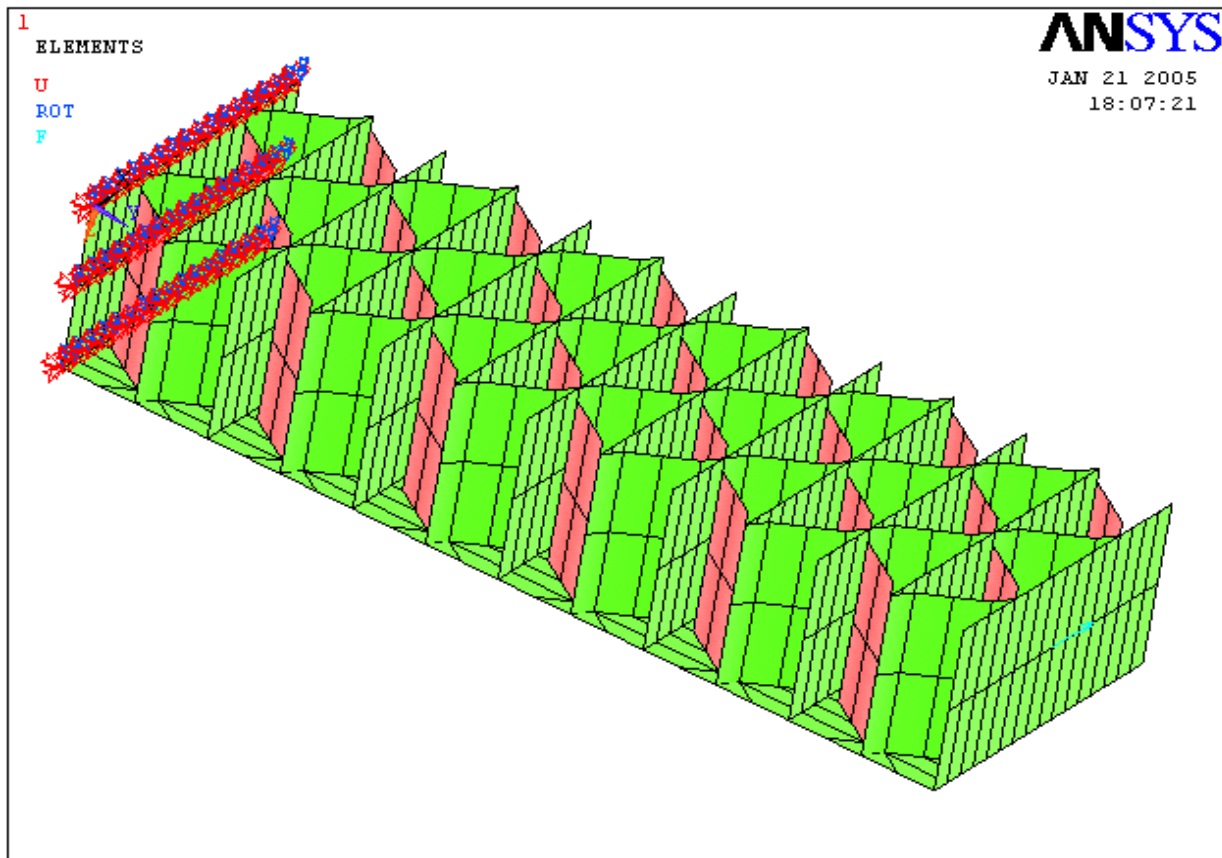


Figure 5.3: ANSYS model for deriving equivalent sandwich beam G_{yx}

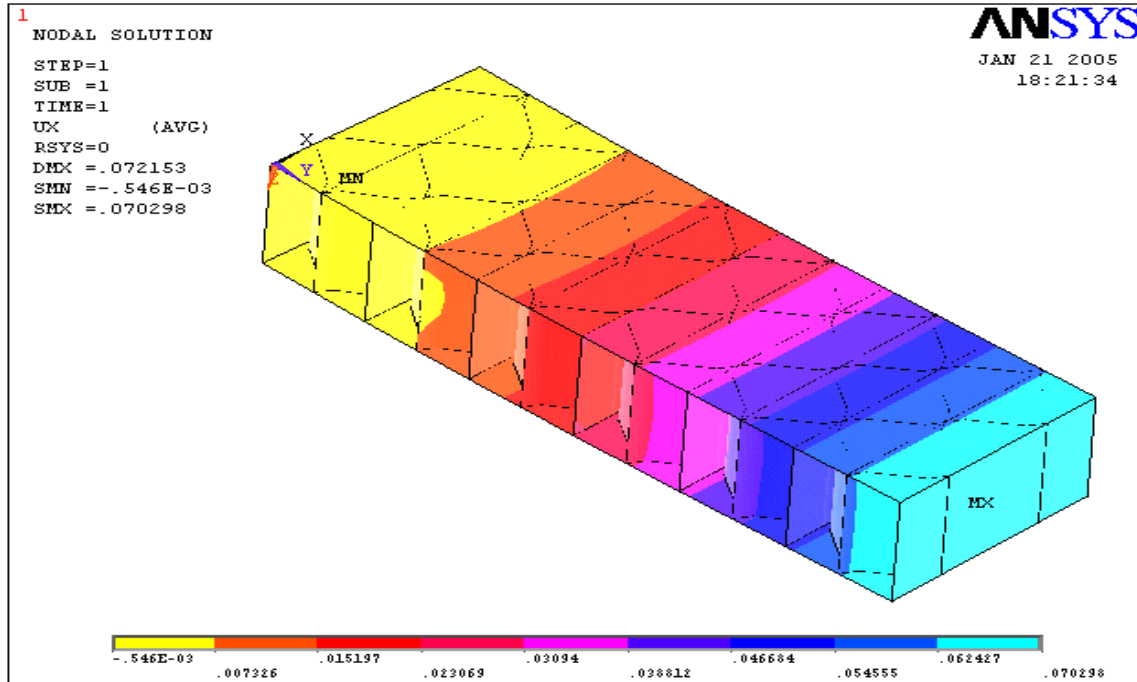


Figure 5.4: Deflection contour for sandwich beam in deriving G_{yx}

The equivalent properties derived from the analysis approach described above are presented in Table 5.1 below. As can be seen from the table, the shear moduli G_{xy} and G_{yx} compare very well. They differ by only about 4%.

Table 5.1: Single-layer equivalent properties of sandwich beam

E_x (psi)	997,306.66
E_y (psi)	819,550.03
G_{xy} (psi)	24,364.14
G_{yx} (psi)	25,423.66

Properties in the vertical (z) direction such as transverse shear (G_{xz} and G_{yz}) and modulus of elasticity in the vertical direction (E_z) are ignored. This is because their contribution to vertical deflection and strain is negligible.

5.3 Verification of Elastic Constants

5.3.1 FEM of Actual Configuration Beam

To verify these properties derived in the previous section, a beam with a span of 15 ft, width of 8 in. and depth of 5 in. is modeled having the sinusoidal core configuration and sandwich construction. The beam is simply supported by constraining nodes for vertical and lateral translations (u_z and u_y) at one end, and vertical translation (u_z) at the other. A concentrated load of 10,000 lb is applied at its midspan. This beam is analyzed using finite elements analysis, and the deflection results at quarter points along the span are recorded (Table 5.2).

5.3.2 FEM of Equivalent Beam

An equivalent beam with the same dimensions is also modeled using one-layered shell elements. The same loading and support conditions as used for the sandwich beam model are also used for this equivalent. Modeling as an orthotropic material, the equivalent properties derived in the previous section is used for this model. After the finite element analysis is performed, the deflection results at quarter points along the span are also noted (Table 5.2).

5.3.3 Hand-Calculation

Further verification of these results is done by performing hand-calculations for the beam using beam theory. Ignoring shear contribution to the deflection (which is a safe assumption in the view of the fact that span/depth > 10), the beam deflection can be calculated from the moment-curvature relationship shown in Equation 5.6 below:

$$EI \frac{d^2v(x)}{dx^2} = M(x) \quad \text{Equation 5.6}$$

From this relationship, the deflection for a simply supported beam with concentrated load at midspan can be expressed by the following formula in Equation 5.7):

$$EIv(x) = \frac{Px^3}{12} - \frac{P[x-L/2]^3}{6} - \frac{PL^2x}{16} \quad \text{Equation 5.7}$$

Three cases are considered for calculating the deflection using the approach above. The three cases vary in the way the flexural stiffness EI is calculated. The following section considers each case.

5.3.3.1 Case 1 (flange-web configuration)

In the first case, the cross-section of the beam is assumed to be composed of top and bottom flanges (representing the face laminates) and nine vertical webs. The distance between successive webs is the same for all elements. These web elements represent the flat and flute laminates which form the core of the sandwich beam. The distance between successive webs is 1 inch. In other words, the idealized model represents a cross-section of the actual sinusoidal core sandwich beam where the flats and flutes are equally spaced. This cross-section is well illustrated in Figure 5.5 below.

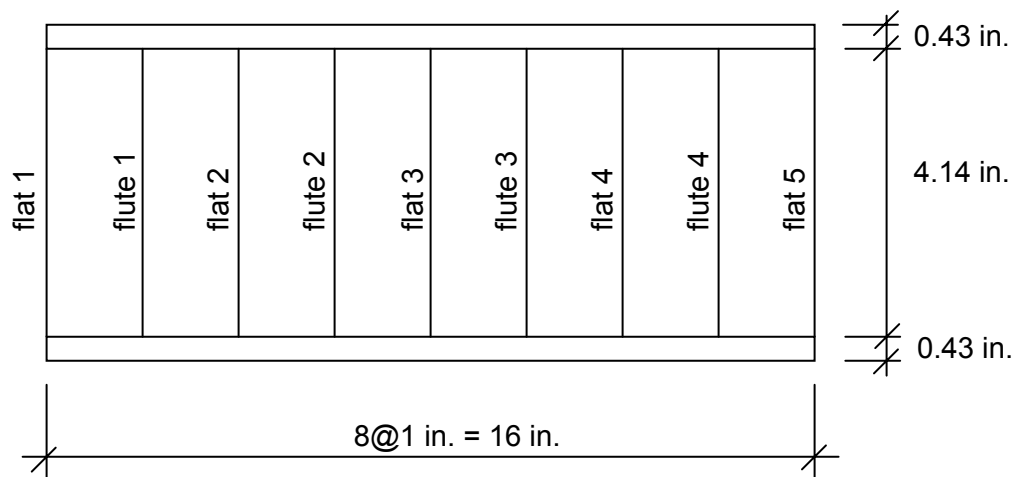


Figure 5.5: Cross-section of sandwich beam for hand calculation – Case 1

The total flexural stiffness is obtained by summing up the stiffnesses of the two faces and the core. The core flexural stiffness is a sum of flexural stiffnesses of all webs making up the core. Thus, the stiffness EI used in Equation 5.7 is:

$$EI = mE_1I_1 + nE_2I_2 \quad \text{Equation 5.8}$$

where, E_1I_1 is the flexural stiffness of one flange, E_2I_2 is the flexural stiffness of one web, m refers to the number of flanges = 2 and n represents the number of webs = 9.

5.3.3.2 Case 2 (3-layered)

In the second case, the beam is analyzed as a three-layered equivalent model. The three layers all have the same width equal to that of the face laminates. The combined thickness of the three layers is the same as the total depth of the beam, with the top and bottom layers retaining their original dimensions. The moment of inertia for each layer is obtained using the parallel axis theorem, so that the equivalent flexural stiffness used in Equation 5.7 is:

$$EI = mE_1I_1 + E_2I_2 \quad \text{Equation 5.9}$$

where, E_1I_1 represents the flexural stiffness of the face layer, E_2I_2 is the flexural stiffness of the middle layer and m symbolizes the number of faces = 2. For the middle layer, the in-plane elastic modulus discussed in Chapter 3 is used for simplification.

5.3.3.3 Case 3 (1-layered)

In the third and final case, the cross-section is treated as having a single layer whose equivalent properties were derived in Section 5.2 and shown in Table 5.1. The calculation of the moment of inertia I was done based on an equivalent rectangular cross-section with width equal to the width of the face laminates. The depth of the

section is equal to the entire depth of the beam. With these properties, the equivalent flexural stiffness EI used in Equation 5.7 above is calculated.

5.3.4 Comparison of Results

Having performed the analysis above, the results for deflection at quarter points along the beam span are presented in Table 5.2. The finite element analysis results for the actual configuration beam model are compared with those from finite element analysis of the equivalent model and hand-calculations.

A closer look at the results in Table 5.2 indicates a very good deflection comparison of the single-layer equivalent beam developed in Section 5.3.2 with the actual configuration model described in Section 5.3.1. The difference recorded for the midspan deflection is less than 0.1%. This is further proof of the accuracy of performing finite element analysis on the less-complicated single-layered equivalent structure. Similarly, the approach described in Section 5.3.3.3 for the hand calculation of a single-layered equivalent beam also yields good results. The difference for the midspan deflection is also less than 0.1%. Thus, rather than performing a finite element analysis on the complex sinusoidal core sandwich beam, the analysis can be carried out with very good results using the less complicated equivalent model. This analysis can be done either by performing finite element modeling on the single layer equivalent or hand calculation using traditional methods in conjunction with the approach described in Section 5.3.3.3.

However, the results of the hand calculation for Cases 1 and 2 (Section 5.3.3.1 and 5.3.3.2) do not compare as well. They each have a difference of over 20% from the actual configuration finite element model. The assumptions made – such as

approximating the core to an arrangement of nine vertical web elements – introduce some errors to the results. The effects of the actual geometry of the core structure are not accounted for. Therefore, the two methods could be used in preliminary calculations or verification of results.

Table 5.2: Comparison of Deflection Results (in.)

Model	1/4-span	Mid-span	3/4-span	Mid-span difference with Actual Config. FEM (%)
FEM of Actual Configuration	9.832	14.363	9.832	
FEM of Equivalent	9.884	14.377	9.884	0.097
Case 1: Hand-Calc (flange-web)	7.363	10.710	7.363	25.434
Case 2: Hand-Calc (3-layer)	7.652	11.129	7.652	22.513
Case 3: Hand-Calc (1-layer)	9.882	14.374	9.882	0.079

5.4 Application to FRP Panel

Having derived the equivalent properties and verified them using a beam model, the approach can now be applied to FRP panels. In this section, the validity of the properties derived is tested for panels. Full deck verification is therefore performed.

In the full panel analysis, an actual panel model with the sinusoidal core configuration and sandwich structure is created using finite element modeling. The full deck has dimensions 15 ft x 7.67 ft x 5 in. It is simply supported over its span of 15 ft and has a total load of 10 kips applied at its mid-span.

However, symmetric conditions are used so that half the span is modeled. This approach reduces the processing time of the ANSYS finite element software. Additionally, because of the complex configuration of the FRP panel, modeling a full-scale deck would exceed the software’s capacity making analysis impossible. As a

result of these limitations, a half-span of 7.5 ft is modeled using elastic shell elements. This model has 66,600 elements and 48,384 nodes. To simulate symmetric conditions, the left end of the panel is constrained for translation in the lateral and vertical directions only (u_y and u_z). On the right end, the nodes are constrained for displacement in the longitudinal direction and rotation about the lateral axis (u_x and Rot_y). A total load of 5 kips is applied on elements within an area of 8 in. x 12 in. on the mid-span of the symmetric model. This load is applied as pressure with a value of 52.0833 psi.

To verify the equivalent properties derived in the previous section, an equivalent panel model is created. The model is made using a single layer of elastic shell elements. The properties presented in Table 5.1 are used for this model. It has the same dimensions, loading conditions and constraints as that for the actual model analyzed in the preceding paragraph.

After finite element analysis is performed on both models, the results are checked and compared for deflection. Deflection results are obtained for two cases. Firstly, at quarter points along the longitudinal centerline, and secondly, at quarter points along the lateral right end of the model. These results are recorded and compared as shown in Table 5.3.

Table 5.3a: Comparison of Deflection Results between Actual Configuration and Equivalent Models. Points in the longitudinal direction along the central line (in.)

	0	22	45	67	90
Actual Config. Model	0	0.4205	0.8070	1.0778	1.2016
Equivalent Model	0	0.4501	0.8273	1.1020	1.2178
% Diff.		6.5739	2.4501	2.1960	1.3303

Table 5.3b: Comparison of Deflection Results between Actual Configuration and Equivalent Models. Points in the lateral direction along the midspan (in.)

	0	23	46	69	92
Actual Config. Model	1.2191	1.1798	1.2016	1.1801	1.2196
Equivalent Model	1.2365	1.2090	1.2178	1.2090	1.2365
% Diff.	1.4072	2.4152	1.3303	2.3904	1.3668

5.5 Summary

From the results presented in Table 5.3, we see very good comparison between the actual and equivalent models. The average difference between results for both models is about 2%. This good comparison shows that we can confidently carry out a stiffness analysis and design using the less complex equivalent model. This makes for a more simplified and yet reliable design approach.

CHAPTER 6 - PARAMETRIC STUDIES FOR OUT-OF-PLANE BEHAVIOR

6.1 Introduction

Having developed and verified an approach for obtaining the equivalent flexural and shear stiffness of the sinusoidal wave core panel in Chapter 5, attention is given in this chapter to developing parametric equations. From these equations, the equivalent stiffness properties from known panel parameters can be obtained. In other words, Chapter 5 dealt with a structure whose components have specific dimensions and properties. Now, however, the focus is directed to obtaining the equivalent stiffness properties for a wider range of parametric values. A systematic approach where each parameter is considered separately is used. This method is based on the assumption that the effects of the parameters are independent of each other.

The parameters used in this study are defined in Tables 6.1 and 6.2 below:

Table 6.1: Face parameters used for stiffness equations

Faces	
E_{x1} and E_{x2}	Young's modulus in x-direction of top and bottom face
E_{y1} and E_{y2}	Young's modulus in y-direction of top and bottom face
t_1 and t_2	Thickness of top and bottom face

Table 6.2: Core parameters used for stiffness equations

Core	
E	Young's Modulus of randomly oriented core material
W	Flute-width of core
L	Half-wavelength of core
H	Depth of core
t	Thickness of core material

The properties, referred to as basic values, are also summarized in Table 6.3. These parametric values represent those for the FRP panels developed by Kansas Structural Composites Inc., the same structure which has been the basis of this research work.

Table 6.3: Basic Properties

Basic Parameters	
E (psi)	1.71E+06
W (in.)	2
L (in.)	4
H (in.)	4.57
t (in.)	0.0898
E_{x1} and E_{x2} (psi)	2.92E+06
E_{y1} and E_{y2} (psi)	1.87E+06
t₁ and t₂ (in.)	0.43
G_{xy1} (psi)	5.46E+05

6.2 Flexural Stiffness Exlyy

The parametric study commences with the flexural stiffness of the panel when subjected to vertical loading. The intent is to understand the bending behavior about the lateral axis of the structure. To study this effect, consideration is given to a beam with a very high span to depth ratio. In this way the less significant shear contribution to deflection can be ignored.

Following a systematic approach, each parameter is first varied within a reasonable range of values while keeping others constant, each time computing the flexural stiffness. The elastic modulus is obtained using the same procedure used in Chapter 5, with the exception that the aim this time is to compute the flexural stiffness EI. Rigid shell elements are placed at the two longitudinal ends of the sandwich beam

model. The beam has a span of 15 ft, width of 8 in. and depth of 5 in., and cantilevered by constraining the nodes at one end for translational and rotational motions. At the other end, a force of 10,000 lb is applied in the vertical direction, causing the beam to bend about its lateral axis. From the deflection results obtained through finite element, $E_x I_{yy}$ can be calculated from Equation 6.1 below:

$$E_x I_{yy} = \frac{P_z L^3}{3\delta_z} \quad \text{Equation 6.1}$$

where, P_z is the applied vertical force, L represents the span of the beam and δ_z symbolizes the vertical end deflection of the beam.

6.2.1 Variation of Stiffness with Core Height, H

While keeping all other parameters constant at their basic values, the core height H is varied within a range of 4.57 in. to 23.57 in. The analysis revealed that the flexural stiffness $E_x I_{yy}$ is more sensitive to the core height than any other parameter. As can be observed from Fig. 6.1, the stiffness varies from about 80,000 ksi to almost 3,000,000 ksi within the range of variation of the core height. This high sensitivity is not surprising when we consider the fact that in general, the moment of inertia is a function of depth to the third degree. The relationship depicted in Fig. 6.1 can be expressed mathematically by the formula below:

$$(E_x I_{yy})_H = x_1 H^4 + x_2 H^3 + x_3 H^2 + x_4 H + x_5 \quad \text{Equation 6.2}$$

where $x_1 = 8.3627E - 04$, $x_2 = -6.9531E - 03$, $x_3 = 5.0966$, $x_4 = -11.2596$ and $x_5 = 29.7750$

Equation 6.2 can be used to compute the flexural stiffness $E_x I_{yy}$ of the Kansas Structural Composite FRP panel for any core height H if all the other parameters are

kept constant at their basic values. An example would be the No-Name Creek Bridge in Russell, Kansas which has a core height of 20.5 in. From Equation 6.2, it would have a stiffness of 2.029E+9 lb-in².

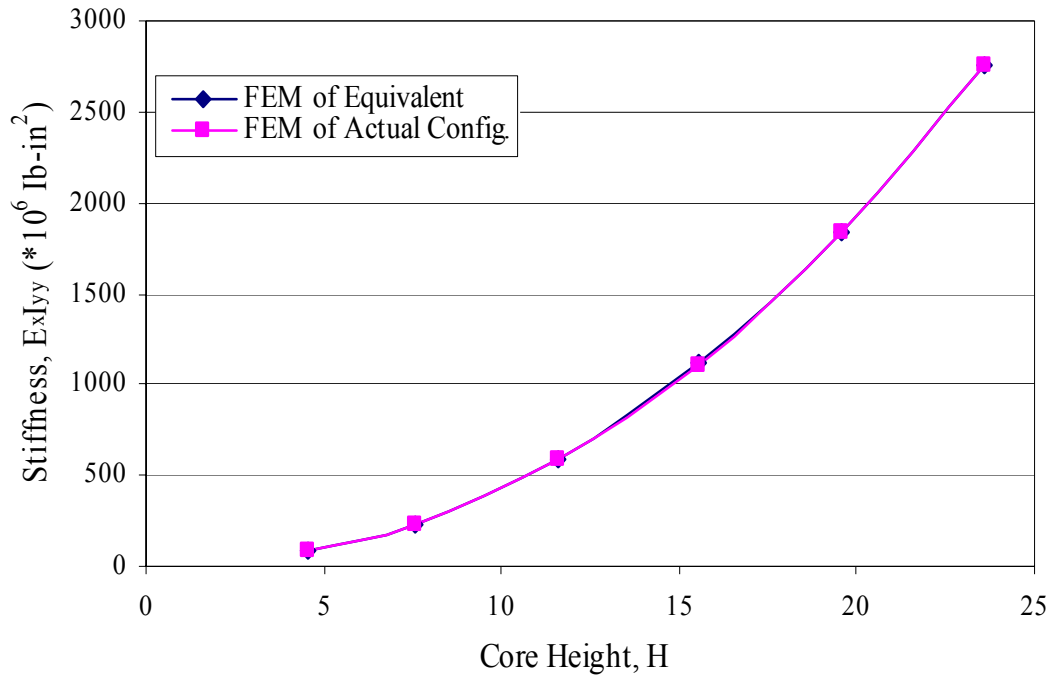


Figure 6.1: Variation of Stiffness with Core Height H

Fig. 6.1 also shows how well the proposed equivalent equation predicts the results of the actual configuration model from the finite element analysis. The difference between both curves is about 0.13%, a very good approximation.

6.2.2 Variation of Stiffness with Face Parameters

The effects on stiffness of the three parameters of the face laminate are the same for both the top and bottom face. Therefore, parametric studies of just the top face would be considered, and the same results could be applied to the bottom.

First, the elastic modulus in the longitudinal direction E_{x1} is varied within a range of 10 ksi to 100,000 ksi, while all other parameters are kept constant at the basic

values. The results of this variation can be visualized in Fig. 6.2. As can be observed, the stiffness is very sensitive to this parameter at lower values, but as E_{x1} increases, the sensitivity decreases having a much gentler gradient. Depending on the value of E_{x1} , the stiffness can be computed from Equation 6.3:

$$E_{x1} I_{yy} = f_1 E_{x1}^4 + f_2 E_{x1}^3 + f_3 E_{x1}^2 + f_4 E_{x1} + f_5 \quad \text{Equation 6.3}$$

for $(0.01 \leq E_{x1} \leq 5)$,

$$f_1 = -0.9163, \quad f_2 = 9.1536, \quad f_3 = -30.628, \quad f_4 = 51.427 \quad \text{and} \quad f_5 = 33.494$$

for $(5 \leq E_{x1} \leq 100)$,

$$f_1 = -3.6338E-06, \quad f_2 = 9.3304E-04, \quad f_3 = -8.6537E-02, \quad f_4 = 3.5812 \quad \text{and} \\ f_5 = 82.283$$

where E_{x1} is in Msi.

Equation 6.3 can be used to calculate the flexural stiffness $E_{x1} I_{yy}$ of the Kansas Structural Composite FRP panel for any value of elastic modulus E_{x1} if all the other parameters are kept constant at their basic values. For example, if for some reason a different top or bottom face material is used that has a different longitudinal elastic modulus with all other properties remaining the same.

It can be noticed from Fig. 6.2, that there is a very good curve fit of the proposed equivalent formula and the actual configuration model results from the finite element analysis. The difference is only about 0.4%.

A similar trend with a variation in elastic modulus in the lateral direction E_{y1} is noticed, though this is a less sensitive parameter since it serves as the secondary modulus in the longitudinal direction. This is depicted in Fig. 6.3. The flexural stiffness is

very sensitive to E_{y1} at lower values, but has a smaller slope at higher values. Again, depending on the value of E_{y1} , the stiffness can be calculated from the following equation (Equation 6.4):

$$E_x I_{yy} = g_1 E_{y1}^4 + g_2 E_{y1}^3 + g_3 E_{y1}^2 + g_4 E_{y1} + g_5 \quad \text{Equation 6.4}$$

for $(0.01 \leq E_{y1} \leq 5)$,

$$g_1 = -2.301, \quad g_2 = 19.64, \quad g_3 = -50.261, \quad g_4 = 53.945 \quad \text{and} \quad g_5 = 58.421$$

for $(5 \leq E_{y1} \leq 100)$,

$$g_1 = -4.68E-07, \quad g_2 = 1.18E-04, \quad g_3 = -1.0484E-02, \quad g_4 = 0.40363 \quad \text{and} \\ g_5 = 86.925$$

where E_{y1} is in Msi.

Equation 6.4 can be used to calculate the flexural stiffness $E_x I_{yy}$ of the FRP panel for any value of lateral elastic modulus E_{y1} if all the other parameters are kept constant at their basic values. For instance, if a different top/bottom face material is used that has a different lateral elastic modulus but all other parameters remain the same.

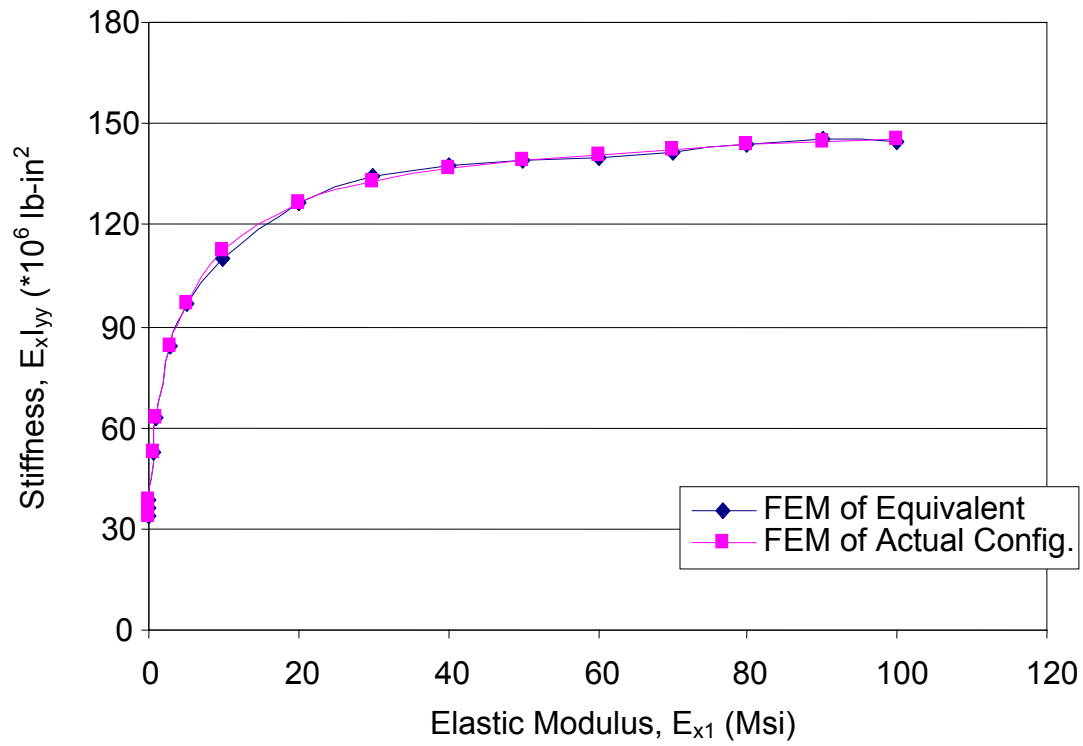


Figure 6.2: Variation of Stiffness with Face Elastic Modulus Ex1

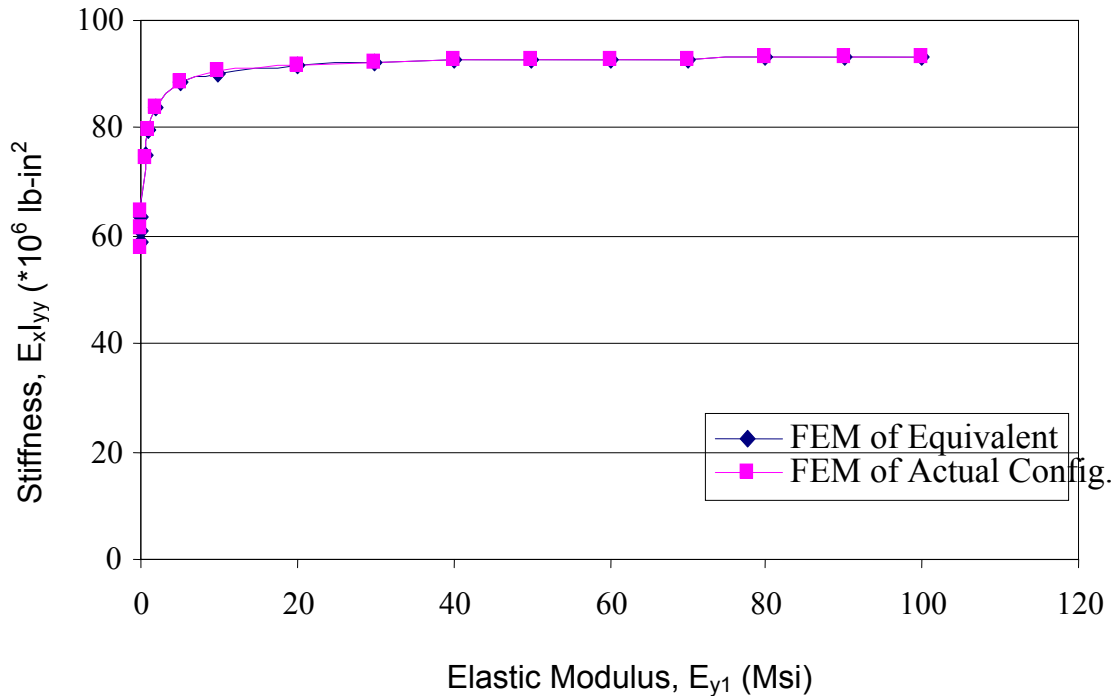


Figure 6.3: Variation of Stiffness with Face Elastic Modulus Ey1

Again, it can be observed from Fig. 6.3 that the proposed equivalent equation well fits the actual configuration model results from the finite element analysis. The difference is only about 0.4%.

The third important parameter is the face thickness. As expected, the panel equivalent stiffness increases with a rise in face thickness. The thickness t_1 is varied from 0.43 in. to 2.5 in. while all other parameters are kept at their constant basic values. Fig. 6.4 presents the relationship of stiffness $E_x I_{yy}$ with the face thickness t_1 . The following formula (Equation 6.5) represents the same relationship:

$$E_x I_{yy} = I_1 t_1^2 + I_2 t_1 + I_3 \quad \text{Equation 6.5}$$

where $I_1 = -8.4707$, $I_2 = 65.015$ and $I_3 = 59.633$

The above equation (Equation 6.5) can be used to compute the flexural stiffness $E_x I_{yy}$ of the FRP panel for any top or bottom face thickness. As an example, if an engineer decides to change just the top face thickness to account for something while retaining the original materials and other panel properties, the stiffness of the structure can be obtained by solving Equation 6.5.

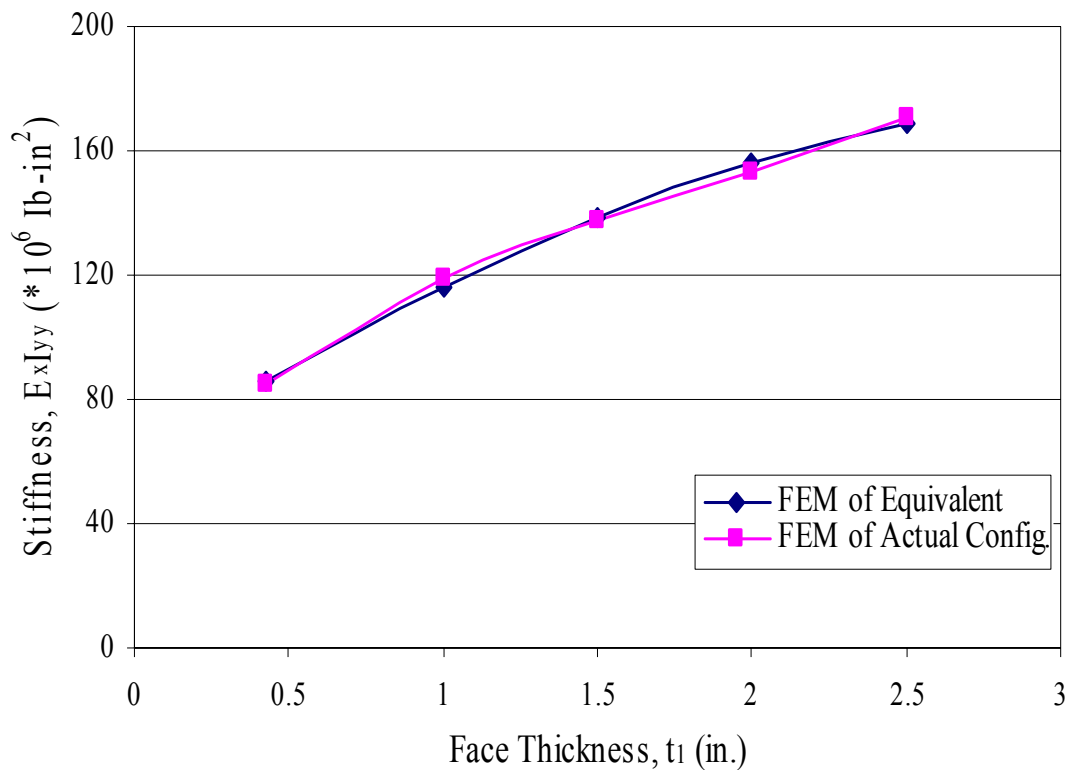


Figure 6.4: Variation of Stiffness with Face Thickness t_1

Once again, it can be seen that there is a very good curve fit between the proposed equivalent equation and the actual configuration model results of the finite element analysis. (Fig. 6.4) The difference is only about 1.4%.

6.2.3 Variation of Stiffness with Core Parameters

Apart from the core height which was discussed in the previous section, the other core parameters include elastic modulus of the core mat E , flute-width W , flute half-wavelength L and core material thickness t .

The elastic modulus of the core material E is varied within a range of 10 ksi to 100,000 ksi. As this variation is done, all other variables are kept constant at their basic

parametric values. The stiffness $E_x I_{yy}$ rises as E increases. The behavior is seen in Fig. 6.5, and the equation representing it is shown in Equation 6.6 below:

$$E_x I_{yy} = n_1 E^2 + n_2 E + n_3 \quad \text{Equation 6.6}$$

where $n_1 = -0.0023$, $n_2 = 3.1857$ and $n_3 = 79.0153$.

Equation 6.6 becomes useful in calculating the stiffness $E_x I_{yy}$ if a different material is used for the flats and flutes of the core. This difference in material brings about a change in the material elastic modulus E . However, for the equation to be valid, all other parameters, including the core mat thickness, have to remain unchanged from the basic parametric values.

As can be noticed in the graph above (Fig. 6.5), the proposed equivalent equation is a very good approximation of the actual configuration model results of the finite element analysis. The difference is only about 0.4%.

Next, the flute-width W is varied within the range of 1 in. to 5 in. with other parameters kept constant. As W rises within that range, the flexural stiffness increases. It is pertinent to note that this is true for the whole section (not a unit width) since the beam width increases with W . In other words, as W increases, the width of the beam correspondingly increases to maintain the number of flutes at four. This logically results in a stiffer section. Fig. 6.6 and Equation 6.7 below well illustrate this relationship:

$$E_x I_{yy} = r_1 W^2 + r_2 W + r_3 \quad \text{Equation 6.7}$$

where $r_1 = 1.1347$, $r_2 = 33.1947$ and $r_3 = 14.8474$.

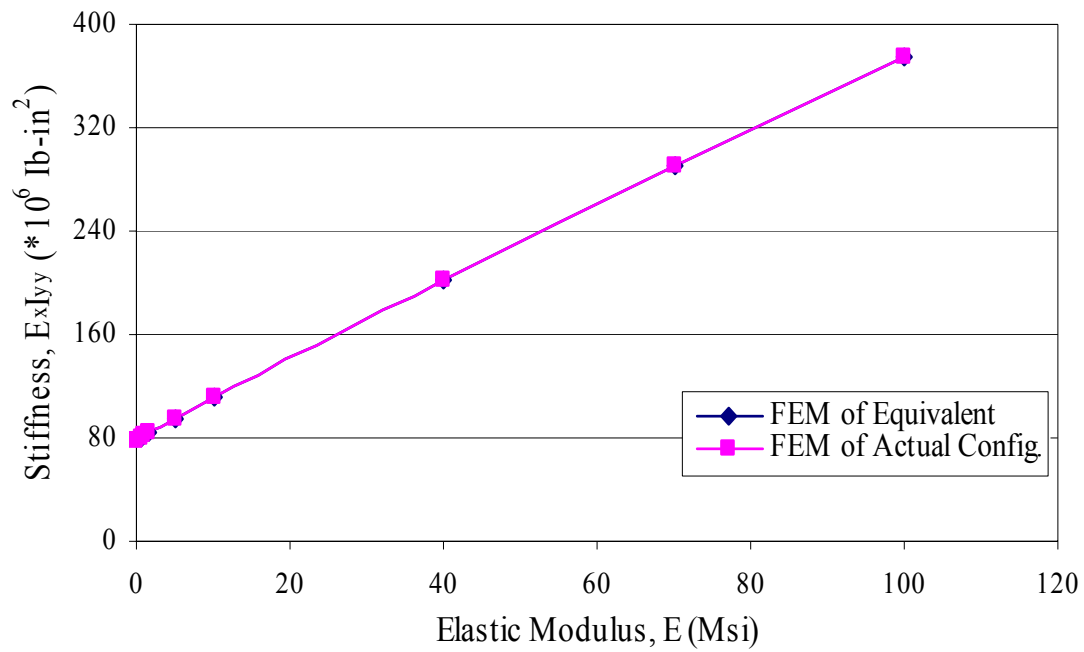


Figure 6.5: Variation of Stiffness with Core Mat Elastic Modulus E

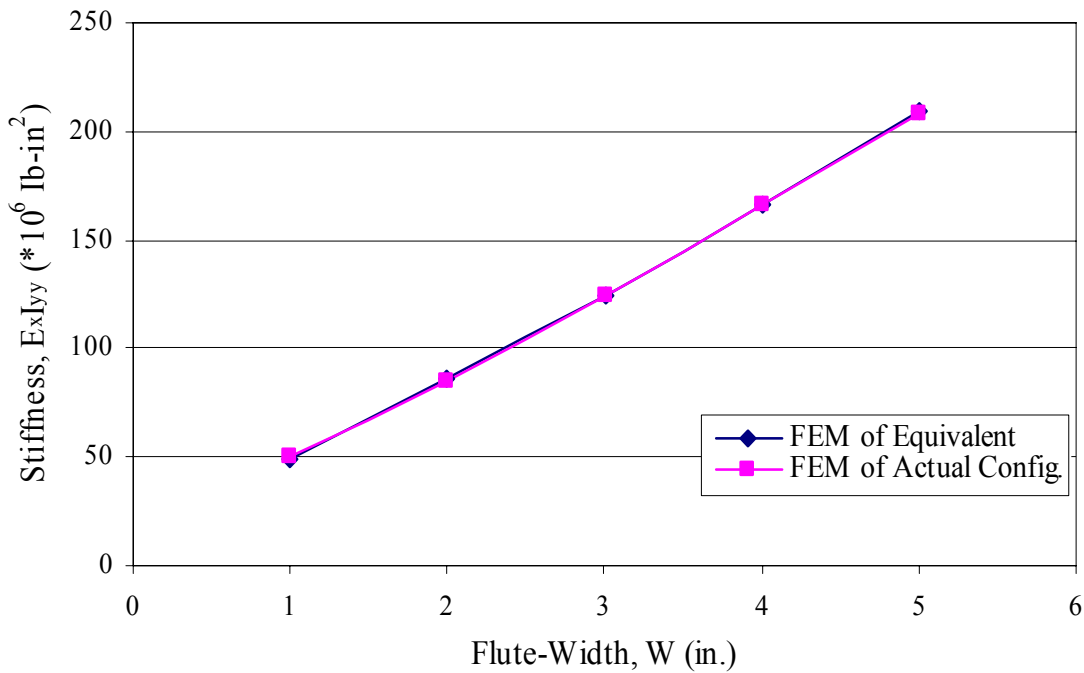


Figure 6.6: Variation of Stiffness with Flute-Width W

This equation (Equation 6.7) is useful in calculating the flexural stiffness $E_x I_{yy}$ when we have a core with a different flute-width W . To use the formula, however, the half-wavelength should not be changed. Also, all other parameters should be unaltered.

The plots in Fig. 6.6 show that the proposed equivalent equation very well fits the results of the actual configuration model from the finite element analysis. There is a difference of only about 0.6%.

Though not as sensitive as flute-width W , the flute half-wavelength L has a similar effect on the stiffness. As it is varied from 4 in. to 14 in., $E_x I_{yy}$ increases as can be observed from Fig. 6.7. The increase in stiffness is understandable when we remember that the component stiffness of the flute in the longitudinal direction rises correspondingly with flute half-wavelength. The equation below (Equation 6.8) represents this trend:

$$E_x I_{yy} = s_1 L^2 + s_2 L + s_3 \quad \text{Equation 6.8}$$

where $s_1 = -0.0433$, $s_2 = 2.2435$ and $s_3 = 76.0774$.

Like the other equations, Equation 6.8 can be used to compute the flexural stiffness $E_x I_{yy}$ for a panel with a given flute half-wavelength L . Again, all other parameters such as the flute-width should be kept at their original basic values.

It can be observed from Fig. 6.7 that there is a good curve fit of the actual configuration model results from finite element analysis by the proposed equivalent formula in Equation 6.8. The difference between both plots is only about 0.3%.

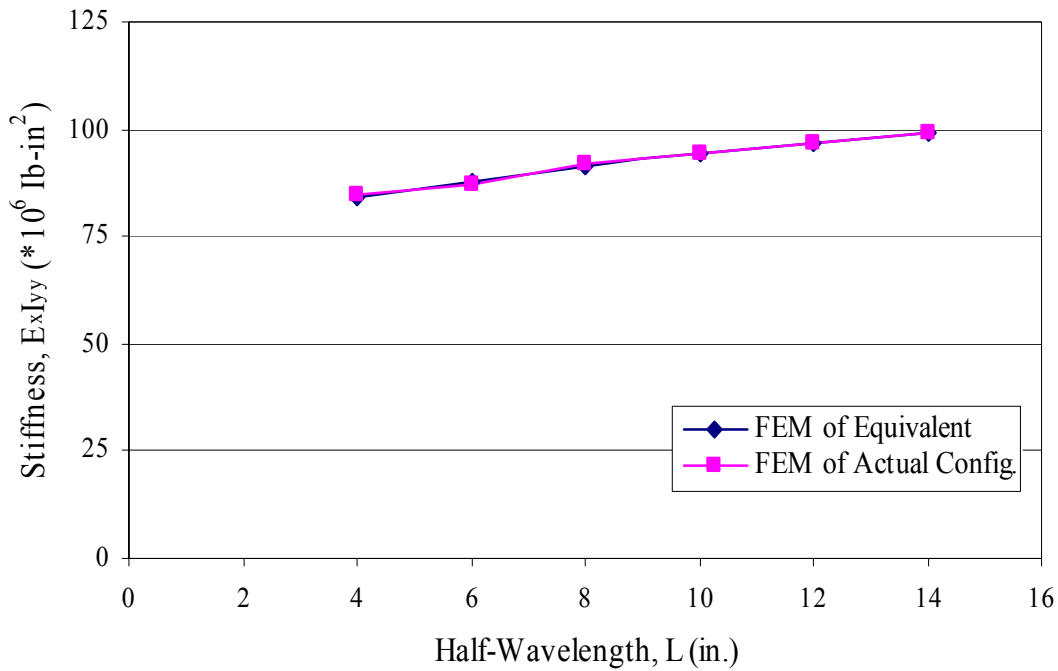


Figure 6.7: Variation of Stiffness with Half-Wavelength L

Finally, the core material thickness t is varied within a range of 0.05 in. to 0.5 in. Within this range, the flexural stiffness increases correspondingly (other parameters kept constant). Fig. 6.8 shows a plot of this relationship, which can also be represented mathematically by the formula (Equation 6.9) below:

$$E_x I_{yy} = p_1 t^2 + p_2 t + p_3 \quad \text{Equation 6.9}$$

where $p_1 = 3.0708$, $p_2 = 67.8971$ and $p_3 = 78.437$

Equation 6.9 is a useful formula in calculating the flexural stiffness $E_x I_{yy}$ for a sinusoidal wave core panel with any given flat/flute thickness. If, for example, a manufacturer or engineer decides to use the same material for the core mat but with an increased (or reduced) thickness, the panel stiffness can be computed from the simplified formula. We note though that, as in previous equations, all other parameters must remain unaltered from their basic parametric values for the equation to be valid.

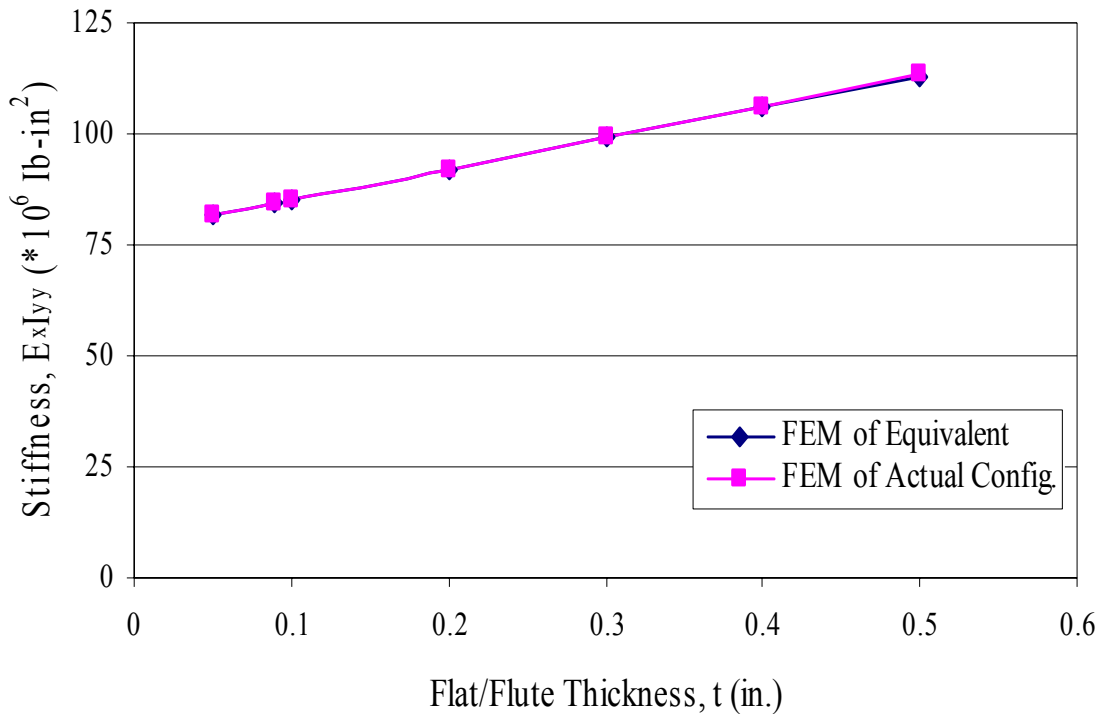


Figure 6.8: Variation of Stiffness with Flat/Flute Thickness t

As can be noticed from Fig. 6.8, the proposed equivalent equation (Equation 6.9) very well approximates the actual configuration model results from the finite element analysis. The difference between both sets of data is less than 0.1%.

6.2.4 Modification Factors

So far, the formulae that have been derived are single-variable equations. Therefore, if more than one parameter is changed from the original basic values, the equations are no longer valid. Hence, in this section, a more general formula for the flexural stiffness $E_x I_{yy}$ in terms of the eight different parameters considered in the previous section is sought. Having understood the link between the various parameters, a more general equation is now derived, using the same systematic approach that was employed in chapter 4. This leads to the concept of modification factors of the

equivalent stiffness for a variation in parameters. This approach assumes that the parameters are independent from each other.

As discussed previously, one of the most important factors influencing the stiffness is the core height. The relationship can be seen in equation 6.2.

6.2.4.1 Face Longitudinal Elastic Modulus Modification Factor, B_1

From Fig. 6.2, it can be noticed that Ex_{lyy} increases with a rise in top face longitudinal modulus of elasticity, and this relation is found in equation 6.3. Similarly, by plotting the modification factor for Ex_1 , $B_1(= E_x I_{yy} / E_x I_{yy}(\text{basic}_x))$ against the ratio $R_1(= E_{x1} / E_{x1(\text{basic})})$, the graph shown in Figure 6.9 is obtained. $Ex_1(\text{basic})$ represents the basic longitudinal modulus of 2,920 ksi and $Ex_{lyy}(\text{basic}_x)$ is the flexural stiffness of the panel at $Ex_1(\text{basic})$. Depending on the value of Ex_1 , the equation can be expressed as follows (Equation 6.10):

$$B_1 = a_1 R_1^4 + a_2 R_1^3 + a_3 R_1^2 + a_4 R_1 + a_5 \quad \text{Equation 6.10}$$

for $(0.01 \leq E_{x1} \leq 5)$,

$$a_1 = -0.79488, \quad a_2 = 2.7195, \quad a_3 = -3.1163, \quad a_4 = 1.792 \quad \text{and} \quad a_5 = 0.39969$$

for $(5 \leq E_{x1} \leq 100)$,

$$a_1 = -1.7404E-06, \quad a_2 = 1.6251E-04, \quad a_3 = -5.6154E-03, \quad a_4 = 9.004E-02 \quad \text{and}$$

$$a_5 = 1.0997$$

where Ex_1 is in Msi.

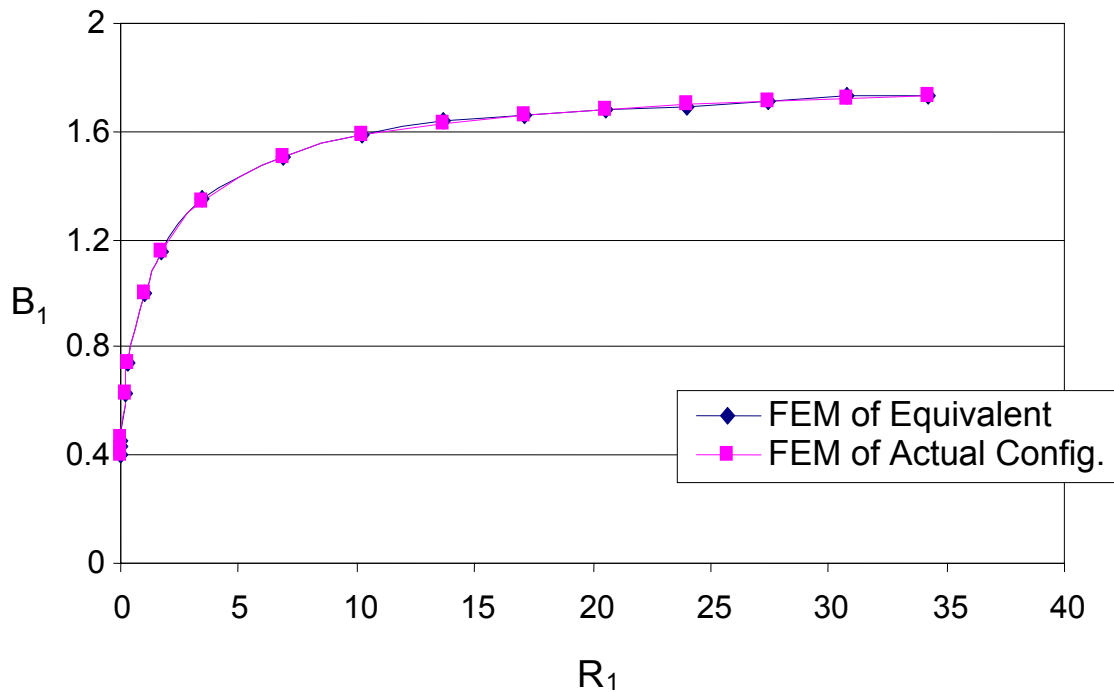


Figure 6.9: Modification Factor by Face Elastic Modulus (1-direction)

6.2.4.2 Face Lateral Elastic Modulus Modification Factor, B₂

The second modification factor required is that with respect to the elastic modulus of the face in the transverse direction E_{y1} . Notice from Fig. 6.3 that as this parameter is varied, the stiffness increases. The lateral elastic modulus modification factor is obtained by varying the ratio $R_2 (= E_{y1} / E_{y1(\text{basic})})$ for the range between 10 ksi and 100,000 ksi, where $E_{y1(\text{basic})}$ is the basic lateral face modulus of 1,870 ksi. By plotting this variation with the modification factor $B_2 (= E_x I_{yy} / E_x I_{yy(\text{basic}_y)})$, the graph in Fig. 6.10 is obtained. $E_x I_{yy(\text{basic}_y)}$ is the flexural stiffness of the panel at $E_{y1(\text{basic})}$. The following equation (Equation 6.11) defines this relationship depending on the value of E_{y1} :

$$B_2 = b_1 R_2^4 + b_2 R_2^3 + b_3 R_2^2 + b_4 R_2 + b_5 \quad \text{Equation 6.11}$$

for $(0.01 \leq E_{y1} \leq 5)$,

$$b_1 = -0.3358, \quad b_2 = 1.5325, \quad b_3 = -2.0973, \quad b_4 = 1.2038 \quad \text{and} \quad b_5 = 0.6972$$

for $(5 \leq E_{y1} \leq 100)$,

$$b_1 = -0.3022E-09, \quad b_2 = 4.3335E-06, \quad b_3 = -2.2743E-04, \quad b_4 = 5.4339E-03 \quad \text{and}$$

$$b_5 = 1.0562$$

where E_{y1} is in Msi.

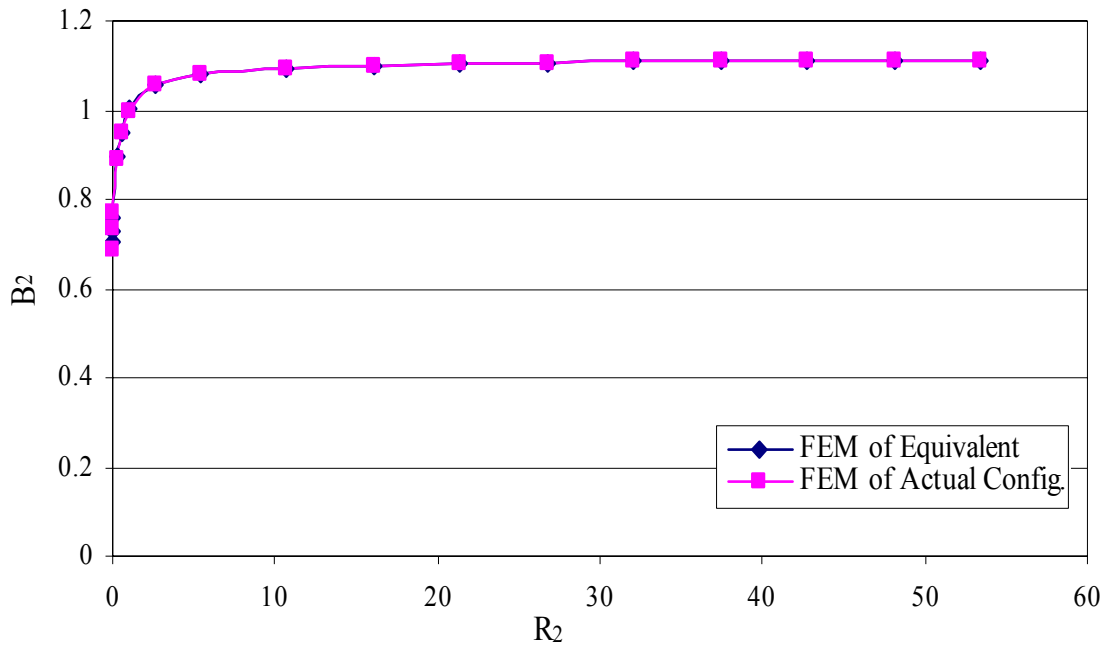


Figure 6.10: Modification Factor by Face Elastic Modulus (2-direction)

6.2.4.3 Face Thickness Modification Factor, B_3

Next, attention is given to the modification factor of the thickness of the top face. It can be recalled from Fig. 6.4 that the stiffness of the panel increases with this parameter, and the relationship was also shown in Equation 6.5. The modification factor

is obtained by varying the thickness ratio $R_3 (= t_1 / t_{1(0.43)})$ within a range of thickness of 0.43 in. to 2.5 in. $t_{1(0.43)}$ represents the basic face thickness of 0.43 in. Plotting $B_3 (= E_x I_{yy} / E_x I_{yy(\text{basic_t1})})$ against R_3 yields the graph shown in Figure 6.11. $E_x I_{yy(\text{basic_t1})}$ is the flexural stiffness of the panel at $t_1(0.43)$. This plot has the following equation for B_3 (Equation 6.12):

$$B_3 = c_1 R_3^2 + c_2 R_3 + c_3 \quad \text{Equation 6.12}$$

where $c_1 = -1.8505E - 02$, $c_2 = 0.3303$ and $c_3 = 0.7046$.

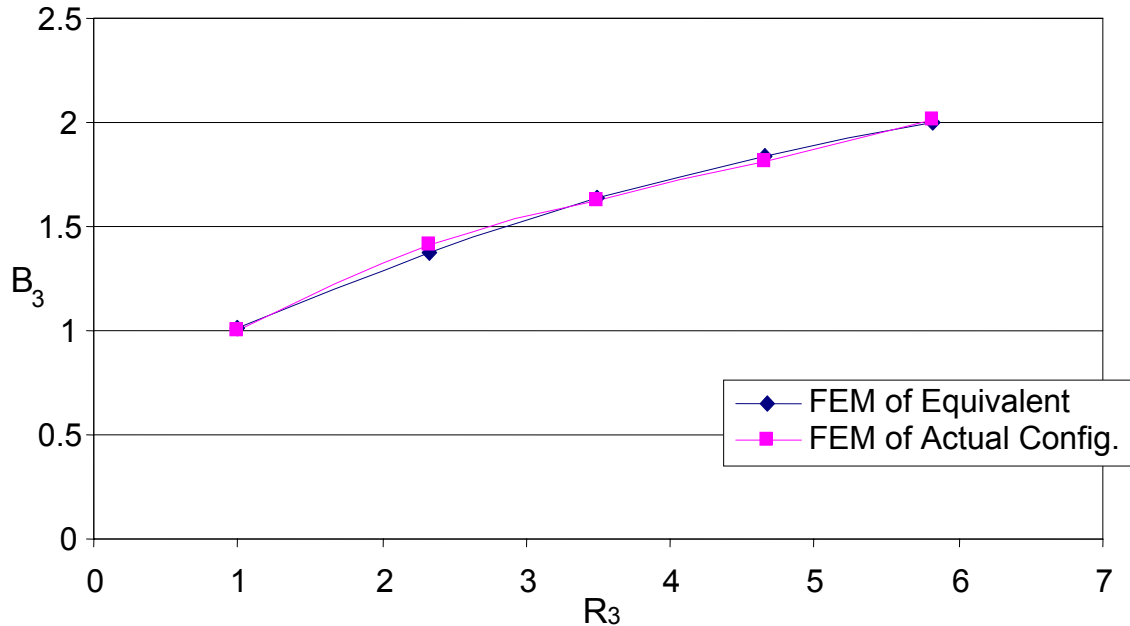


Figure 6.11: Modification Factor by Face Thickness

6.2.4.4 Core Mat Elastic Modulus Modification Factor, B_4

From Fig. 6.5 and Equation 6.6, it was seen that one of the very important parameters of the core is the elastic modulus of its material E . As E increases, so does the flexural stiffness. The equation for modification factor of the stiffness due to E is

sought. This is derived by computing the elastic modulus ratio $R_4 (= E / E_{(1.71)})$ and the corresponding modification factor $B_4 (= E_x I_{yy} / E_x I_{yy}(\text{basic_E}))$. $E_{(1.71)}$ is the basic core mat elastic modulus of 1,710 ksi, while $E_x I_{yy}(\text{basic_E})$ represents the flexural stiffness of the panel at $E_{(1.71)}$. Plotting B_4 versus R_4 produces the graph in Fig. 6.12 and its equation is as follows (Equation 6.13):

$$B_4 = d_1 R_4^2 + d_2 R_4 + d_3 \quad \text{Equation 6.13}$$

where $d_1 = -7.8268E-05$, $d_2 = 6.4427E-02$ and $d_3 = 0.9345$.

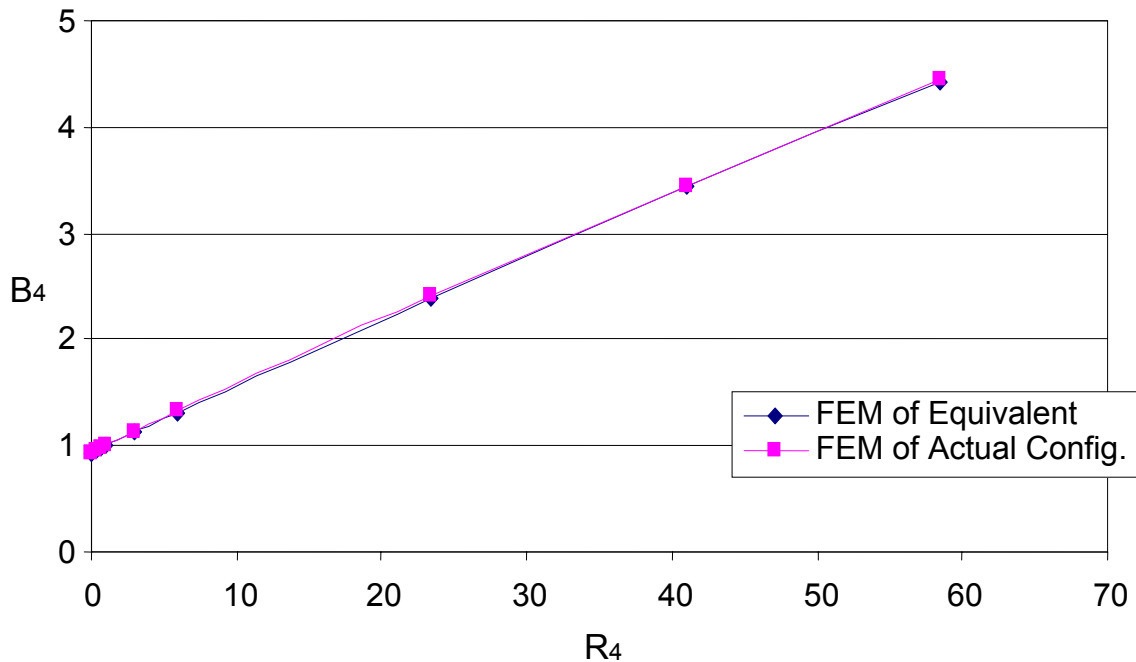


Figure 6.12: Modification Factor by Core Mat Elastic Modulus

6.2.4.5 Core Flute-Width Modification Factor, B_5

Another very significant parameter of the core is its flute-width W . An increase in W results in a rise in the panel stiffness, as shown from Fig. 6.6 and Equation 6.7. Similarly, by plotting the modification factor for flute-width, $B_5 (= E_x I_{yy} / E_x I_{yy}(\text{basic_W}))$

against the ratio $R_5 (= W / W_{(2)})$, the graph in Fig. 6.13 results. $W(2)$ represents the basic flute-width of 2 in. and $E_{x'yy}(\text{basic}_W)$ is the flexural stiffness of the panel when the flute-width is 2 in. The equation (Equation 6.14) can be expressed as follows:

$$B_5 = k_1 R_5^2 + k_2 R_5 + k_3 \quad \text{Equation 6.14}$$

where $k_1 = 5.3623\text{E-}02$, $k_2 = 0.7844$ and $k_3 = 0.1754$.

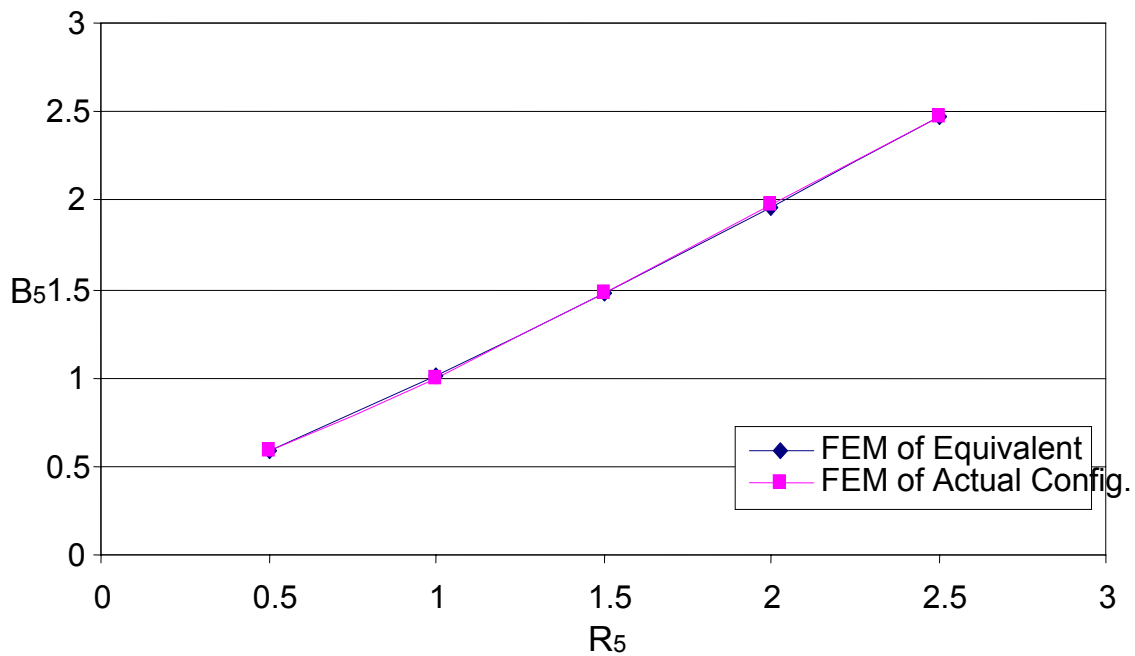


Figure 6.13: Modification Factor by Flute Width

6.2.4.6 Core Half-Wavelength Modification Factor, B_6

Next, consideration is given to the modification factor of the stiffness due to the half-wavelength L . From Fig. 6.7, the stiffness increases with a rise in half-wavelength. This can also be seen from Equation 6.8. This same trend is observed from the plot of the modification factor $B_6 (= E_{x'yy} / E_{x'yy}(\text{basic}_L))$ against the ratio $R_6 (= L / L_{(4)})$. (Fig. 6.14)

Here, $L(4)$ represents the basic half-wavelength of 4 in. and $E_{xlyy}(\text{basic}_L)$ is the flexural stiffness of the panel when the L is 4 in. The formula is shown in Equation 6.15.

$$B_6 = m_1 R_6^2 + m_2 R_6 + m_3 \quad \text{Equation 6.15}$$

where $m_1 = -8.1937E-03$, $m_2 = 0.1060$ and $m_3 = 0.8988$.

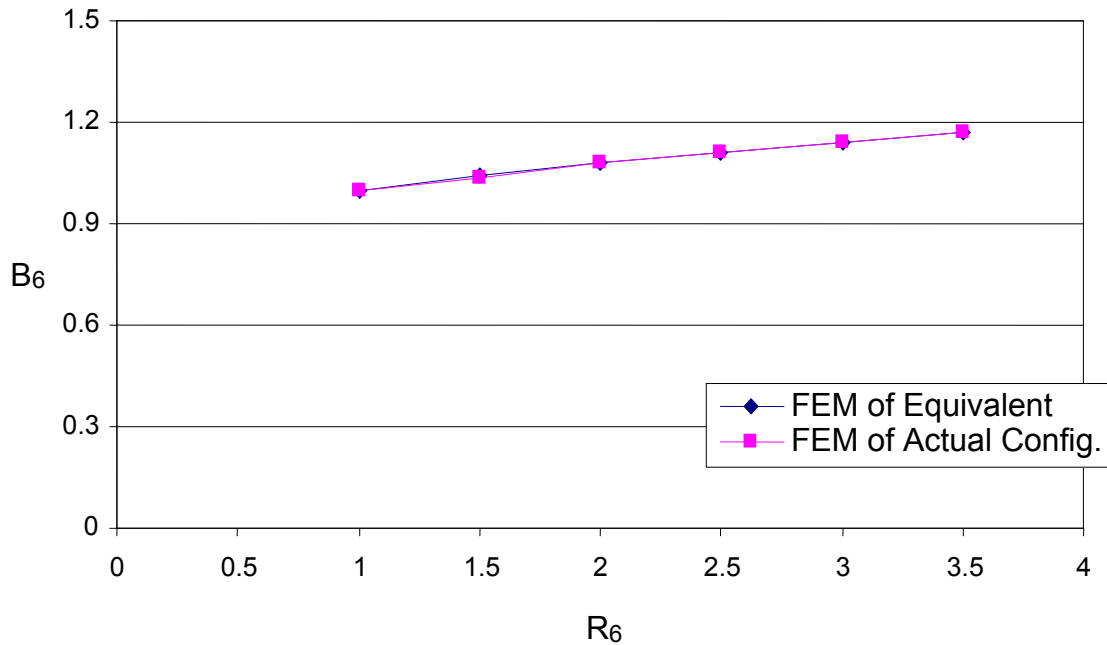


Figure 6.14: Modification Factor by Half-Wavelength

6.2.4.7 Core Material Thickness Modification Factor, B_7

Finally, focus is directed to the modification factor of the stiffness due to the core mat thickness t . Flexural stiffness increases with the thickness of the core material, and this behavior is found in Fig. 6.8 and Equation 6.9. The thickness ratio $R_7 (= t / t_{(0.0898)})$ is computed for a range of t between 0.05 in. and 0.5 in. where $t_{0.0898}$ is the basic flat/flute thickness, 0.0898 in. In Fig. 6.15, the modification factor $B_7 (= E_{xlyy} / E_{xlyy}(\text{basic}_t))$ is plotted against R_6 . $E_{xlyy}(\text{basic}_t)$ is the flexural stiffness of the

panel at $t=0.0898$. The expression for the flat/flute thickness modification factor can be written as follows:

$$B_7 = p_1 R_7^2 + p_2 R_7 + p_3 \quad \text{Equation 6.16}$$

where $p_1 = 2.9257E - 04$, $p_2 = 7.2037E - 02$ and $p_3 = 0.9267$.

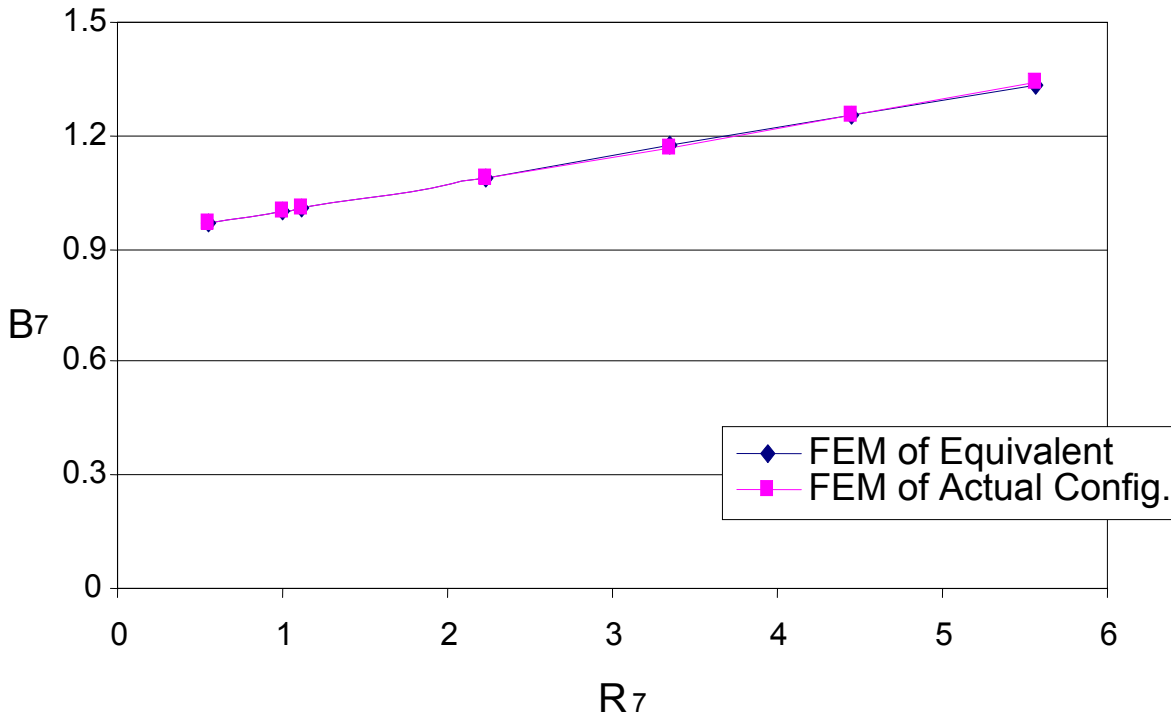


Figure 6.15: Modification Factor by Flat/Flute Thickness

6.2.5 Formula for Predicting Flexural Stiffness $E_x I_{yy}$

Having derived and discussed the interrelationship between panel parameters, the following formula is now proposed for calculating the flexural stiffness $E_x I_{yy}$:

$$E_x I_{yy} = B_1 B_2 B_3 B_4 B_5 B_6 B_7 (E_x I_{yy})_H \quad \text{Equation 6.17}$$

where B_1 , B_2 , B_3 , B_4 , B_5 , B_6 , B_7 and $(E_x I_{yy})_H$ can be obtained from Equations 6.2, 6.10, ..., 6.16

Though the above equation was derived based on variation of just the top face, the same formula can be applied to the two faces of the sandwich structure. New modification coefficients are simply introduced to account for the variation in the bottom face. These new factors have the same formulae as those of the top face. Thus, the modification factors used in Equation 6.17 become:

$$B_i = B_{i1}B_{i2} \quad \text{Equation 6.18}$$

where B_{i1} and B_{i2} refer to the modification factors for top and bottom faces respectively and $i = 1, 2, \dots, 7$

It must also be noted that the equation is valid for a beam with a width equal to four times the flute-width. Hence, if the flute-width is 2 in., the width of the beam for the computation of E_{xlyy} is 8 in. This was the assumption made in the derivation of the formula.

6.3 Flexural Stiffness E_{ylxx}

The next property now studied is the flexural stiffness of the panel when subjected to bending about the longitudinal axis E_{ylxx} . Although this property is not as significant as E_{xlyy} , it still has some contribution to the stiffness of the panel. This effect is analyzed by considering a beam with a very high span to depth ratio, just as was done in the previous case. The purpose of this approach is to neglect the shear contribution of the beam to deflection.

The same systematic approach is followed by first varying each parameter within a reasonable range of values while keeping others constant, each time computing the flexural stiffness. The sandwich beam model used for this phase has its span L in the lateral direction measuring 15 ft. It has a width of 8 in. in the longitudinal direction and a

depth of 5 in. It is cantilevered at one of the lateral ends, and a force P_z of 10,000 lb is applied at its other end causing bending about its longitudinal axis. From the deflection results, $E_y I_{xx}$ can be calculated using the following formula:

$$E_y I_{xx} = \frac{P_z L^3}{3\delta_z} \quad \text{Equation 6.19}$$

6.3.1 Variation of Stiffness with Core Height, H

Just as in the case of $E_x I_{yy}$, the core height H is the most sensitive of all the parameters. It is varied within the same range of 4.57 in. to 23.57 in., while other parameters are kept constant. As can be observed from Fig. 6.16, the stiffness $E_y I_{xx}$ varies from about 70,000 ksi to almost 1,800,000 ksi within the range of variation of the core height. However, as sensitive as this is, a comparison with $E_x I_{yy}$ reveals that the latter is a more sensitive (and hence, more important) stiffness property of the panel. The relationship between $E_y I_{xx}$ and H can be expressed by equation 6.20:

$$(E_y I_{xx})_H = y_1 H^4 + y_2 H^3 + y_3 H^2 + y_4 H + y_5 \quad \text{Equation 6.20}$$

where $y_1 = 5.0598E-05$, $y_2 = -4.9089E-03$, $y_3 = 3.2923$, $y_4 = -1.9895E-02$ and $y_5 = 2.9739E-02$.

Equation 6.20 becomes very useful when it is intended to compute the flexural stiffness $E_y I_{xx}$ of an FRP sinusoidal wave core panel for any core height H if all the other parameters are kept constant at their basic parametric values. For the No-Name Creek Bridge in Russell, Kansas which has a core height of 20.5 in., for example, $E_y I_{xx}$ would have a value of about $1,350E+6$ lb-in².

It is also noticed from Fig. 6.16 that the proposed equivalent stiffness equation as a function of core height H predicts accurately the actual configuration model results

from the finite element analysis. The difference between both sets of data is only about 0.05%.

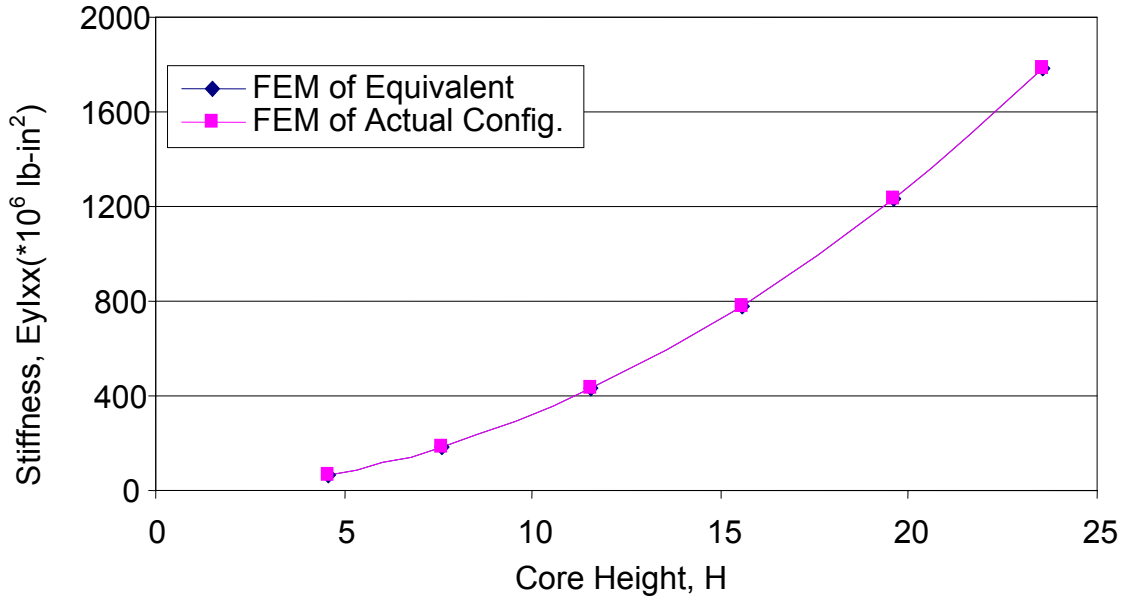


Figure 6.16: Variation of Stiffness with Core Height H

6.3.2 Variation of Stiffness with Face Parameters

This step involves varying the elastic modulus in the lateral direction E_{y1} within a range of 10 ksi to 100,000 ksi, while keeping other parametric constants at their basic values. Observe from Fig. 6.17 an illustration of this variation. It can be noticed that the stiffness is more sensitive to this parameter at lower values. As E_{y1} increases however, the sensitivity decreases. The flexural stiffness can be computed as follows, depending on the value of E_{y1} :

$$E_y I_{xx} = g_1 E_{y1}^4 + g_2 E_{y1}^3 + g_3 E_{y1}^2 + g_4 E_{y1} + g_5 \quad \text{Equation 6.21}$$

for $(0.01 \leq E_{y1} \leq 5)$,

$$g_1 = -7.6158, \quad g_2 = 62.834, \quad g_3 = -1.4832E + 02, \quad g_4 = 1.3691E + 02 \quad \text{and}$$

$$g_5 = 12.307$$

for $(5 \leq E_{y1} \leq 100)$,

$$g_1 = -1.9115E - 06, \quad g_2 = 4.8673E - 04, \quad g_3 = -4.4595E - 02, \quad g_4 = 1.8173 \quad \text{and}$$

$$g_5 = 76.027$$

where E_{y1} is in Msi.

Again, Equation 6.21 becomes valuable when it is desired to compute the flexural stiffness $E_{y1}I_{xx}$ for any value of elastic modulus E_{y1} if all other parameters are kept at their original basic values. The proposed equivalent formula in Equation 6.21 well predicts the actual configuration model finite element results, with a difference of only about 0.3%.

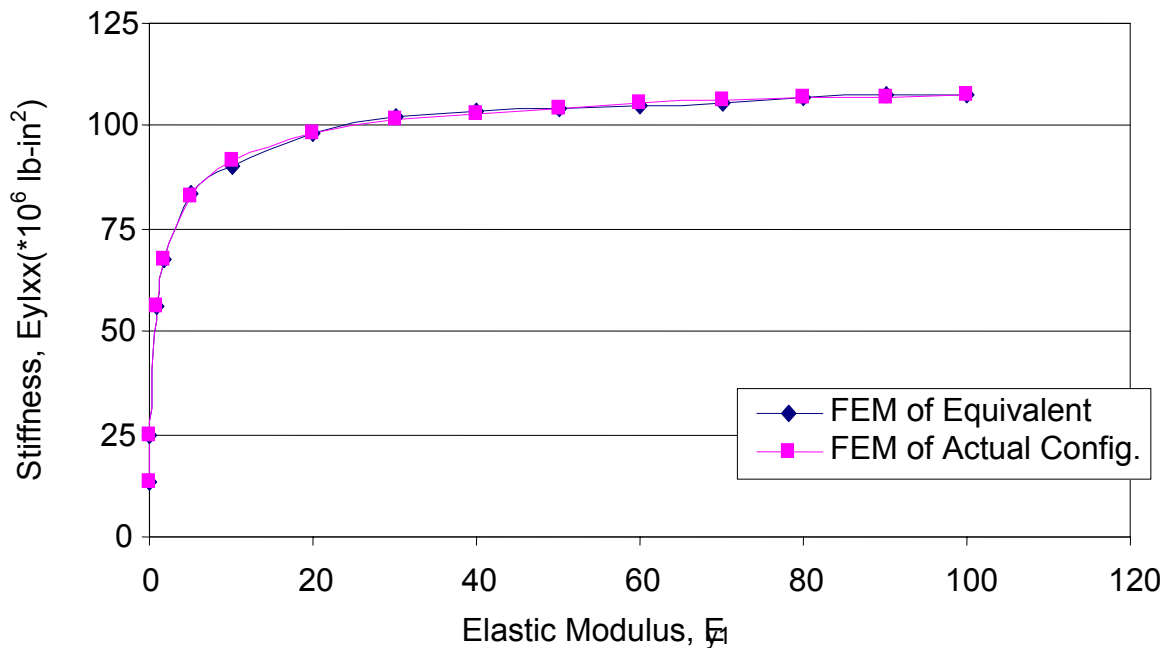


Figure 6.17: Variation of Stiffness with Face Elastic Modulus E_{y1}

Similarly, the flexural stiffness is very sensitive to Ex1 at lower values, but has a smaller slope at higher values. It is however a less sensitive parameter when compared to Ex1. This is because Ey1 is the primary modulus in the lateral direction, while Ex1 is secondary. The graph of stiffness against Ex1 (with other parameters kept constant) is depicted in Fig. 6.18. Depending on the value of Ex1, the stiffness can be calculated from Equation 6.22 below:

$$E_y I_{xx} = f_1 E_{x1}^4 + f_2 E_{x1}^3 + f_3 E_{x1}^2 + f_4 E_{x1} + f_5 \quad \text{Equation 6.22}$$

for $(0.01 \leq E_{x1} \leq 5)$,

$$f_1 = -3.4362E - 02, \quad f_2 = 0.6861, \quad f_3 = -4.6155, \quad f_4 = 14.393 \quad \text{and} \quad f_5 = 50.114$$

for $(5 \leq E_{x1} \leq 100)$,

$$f_1 = -9.2781E - 07, \quad f_2 = 2.3573E - 04, \quad f_3 = -2.1479E - 02, \quad f_4 = 0.8592 \quad \text{and} \\ f_5 = 67.658$$

where Ex1 is in Msi.

Equation 6.22 can be used to compute the stiffness $E_y I_{xx}$ of the panel for any given value of elastic modulus Ex1.

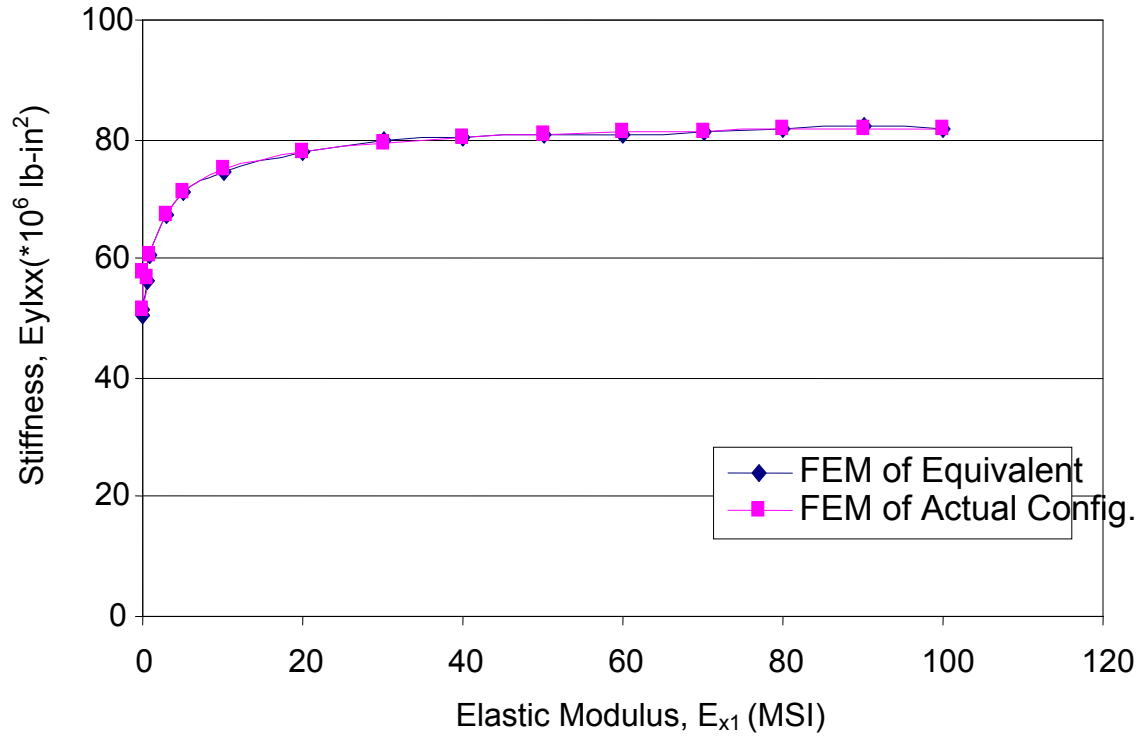


Figure 6.18: Variation of Stiffness with Face Elastic Modulus E_{x1}

A very good fit of the proposed equivalent formula (Equation 6.22) and the actual configuration model results from the finite element analysis can be seen from Fig. 6.18. The difference between both sets is approximately 0.25%.

The next parameter is the face thickness t_1 . As this parameter is varied from 0.43 in. to 2.5 in. (with other parameters kept constant), the stiffness increases from about 68,000 ksi to 135,000 ksi. Fig. 6.19 and Equation 6.23 show this relationship of stiffness $E_y I_{xx}$ with the face thickness t_1 .

$$E_y I_{xx} = I_1 t_1^2 + I_2 t_1 + I_3 \quad \text{Equation 6.23}$$

where $I_1 = -6.7217$, $I_2 = 51.146$ and $I_3 = 48.783$.

If for some reason a need arises for an engineer or manufacturer to change the thickness of the top or bottom face without altering other properties of the panel, Equation 6.23 could be used to obtain the new stiffness Ey_{lxx} .

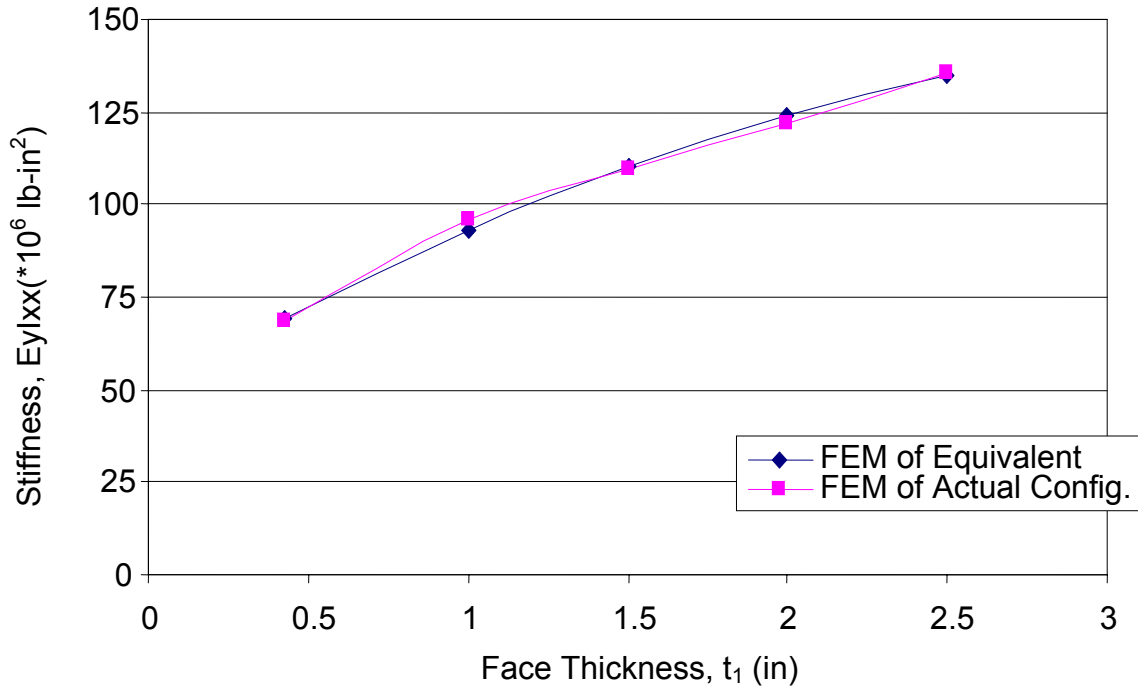


Figure 6.19: Variation of Stiffness with Face Thickness t_1

The difference between the proposed equivalent equation and the actual configuration model results from finite element analysis is about 1.6%, which is a good approximation (Fig. 6.19).

6.3.3 Variation of Stiffness with Core Parameters

The core parameters which affect the flexural stiffness Ey_{lxx} include core height H , elastic modulus of the core mat E , flute-width W , flute half-wavelength L and core material thickness t . The relationship with core height has been discussed previously. Its equation was developed and shown in Equation 6.20. In this section equations relating the stiffness and the other parameters are derived.

The first parameter to be given attention is the elastic modulus of the core material E . This parameter is varied within a range of 10 ksi to 100,000 ksi. As observed from the results, increasing E also increases the stiffness. $E_y I_{xx}$ rises from about 65,000 ksi to 120,000 ksi. Fig. 6.20 describes this behavior pictorially, which can also be seen from Equation 6.24 below:

$$E_y I_{xx} = n_1 E^2 + n_2 E + n_3 \quad \text{Equation 6.24}$$

where $n_1 = -1.5034E - 03$, $n_2 = 0.6822$ and $n_3 = 67.022$.

A different material may be used for the core mat. This would mean that the elastic modulus E would change. If this happens, Equation 6.24 becomes handy in calculating the new flexural stiffness $E_y I_{xx}$. However, all the other panel parameters have to remain unaltered for the equation to be valid.

From the graphs in Fig. 6.20, it can be observed that the proposed equivalent equation (Equation 6.24) very well approximates the actual configuration FEM results. The difference is only about 0.3%.

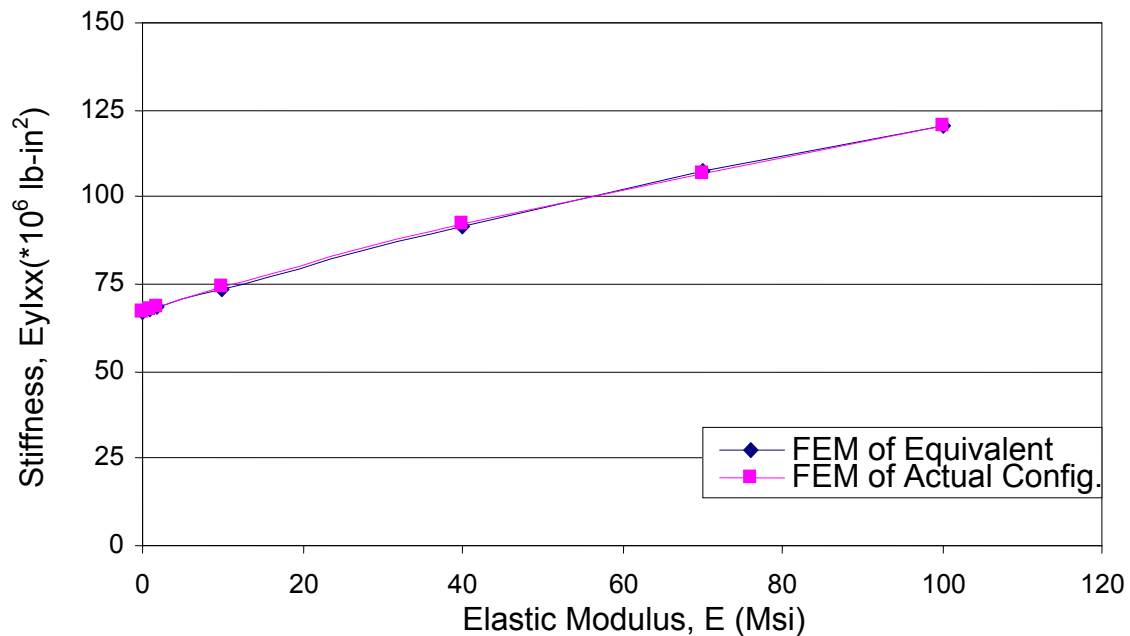


Figure 6.20: Variation of Stiffness with Core Mat Elastic Modulus E

Next, the flute-width W is varied within the range of 1 in. to 5 in. keeping other parameters constant. As revealed by the results from the analysis, increasing W also increases the flexural stiffness $E_{y|xx}$. This increase is due to the fact that the component stiffness of the flute in the lateral direction rises correspondingly with increased flute-width. In other words, when W increases, more core material is aligned in the lateral direction thus providing more stiffness in that direction. Fig. 6.21 and Equation 6.25 below show this relationship:

$$E_{y|xx} = r_1 W^2 + r_2 W + r_3 \quad \text{Equation 6.25}$$

where $r_1 = -0.4755$, $r_2 = 7.679$ and $r_3 = 55.579$.

Equation 6.25 can be used when there is a need to calculate the flexural stiffness $E_{y|xx}$ at any given value of flute width W . All other parameters must remain the same as their original basic values.

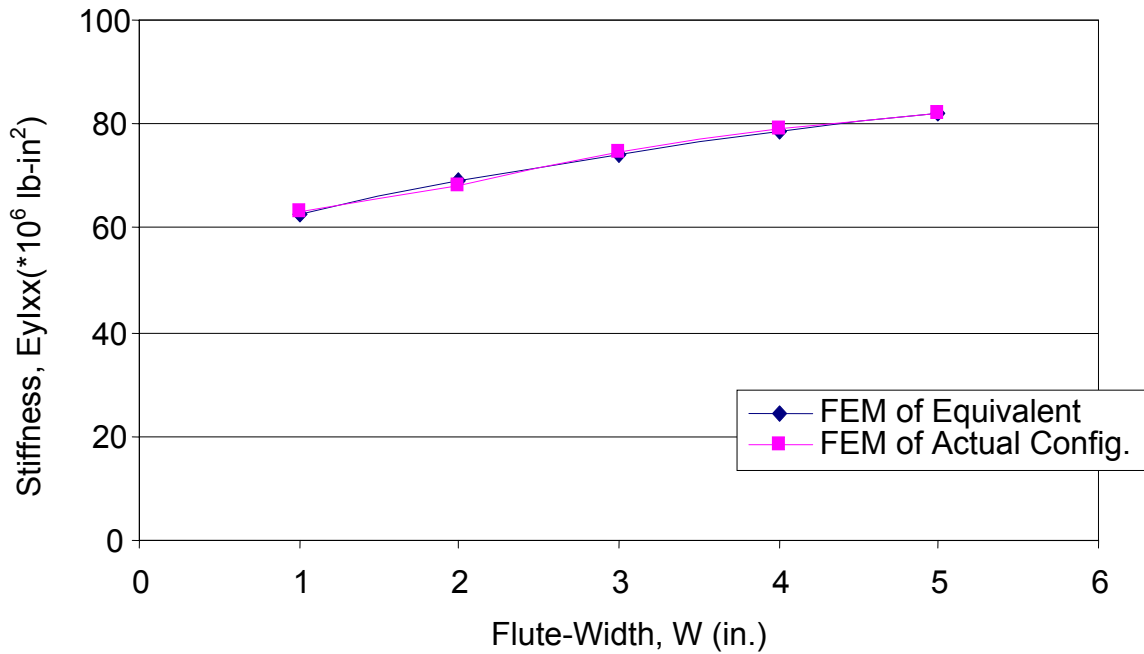


Figure 6.21: Variation of Stiffness with Flute-Width W

The proposed equivalent equation (Equation 6.25) fits the actual configuration model results from finite element analysis. The difference is just about 0.5%.

The flute half-wavelength L has a similar effect on the stiffness. It is varied from 4 inches to 12 inches, keeping other parameters at their constant basic values. As can be noticed from Fig. 6.22, Eylxx increases as L increases. This increase in stiffness is true for the entire cross-section of the beam. As L increases, the width of the beam rises correspondingly to maintain the number of half-wavelengths at two. Therefore the results obtained are always per two half-wavelengths. (This is akin to slab design where unit width is used). Since the section increases with L, Exlyy increases also. This can also be seen in Equation 6.26.

$$E_y I_{xx} = s_1 L^2 + s_2 L + s_3 \quad \text{Equation 6.26}$$

where $s_1 = 0.1260$, $s_2 = 12.494$ and $s_3 = 16.124$.

For any given value of L , the flexural stiffness $E_y I_{xx}$ can be computed using Equation 6.26 provided that the other parameters remain unchanged from their basic parametric values.

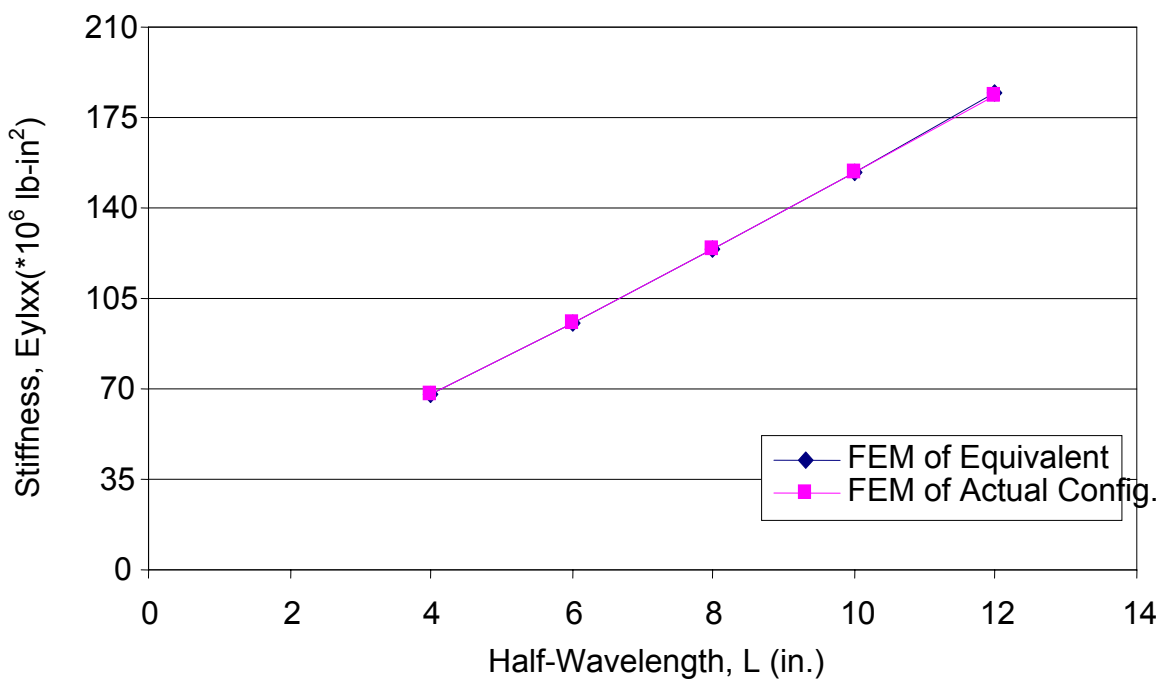


Figure 6.22: Variation of Stiffness with Half-Wavelength L

It can be observed from Fig. 6.22 that the proposed equivalent equation (Equation 6.26) very well approximates the actual configuration model results from finite elements, differing only by about 0.2%.

Lastly, the core material thickness t is varied from 0.05 in. and 0.5 in. Within this range, the flexural stiffness increases correspondingly. This increase is shown in the plot in Fig. 6.23, which can also be represented mathematically by the formula below:

$$E_y I_{xx} = p_1 t^2 + p_2 t + p_3 \quad \text{Equation 6.27}$$

where $p_1 = 5.3457$, $p_2 = 19.766$ and $p_3 = 66.315$.

Equation 6.27 can be used to obtain the flexural stiffness $E_y I_{xx}$ for any given value of core mat thickness. For example, if the same material is used for the core mat but a different thickness is needed for some reason. As in previous cases, all other parameters must remain unaltered from their original basic values for the equation to be valid.

The difference between the proposed equivalent equation and the actual configuration finite element model is about 0.15%. This illustrates that Equation 6.27 provides a very good curve fit.

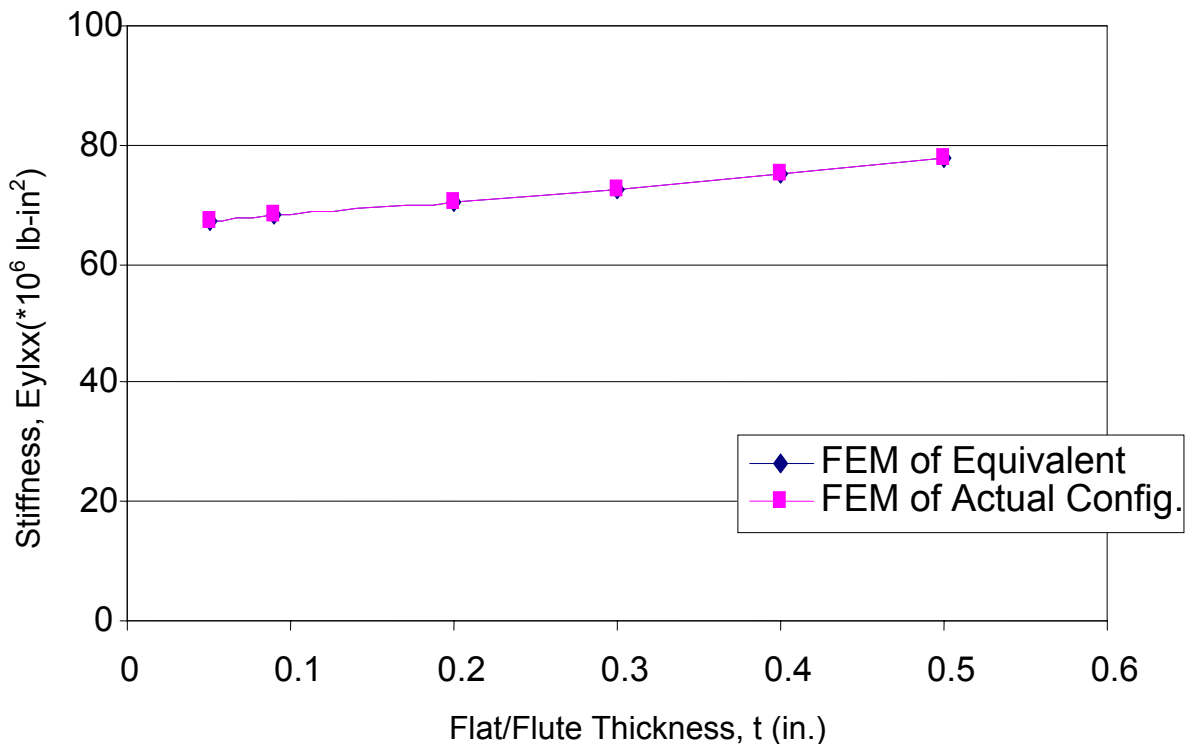


Figure 6.23: Variation of Stiffness with Flat/Flute Thickness t

6.3.4 Modification Factors

A more general formula for the flexural stiffness E_{ylxx} in terms of the eight different parameters considered in the previous section can now be derived. The same systematic approach as was followed for flexural stiffness E_{xlyy} is used. The concept of modification factors of the equivalent stiffness for a variation in parameters is employed. First of all, it was noticed that one of the most important factors influencing the stiffness is the core height. This relationship can be seen in Equation 6.20 and Fig. 6.16.

6.3.4.1 Face Lateral Elastic Modulus Modification Factor, C_1

Fig. 6.17 and Equation 6.21 showed that E_{ylxx} increases with a rise in top face lateral modulus of elasticity. A plot of the modification factor for E_{y1} , $C_1(= E_{y1}I_{xx} / E_{y1(basic)}I_{xx})$ against the ratio $S_1(= E_{y1} / E_{y1(basic)})$, reveals a similar trend. This trend can be seen in the graph in Fig. 6.24. The term $E_{y1(basic)}$ represents the basic lateral modulus of 1,870 ksi and $E_{ylxx(basic)}$ symbolizes the flexural stiffness of the panel at $E_{y1(basic)}$. The following equation (Equation 6.28) can be used to compute the modification factor:

$$C_1 = a_1 S_1^4 + a_2 S_1^3 + a_3 S_1^2 + a_4 S_1 + a_5 \quad \text{Equation 6.28}$$

for $(0.01 \leq E_{y1} \leq 5)$,

$$a_1 = -1.3816, \quad a_2 = 6.0956, \quad a_3 = -7.6948, \quad a_4 = 3.7982 \quad \text{and} \quad a_5 = 0.1826$$

for $(5 \leq E_{x1} \leq 100)$,

$$a_1 = -3.4678E-07, \quad a_2 = 4.7219E-05, \quad a_3 = -2.3135E-03, \quad a_4 = 5.0415E-02 \quad \text{and}$$

$$a_5 = 1.1279$$

where E_{y1} is in Msi.

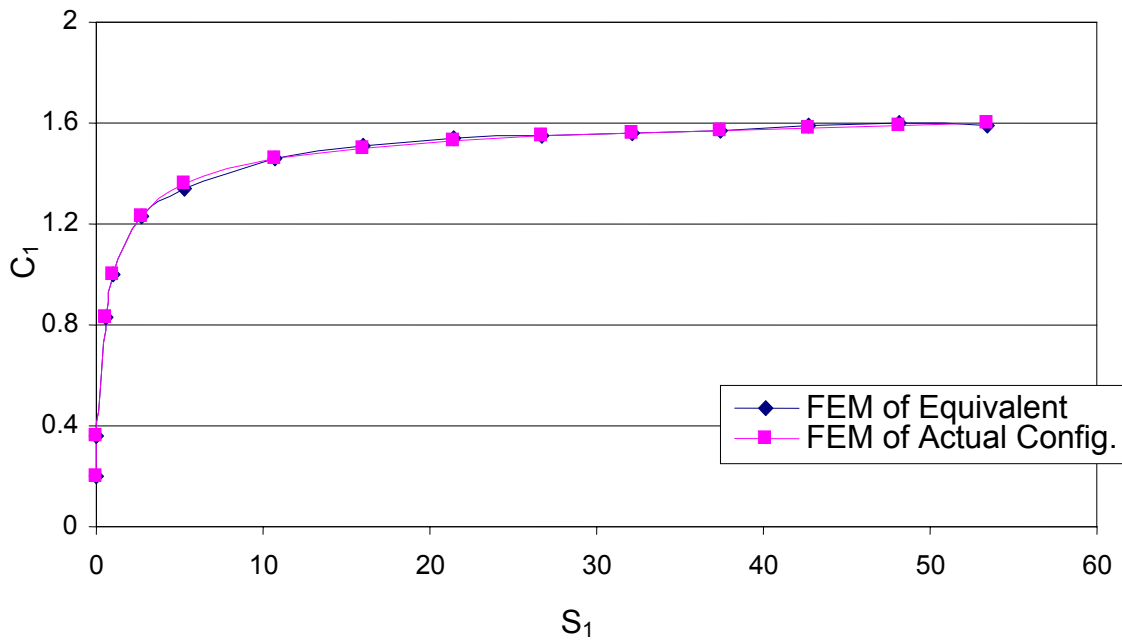


Figure 6.24: Modification Factor by Face Elastic Modulus (2-direction)

6.3.4.2 Face Longitudinal Elastic Modulus Modification Factor, C₂

Next consider is given to the modification factor with respect to the elastic modulus of the face in the longitudinal direction E_{x1} . Notice from Fig. 6.18 (as well as Equation 6.22) that as this parameter is varied, the stiffness increases. It was also explained that since E_{x1} is a secondary modulus in the lateral direction, it is a less sensitive parameter compared with E_{y1} . The modification factor is obtained by varying the ratio $S_2 (= E_{x1} / E_{x1(\text{basic})})$ for the range between 10 ksi and 100,000 ksi (with all other parameters kept constant at their basic values), where $E_{x1(\text{basic})}$ is the basic longitudinal face modulus of 2,920 ksi. If the modification factor $C_2 (= E_{y|_{xx}} / E_{y|_{xx}(\text{basic}_x)})$ is plotted against S_2 , the graph in Fig. 6.25 is obtained. $E_{y|_{xx}(\text{basic}_x)}$ represents the flexural stiffness of the panel at $E_{x1(\text{basic})}$. The following equation (Equation 6.29) defines this relationship depending on the value of E_{x1} :

$$C_2 = b_1 S_2^4 + b_2 S_2^3 + b_3 S_2^2 + b_4 S_2 + b_5 \quad \text{Equation 6.29}$$

for $(0.01 \leq E_{x1} \leq 5)$,

$$b_1 = -3.7061E-02, \quad b_2 = 0.2534, \quad b_3 = -0.5838, \quad b_4 = 0.6235 \quad \text{and} \quad b_5 = 0.7435$$

for $(5 \leq E_{x1} \leq 100)$,

$$b_1 = -5.0797E-07, \quad b_2 = 4.705E-05, \quad b_3 = -1.6041E-03, \quad b_4 = 0.025097 \quad \text{and}$$

$$b_5 = 1.0448.$$

where E_{x1} is in Msi.

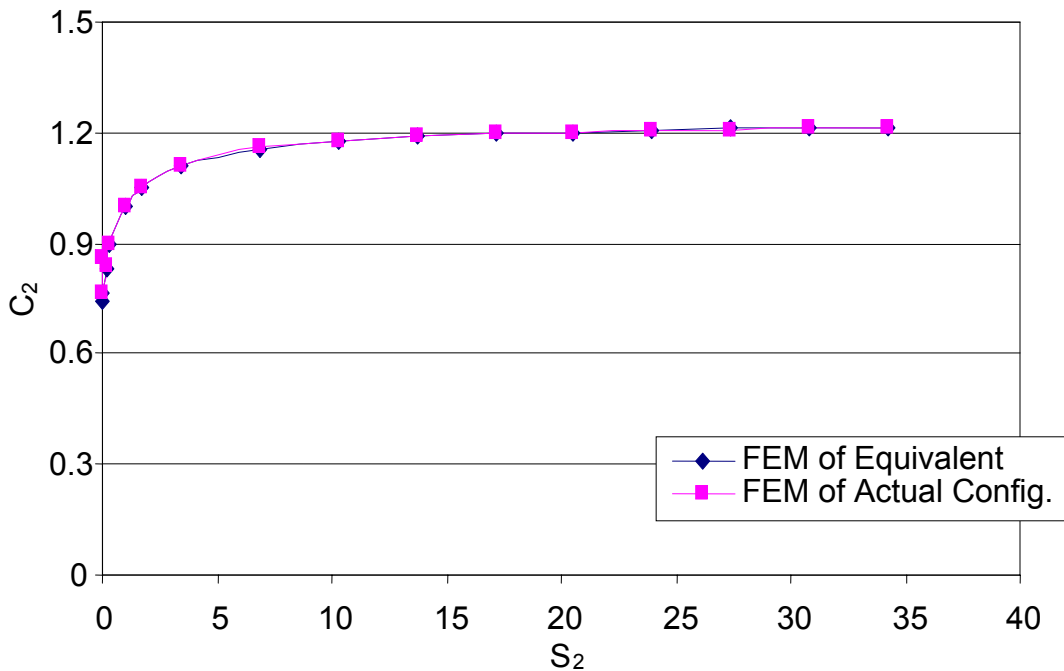


Figure 6.25: Modification Factor by Face Elastic Modulus (1-direction)

6.3.4.3 Face Thickness Modification Factor, C₃

The next modification factor considered is that with respect to the thickness of the top face. It can be recalled from Fig. 6.19 that the stiffness of the panel increases with an increase in face thickness t_1 . The relationship is also shown in Equation 6.23.

The modification factor can now be derived by varying the thickness ratio $S_3 (= t_1 / t_{1(0.43)})$ within a range of thickness of 0.43 in. to 2.5 in., where $t_{1(0.43)}$ represents the basic face thickness of 0.43 in. A plot of $C_3 (= E_y I_{yy} / E_y I_{yy(\text{basic_}t1)})$ against S_3 yields the graph shown in Fig. 6.26. The flexural stiffness of the panel when t_1 is 0.43 in. is represented by the term $E_y I_{yy(\text{basic_}t1)}$. This plot has the following equation:

$$C_3 = c_1 S_3^2 + c_2 S_3 + c_3 \quad \text{Equation 6.30}$$

where $c_1 = -1.8196E - 02$, $c_2 = 0.322$ and $c_3 = 0.7142$.

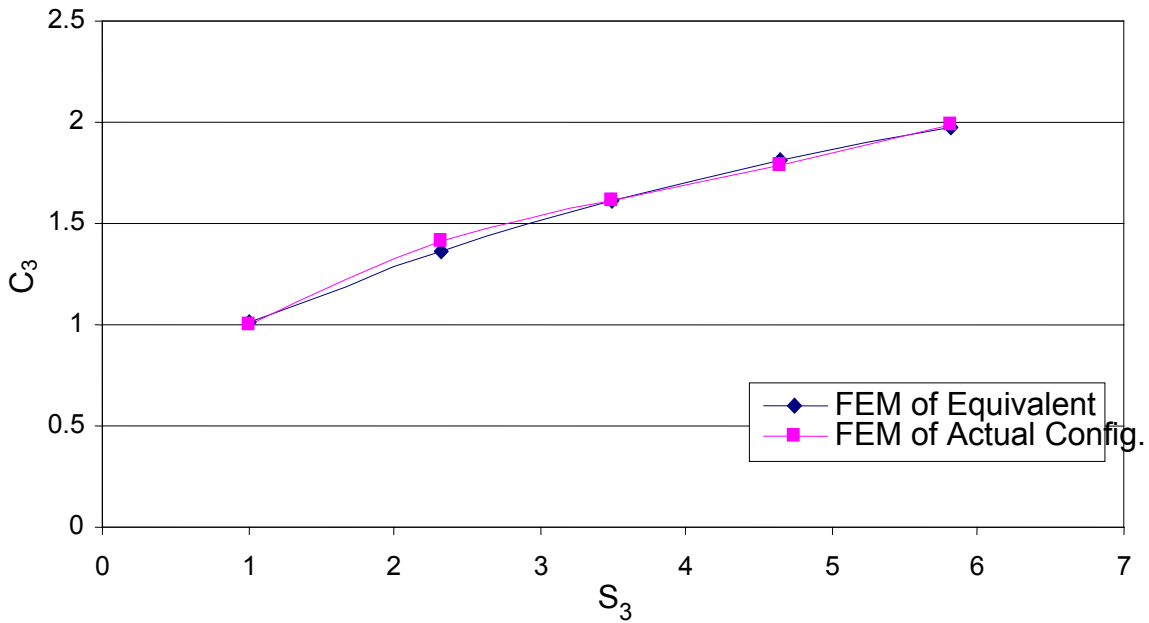


Figure 6.26: Modification Factor by Face Thickness

6.3.4.4 Core Mat Elastic Modulus Modification Factor, C_4

From Fig. 6.20 and Equation 6.24, the relationship between the modulus of elasticity of the core mat and the flexural stiffness was shown. As the elastic modulus E increases, so does the flexural stiffness. Derivation of the equation for modification factor of the stiffness due to E is of interest. This is performed by computing the elastic

modulus ratio $S_4 (= E / E_{(1.71)})$ and the corresponding modification factor $C_4 (= E_y I_{xx} / E_y I_{xx}(\text{basic_E}))$ as E varies from 10 ksi to 100,000 ksi while all the other variables are kept constant at their basic parametric values. $E_{(1.71)}$ is the basic core mat elastic modulus of 1,710 ksi, while the term $E_y I_{xx}(\text{basic_E})$ represents the flexural stiffness of the panel at $E_{(1.71)}$. Plotting C_4 versus S_4 produces the graph in Fig. 6.27 whose equation is:

$$C_4 = d_1 S_4^2 + d_2 S_4 + d_3 \quad \text{Equation 6.31}$$

where , $d_2 = 1.7096E - 02$ and $d_3 = 0.9822$.

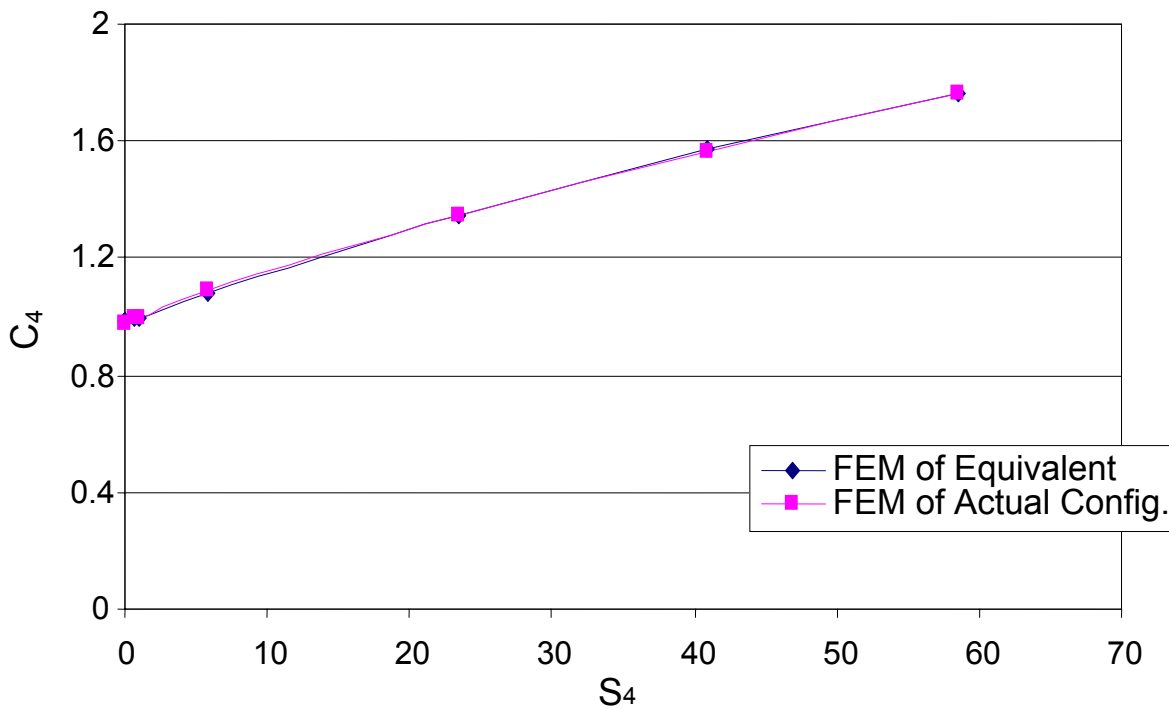


Figure 6.27: Modification Factor by Core Mat Elastic Modulus

6.3.4.5 Core Flute-Width Modification Factor, C_5

An increase in the flute-width W results in a rise in the panel flexural stiffness $E_{yI_{xx}}$. This can be observed from Figure 6.21 and Equation 6.25. A plot of the modification factor for flute-width, $C_5 (= E_{yI_{xx}} / E_{yI_{xx}(\text{basic}_W)})$ against the ratio $S_5 (= W / W_{(2)})$ shows a similar behavior. This relationship is seen from the graph in Fig. 6.28. $W(2)$ represents the basic flute-width of 2 in. and $E_{yI_{xx}}(\text{basic}_W)$ is the flexural stiffness of the panel when the flute-width is 2 in. To calculate this modification factor, Equation 6.32 can be used:

$$C_5 = k_1 S_5^2 + k_2 S_5 + k_3 \quad \text{Equation 6.32}$$

where $k_1 = -2.7848E-02$, $k_2 = 0.2249$ and $k_3 = 0.8137$.

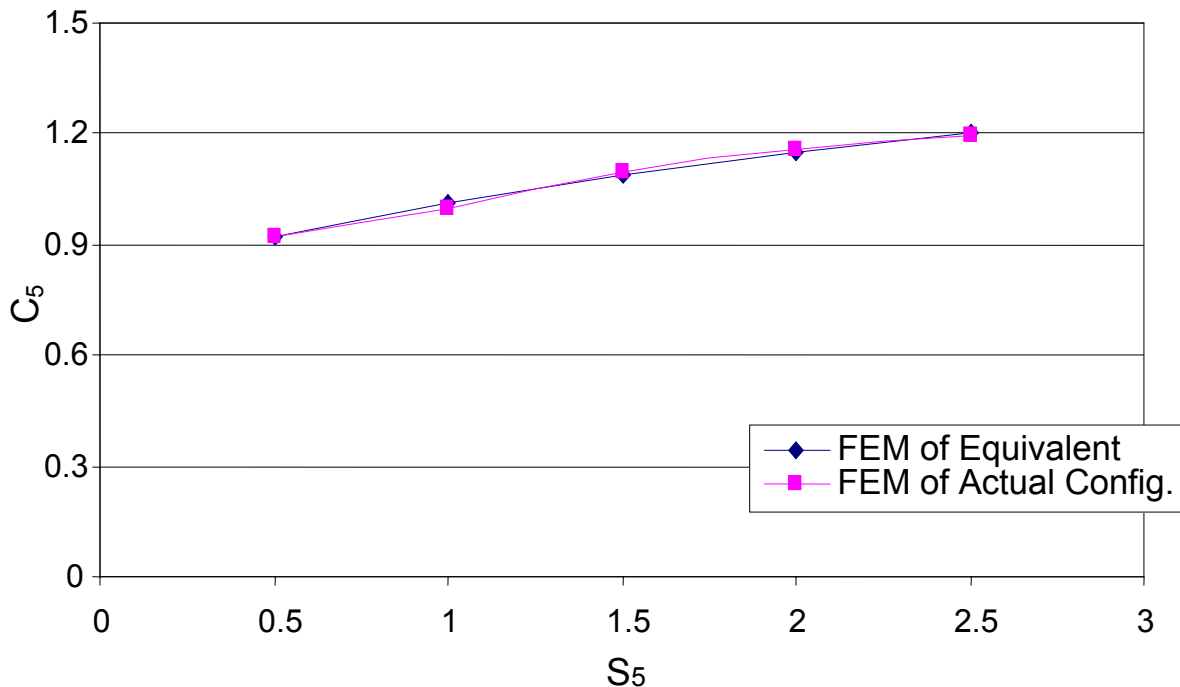


Figure 6.28: Modification Factor by Flute Width

6.3.4.6 Core Half-Wavelength Modification Factor, C_6

Next an equation for the modification factor of the stiffness due to the half-wavelength L is derived. From Figure 6.22, a rise in half-wavelength results in an increase in the stiffness. Equation 6.26 also shows this. By plotting the modification factor $C_6 (= E_y I_{yy} / E_y I_{yy}(\text{basic_L}))$ against the $S_6 (= L / L_{(4)})$ ratio, a similar behavior is noted. (Fig. 6.29) $L(4)$ represents the basic half-wavelength of 4 in. and $E_y I_{yy}(\text{basic_L})$ is the flexural stiffness of the panel at $L(4)$. The modification factor C_6 can be calculated as follows:

$$C_6 = m_1 S_6^2 + m_2 S_6 + m_3 \quad \text{Equation 6.33}$$

where, $m_1 = 2.9518E - 02$ $m_2 = 0.7317$ and $m_3 = 0.2361$.

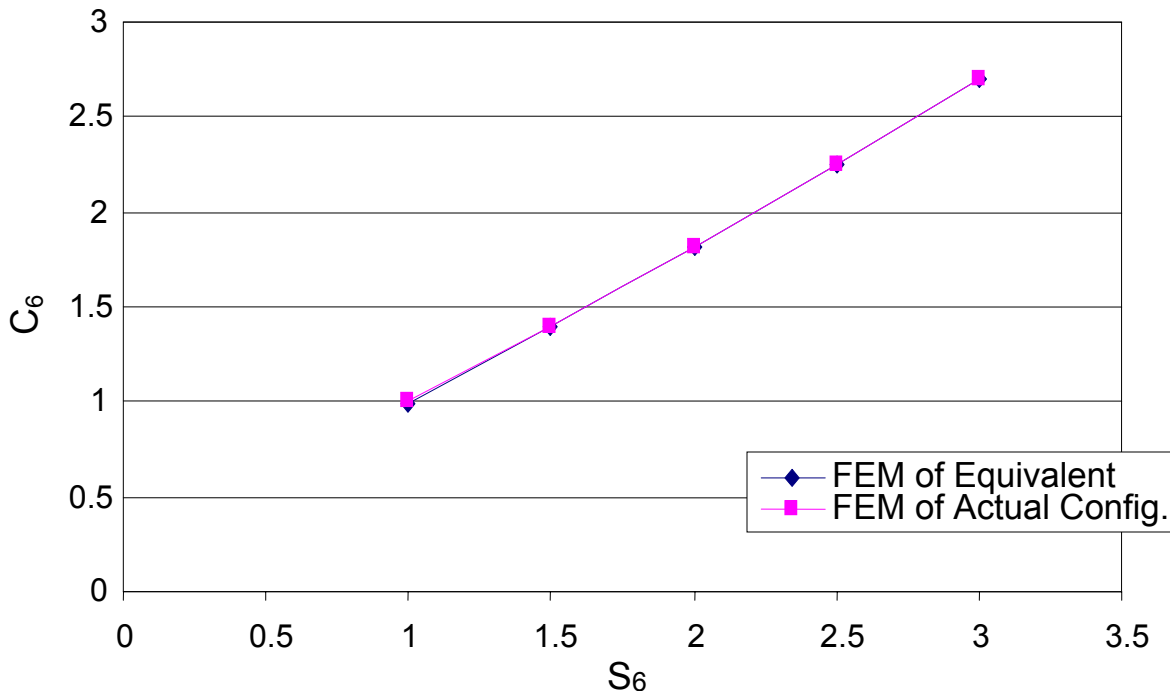


Figure 6.29: Modification Factor by Half-Wavelength

6.3.4.7 Core Material Thickness Modification Factor, C_7

The final modification factor derived is that due to the core mat thickness t . Flexural stiffness increases with the thickness of the core material, as shown in Fig. 6.23 and Equation 6.27. The thickness ratio $S_7 (= t / t_{(0.0898)})$ is computed for a range of t from 0.05 inch to 0.5 inch. $t_{0.0898}$ is the basic flat/flute thickness of 0.0898 inch. In Fig. 6.30, the modification factor $C_7 (= E_y I_{xx} / E_y I_{xx(\text{basic}_t)})$ is plotted against S_7 , where $E_y I_{xx(\text{basic}_t)}$ refers to the flexural stiffness of the panel at $t_{0.0898}$. The formula for the flat/flute thickness modification factor can be expressed as follows:

$$C_7 = p_1 S_7^2 + p_2 S_7 + p_3 \quad \text{Equation 6.34}$$

where $p_1 = 6.3114E-04$, $p_2 = 2.5988E-02$ and $p_3 = 0.9709$.

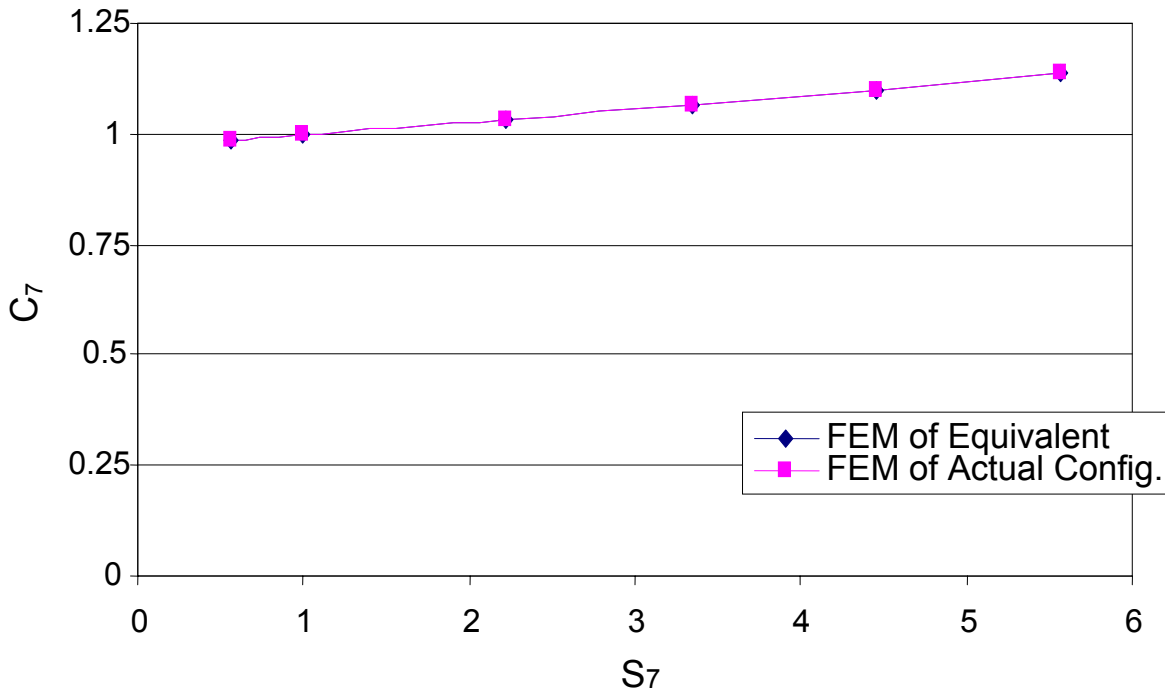


Figure 6.30: Modification Factor by Flat/Flute Thickness

6.3.5 Formula for Predicting Flexural Stiffness $E_y I_{xx}$

The previous sections discussed interrelationship between the various panel parameters. With these results, the following equation is now proposed for calculating the flexural stiffness $E_y I_{xx}$:

$$E_y I_{xx} = C_1 C_2 C_3 C_4 C_5 C_6 C_7 (E_y I_{xx})_H \quad \text{Equation 6.35}$$

where C_1 , C_2 , C_3 , C_4 , C_5 , C_6 , C_7 and $(E_y I_{xx})_H$ can be obtained from Equations 6.20, 6.28, ..., 6.34

Like the case of flexural stiffness in the longitudinal direction $E_x I_{yy}$, it can be noticed here that Equation 6.35 is derived based on the variation of just the top face. However, the same formula can be applied to the two faces of the sandwich structure. The same assumption as was done previously is made. That is, introducing new modification coefficients which take into account the variation in the bottom face. The new factors have the same formulae as those of the top face. The modification factors in Equation 6.35 can thus be modified as follows:

$$C_i = C_{i1} C_{i2} \quad \text{Equation 6.36}$$

where C_{i1} and C_{i2} refer to the modification factors for top and bottom faces respectively and $i = 1, 2, \dots, 7$.

It is pertinent to note that the equation is valid for a beam with a width equal to twice the half-wavelength. Hence, if the half-wavelength is 4 inches, the width of the beam for the computation of $E_y I_{xx}$ is 8 inches. This was the assumption made in the derivation of the formula.

6.4 Equivalent Shear Stiffness $G_{xy}A_s$

It was discussed previously that the shear contribution to deflection is sometimes ignored in structural analysis, because for long beams this contribution is not significant. For deep beams, however, the shear contribution has to be included in the traditional beam deflection equation, because it can become a major factor in the structure's behavior.

In this section, parametric studies are performed with the objective of deriving an equation for the shear stiffness of the sinusoidal sandwich beam. Even in cases where the shear contribution can be ignored, we sometimes need to input its value for analysis purposes. The proposed equation can therefore be helpful in those cases also.

Just as was mentioned previously, the approach employed to derive the shear stiffness considers the fact that the total deflection of the beam model is a summation of both the bending and shear deflections. This is illustrated by Equation 6.37 below for a cantilever beam of span L , flexural stiffness EI , shear stiffness GA and with a point load P at its free end:

$$\Delta = \frac{PL^3}{3EI} + \frac{PL}{GA_s} \quad \text{Equation 6.37}$$

The beam for this study is modeled as a cantilever with span L . The nodes on one of its ends are fixed for all degrees of freedom. At the other end, the nodes are kept free, and a point load P_y is applied in the lateral direction. This causes bending in the lateral direction (y) about the vertical axis (z), and shear of the longitudinal-lateral (x - y) plane. The shear modulus G_{xy} ($= G_{yx}$) can be calculated from the total deflection using the following formula:

$$G_{xy}A_s = \frac{P_y L}{(\delta_y - (P_y L^3 / 3E_x I_{zz}))} \quad \text{Equation 6.38}$$

The flexural stiffness $E_x I_{zz}$ is computed from $E_x I_{yy}$ in Equation 6.17 and the given cross-section using the following relation:

$$E_x I_{zz} = E_x I_{yy} \frac{I_{zz}}{I_{yy}} \quad \text{Equation 6.39}$$

The method employed to develop the shear stiffness equations is the same systematic approach that has been used in this work, where the concept of modification factors come to play. First though, the stiffness equations as a function of individual variables are derived.

6.4.1 Variation with Parameters

The elastic modulus in the longitudinal direction E_{x1} is first varied within a range of 1,000 ksi to 100,000 ksi, keeping other parameters constant. With each change in this parameter, $G_{xy}A_s$ is computed using Equations 6.38 and 6.39. To obtain E_{x1} , Equation 6.3 is used. The shear stiffness increases rapidly within lower values of E_{x1} , but this increase has a smaller rate as the elastic modulus increases. The relationship between the shear stiffness and elastic modulus can be seen from the results plotted in Fig. 6.31. It can also be expressed by the equation below:

$$(G_{xy}A_s)_{E_{x1}} = aE_{x1}^n \quad \text{Equation 6.40}$$

where $a = 4.9321E + 04$, $n = 0.1933$ and E_{x1} is in psi.

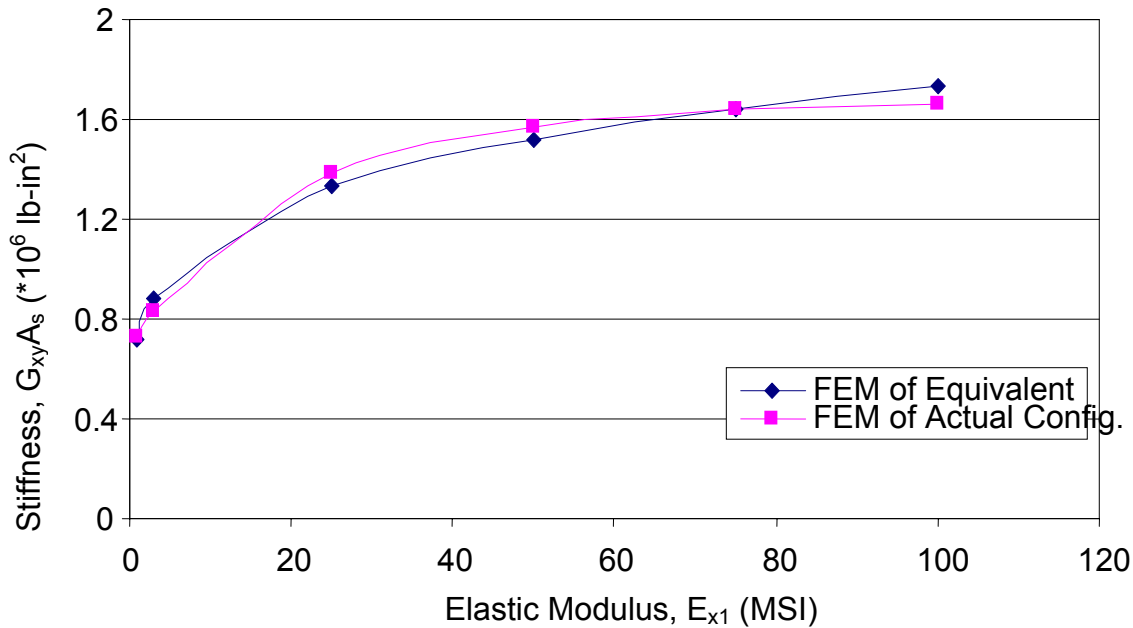


Figure 6.31: Variation of Stiffness with Face Elastic Modulus E_{x1}

As can be observed from Fig. 6.31, the proposed equivalent formula in Equation 6.40 well predicts the actual configuration model results from the finite element analysis. The difference between both sets of data is only about 3%.

Next, the shear modulus of the top face G_{xy1} is varied from 500 ksi to 10,000 ksi. The stiffness rises following the same trend as the case of E_{x1} . Equations 6.38 and 6.39 are used to compute $G_{xy}A_s$. To obtain E_{xlyy} for the variation of G_{xy1} , the Equation 6.41 below is used.

$$E_{xlyy} = wG_{xy1}^v \quad \text{Equation 6.41}$$

where $w = 4.8306E + 07$, $v = 4.8236E - 02$ and G_{xy1} is in psi.

Equation 6.41 was developed during the parametric studies of flexural stiffness E_{xlyy} . However, because G_{xy1} is not a significant contributing factor to flexural stiffness E_{xlyy} , Equation 6.41 is not incorporated in Equation 6.17 developed previously, and

nothing has been mentioned about it thus far. It is discussed in this section since its influence on the shear stiffness is important.

From the results of shear stiffness obtained by varying G_{xy1} , the plot in Fig. 6.32 is produced. The equation of this plot is shown below:

$$G_{xy} A_s = k G_{xy1}^m \quad \text{Equation 6.42}$$

where $k = 2.4995E + 05$, $m = 8.7095E - 02$ and G_{xy1} is in psi.

The plots in Fig. 6.32 show that Equation 6.42 proposed for the equivalent shear stiffness as a function of the face shear modulus G_{xy1} well predicts the actual configuration finite element model results. The difference between both data sets is approximately 1.6%.

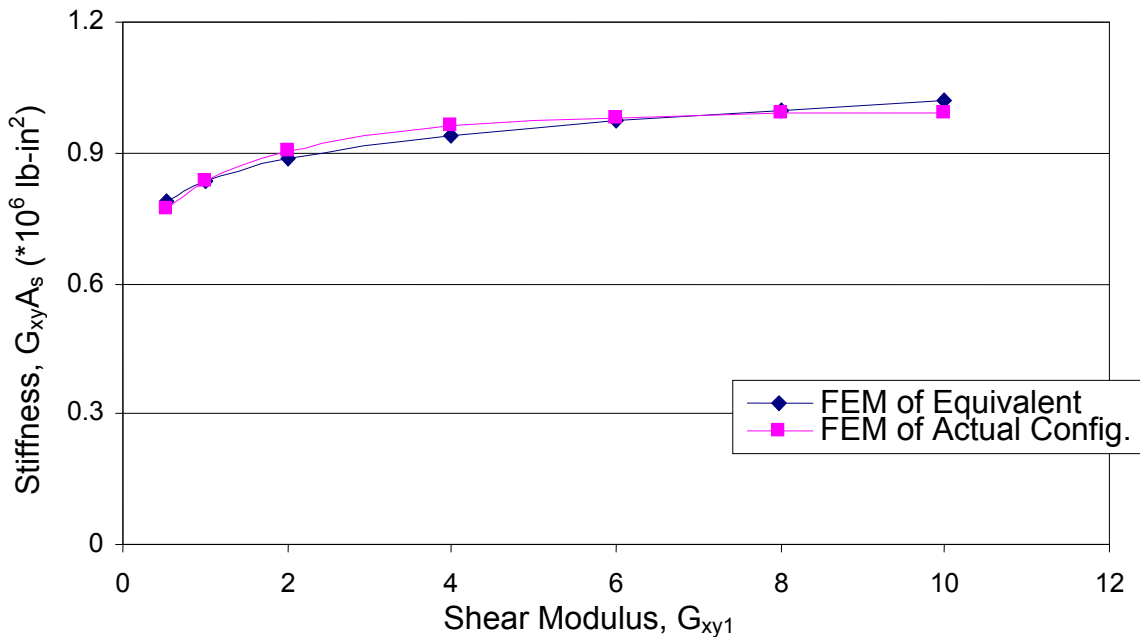


Figure 6.32: Variation of Stiffness with Face Shear Modulus G_{xy1}

The third parameter considered is the top face thickness t_1 . This parameter is varied from 0.43 in. to 2.5 in. while other parameters are kept constant at their basic parametric values. It can be observe from the plot in Fig. 6.33 that the shear stiffness increases with the face thickness, and this parameter is the most sensitive of all. The shear stiffness $G_{xy}A_s$ for each thickness value is computed using Equation 6.38. Equations 6.5 and 6.39 are used to compute the needed flexural stiffness.

The relationship between the shear stiffness $G_{xy}A_s$ and the face thickness t_1 is shown by the following formula:

$$G_{xy}A_s = r + st_1 \tag{Equation 6.43}$$

where $r = 5.5314E + 05$, $s = 1.0295E + 06$ and t_1 is in inches.

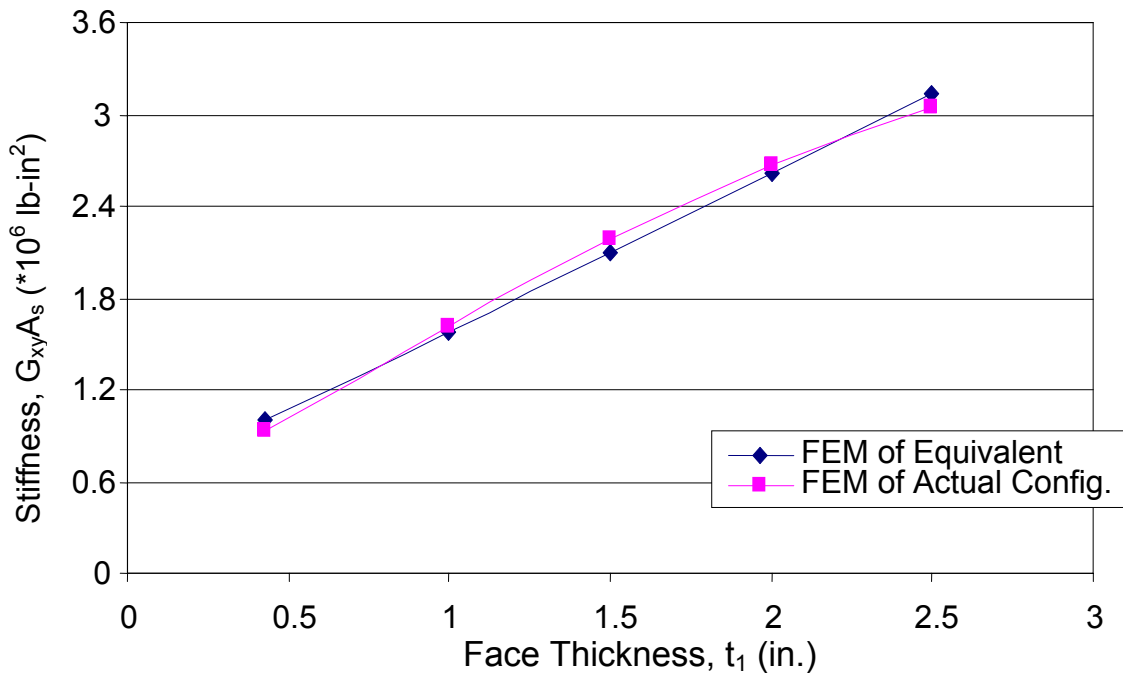


Figure 6.33: Variation of Stiffness with Face Thickness t_1

Again, the proposed equation for equivalent shear stiffness in terms of face thickness (Equation 6.43) very well predicts the actual configuration finite element model results obtained from the analysis. This good curve fit can be noticed from Fig. 6.33. The difference between the proposed and the actual data sets is only about 3%.

Finally, the relationship between the shear stiffness and the core height is studied. The core height H is varied between 4.57 in. and 19.57 in. Using the same approach as in the previous parameters, the shear stiffness $G_{xy}A_s$ is computed using Equation 6.38. The flexural stiffness Ex_{lzz} is first calculated from Equations 6.2 and 6.39. As the core height increases, so does the shear stiffness. This is seen in Fig. 6.34 and the equation below.

$$G_{xy}A_s = qH^p \quad \text{Equation 6.44}$$

where $q = 3.3137E + 05$, $p = 0.5760$ and H is in inches.

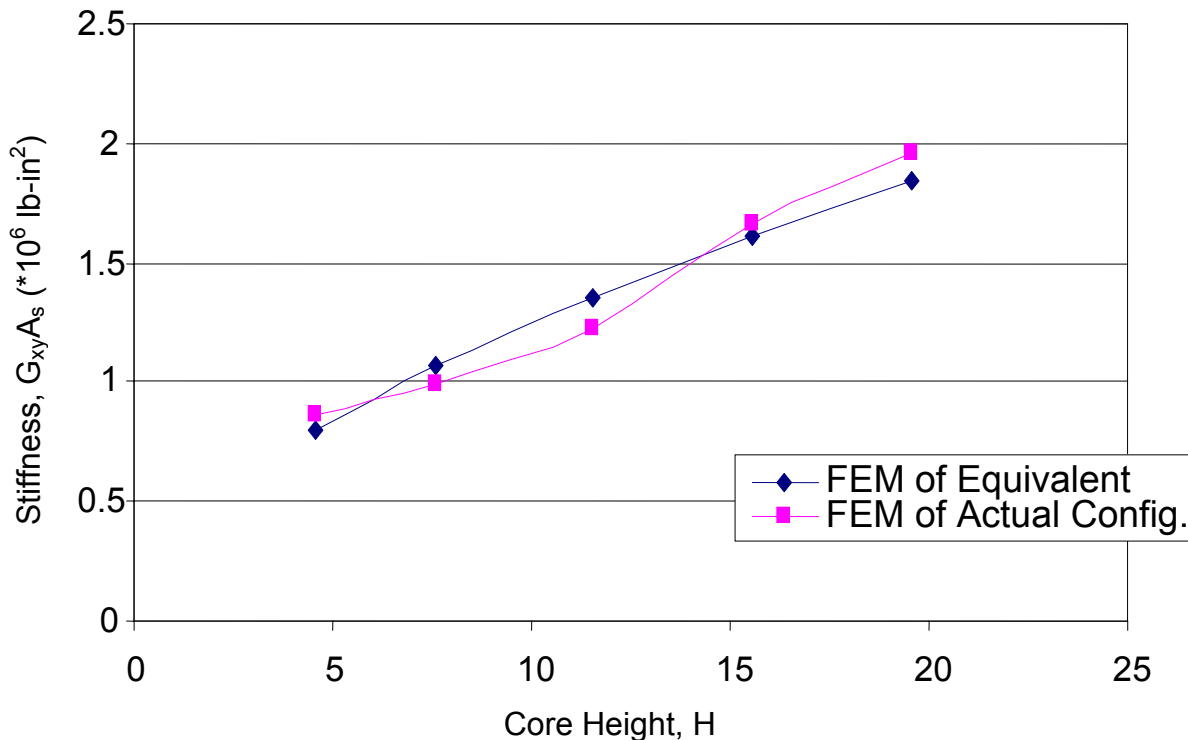


Figure 6.34: Variation of Stiffness with Core Height H

Equations 6.40, 6.42, 6.43 and 6.44 could be used to compute the shear stiffness $G_{xy}A_s$ of the FRP sinusoidal wave core sandwich panel when only one of its parameters is changed from the original basic value. If, for example, the thickness of the top face is changed for some reason and all the other parameters are unaltered from their basic values, Equation 6.43 could be used to calculate $G_{xy}A_s$.

6.4.2 Modification Factors

To derive a formula for the shear stiffness in terms of the four parameters discussed in the previous section, the same systematic approach that was used for the flexural stiffnesses E_{xlyy} and E_{ylxx} is followed. Modification factors of the stiffness in terms of the individual parameters are first sought, and then the general formula as a function of these factors is derived.

As was discussed previously, one of the important parameters influencing the shear stiffness is the elastic modulus of the face in the longitudinal direction. The relationship was derived and shown in Equation 6.40. This equation forms the base of the proposed general formula.

6.4.2.1 Face Shear Modulus Modification Factor, D_1

The first modification factor derived is that relating to the shear modulus of the face G_{xy1} . It was shown that the beam equivalent shear stiffness increases with the face shear modulus. The equation derived to show that relationship can be seen in Equation 6.42. The plot in Fig. 6.32 also illustrates this trend. To obtain the equation for modification factor by this parameter, the shear modulus ratio $T_1 (= G_{xy1} / G_{xy1(0.546)})$ is calculated for a range of G_{xy1} of 500 ksi to 10,000 ksi. The modification factor $D_1 (= G_{xy}A_s / G_{xy}A_{s(\text{basic}_G)})$ is then plotted against T_1 , and this is shown in Fig. 6.35. The

terms $G_{xy1}(0.546)$ and $G_{xyAs}(\text{basic_G})$ represent the basic face shear modulus of 546 ksi and the corresponding equivalent shear stiffness respectively. The plot in Fig. 6.35 can also be expressed by the following equation:

$$D_1 = bT_1^m \quad \text{Equation 6.45}$$

where $b = 1.0250$ and $m = 8.7095E - 02$.

6.4.2.2 Face Thickness Modification Factor, D_2

Next, the thickness ratio $T_2 (= t_1 / t_{1(0.43)})$ is varied within a range of thickness of 0.43 in. to 2.5 in. The modification factor by face thickness is obtained by computing the ratio $D_2 (= G_{xy}A_s / G_{xy}A_{s(\text{basic_}t1)})$ for each thickness ratio value. The term $t1(0.43)$ refers to the basic face thickness value of 0.43 in., while $G_{xyAs}(\text{basic_}t1)$ is the equivalent shear stiffness at $t1(0.43)$. It can be recalled from Equation 6.43 and Fig. 6.33 that the face thickness is the most sensitive of all the parameters. There is a linear increase in the stiffness as $t1$ rises. A plot of D_2 against T_2 as shown in Fig. 6.36 reveals the same linear relationship. Mathematically, it can be written as follows:

$$D_2 = c + dT_2 \quad \text{Equation 6.46}$$

where $c = 0.5954$ and $d = 0.4765$.

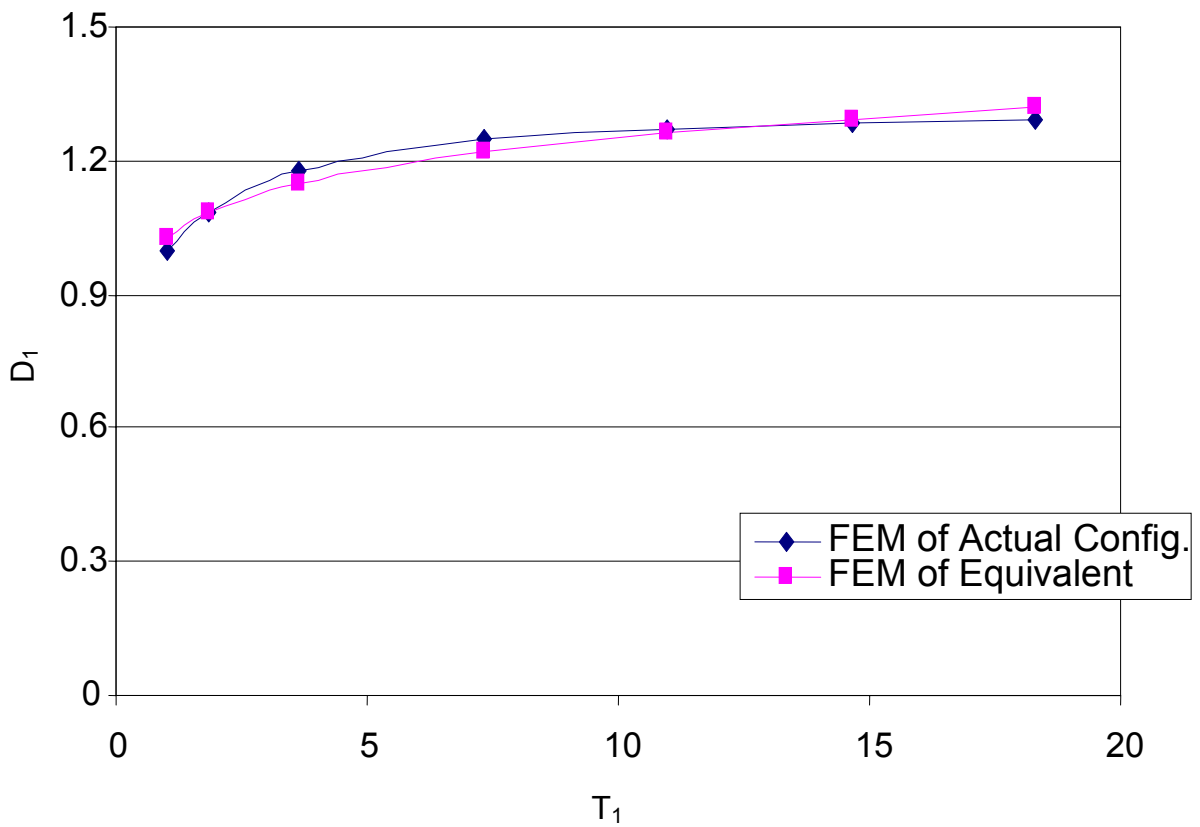


Figure 6.35: Modification Factor by Face Shear Modulus

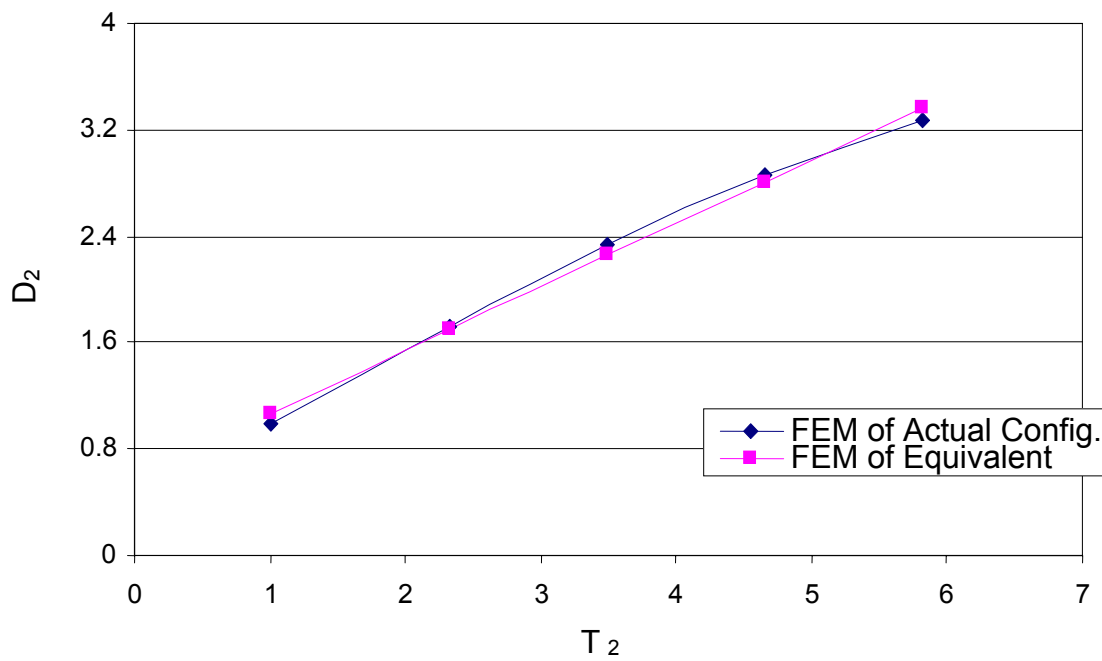


Figure 6.36: Modification Factor by Face Thickness

6.4.2.3 Core Height Modification Factor, D_3

Finally, the modification factor by core height is derived. From Equation 6.44 and Fig. 6.34, it can be observed that increasing the depth of the core results in a corresponding increase in the equivalent shear stiffness. To derive the equation for the modification factor, the thickness of the core is varied within a range of 4.57 in. to 19.57 in., and the ratio $T_3 (= H/H_{(4.57)})$ is computed for each variation. Each corresponding stiffness ratio $D_3 (= G_{xy}A_s / G_{xy}A_{s(\text{basic}_H)})$ is also computed, and D_3 is plotted against T_3 . The resulting plot is shown in Fig. 6.37. $H(4.57)$ is the basic core height of 4.57 in., and $G_{xy}A_{s(\text{basic}_H)}$ represents the equivalent shear stiffness when H is 4.57 in. The core height modification factor can thus be calculated using the formula:

$$D_3 = zT_3^p \quad \text{Equation 6.47}$$

where $z = 0.9271$ and $p = 0.5760$.

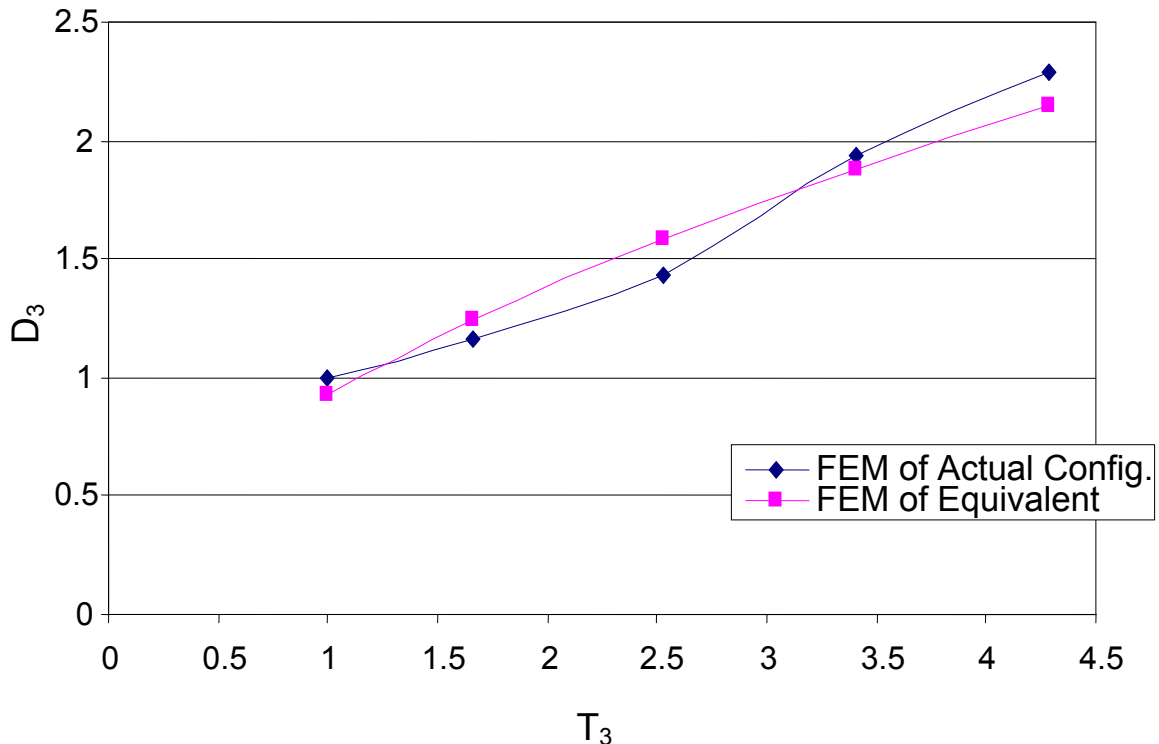


Figure 6.37: Modification Factor by Core Height

6.4.3 Formula for Predicting Shear Stiffness $G_{xy}A_s$

Having studied the inter-relationship between the four different parameters for equivalent shear stiffness using the systematic approach above, they can all be put together into a general equation of the following proposed form (Equation 6.48):

$$G_{xy}A_s = D_1 D_2 D_3 (G_{xy}A_s)_{E_x1} \quad \text{Equation 6.48}$$

where D_1 , D_2 , D_3 and $(G_{xy}A_s)_{E_x1}$ can be obtained from Equations 6.40, 6.45, ..., 6.47

6.5 Application of Stiffness Properties to Deck Model

The stiffness properties derived were based on a beam model. However, since decks can be viewed as a combination of several beams, the stiffness properties just derived could be extended to decks. Decks are sometimes designed as beams with a certain width such as a unit. The design results are then extended to the entire deck. In the derivations we have made so far, the analyses were performed using a beam with width equal to 4 flute-widths (for stiffness in longitudinal direction), or 2 half-wavelengths (for stiffness in lateral direction). Hence, the equivalent stiffness properties of a sinusoidal-wave core sandwich deck system will consider a representative beam cross-section with the same width just described. In other words, instead of talking about stiffness per unit width, we will be dealing with stiffness per 4-flute-width or per 2-half-wavelength.

In deriving the stiffness equations, one parameter is varied and all others are kept constant. With the assumption that these parameters are independent from each other, a systematic approach was followed to derive modification factors. These individual equations can be seen in the previous section. As expected with any curve fitting approach, the equations do not perfectly fit the data. However, the deviation and

variation in each of these equations are acceptably small. For instance, talking about the most important stiffness property, the flexural stiffness in the longitudinal direction $E_x I_{yy}$, the average difference between the derived equation and actual data for all data sets of core height H was approximately 0.13%. For modification factor by elastic modulus of top face in longitudinal direction, it was about 0.24%. Tables 6.4 to 6.6 below summarize these differences for the three stiffness properties. The differences in Table 6.4 were calculated based on the data and graphs in Figs. 6.1 to 6.8. Table 6.5 was derived from Figs. 6.16 to 6.23. And the results in Table 6.6 were computed from Figs. 6.31 to 6.34.

The question that arises is: What happens when these individual equations are combined to yield the general stiffness formulae in Equations 6.17, 6.35 and 6.48? How accurate will the results be? To prove that a high level of accuracy will still exist, two phases of verification are carried out.

Table 6.4: Average difference between equation and actual data for Flexural Stiffness $E_x I_{yy}$

Parameter	Average % diff.
H	0.13
E_{x1}	0.24
E_{y1}	0.36
t_1	1.46
E	0.39
W	0.66
L	0.28
t	0.09

Table 6.5: Average difference between equation and actual data for Flexural Stiffness $E_y I_{xx}$

Parameter	Average % diff.
H	0.05
E_{x1}	0.14
E_{y1}	0.31
t_1	1.62
E	0.31
W	0.53
L	0.21
t	0.16

Table 6.6: Average difference between equation and actual data for Flexural Stiffness $G_{xy} A_s$

Parameter	Average % diff.
H	6.54
E_{x1}	3.26
G_{xy1}	1.62
t_1	3.27

6.5.1 Verification Phases

6.5.1.1 Phase I

In this phase, we investigate if the basic parameters used in the derivation maintain an acceptable level of accuracy. This is necessary because if the equations don't hold true for these basic parameters, they would certainly not work for others.

The model used in this verification is a simply-supported deck with the dimensions 15 ft x 7.75 ft x 5 in. A load of 5 kips is applied at the mid-span as pressure on elements measuring 8 in. x 12 in. A comparison of the actual sinusoidal wave-core sandwich deck with its equivalent derived from the proposed equations is sought. The values of the parameters for the actual model are shown in Table 6.3.

With these parameters, the flexural and shear stiffness values are computed using Equations 6.17, 6.35 and 6.48. It should also be noted that the stiffnesses calculated from those equations are not per unit width, but per 4-flute-width or per 2-half-wavelength. Thus the moment of inertia (I_{yy} or I_{xx}), or shear area (A_s) is calculated based on the width of this given cross-section. The equivalent panel elastic modulus in the longitudinal and lateral directions (E_x and E_y), as well as the equivalent shear modulus (G_{xy}) can then be evaluated. These properties are shown in Table 6.7. These are used as inputs in a simple model of single layered shell elements with the same dimensions and loading conditions. A first-order finite element analysis is performed, and the deflection results recorded as can be observed from Table 6.8. The comparison is done for both the longitudinal and lateral directions. Table 6.8 also shows the FEM results of the actual sandwich model.

Table 6.7: Equivalent stiffness values and corresponding moduli

$E_x I_{yy}$ (lb-in ²)	8.6557E+07
$E_y I_{xx}$ (lb-in ²)	6.9774E+07
$G_{xy} A_s$ (lb-in ²)	8.9317E+05
E_x (psi)	1.0387E+06
E_y (psi)	8.3729E+05
G_{xy} (psi)	2.6795E+04

Table 6.8a: Comparison of deflection results. Points in the longitudinal direction along the central line.

Distance (in.)	0	22	45	67	90
Actual Config FEM	0	0.4205	0.8070	1.0778	1.2016
Equivalent FEM (Equation)	0	0.4315	0.8276	1.1023	1.2182
% Diff.		2.5356	2.4796	2.2226	1.3627

Table 6.8b: Comparison of deflection results. Points in the lateral direction along the midspan

Distance (in.)	0	23	46	69	92
Actual Config. FEM	1.2191	1.1798	1.2016	1.1801	1.2196
Equivalent FEM (Equation)	1.2369	1.2093	1.2182	1.2093	1.2369
% Diff.	1.4391	2.4394	1.3627	2.4146	1.3987

A closer look at the two sets of results reveals a very good comparison. The difference between the maximum deflection values of both models is about 1.4%. Therefore, we can conclude that the proposed equations work satisfactorily well for the basic model.

6.5.1.2 Phase II

Here the stiffness equations are verified by considering a sandwich panel whose properties all differ from those of the basic model. The approach is the same as in Phase I. The verification model has the following properties:

Table 6.9: Panel properties

Span (ft.)	18
Width (ft.)	12
Depth (in.)	9

To simulate conditions similar to practical situations, the loading used is the design tandem in LRFD. The deck is loaded with just one axle of the tandem placed at midspan for the worst deflection condition. The wheel of each axle 12.5 kips, and spaced at 6 ft. The wheel load is distributed over elements within an area 15 in. x 16 in. Fig. 6.38 shows the ANSYS model with the wheel loads applied on elements. Only half the deck is modeled using symmetric conditions. The boundary conditions used to simulate symmetry can be seen in Fig. 6.39. The parameters for the actual sinusoidal wave-core sandwich deck are displayed in Table 6.10.

Table 6.10: Sandwich parameters

Properties	Values
E_{x1} and E_{x2} (psi)	1.50E+06
E_{y1} and E_{y2} (psi)	1.20E+06
t_1 and t_2 (in.)	0.5
G_{xy1} (psi)	2.00E+05
E (psi)	5.00E+05
L (in.)	6
W (in.)	4
H (in.)	8.5
t (in.)	0.1

With the sandwich parameters the equivalent flexural and shear stiffness values for the deck can be calculated as was done in the previous example from Equations 6.17, 6.35 and 6.48. From these the elastic and shear moduli of the equivalent structure are evaluated. Table 6.11 summarizes these properties. The equivalent structure modeled by ANSYS can be observed in Figs. 6.40 and 6.41, which show the loading and boundary conditions.

Table 6.11: Equivalent stiffness values and corresponding moduli

$E_x I_{yy}$ (lb-in²)	4.00E+08
$E_y I_{xx}$ (lb-in²)	2.57E+08
$G_{xy} A_s$ (lb-in²)	1.10E+06
E_x (psi)	4.12E+05
E_y (psi)	3.53E+05
G_{xy} (psi)	9.19E+03

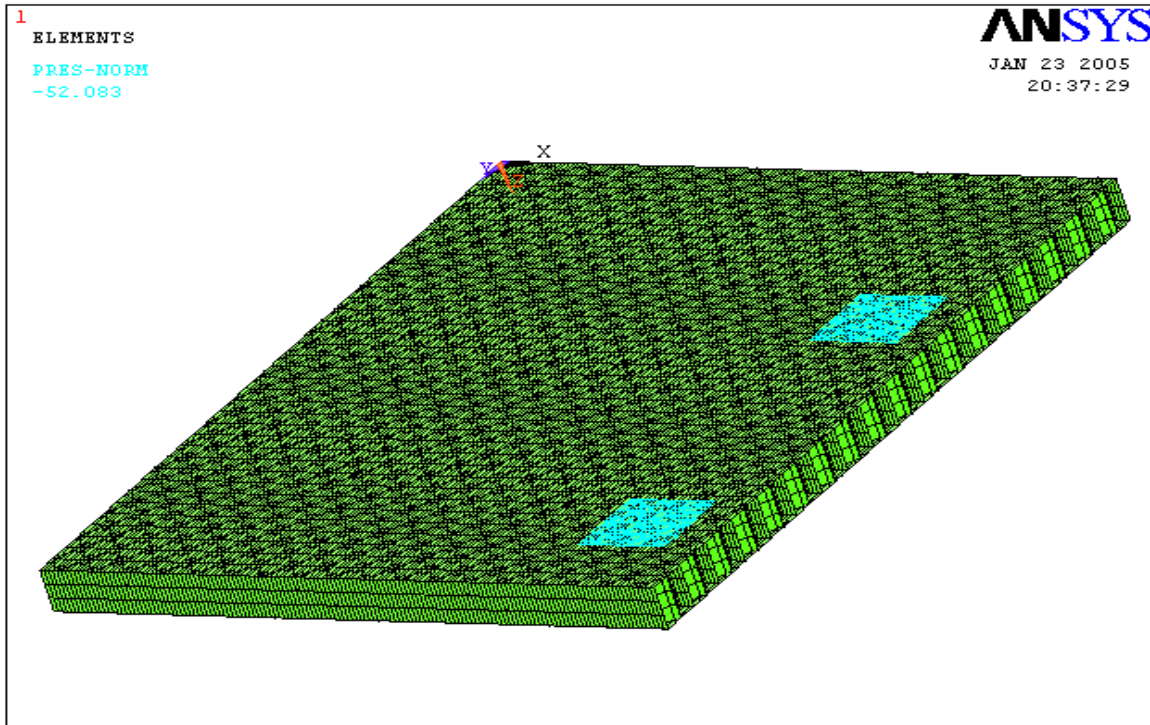


Figure 6.38: Model of actual FRP sinusoidal core panel – Phase II loading

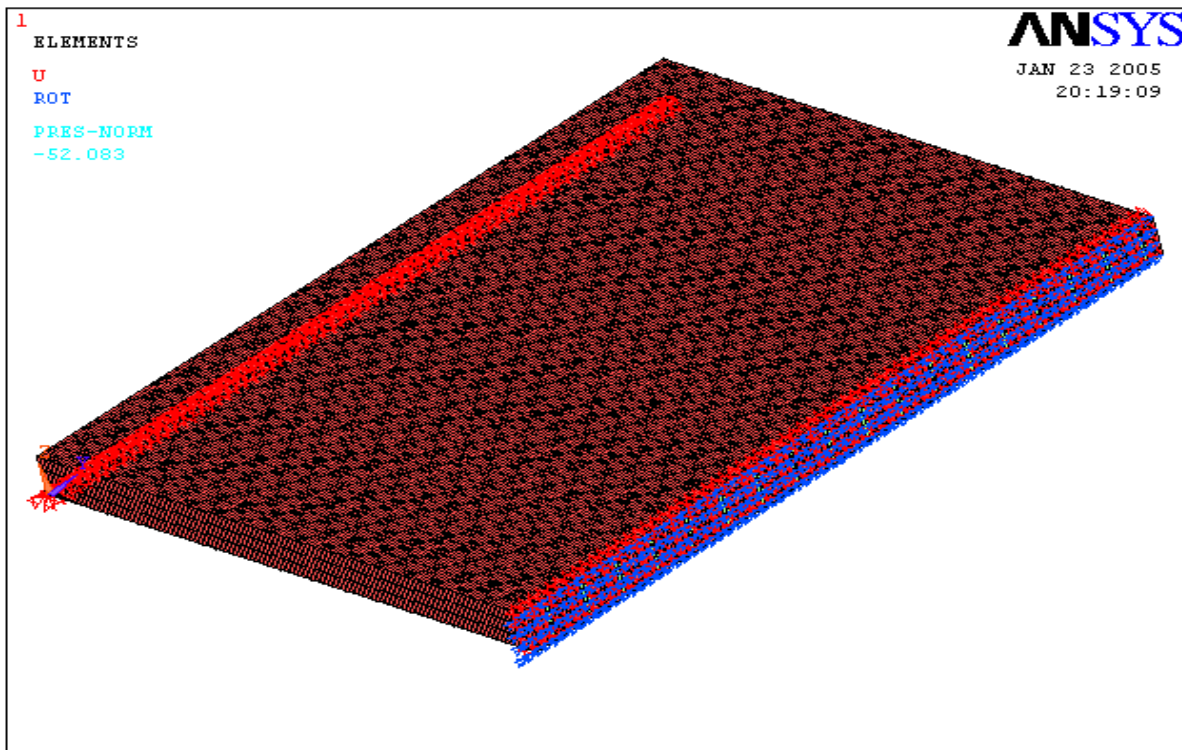


Figure 6.39: Model of actual FRP sinusoidal core panel – Phase II boundary conditions

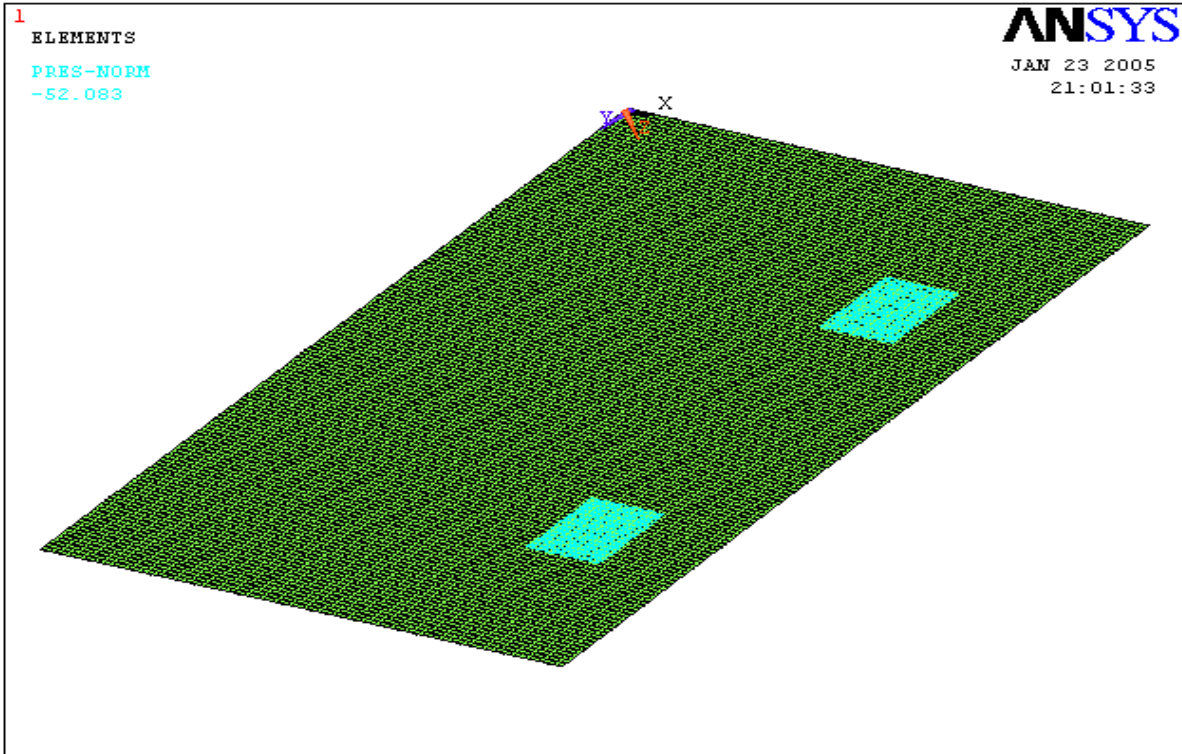


Figure 6.40: Model of equivalent FRP panel – Phase II loading

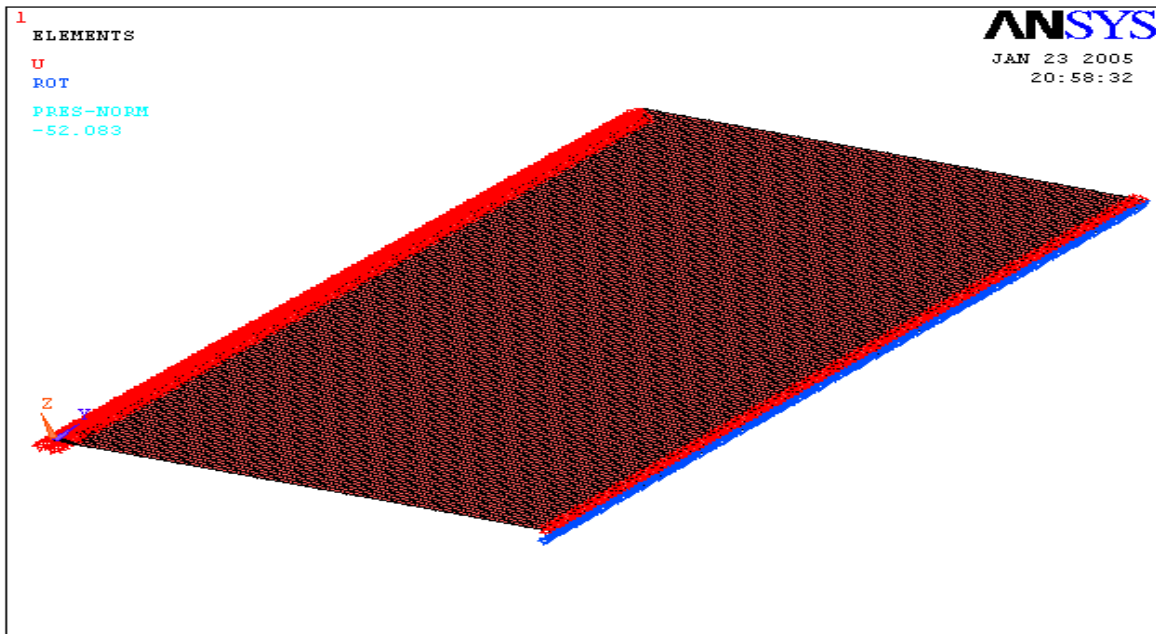


Figure 6.41: Model of equivalent FRP panel – Phase II boundary conditions

A first-order finite element analysis is carried out for both models – the actual and the equivalent – and the deflection results are noted. These results are summarized for various locations in the longitudinal and lateral directions of the panel. (Table 6.12) Figs. 6.42 and 6.43 show the vertical deflection contours for the actual configuration and the equivalent models respectively.

Table 6.12a: Comparison of deflection results (in.). Points in the longitudinal direction along the central line (in.)

x	Actual Config. FEM	Equivalent FEM (Equation)	% diff.
0	0	0	
18	0.76301	0.7062	7.4455
36	1.4822	1.3507	8.8719
54	2.1113	1.9504	7.6209
72	2.6036	2.4033	7.6932
90	2.9165	2.6917	7.7079
108	3.0232	2.7907	7.6905

Table 6.12b: Comparison of deflection results (in.). Points in the lateral direction along the midspan (in.)

y	Actual Config. FEM	Equivalent FEM (Equation)	% diff.
0	3.4883	3.1563	9.5175
36	3.1458	2.8877	8.2046
72	3.0232	2.7907	7.6905
108	3.1478	2.8877	8.2629
144	3.4907	3.1563	9.5797

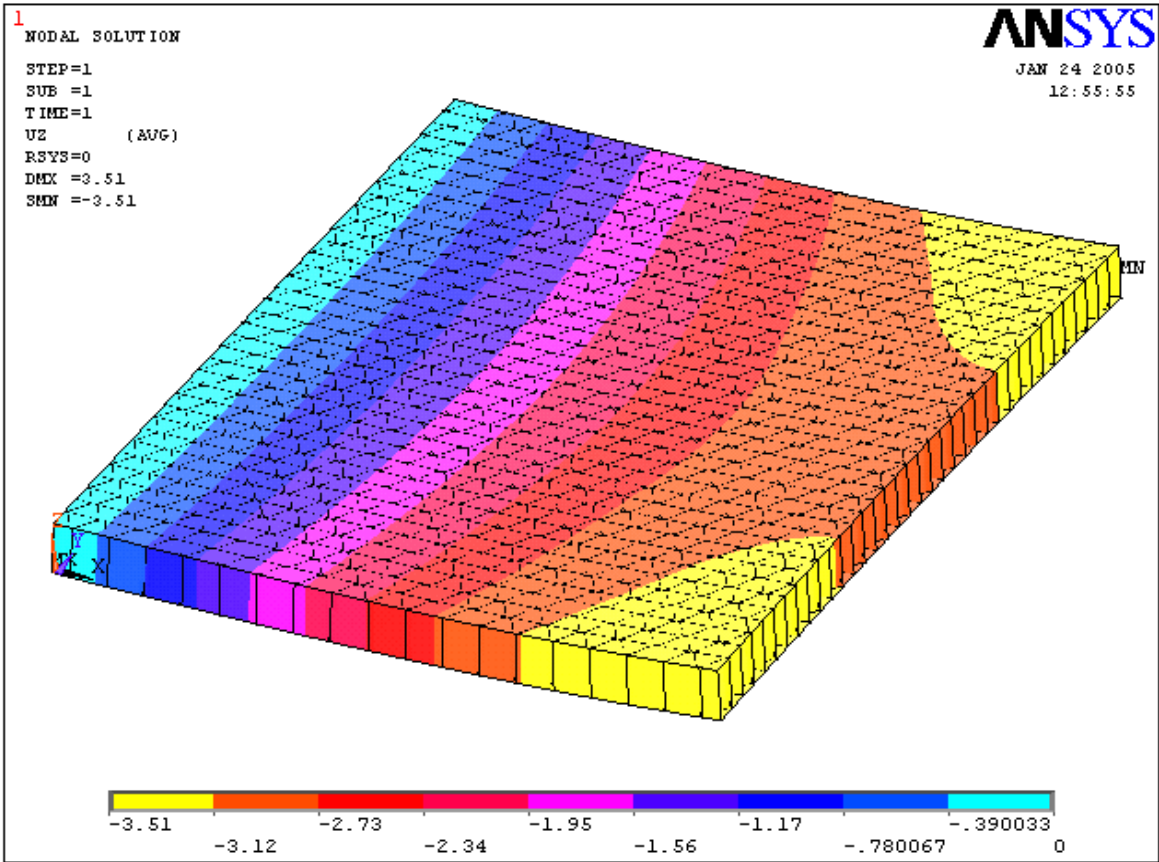


Figure 6.42: Deflection contour of actual FRP sinusoidal core panel

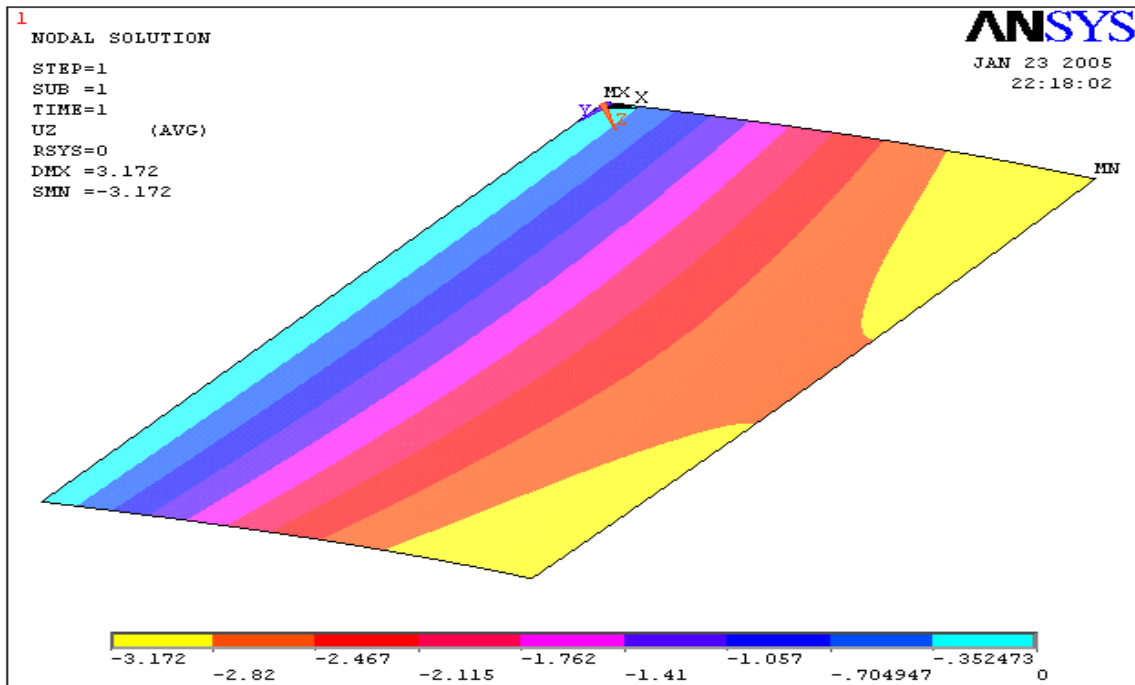


Figure 6.43: Deflection contour of equivalent FRP panel

A very good comparison (considering the complexity of the sandwiched deck) can be noted between the sets of results shown in Table 6.12. The average difference in deflections between the actual and equivalent models is approximately 8%. Visual observation of Figs. 6.42 and 6.43 shows comparable results for both models.

Thus, we can say that the proposed equations work well for this model. They can therefore be used with a high degree of confidence in obtaining simplified single-layer equivalent properties of the complex FRP sinusoidal wave core sandwich panel.

CHAPTER 7 - STRUCTURAL ANALYSIS WITH WEARING SURFACE

7.1 Introduction

Usually in structural design of bridges, the wearing surface is not considered a structural component. It is taken into account only during the computation of the dead loads. In the AASHTO LRFD code, for instance, the uncertainty of the presence of the wearing surface during the life of the bridge is accounted for by means of maximum and minimum load factors (Barker and Pucket 1997). This is understandable when we remember that the life of the wearing surface is much less than the structural deck itself. The life span of a thin wearing surface (usually less than 1 in. thick) for example, over an orthotropic steel deck and consisting of a layer of adhesive/cement matrix is usually less than 5 years (Hulsey et al. 2002). Latex modified concrete overlays theoretically have a useful life of approximately 20 years. Thin polymer overlays have an anticipated life of 20 years or greater (Calvo and Meyers 1991). Mastic asphalt (a mixture of asphalt cement, filler and coarse aggregate) has a life expectancy of 25 years (Hicks et al. 2000).

To achieve the benefits of serviceability and high performance of the wearing surface, the following requirements have to be met (Hicks et al. 2000):

7.1.1 Bond

Good bonding will ensure that the wearing surface acts compositely with the deck. It will also prevent delamination, especially when the structure experiences large deflections. These large deflections cause high interlaminar stresses which can result in the wearing surface breaking apart or separating from the deck if the bond is weak.

7.1.2 Durability

A bridge is designed for different types of loads and conditions. The wearing surface must also be able to withstand traffic loads as well as other harsh environmental conditions without rutting, shoving or wearing.

7.1.3 Fatigue Strength and Flexibility

The wearing surface must have sufficient fatigue strength and flexibility to prevent cracks under different loading conditions. This is important not only for long life but also for maintaining the water-proofing ability of the overlay.

7.1.4 Weight

The bridge designer should ensure that the wearing surface has as minimum a weight as possible compared to the deck itself. This is done by proper selection of overlay materials and thickness.

7.1.5 Rideability

The wearing surface should also be very smooth to ride on which makes for the comfort of road users.

7.2 Stiffness Contribution of Wearing Surface

The contribution of wearing surface to the stiffness of the deck is now examined. This contribution is usually ignored in practice since the overlay is not usually considered as a structural component of the deck and its contribution to the overall stiffness of concrete deck is relatively small. If this contribution is relatively significant however, such as in the case of FRP deck, it can be utilized in a typical bridge design.

In this study, it is assumed that the requirements for optimum wearing surface performance as discussed previously have been met. In particular, it is assumed that

the bond between the wearing surface and the deck is adequately strong so that there is no delamination, and that the overlay material is durable to prevent wear. A method for computing the stiffness contribution of the overlay is sought and verified.

7.3 Finite Element Modeling

It was shown in Chapters 5 and 6 that the complicated sinusoidal wave core sandwich panel can be accurately modeled as a single layered structure with equivalent properties which were derived. Since the focus in this section is on stiffness contribution, the model used here is the stiffness-based single-layered equivalent of the FRP sinusoidal wave-core sandwich beam. The equivalent model is used instead of the actual model because as was discussed, it is much less complicated but gives approximately the same stiffness results. To model the additional layer of wearing surface, structural layered shell elements are used. A two-layered beam model is created with the bottom layer representing the equivalent deck and the top the wearing surface.

The beam used has the same configuration and material properties as those of the panel manufactured by Kansas Structural Composites Inc., which has been the basis of this research work. These parametric values can be seen in Table 6.3 of Chapter 6. The span of the beam is 15 ft, the width is 8 in. and the depth is 5 in. The single-layered equivalent properties for this structure were derived in Chapter 5 and shown in Table 5.1.

In testing for the stiffness contribution of the wearing surface material, two independent variables are identified and noted. These are the elastic modulus and

thickness of the overlay material. They are designated as E_{ws} and t_{ws} respectively. These parameters are varied, and the beam stiffness computed.

To obtain the flexural stiffness, the beam is modeled as a cantilever of span L and subjected to a point load P at the free end which causes bending. As was discussed in Chapter 5, the shear contribution to deflection can be ignored because it is insignificant for long beams. The stiffness EI can be computed from the deflection results δ using the formula in Equation 7.1 below:

$$EI = \frac{PL^3}{3\delta} \quad \text{Equation 7.1}$$

The stiffness obtained with each variation of E_{ws} and t_{ws} is compared with that when the beam has no wearing surface (Table 5.1) to investigate how much contribution the overlay provides.

The wearing surface Young's modulus E_{ws} is varied within the range of 250 ksi to 5,000 ksi, and the thickness t_{ws} from 0.25 in. to 2 in. Fig. 7.1 well illustrates the stiffness contribution of the wearing surface to the entire structure. It shows a plot of F (representing the ratio of beam stiffness with overlay to that without overlay) against E_{ws} for the different values of t_{ws} .

As can be observed from the graph, the wearing surface can contribute quite significantly to the stiffness of the structure. Consider a practical case of the polysulphide epoxy overlay, for example, to illustrate this. Typical values for the elastic modulus and thickness are 2.75 GPa (400 ksi) and 0.375 in. respectively (Stenko and Chawalwala 2001). An interpolation from Fig. 7.1 shows that the stiffness of the beam taking into consideration the wearing surface is about 15% more than when the wearing surface is not accounted for. This contribution could be taken advantage of in the design

of the structure. However, it must be borne in mind that very high values of Young's modulus (such as 5,000 ksi) for wearing surface on FRP decks are not realistic.

It is pertinent to note, however, that the analysis just performed holds true under ideal conditions. These include the assumption that there is perfect bonding between the wearing surface material and top face laminate. Also implied is that durability conditions are met and therefore no wear nor degradation of the overlay material exists.

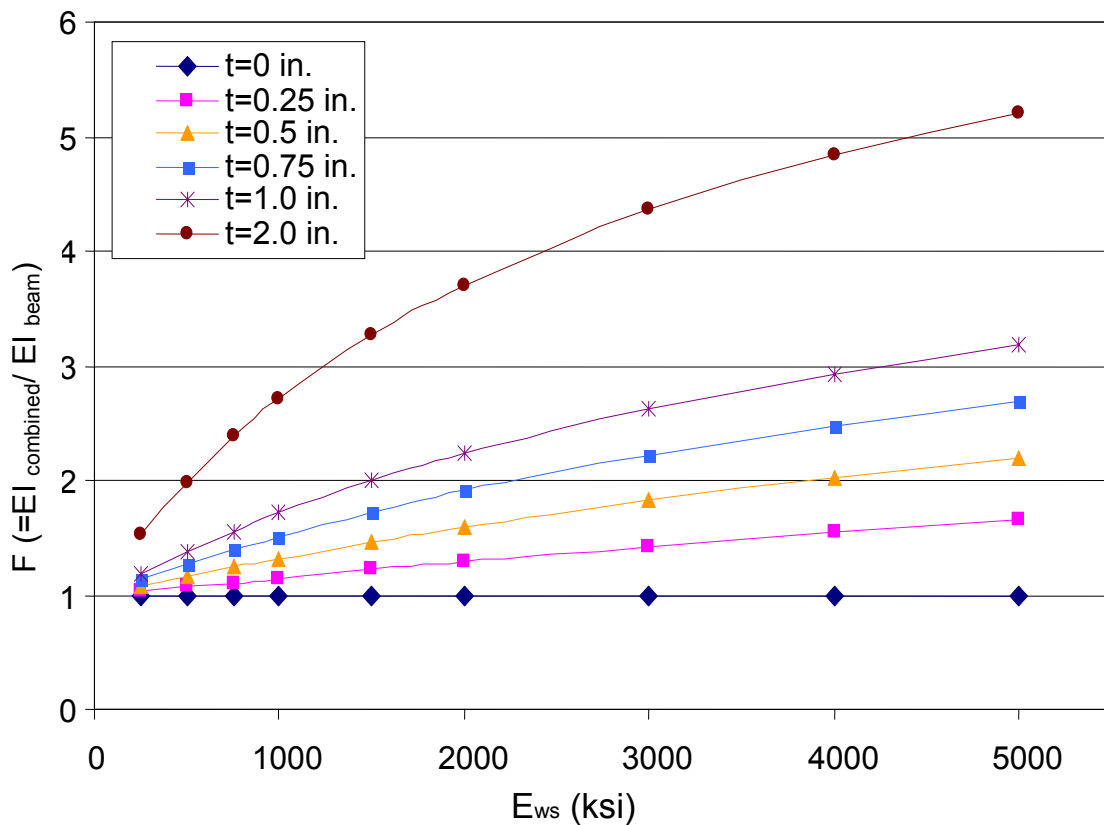


Figure 7.1: Stiffness contribution of wearing surface

7.4 Derivation of Stiffness

Apart from deriving the stiffness using the finite element approach described in the previous section, two other methods are now proposed and tested against the finite element results obtained. These methods involve using traditional beam analysis approach. They differ in the way the stiffness of the core is calculated and are discussed in the foregoing sections.

7.4.1 Hand Calculation Based on Equivalent Beam – Method 1

In this first method, the stiffness of the beam is computed for a two-layered structure, the top representing the wearing surface and the bottom, the equivalent structural beam developed in Chapter 5. It is noted that the two materials are dissimilar. Hence, the analysis starts with obtaining a transformed section. Fig. 7.2 below illustrates this process of transforming the section to the same material. This is done by transforming the overlay material to an equivalent beam material using the modular ratio, m ($=E_{ws}/E_{beam}$).

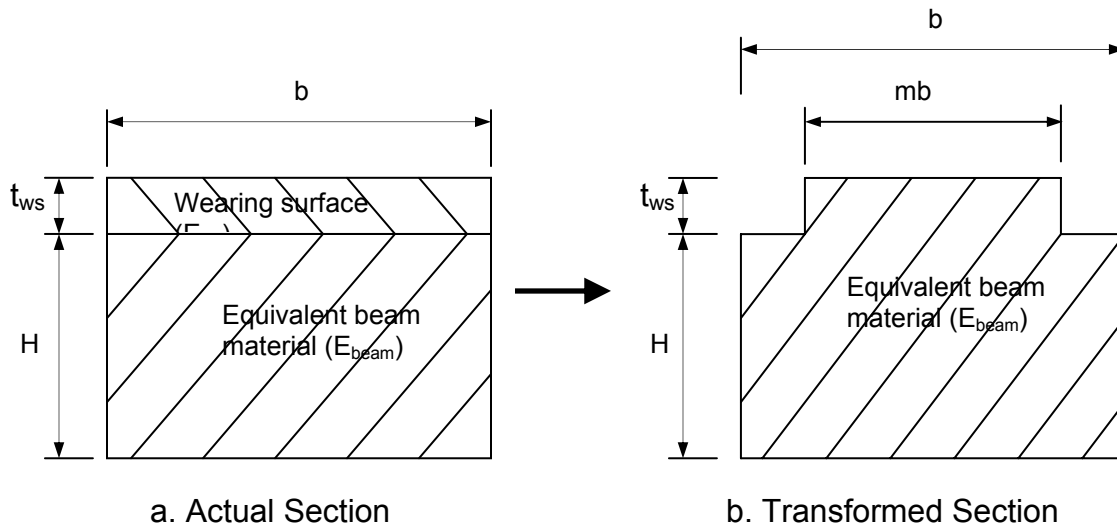


Figure 7.2: Transformation of two-layered section

With the transformed section in Fig.7.2b, the distance from the top fibers of the cross-section to the centroidal axis \bar{y} can be computed using the formula in Equation 7.2:

$$\bar{y} = \frac{\sum_{i=1}^n A_i \bar{y}_i}{\sum_{i=1}^n A_i} \quad \text{Equation 7.2}$$

where A_i and \bar{y}_i symbolize the area and centroid of each layer of a given section. For the section in Fig. 7.2, the above equation (Equation 7.2) reduces to the form:

$$\bar{y} = \frac{H^2 + mt_{ws}^2 + 2Ht_{ws}}{2(H + mt_{ws})} \quad \text{Equation 7.3}$$

Having found the location of the centroid, the total stiffness of the section can be obtained by a superposition of the stiffness values of individual layers. Thus,

$$(EI)_{\text{total}} = (EI)_{\text{beam}} + (EI)_{ws} \quad \text{Equation 7.4}$$

$(EI)_{\text{beam}}$ and $(EI)_{ws}$ are evaluated using the parallel axis theorem for moment of inertia I , noting the position of the centroid. The theorem states that the moment of inertia of an area about any axis I is equal to the moment of inertia of the same area about a parallel axis passing through the area's centroid I_0 , added to the product of the same area and the square of the distance between the two axes. This can be stated mathematically as follows:

$$I = I_0 + A\bar{y}^2 \quad \text{Equation 7.5}$$

Therefore, the flexural stiffness of the beam can be calculated by the following equation:

$$(EI)_{\text{beam}} = E_{\text{beam}} bH \left(\frac{H^2}{12} + \left(\frac{H}{2} + t_{ws} - \bar{y} \right)^2 \right) \quad \text{Equation 7.6}$$

Following the same procedure, the stiffness for the wearing surface can also be computed using the section in Fig. 7.2. This can be expressed thus:

$$(EI)_{ws} = E_{ws} t_{ws} b \left(\frac{t_{ws}^2}{12} + \left(y - \frac{t_{ws}}{2} \right)^2 \right) \quad \text{Equation 7.7}$$

7.4.3 Hand Calculation Based on Simplified Actual Beam Configuration –

Method 2

In this second technique, the flexural stiffness is computed for the actual sinusoidal wave core sandwich beam at a section where the flats and flutes are equally spaced. It must be noted however that this is an approximate method which does not take full account of the actual core geometry. Implicit in this approach is the assumption that the core constituents (the flats and flutes) are simply parallel components along the span of the beam instead of the sinusoidal wave configuration.

The section is made up of three dissimilar materials – the face, core mat and wearing surface. Therefore, just as was done in Section 7.4.1 (method 1), the analysis commences with obtaining a transformed section. This transformed section is in the form of an I-beam as shown in Fig. 7.3. In the figure, t represents the summation of the thickness of all flats and flutes of the actual section.

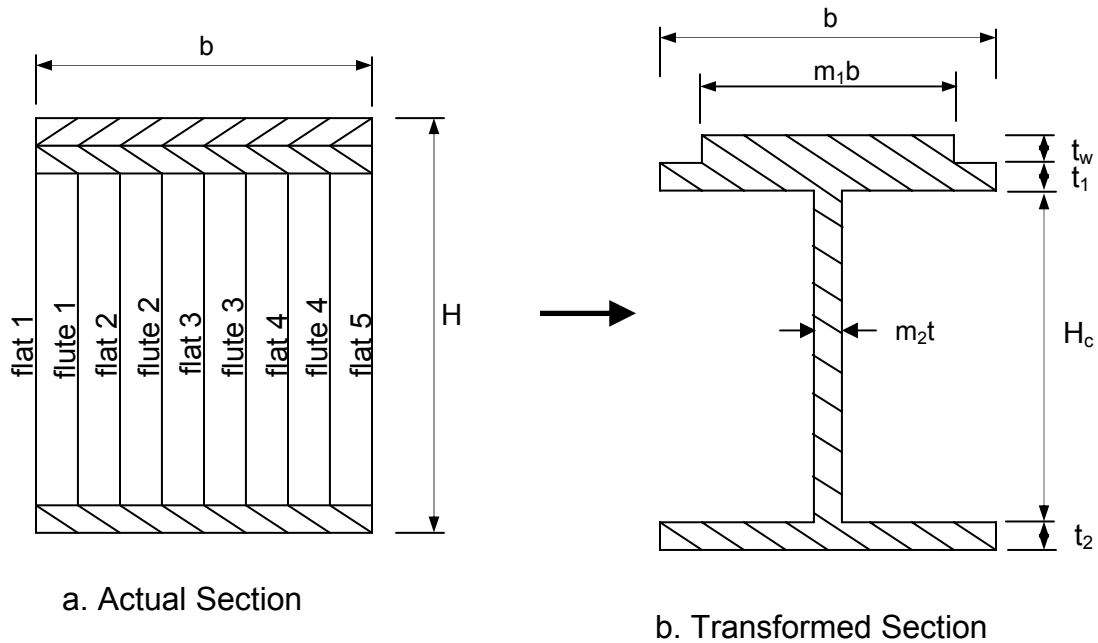


Figure 7.3: Transformation of sinusoidal wave core sandwich section

Equation 7.2 is used to compute the location of the centroid of the transformed section in Fig 7.3b. The equation becomes:

$$\bar{y} = \frac{b(m_1 t_w \bar{y}_1 + t_1 (\bar{y}_2 + \bar{y}_4)) + m_2 t H_c \bar{y}_3}{b(m_1 t_w + 2t_1) + m_2 t H_c} \quad \text{Equation 7.8}$$

where \bar{y}_1 , \bar{y}_2 , \bar{y}_3 and \bar{y}_4 represent the distance from the top fibers of the section to the centroid of the wearing surface, top face, core and bottom face, respectively. The wearing surface and core are transformed into the same material used for the top/bottom face using the modification factors m_1 ($=E_{ws}/E_{top_face}$) and m_2 ($=E_{core}/E_{top_face}$).

With the centroid of the section calculated, the total stiffness of the section $(EI)_{total}$ is obtained using the same superposition technique shown in Equation 7.4 in conjunction with the parallel axis theorem presented in Equation 7.5.

7.5 Method Verification

The two classical beam methods just discussed in the previous section are now compared with the finite element analysis procedure described in Section 7.3. The objective here is to investigate which approach provides a better approximation of the results from finite elements. To perform this task, the properties of the wearing surface are varied within certain ranges. For each property set, the flexural stiffness is computed for the entire structure using methods 1 and 2 in Section 7.4. The results are then compared with those from finite element analysis of corresponding property sets.

As has been explained, the two important properties of the wearing surface having significant effect on the stiffness are the Young's modulus E_{ws} and the thickness t_{ws} . The Young's modulus is varied within the range of 250 ksi to 5,000 ksi, and the thickness from 0.25 in. to 2 in. Figs. 7.4 to 7.8 show the variation of the structure's flexural stiffness EI with wearing surface elastic modulus E_{ws} at varying overlay thickness t_{ws} . The figures also show how the two traditional analysis methods compare with the finite element approach. It can also be observed that logically in each of the three cases, EI increases with both E_{ws} and t_{ws} .

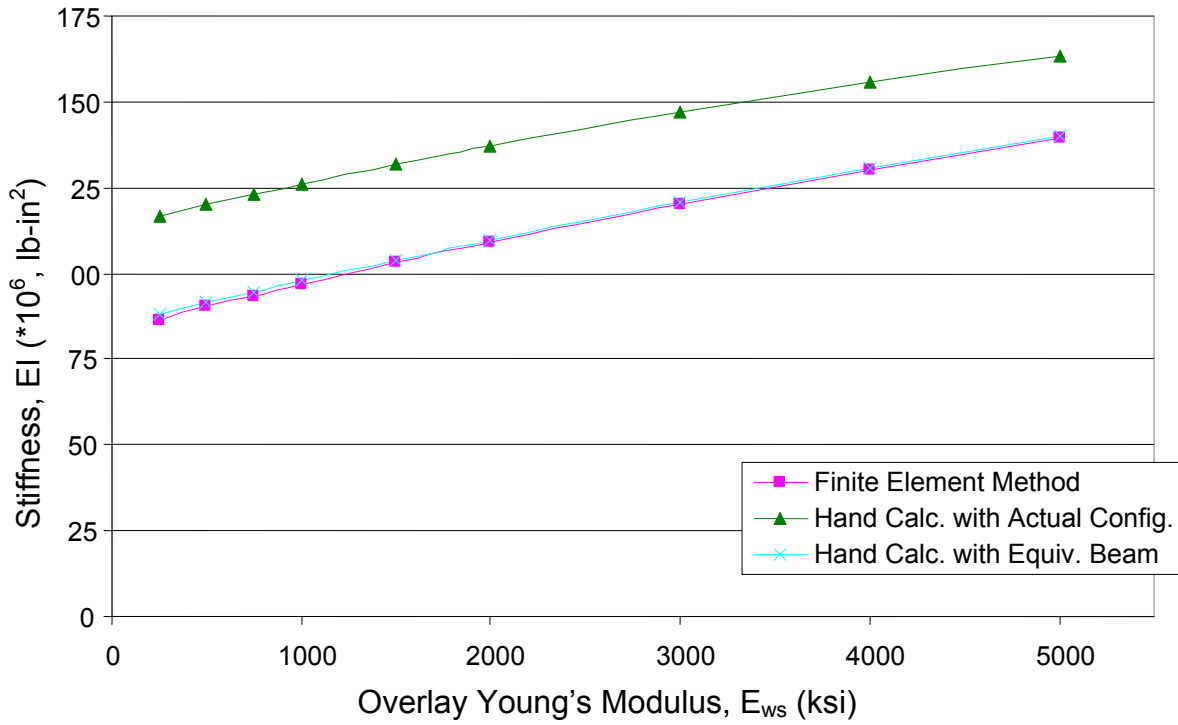


Figure 7.4: Variation of EI with E_{ws} at $tws = 0.25$ in.

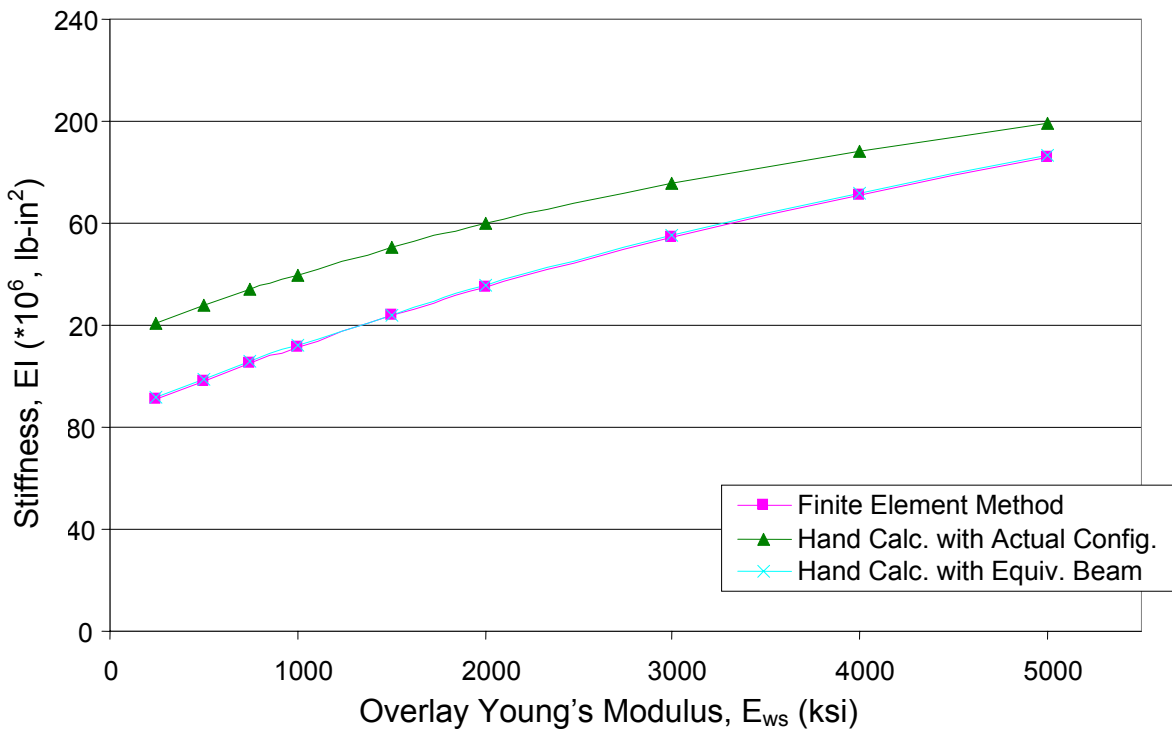


Figure 7.5: Variation of EI with E_{ws} at $tws = 0.5$ in.

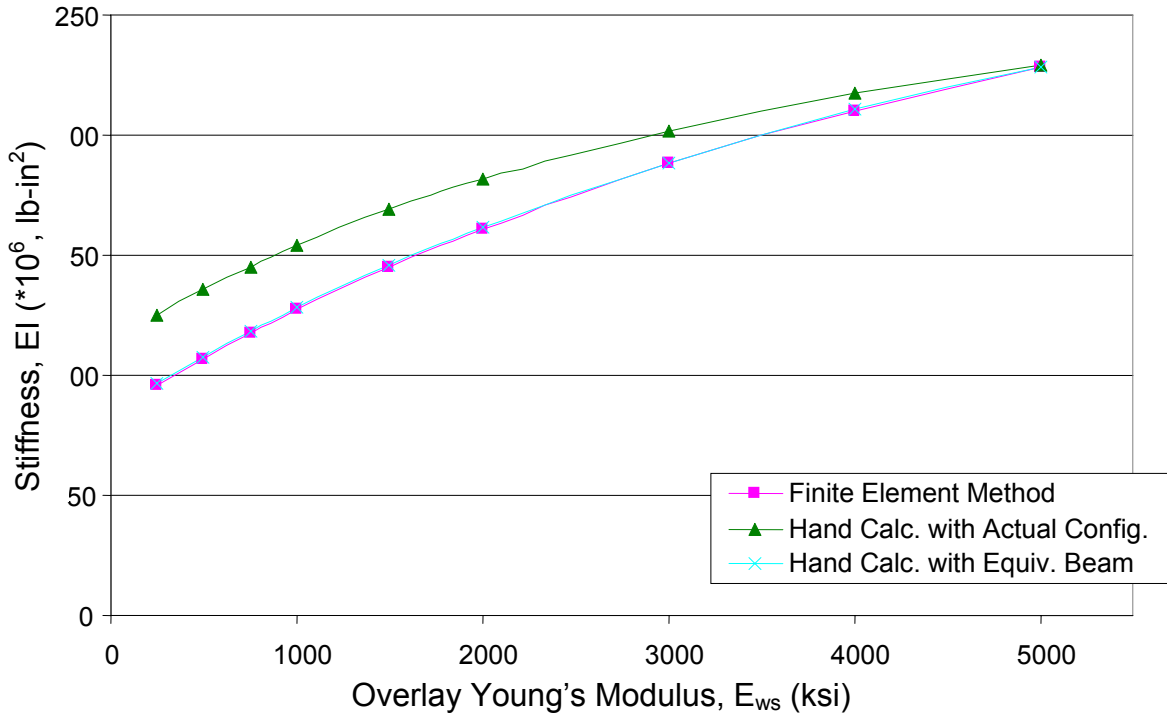


Figure 7.6: Variation of EI with Ews at tws = 0.75 in.

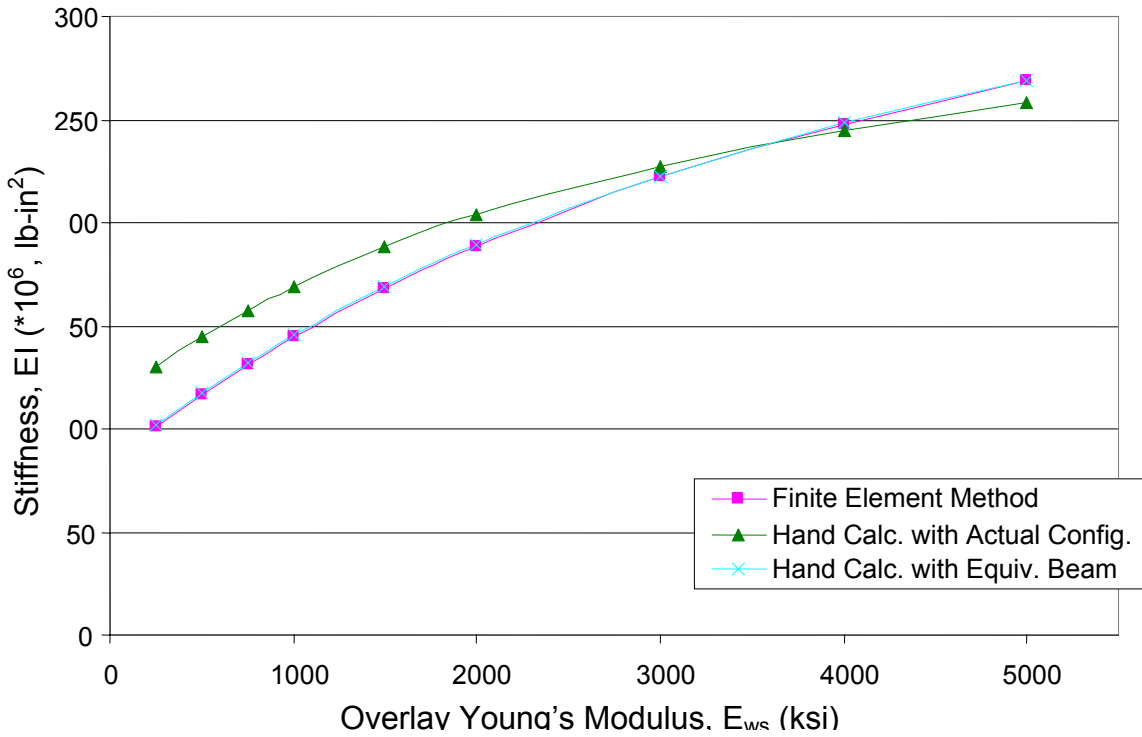


Figure 7.7: Variation of EI with Ews at tws = 1.0 in.

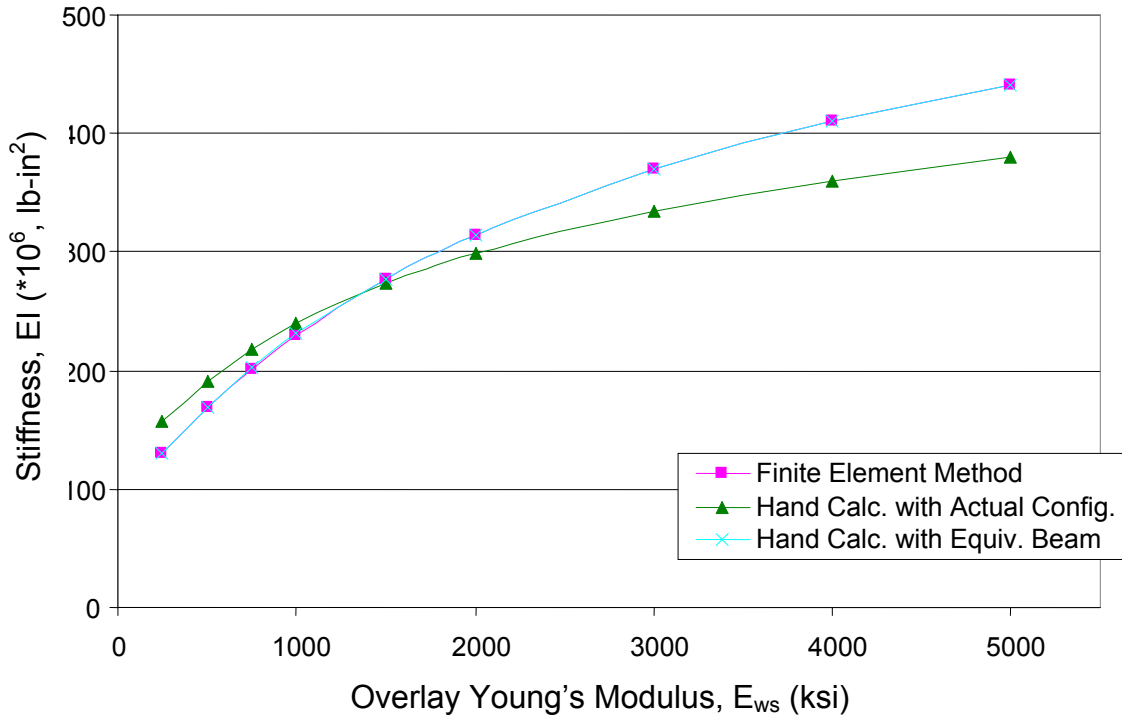


Figure 7.8: Variation of EI with E_{ws} at t_{ws} = 2.0 in.

It can be observed from all five graphs above (Figs. 7.4 to 7.8) that the hand calculation with equivalent beam method (Section 7.4.1) has consistently very good matched with the finite element method. The average difference between both plots in each of the five graphs is about 0.5%, an excellent approximation. The significance of this is that with the approach described in Section 7.4.1 (method 1), the stiffness properties of the beam with a layer of wearing surface can be computed with a high level of confidence. The results predicted from finite element analysis will be pretty much the same. As has been seen, the beam equivalent properties will first have to be derived from the approach and equations discussed in Chapters 5 and 6.

On the other hand, Figs. 7.4 – 7.8 show that the hand calculation with simplified actual beam configuration approach (Section 7.4.2) does not fit the finite element results

as well. The maximum difference between both plots is about 20%. This relatively large difference is easy to comprehend when note is taken of the assumptions made in this approach. It was assumed that the core is made up of parallel web elements running along the longitudinal axis of the beam, instead of the actual sinusoidal wave core pattern. This assumption simplifies the calculations tremendously, but introduces the deviation from the finite element analysis. Although this method does not produce as accurate results as does method 1, it can be used for preliminary design or as a check for stiffness calculations. Since there is no need for a computation of equivalent beam stiffness properties following the approach in Chapters 5 and 6, the method is less demanding.

CHAPTER 8 - THERMAL ANALYSIS

8.1 Introduction

So far in this research work, the results obtained pertain only to a structure at the “stress free” temperature, which is the temperature at which the structure is assumed to be free of stress when no load is applied. In real-life situations however, changes in temperature of the structure are commonplace during manufacturing, construction and service life. These changes can cause high stresses which could have very significant effects on FRP materials. Therefore in this chapter, a thermal study is carried out to investigate the level of stress at the interface between the top face and the core of the sinusoidal wave core sandwich panel. This location is selected for the study because one of the main causes of failure of the sandwich panel is delamination of the face laminate from the sandwiched core (Kalny 2003). While this is not a failure analysis, the results obtained will furnish the reader with a general idea of the effects of temperature on this highly indeterminate structure. The effects of two types of temperature changes – differential and uniform – will be analyzed.

When a body of say, length L experiences a change in temperature ΔT , a corresponding change in its dimension ΔL is observed. This change in dimension is proportional to the body's initial dimension and the temperature change. Thus thermal strains in the body can be computed using the following linear relation:

$$\varepsilon^{\text{thermal}} = \frac{\Delta L}{L} = \alpha \Delta T \quad \text{Equation 8.1}$$

where α is the proportionality constant between the thermal strain and temperature change from some reference temperature. This constant is known as the coefficient of thermal expansion.

When dealing with an orthotropic material, such as the face laminates described in Section 3.3 (Chapter 3), thermal strains in two different directions can be defined. These are the strains in the longitudinal and transverse directions, and are given by the following equations (Agarwal and Broutman 1980):

$$\varepsilon_L^{thermal} = \alpha_L \Delta T \quad \text{Equation 8.2a}$$

$$\varepsilon_T^{thermal} = \alpha_T \Delta T \quad \text{Equation 8.2b}$$

where α_L and α_T represent the longitudinal and transverse coefficient of thermal expansion respectively.

All resins have positive thermal expansion coefficients which are within the range of about $30 \times 10^{-6}/^\circ\text{C}$ and $100 \times 10^{-6}/^\circ\text{C}$. E-glass, on the other hand, has a low coefficient of thermal expansion of about $5.04 \times 10^{-6}/^\circ\text{C}$. In the fiber direction, carbon fibers have a negative coefficient of $-0.99 \times 10^{-6}/^\circ\text{C}$, while in the direction transverse to the fibers, its coefficient is $16.7 \times 10^{-6}/^\circ\text{C}$ (Barbero 1999).

8.2 Determination of Lamina Thermal Expansion Coefficients

It was mentioned previously that composite materials have two coefficients of thermal expansion. Expressions to calculate these constants are well documented in literature such as Agarwal and Broutman (1980) and Barbero (1999). These equations are shown in this section to illustrate their application in the present study. For a lamina (a layer or ply of composite material), the thermal coefficient in the fiber direction α_1 can be computed from Equation 8.3 below:

$$\alpha_1 = \frac{1}{E_1} (\alpha_f E_f V_f + \alpha_m E_m V_m) \quad \text{Equation 8.3}$$

where α_f and α_m refer to the coefficients of thermal expansion for fibers and matrix, E_f and E_m symbolize the elastic modulus of the fiber and matrix, E_1 is the equivalent elastic modulus of the lamina which can be evaluated from the Rule of Mixtures discussed in Chapter 3 (Equation 3.6) and V_f and V_m are the fiber and matrix volume fractions related by the expression,

$$V_f + V_m = 1 \quad \text{Equation 8.4}$$

In the direction perpendicular to the fibers, the thermal expansion coefficient can be computed from the equation below:

$$\alpha_2 = (1 + \nu_f)\alpha_f V_f + (1 + \nu_m)\alpha_m V_m - \alpha_1 \nu_{12} \quad \text{Equation 8.5}$$

where ν_f and ν_m represent the fiber and matrix Poisson's ratios and ν_{12} is the major Poisson's ratio of the lamina which can also be computed from the Rule of Mixtures discussed in Chapter 3 (Equation 3.10).

It can be noted from Equations 8.3 and 8.5 that it is possible to tailor the thermal coefficient to specific needs by changing the fiber volume fraction and this is an advantage possessed by composite materials. It is also pertinent to note that the longitudinal thermal coefficient α_1 is usually smaller than the transverse thermal coefficient α_2 . This is because the thermal expansion behavior in the longitudinal direction is dominated more by the fibers which usually have a smaller coefficient of expansion than the matrix. On the other hand, in the transverse direction, the behavior is controlled more by the matrix material and hence causes the composite to experience greater changes in dimension in this direction.

For randomly oriented composite plies such as that of the core material (Table 3.1 in Chapter 3), the behavior of the material is assumed to be isotropic in the plane of

the layer. The thermal expansion coefficient α_q can therefore be obtained using the relationship in the following equation (Barbero 1999):

$$\alpha_q = \frac{\alpha_1 + \alpha_2}{2} + \frac{\alpha_1 - \alpha_2}{2} \left(\frac{E_1 - E_2}{E_1 + (1 + 2\nu_{21})E_2} \right) \quad \text{Equation 8.6}$$

where E_2 is the transverse elastic modulus of the composite which can be computed from Equation 3.9 and ν_{21} is the minor Poisson's ratio obtained from Equation 3.11 (Chapter 3).

The constituents of the laminae used for the sandwich panels of the present study are E-glass fibers and polyester resin matrix. The properties of these materials are shown in Table 8.1 (Barbero 1999 and Davalos et al. 2001). In Table 8.2, the thermal expansion coefficients of each lamina making up the panel can be seen. These coefficients are computed based on the formulations just discussed in this section and the properties in Table 3.1 (Chapter 3).

Table 8.1: Properties of constituent materials

Material	$\alpha \cdot 10^{-6} (/^{\circ}\text{C})$	E (GPa)	ν
Polyester Resin	30	5.06	0.3
Glass Fibers	5.04	72.4	0.255

Table 8.2: Laminae thermal coefficients of expansion

Ply Name	Orientation	$\alpha_1 \cdot 10^{-6} (/^{\circ}\text{C})$	$\alpha_2 \cdot 10^{-6} (/^{\circ}\text{C})$	$\alpha_q \cdot 10^{-6} (/^{\circ}\text{C})$
Bond Layer	Random	19.4013	25.7162	22.5588
CM3205	0 or 90	8.1114	25.4062	
CM3205	Random	17.1390	24.4021	20.7706
UM1810	0	7.7253	24.4050	
UM1810	Random	14.3208	21.4387	17.8798
Core Mat	Random	17.1390	24.4021	20.7706

8.3 Determination of Laminate Thermal Expansion Coefficients

Once the laminae coefficients of thermal expansion have been computed from Section 8.2, the effective laminate coefficients of thermal expansion can be developed. (A laminate refers to an arrangement of an arbitrary number of laminae. Each lamina has its plane of elastic symmetry in the plane of the laminate). This can be done if the stacking configuration of the laminate is known. The configuration and laminae orientation of the sandwich panel face laminates used in this study can be seen in Fig. 3.2 (Chapter 3). First, the thermal coefficients are derived from the thermal force resultants. These force resultants are expressed in terms of the laminae stiffness properties \bar{Q}_{ij}^k in the global x-y coordinate system by the following equations (Whitney et al. 1982):

$$N_x^T = \sum_{k=1}^n (\bar{Q}_{11}^k \alpha_x^k + \bar{Q}_{12}^k \alpha_y^k + \bar{Q}_{16}^k \alpha_{xy}^k) (h_k - h_{k-1}) \Delta T \quad \text{Equation 8.7a}$$

$$N_y^T = \sum_{k=1}^n (\bar{Q}_{12}^k \alpha_x^k + \bar{Q}_{22}^k \alpha_y^k + \bar{Q}_{26}^k \alpha_{xy}^k) (h_k - h_{k-1}) \Delta T \quad \text{Equation 8.7b}$$

$$N_{xy}^T = \sum_{k=1}^n (\bar{Q}_{16}^k \alpha_x^k + \bar{Q}_{26}^k \alpha_y^k + \bar{Q}_{66}^k \alpha_{xy}^k) (h_k - h_{k-1}) \Delta T \quad \text{Equation 8.7c}$$

The stiffness properties \bar{Q}_{ij}^k have been discussed in Section 3.3 and the laminate nomenclature is shown in Fig. 3.3. The thermal coefficients of the kth lamina α_x^k , α_y^k and α_{xy}^k can be obtained from the lamina fiber orientation θ by the following formulae:

$$\alpha_x^k = \alpha_1^k \cos^2 \theta_k + \alpha_2^k \sin^2 \theta_k \quad \text{Equation 8.8a}$$

$$\alpha_y^k = \alpha_1^k \sin^2 \theta_k + \alpha_2^k \cos^2 \theta_k \quad \text{Equation 8.8b}$$

$$\alpha_{xy}^k = 2\alpha_1^k \cos \theta_k \sin \theta_k - 2\alpha_2^k \cos \theta_k \sin \theta_k \quad \text{Equation 8.8c}$$

The effective thermal coefficient for a balanced-symmetric laminate (such the face laminates of the present study shown in Fig. 3.2) can then be written in terms of the thermal force resultants of Equation 8.7 by the following formulae:

$$\alpha_x = \frac{A_{22}N_x^T - A_{12}N_y^T}{(A_{11}A_{22} - A_{12}^2)\Delta T} \quad \text{Equation 8.9a}$$

$$\alpha_y = \frac{A_{11}N_y^T - A_{12}N_x^T}{(A_{11}A_{22} - A_{12}^2)\Delta T} \quad \text{Equation 8.9b}$$

$$\alpha_{xy} = N_{xy}^T / A_{66} \Delta T = 0 \quad \text{Equation 8.9c}$$

where α_x , α_y and α_{xy} symbolize the laminate effective longitudinal, transverse and shear coefficients of thermal expansion respectively and the A_{ij} terms represent the terms of the extensional stiffness matrix $[A]$ which can be computed from Equation 3.20 (Chapter 3).

The effective coefficients of expansion of the face laminates and the core material computed based on Equations 8.7 to 8.9 are shown in Table 8.3. A more detailed worksheet of the computation can be viewed in Appendix C.

Table 8.3: Thermal expansion coefficients of face laminates and core

Component	$\alpha_x * 10^{-6} (/ ^\circ\text{C})$	$\alpha_y * 10^{-6} (/ ^\circ\text{C})$	$\alpha_q * 10^{-6} (/ ^\circ\text{C})$
Faces	12.2939	19.7187	
Core Mat			20.7706

8.4 Case Study – Crawford County Bridge

Thermal studies carried out in this chapter are performed on FRP panels used over a rehabilitated bridge in Crawford County, Kansas. It must be emphasized first of all that this case study is simply a conceptual one. It is performed primarily to help the

reader appreciate the analysis approach employed, and have a general idea of the FRP bridge's performance under thermal loading. The data used in the analysis are utilized to meet that end. The bridge was originally an asphalt-on-steel deck supported by 14 W21 x 68 I-beam stringers (Gill 1998). It was then replaced by the KSDOT with fiber-reinforced polymer sandwich panels manufactured by Kansas Structural Composites, Inc in 1999. The entire bridge was 45 ft long and 32 ft wide. The deck panels were 32 ft by 9 ft and were laid across the longitudinal stringers, perpendicular to traffic. The panels were bolted onto specially designed saddles and the already existing I-beams. Fig. 8.1 shows the FRP panels resting on the saddle beams during the construction stage of the project.



Figure 8.1: Construction of Crawford County Bridge showing FRP panels and Saddle Beams

The temperature data used in this thermal study is obtained from measurements performed by Kansas Department of Transportation on the bridge each day from December 2002 to July 2004 (Meggers 2005). Temperature measurements of the top and bottom faces of the bridge were taken every two hours. The ambient temperatures were also measured each time. The temperature measurements performed on the bridge for a one-year period from August 2003 to July 2004 are first examined to determine which days are critical. First, a linear temperature distribution is assumed along the depth of the sandwich panel section. Critical cases are obtained by computing the temperature gradient of the section and comparing with the ambient (reference) temperature. The objective is to obtain two one-week spans representing the coldest and warmest week of the year. These weeks will include the worst thermal conditions. The data sets with the highest temperature gradients and largest differences from the reference represent the critical cases of interest. From this data analysis, the coldest week is found to be February 7 – 13, 2004, while the warmest is June 21 – 27, 2004. The temperature measurements by the Kansas Department of Transportation for these weeks can be seen in Figs. 8.2 and 8.3. The figures show temperatures at the top and bottom of the panel as well as the ambient temperature for every two hours of those two weeks.

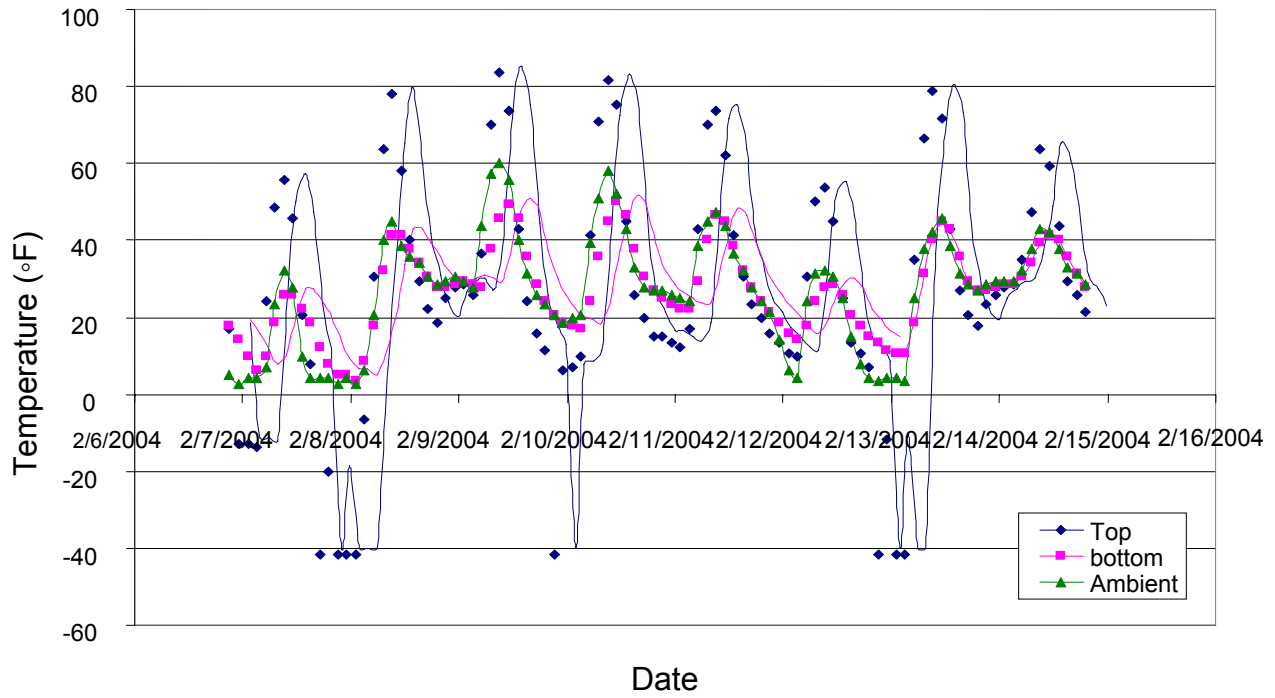


Figure 8.2: Crawford County bridge temperature measurements by Kansas DOT for Feb. 7-13, 2004

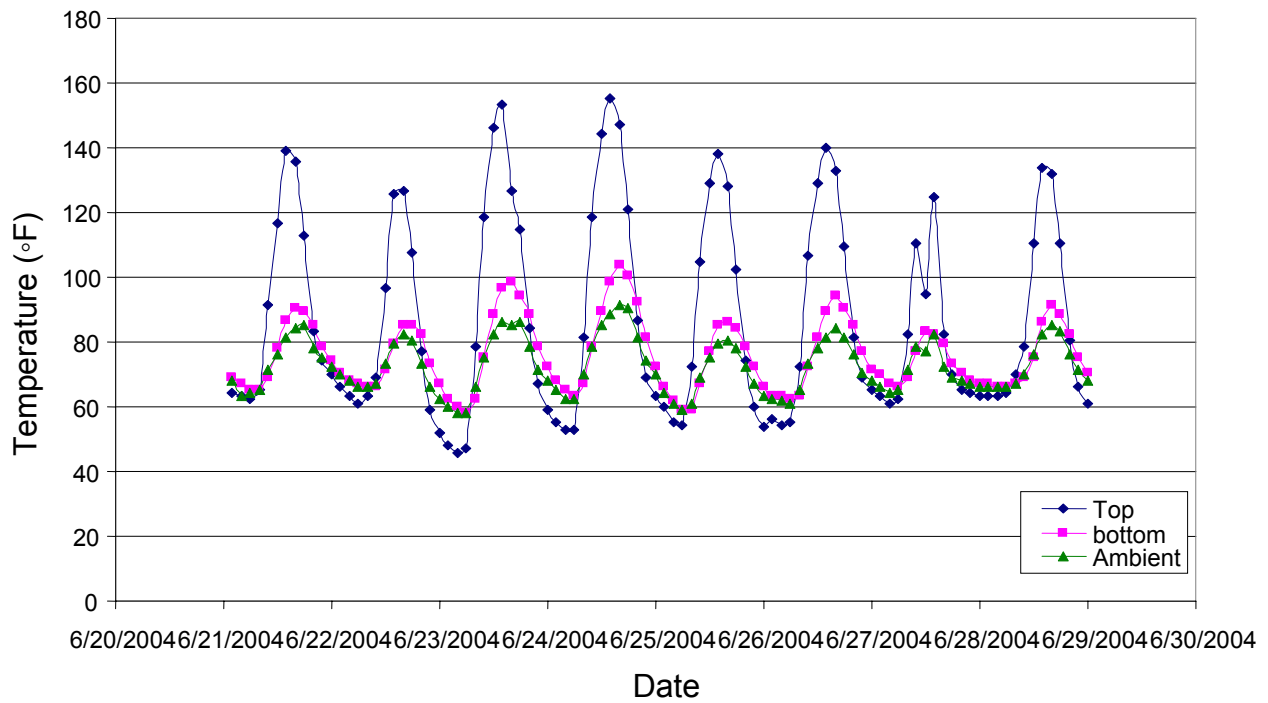


Figure 8.3: Crawford County bridge temperature measurements by Kansas DOT for June 21-27, 2004

8.5 Finite Element Modeling

For the purpose of this study, a portion of the panel, 8 ft long by 9 ft wide by 5 in. deep is modeled. The modeling of the bridge follows the same technique discussed in Section 3.4.1 (Chapter 3). Structural shell elements are employed. The model has a total of 83,328 elements and 60,466 nodes. Since the Crawford County Bridge was manufactured by Kansas Structural Composites Inc., the material properties of the core mat and face laminates shown in Tables 3.1 and 3.2 are used.

Two modeling cases are considered and compared for worst case thermal behavior. The first case deals with the panel with simple supports, while the second considers continuous supports in view of the saddle beams on which the panels are bolted. The thermal analysis is performed for the worst case temperature data set of each day from Figs. 8.2 and 8.3. This gives a total of fourteen thermal load cases for the two weeks applied on each model. The objective of the analysis is to study the thermal stress levels of the interface between the top face and core where delamination often occurs and to know the general stress distribution in the panel.

Bridges experience both daily and seasonal temperature variations. It has been observed that these fluctuations in temperature can be divided into two separate components – a gradient and a uniform change (Barker and Puckett 1997). These two components form the basis of the thermal study conducted in this work and discussed in the succeeding sections. It is good to note that even though these stresses may not be as significant as those from mechanical static or dynamic loads, their impact may become felt after a long period of time due to possible fatigue as a result of cyclic thermal loading.

8.6 Structural Behavior due to Gradient Temperature Change

Significant temperature differences between the top and bottom faces of the panel result in high temperature gradients across the section's depth. This could result in temperature induced curvatures which introduce internal stresses not only in the interface between the top face and core, but in the entire structure. This in turn could lead to delamination of the top face from the core. Because of the importance of these stresses, the thermal behavior of the panel due to these differential temperatures is now examined.

The ambient temperature is taken as the reference temperature for the purpose of the present analysis. Reference temperature actually refers to the temperature at which the structure is considered to be free of stress if no mechanical static or dynamic loads are applied. At ambient temperatures, residual stresses already exist caused by temperature changes between fabrication and room temperatures during the manufacturing stage of the composite structure. These residual stresses are however ignored for the purpose of this study.

The thermal load cases are applied on the model as described in the previous section, and the maximum stresses at the interface between the top face and core are recorded. The stresses focused on primarily are normal stresses in the vertical (thickness) direction σ_z which can cause pulling away of the face from the core, as well as shear stresses τ_{xz} and τ_{yz} which may result in shearing away of the top face from the core. (The x-direction is the longitudinal direction of the panel while the y-direction is the transverse). Other stresses (σ_x , σ_y and τ_{xy}) are also noted. It is worthy of note that the sign convention for the normal nodal stresses σ_z is very important. In the finite element

model of this work, positive stress σ_z tends to pull the top face in the positive direction – away from the core – and hence cause delamination. The negative stress, on the other hand, works against delamination and is therefore of benefit to the panel for this effect. If some other effects are studied, such as local buckling of web elements, the negative stress values of σ_z will be of significance. Hence in the case of σ_z , interest in this study focuses on the positive values. For other stresses (τ_{xz} , τ_{yz} , σ_x , σ_y and τ_{xy}), the sign convention is immaterial since the isotropic interface have the same effects in both directions (x and y).

8.6.1 Case 1 – Modeling and Analysis of Simply Supported Panel

To model the simple supports of the panel, the nodes of the bottom face at one end of the structure are constrained for translational displacements in the three orthogonal directions – x, y and z – to simulate a pin support. At the other end, a roller in the longitudinal (x) direction is modeled by constraining the vertical (z) and lateral (y) translations. In Fig. 8.4, the ANSYS model showing the support conditions can be seen. Figs. 8.5 and 8.6 show the graphs of the six different stresses (σ_x , σ_y , σ_z , τ_{xz} , τ_{yz} and τ_{xy}) from the thermal analysis for the two separate weeks in February and June. The stresses recorded are the maximum stresses of the panel. As we will see, these maximum stresses occur at the supports of the structure for reasons that will be explained later.

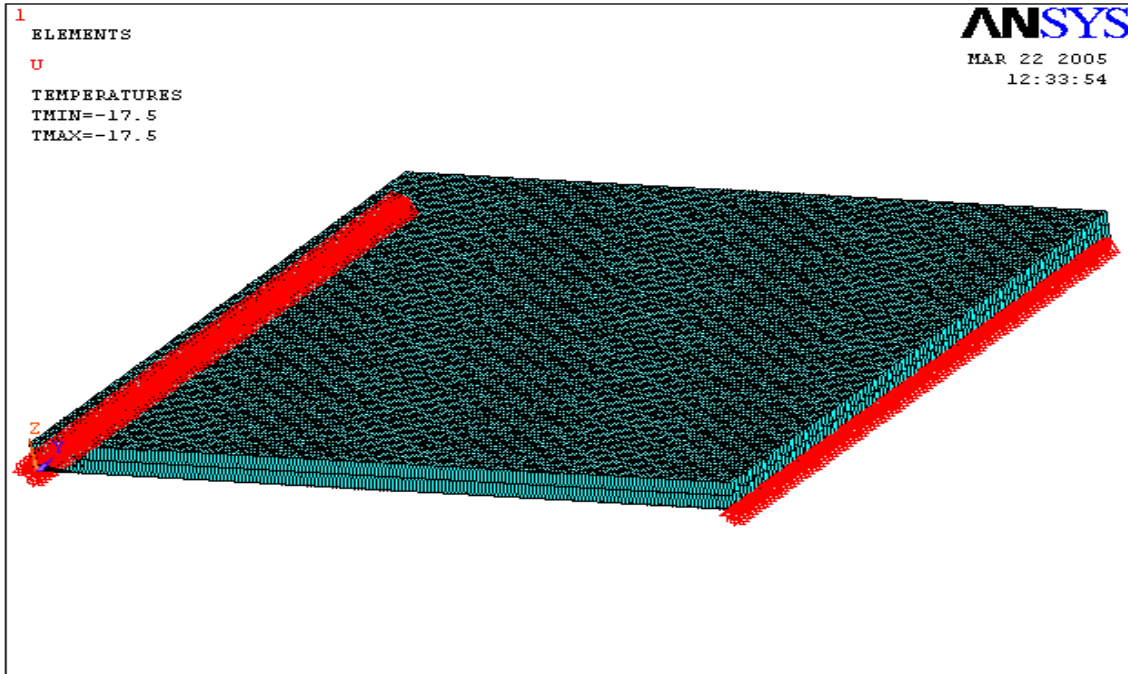


Figure 8.4: ANSYS model showing simple support conditions

It can be noted from Figs 8.5 and 8.6 that the normal stress σ_z and shear stresses τ_{xz} and τ_{yz} are very significant in comparison with the other stresses. For the coldest week (Fig. 8.5), these significant stresses have maximum values of 74 psi, 56 psi and 60 psi respectively. The values for the warmest week (Fig. 8.6) are 54 psi, 57 psi and 63 psi respectively. All maximum stress values were noted to occur at the location of the pinned support. This is because high reaction forces are induced during loading. This is explained further in Section 8.6.3. It must be borne in mind that the values recorded for σ_z are the maximum positive stresses which has the tendency to separate the top face from the core.

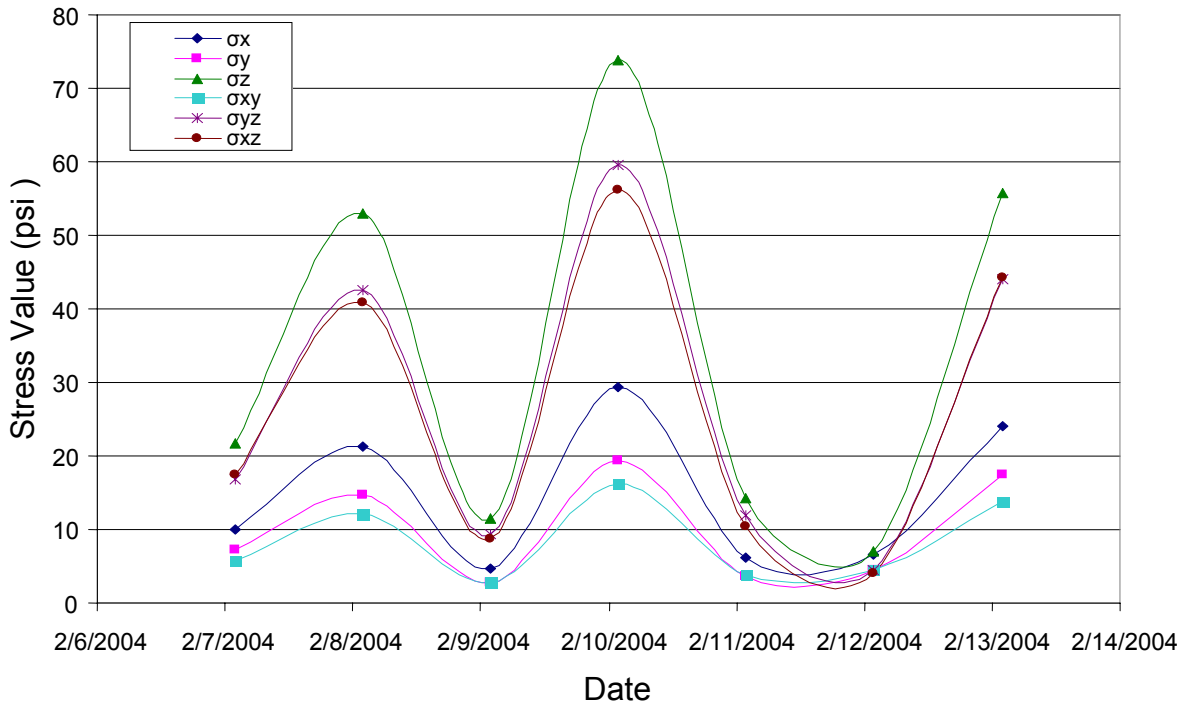


Figure 8.5: Thermal stresses due to gradient temperature changes of Case 1 (Feb. 7-13, 2004)

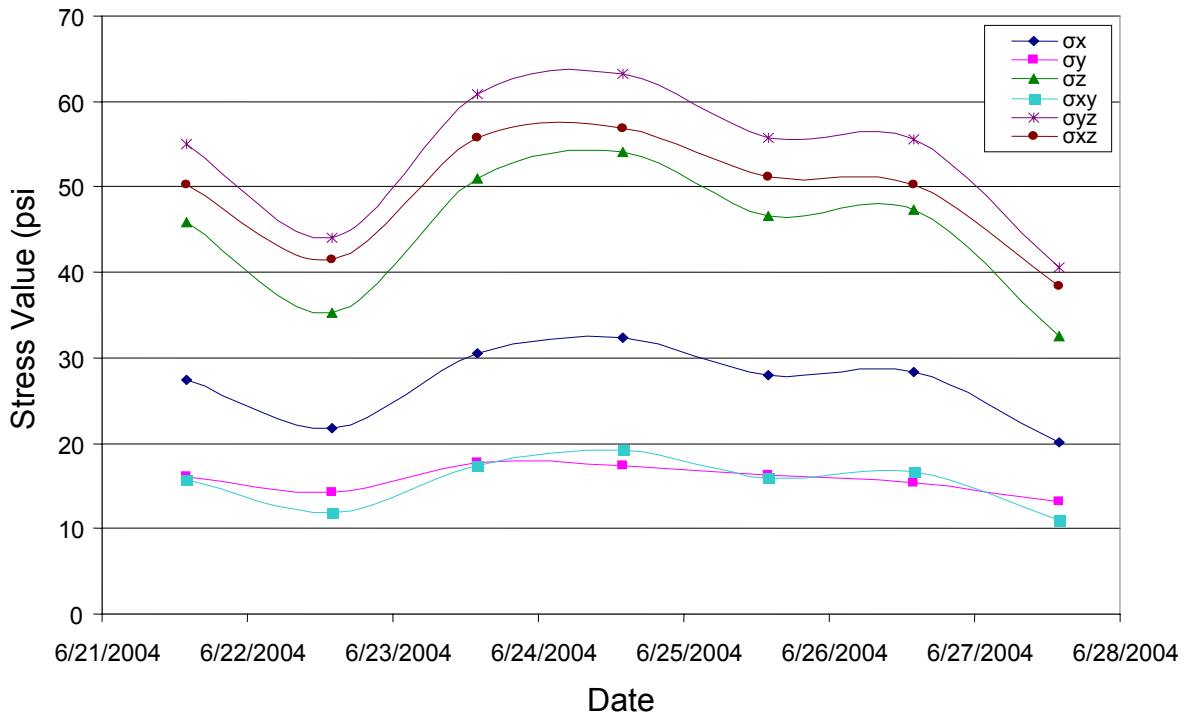


Figure 8.6: Thermal stresses due to gradient temperature changes of Case 1 (June 21-27, 2004)

To help better appreciate conceptually the significance of these stress values, consider the properties of polyester resin which is the matrix used on the bonding layer in the interface between the top face and the core. The tensile and shear strengths have the same value of 75.9 Mpa (11,000 psi) (Barbero 1999). According to the maximum stress failure theory, failure of a layer occurs when at least one of the stresses in material coordinates exceeds the corresponding specified allowable value. Therefore failure takes place if any of the following conditions in Equation 8.10 is met:

$$\sigma_L > F_L \quad \text{Equation 8.10a}$$

$$\sigma_T > F_T \quad \text{Equation 8.10b}$$

$$\sigma_{LT} > F_{LT} \quad \text{Equation 8.10c}$$

where σ_L , σ_T and σ_{LT} are the longitudinal, transverse and shear stresses in the layer, and F_L , F_T and F_{LT} represent the corresponding allowable values. Of course, for the longitudinal and transverse directions, care must be taken to note whether the stress is compressive or tensile and the comparison should be made with the corresponding strength.

Suppose the allowable tensile and shear stresses have the same value of 5 Mpa (725 psi). It is obvious from Equation 8.10 that the maximum stresses σ_z , τ_{xz} and τ_{yz} (74 psi, 57 psi and 63 psi) are well below failure. This would mean that under thermal conditions alone, the bond in the interface will be maintained. Again it must be emphasized that this analysis is only conceptual. It furnishes the reader a general idea of the thermal behavior of the panel. Actually, in many design cases, thermal loads do not usually exceed any strength limit state, but the loads can be of concern regarding serviceability (Barker and Puckett 1997).

8.6.2 Case 2 – Modeling and Analysis of Continuously Supported Panel

In this next case, continuous supports are modeled for the panel resting on four equally spaced saddle beams which are bolted to the panel. Pinned connections are simulated by constraining the nodes of the bottom face at the location of the supports for translational displacements in all three directions – x, y and z. Fig. 8.7 shows the ANSYS model illustrating the continuous boundary conditions. In Figs. 8.8 and 8.9, graphs are presented to show the six different stresses (σ_x , σ_y , σ_z , τ_{xz} , τ_{yz} and τ_{xy}) from the thermal analysis for the two separate weeks in February and June. The stresses recorded are the maximum stresses experienced by the panel.

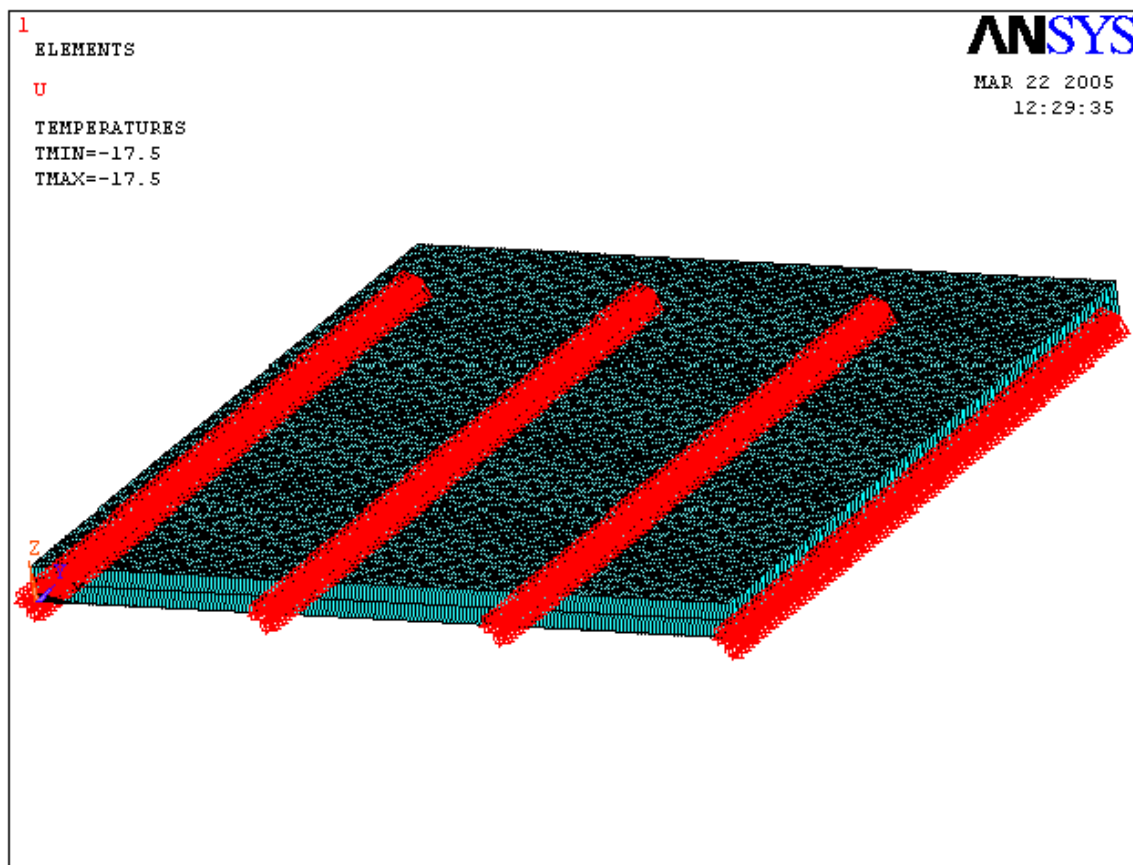


Figure8.7: ANSYS model showing continuous support conditions

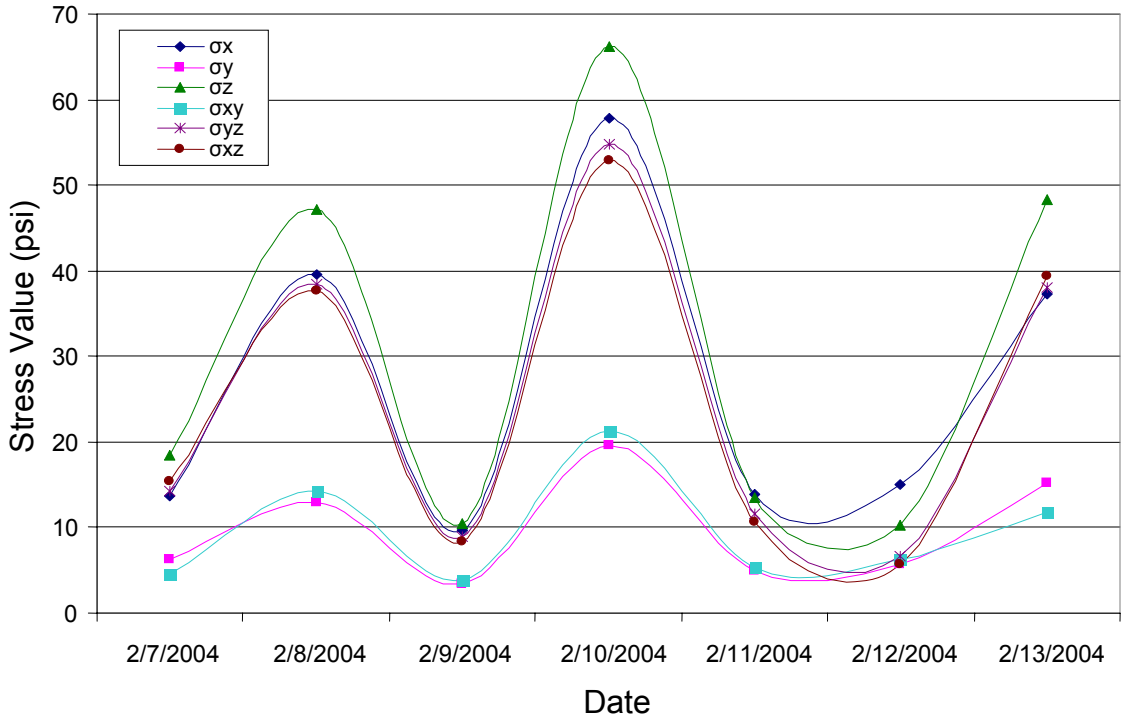


Figure 8.8: Thermal stresses due to differential temperature changes of Case 2 (Feb. 7-13, 2004)

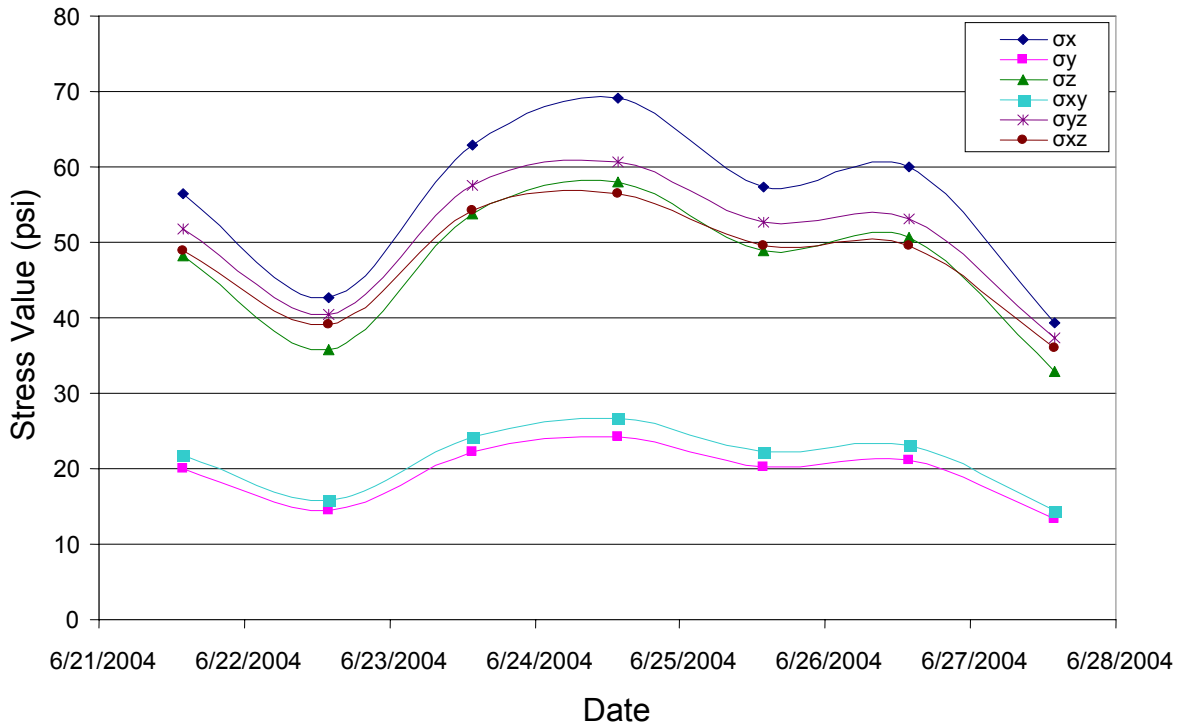


Figure 8.9: Thermal stresses due to differential temperature changes of Case 2 (June 21-27, 2004)

The graphs in Figs 8.8 and 8.9 are very similar to those for case 1 in Figs. 8.5 and 8.6. Again σ_z , τ_{xz} and τ_{yz} are very significant when compared with σ_y and τ_{xy} . From Fig. 8.8, the coldest week records maximum values for these significant stresses as 66 psi, 53 psi and 55 psi respectively. For the warmest week, these values are 58 psi, 56 psi and 61 psi (Fig. 8.9). Just as in the case of the simply supported panel, the maximum stresses here are observed to occur at the supports of the structure. There are, however some significant differences between cases 1 and 2 as discussed in the following section.

8.6.3 Comparison between Results of Simple and Continuous Supports

Figs. 8.10 and 8.11 show comparisons of the normal stresses in the longitudinal direction σ_x for the simply and continuously supported panels. It can be observed from the figures that σ_x is very significant for the case of the continuously supported panel. The maximum values for this stress for the coldest and warmest weeks are 58 psi and 69 psi. For the simply supported panel however, this stress has corresponding maximum values of only 29 psi and 32 psi. This significant difference can be explained by understanding the constraint conditions in the panel. For the simply supported panel, the structure is free to translate in the longitudinal (x) direction at the roller support. On the other hand, the continuously supported panel induces reactions and forces in the x-direction at the supports and the entire structure which accounts for the higher normal stress σ_x .

Figs. 8.12 to 8.17 show similar comparisons for σ_z , τ_{xz} and τ_{yz} . It is interesting to note that unlike in the case of σ_x , the simply supported panel shows consistently

higher values of σ_z , τ_{xz} and τ_{yz} than the continuously supported panel. This difference can be better understood when we think about what happens to the panel when it is subjected to a gradient temperature change. If, for instance, a panel is subjected to sunshine, the top face heats up more than the bottom face. As a result of this non-uniform heating, there is a differential in temperature between both faces which results in a bowing upward of the panel. For a panel that has internal restraints, compatibility actions are induced. On the other side of the coin, a simply supported panel will have internal stress due to the piecewise linear temperature gradient (Barker and Puckett 1997). This could be the result of the slightly higher values of σ_z , τ_{xz} and τ_{yz} for the simply supported panel. Additionally, the vertical reactions and forces in the continuously supported panel are distributed to more supports than in the case of the simply supported structure making the latter structure develop higher vertical stress values at its supports.

Because the high stress values noted for the structure are related to induced reactions at restraints, it is little wonder that the maximum values occur at the supports of the structure. This is true for both the simply and continuously supported panels.

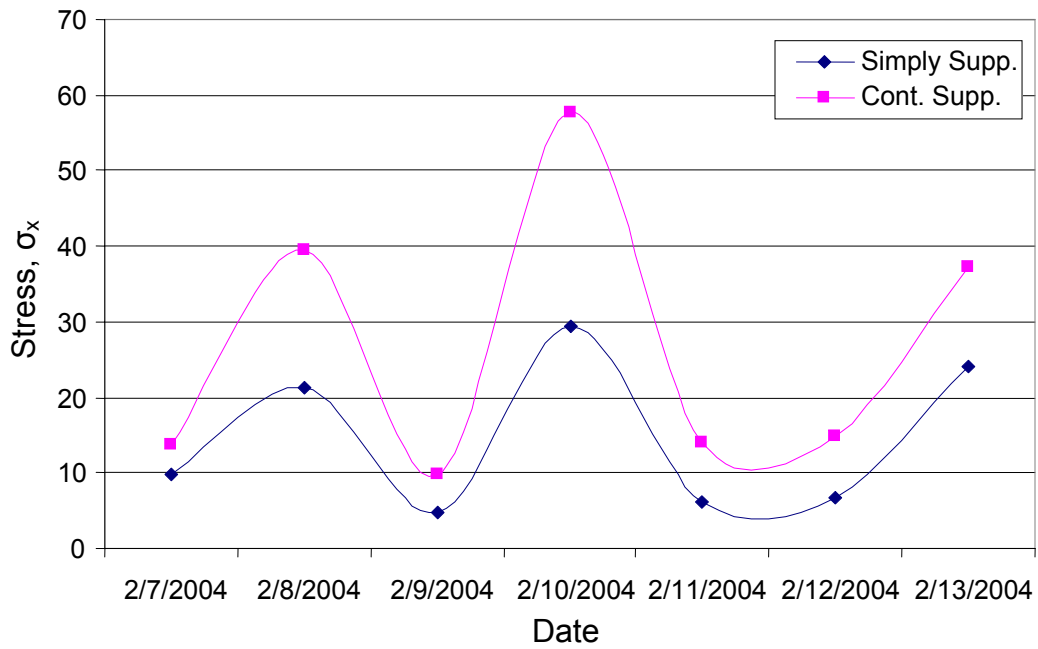


Figure 8.10: Comparison of σ_x (psi) for Simply and Continuously Supported Panels (Feb.)

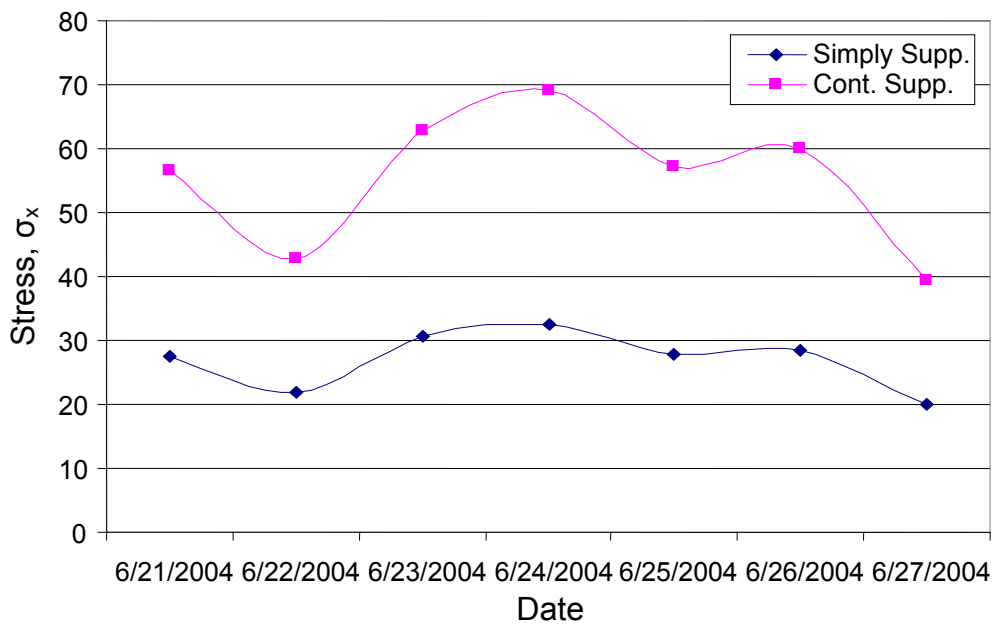


Figure 8.11: Comparison of σ_x (psi) for Simply and Continuously Supported Panels (June)

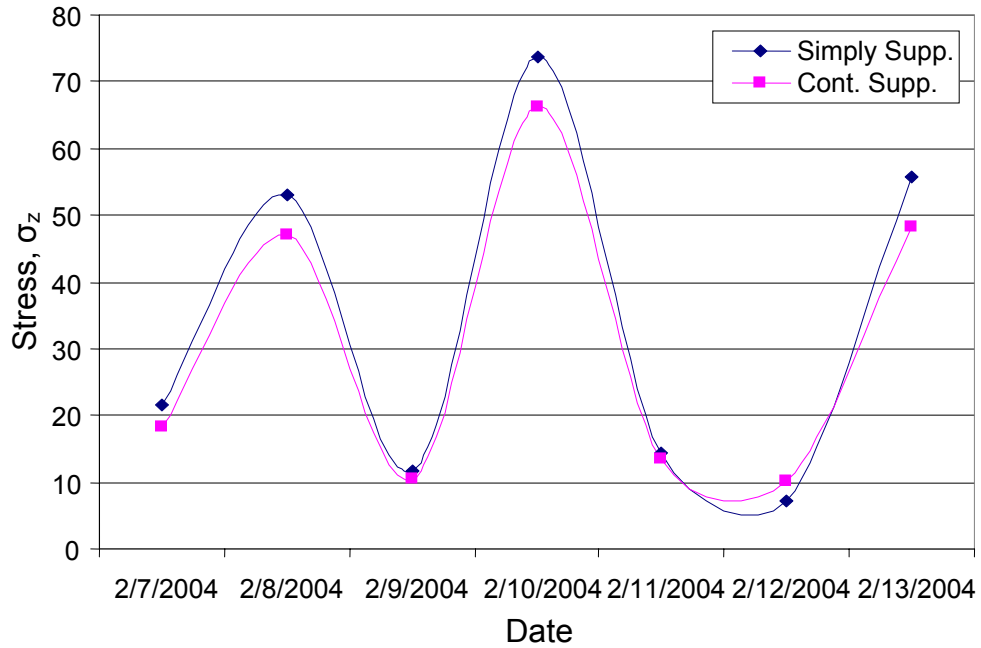


Figure 8.12: Comparison of σ_z (psi) for Simply and Continuously Supported Panels (Feb.)

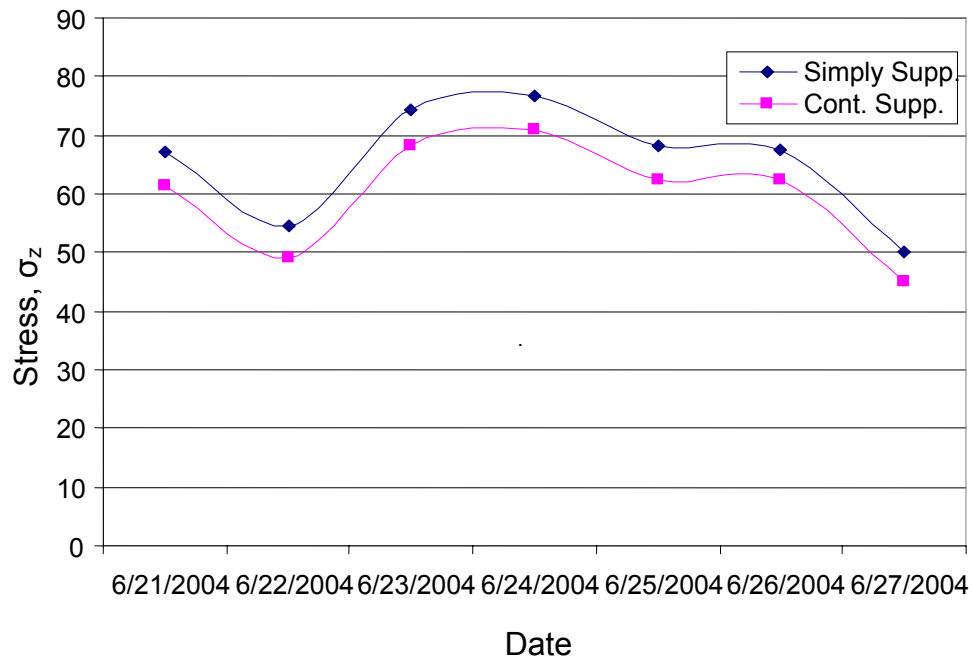


Figure 8.13: Comparison of σ_z (psi) for Simply and Continuously Supported Panels (June)

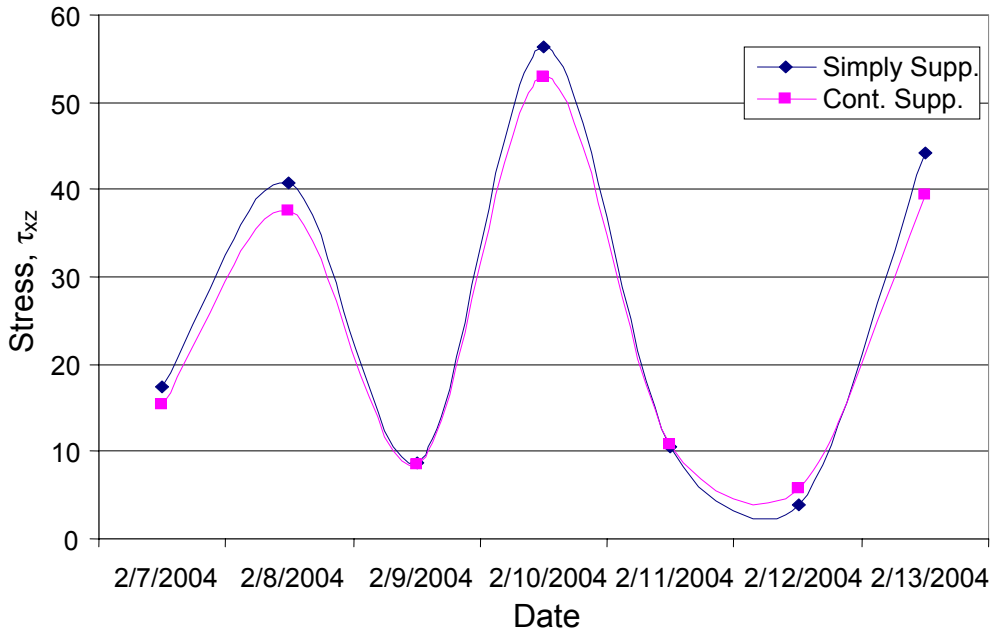


Figure 8.14: Comparison of τ_{xz} (psi) for Simply and Continuously Supported Panels (Feb.)

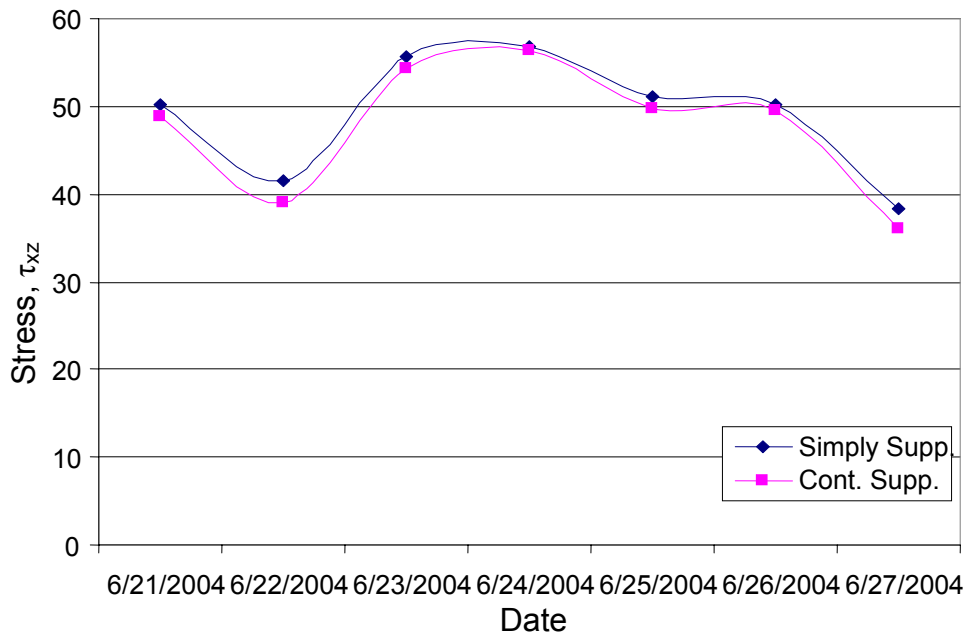


Figure 8.15: Comparison of τ_{xz} (psi) for Simply and Continuously Supported Panels (June)

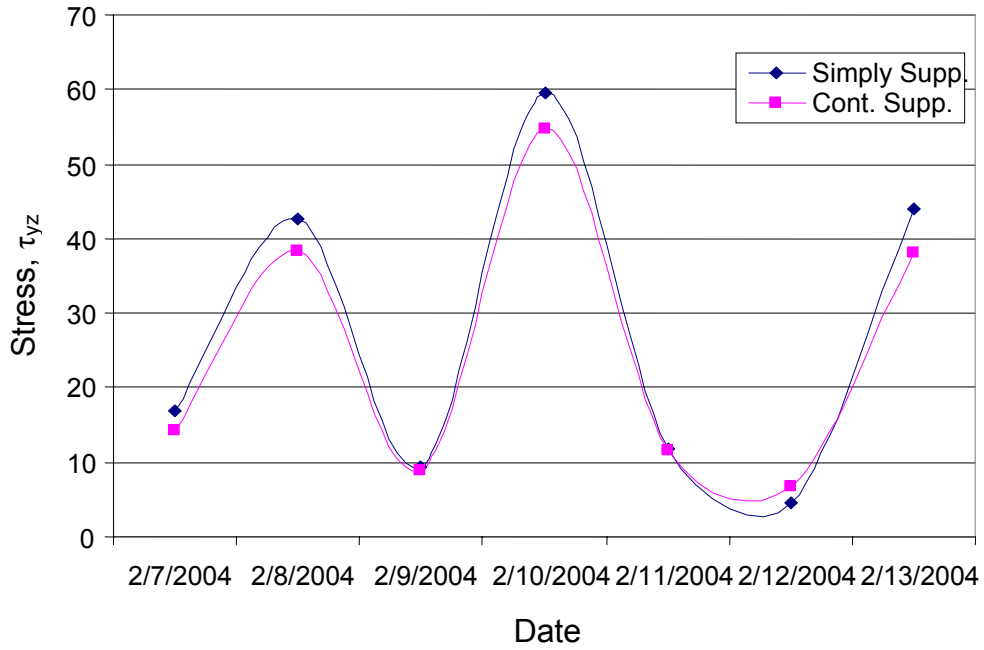


Figure 8.16: Comparison of τ_{yz} (psi) for Simply and Continuously Supported Panels (Feb.)

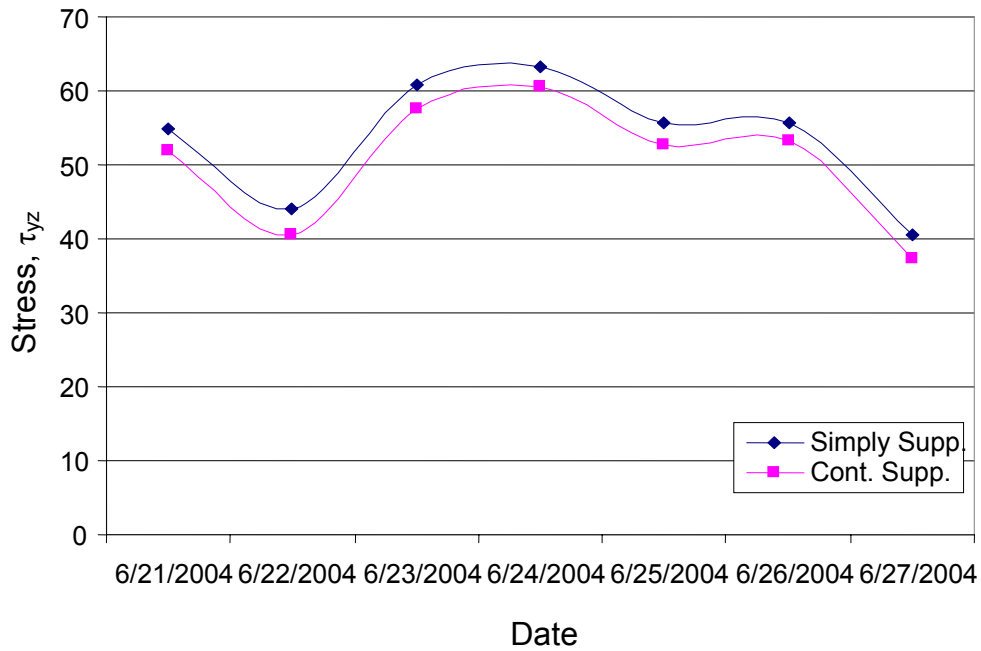


Figure 8.17: Comparison of τ_{yz} (psi) for Simply and Continuously Supported Panels (June)

8.7 Structural Behavior due to Uniform Temperature Change

In uniform temperature change, the entire structure experiences a change in temperature by a constant amount. The effect on the structure is a lengthening or shortening of the bridge which induces stresses (forces and reactions). In studying the behavior of the panel due to this uniform change, a temperature range of the structure is first determined. The limits of this range are based on temperatures within which the structure will stay irrespective of structure types. This range is used to establish the value of temperature change with respect to a reference (such as construction temperature) that should be used in a thermal analysis. AASHTO standards define this range for certain materials such as steel and concrete (Barker and Puckett 1997). However, the specifications for FRP materials are not available. The temperature of the structure is a function of thermal properties such as specific heat of the material, mass, heat conductivity and surface-to-volume ratio.

Therefore, to establish these bounds for the purpose of this study, the temperature data collected for the Crawford County Bridge during August 2003 through July 2004 (Section 8.4) is examined. The structure's maximum and minimum temperatures obtained from this examination are 132.5 °F (July 12, 2004) and -17.5 °F (Feb. 8, 2004) respectively. Thus, a temperature range of -20 °F to 135 °F is assumed for analysis purpose.

Next, a reference temperature is assumed. As was discussed in Section 8.6, this temperature is that at which the structure is considered to be free of stress if no mechanical static or dynamic loads are applied. In this study however, an assumed

construction temperature is chosen and residual stresses which may exist in the bridge are ignored. The temperature assumed at construction is 40 °F.

The same finite element model as used in Section 8.6 is employed in this section. Two cases are examined – temperature rise and fall of the construction temperature with respect to the upper and lower bounds. Each of these two cases is examined for the two different structural boundary conditions described in Sections 8.6.2 and 8.6.3. The rise and fall in temperature are computed from Equations 8.11 and 8.12 respectively:

$$\Delta T_{\text{Rise}} = T_U - T_R \quad \text{Equation 8.11}$$

$$\Delta T_{\text{Fall}} = T_L - T_R \quad \text{Equation 8.12}$$

where TU and TL represent the upper and lower limits of the assumed temperature range, and TR refers to the selected reference temperature.

The results of the finite element analysis for both temperature rise and fall are presented in Table 8.4. The table shows the maximum values of the six different stresses – σ_x , σ_y , σ_z , τ_{xz} , τ_{yz} and τ_{xy} – at the interface between the top face and core. A comparison between simple and continuous supports can be observed. All maximum stress values occur at the location of the supports of the panel for the same reason as was explained in Section 8.6.3. The restraints in the structure cause high stresses to be induced. As was explained in Section 8.6, the values recorded for σ_z are the maximum positive stresses which have the tendency to separate the top face from the core.

It can be noticed from Table 8.4 that the stress results for temperature rise are consistently higher than those for temperature fall for all stresses. This is simply

because the rise in temperature in this particular analysis is greater than the fall, with respect to the reference (assumed construction) temperature. Induced stresses and strains are a function of and proportional to temperature difference as can be noticed conceptually from Equation 8.1, 8.2 or 8.7.

Of interest also is the comparison between the results of the simply and continuously supported panels. In each case of temperature rise and fall, the continuously supported panel produces higher values than the simply supported for all corresponding stresses. It is not difficult to understand why this is the case when we consider the structural behavior of a panel under uniform temperature change. Under this effect, the bridge lengthens or shortens depending on thermal properties. Constraints in the structure cause reactions and forces to develop. Thus the continuously supported structure experiences higher values of induced stresses. It can therefore be said that subjected to uniform temperature changes, a simply supported panel will perform structurally better than a similar panel having continuous supports assuming other factors remaining unchanged.

Table 8.4: Thermal stresses (psi) for uniform temperature change of panel

Temp.	Boundary Condtion	σ_x	σ_y	σ_z	τ_{xy}	τ_{yz}	τ_{xz}
Temp. Rise	Simple Support	-67.014	-49.85	100.93	-52.428	84.446	-73.117
	Continuous Support	-181.63	-64.131	132.57	-71.994	102.49	-87.943
Temp. Fall	Simple Support	40.561	30.172	62.447	31.733	-51.112	44.255
	Continuous Support	109.93	38.816	73.498	43.575	-62.032	53.228

CHAPTER 9 - CONCLUSIONS AND RECOMMENDATIONS

9.1 Summary

This study has focused primarily on employing finite element modeling techniques to evaluate the performance of a highly indeterminate and complex fiber reinforced polymer (FRP) sandwich bridge panel. The panel system is composed of a sinusoidal wave honeycomb core sandwiched by top and bottom face laminates. In view of the complexity of the core geometry, an effort was made to transform the panel section into an equivalent solid orthotropic plate. In this regard, a distinction was made between axial and bending behaviors, and equivalent properties were developed correspondingly.

The equivalent properties due to in-plane (axial) response were derived for the three different parts of the panel. Micro- and macro- mechanics were employed in computing the properties of the top and bottom face laminates, and a finite element approach was developed for obtaining the equivalent core properties in the three orthogonal directions. Once the method for the core was verified, parametric studies were performed to derive equations of the elastic modulus in the three directions as functions of core parameters. The equations were formulated using curve fitting techniques and regression analysis. The in-plane properties of the entire panel can be easily calculated once the properties of the core and face laminates are known.

In comparison, equivalent properties relating to out-of-plane (bending) behavior of the panel were developed for the whole sandwich structure – top face, core and bottom face – acting as a single orthotropic plate, since the out-of-plane properties cannot be simply added together from the components. A finite element approach was

devised to obtain the equivalent stiffness constants – flexural and shear – of the single layered structure. These constants were verified both for a beam and a panel. Once the verification was done, parametric studies were carried out to develop equations for shear and flexural stiffnesses. The techniques used to develop these equations were the same as in the case of the in-plane behavior – curve fitting and regression analysis.

The effect on structural stiffness of a layer of wearing surface was also studied. With the assumption that perfect bonding exists between the overlay material and the panel top face, the stiffness contribution of the wearing stiffness was examined. This was done by adding a new layer of elements on the previously developed equivalent orthotropic plate. A simplified method to compute this increased stiffness of the structure was proposed.

Finally, a conceptual study of the thermal behavior of the panel was conducted to present the reader with an overview of the level of stresses in the panel. Thermal expansion coefficients of the panel components were first computed. A distinction was made between gradient and uniform temperature changes, and thermal studies were performed for each case. The interface between the top face and the core was given primary attention since failure through delamination is a major concern at that location.

9.2 Conclusions

The sinusoidal wave core FRP sandwich panel is a highly indeterminate structure. Based on the study performed and presented in this research work, the conclusions made can be summarized as below.

To analyze and design the FRP honeycomb core for in-plane (axial) behavior, its complex configuration can be simplified to an equivalent solid plate. The elastic

properties of this equivalent structure can be computed using the formulation presented in this work. These equations are summarized as follows. In the longitudinal (x) direction, the formula for the elastic modulus E_x as a function of flute half-wavelength L (in.), flute-width W (in.), core height H (in.), flat/flute thickness t (in.) and core mat modulus of elasticity E_{11} (psi) can be represented as (Equation 4.12),

$$E_x = KL^m H^p W^n t E_{11} \quad \text{Equation 9.1}$$

where $K = 1.0580$, $m = -5.2332E - 02$, $p = 4.7176E - 02$ and $n = -1.0083$.

In the transverse direction, elastic modulus E_y (psi) as a function of the same parameters can be computed using the following equation (Equation 4.24):

$$E_y = S L^k H^r t^q (C + \ln W) E_{11} \quad \text{Equation 9.2}$$

where $S = 9.3770E + 01$, $k = -3.4594$, $r = -2.5138E - 02$, $q = 2.2267$ and $C = 0.3069$.

Finally, the elastic modulus in the vertical direction E_z (psi) can be calculated using the formula (Equation 4.36):

$$E_z = D W^g L^u H^v t E_{11} \quad \text{Equation 9.3}$$

where $D = 3.8002$, $g = -0.7194$, $u = -0.3538$ and $v = -2.5096E - 02$.

This formulation could be useful in the analysis and design of structural members where axial effects are of paramount importance such as columns. For a sandwich structure – where the core is enveloped by top and bottom faces – the elastic properties of the faces can be computed separately using macro-mechanics approach described in this work.

The analysis of the sandwich panel for out-of-plane behavior (bending) was also performed. The entire complicated panel can be reduced to an equivalent solid orthotropic plate whose flexural and shear properties can be calculated from the

equations formulated in this work. This approach comes handy when dealing with bridge decks whose behavior is governed by bending and perhaps shear response. The equations are summarized as follows. Flexural stiffness for bending about the transverse (y) axis causing strain in the longitudinal (x) direction E_{xlyy} can be represented by the following formula (Equation 6.17)

$$E_{xlyy} = B_1 B_2 B_3 B_4 B_5 B_6 B_7 (E_{xlyy})_H \quad \text{Equation 9.4}$$

where $B_1, B_2, B_3, B_4, B_5, B_6, B_7$ are modification factors for face longitudinal Young's modulus, face transverse Young's modulus, face thickness, core mat elastic modulus, core flute-width, core half-wavelength and core mat thickness respectively which can be computed from Equations 6.10 to 6.16. $(E_{xlyy})_H$ is the flexural stiffness equation as a function of core height H alone with other parameters kept constant at their basic values (Equation 6.2). The basic values are shown in Table 6.3 (Chapter 6). It must be noted that the stiffness equation for E_{xlyy} is not per unit width, but for a section whose width is four times the flute-width.

Flexural stiffness for bending about the longitudinal (x) axis causing strain in the transverse (y) direction E_{ylxx} can be shown mathematically as follows (Equation 6.35):

$$E_{ylxx} = C_1 C_2 C_3 C_4 C_5 C_6 C_7 (E_{ylxx})_H \quad \text{Equation 9.5}$$

where $C_1, C_2, C_3, C_4, C_5, C_6, C_7$ are modification factors for face transverse Young's modulus, face longitudinal Young's modulus, face thickness, core mat elastic modulus, core flute-width, core half-wavelength and core mat thickness respectively which can be computed from Equations 6.28 to 6.34. $(E_{ylxx})_H$ is the flexural stiffness equation as a function of core height H alone with other parameters kept constant at their basic values

(Equation 6.20). The stiffness equation for E_{ylxx} is not per unit width, but for a section whose width is twice the half-wavelength.

Lastly, the shear stiffness $G_{xy}A_s$ can be computed using the following expression (Equation 6.48):

$$G_{xy}A_s = D_1 D_2 D_3 (G_{xy}A_s)_{E_{x1}} \quad \text{Equation 9.6}$$

where D_1 , D_2 and D_3 are modification factors for face shear modulus, face thickness and core height which are shown in Equations 6.45 to 6.47. $(G_{xy}A_s)_{E_{x1}}$ refers to the shear stiffness in terms of the face longitudinal Young's modulus alone when other parameters are held constant at their basic values, and can be seen in Equation 6.40.

In many designs, the contribution to structural stiffness of the wearing surface is not considered. From this research, it was found that the overlay may contribute significantly to the stiffness of the FRP sandwich panel, depending of the elastic modulus and thickness of the material used. This contribution could be utilized by structural analysts and designers. Using the properties developed for the equivalent solid orthotropic plate, the stiffness of the entire structure with a layer of wearing surface can be computed using the traditional methods described or the finite element approach discussed.

The conceptual thermal analysis performed in this work compared the same panel under two different boundary conditions – simple and continuous support. The finite element study showed that under uniform temperature change all stresses at the interface were consistently higher for the case of the continuously supported panel. This is because of forces and reactions induced as the structure tries to lengthen or shorten. In the case of the simple supports however, fewer constraints would imply less induced

forces and reactions. This is especially so since one end of the simple supports is a roller. For the differential temperature change, it was observed that the normal stress in the longitudinal direction σ_x was higher for the continuously supported panel than for the simply supported. This was due to the fact that the latter structure was free to translate longitudinally at the roller support, while this freedom was constrained at all supports in the former structure. Hence greater induced stresses for σ_x were noted for the continuously supported panel.

9.3 Recommendations for Further Research

Some recommendations are now presented to provide some insight on further research needed.

➤ Non-linear analysis

One of the main concerns of this highly indeterminate and complex structure is its non-linear behavior. Although FRP materials (such as E-Glass) are linearly elastic, the structure as a whole behaves non-linearly. This work concentrated on performing finite element analysis within the linear range of the structure. Further research is therefore needed to investigate non-linear behavior. It was mentioned that a major failure mode experienced by sandwich structures is delamination. Another potential source of failure is local buckling of the flats and flutes. Therefore non-linear analysis with a view to investigating failure would no doubt be essential.

➤ Effective width formulation

The effective width is a very important parameter in the design of bridge decks. It is the distance over which the concentrated wheel load is assumed to be uniformly distributed. Design standards exist for bridges of different materials such as reinforced

concrete. However, none exists for the FRP bridge type considered in this work. Once the effective width of a bridge is known, the design is done only for that portion of the structure. This design can be safely applied to the entire structure. Hence the development of effective width for this panel type will most certainly be beneficial.

➤ **Wearing surface bond**

The study on wearing surface assumed that the bond existing in the interface between the overlay and the top face is perfect. Though this is a requirement for achieving the benefits of a wearing surface, it goes without saying that this is not true in actual practice due to many imperfections. Hence, the level of stress that exists in this interface has to be investigated. This would aid in the conceptual design, material selection and construction of the wearing surface.

➤ **Full deck modeling**

Because of the limitation in number of elements of the finite element software employed in this study (ANSYS 9.0 University Advanced version), it was impossible to model a full deck. For example, to build a very small model of 15 feet x 7.5 feet x 5 inches, it would require about 133,200 elements since a minimum of 4 elements are required to model a sine wave. However, the element capacity of the available software is 128,000. Modeling a full deck would be beneficial for different applications such as comparing field results with finite element analysis, developing effective width equations and performing non-linear analysis. Hence devising methods to create finite element models of the full FRP sinusoidal wave-core sandwich deck will be helpful.

REFERENCES

- Agarwal, B. D. and Broutman, L. J. (1980). "Analysis and Performance of Fiber Composites", *John Willey and Sons, Inc.*, New York, U.S.A.
- Alampalli, S. (2000). "Modal Analysis of a Fiber-Reinforced Polymer Composite Highway Bridge", *Proceedings of SPIE -- The International Society for Optical Engineering*, vol 4026 (I), pp 21-25
- Babael, K. and Hawkins, N. M. (1990). "Performance of Bridge Deck Concrete Overlays", *ASTM Special Technical Publication*, no.1100, pp 95-108
- Bakeri, P.A. and Sunder, S.S. (1990). "Concepts of Hybrid FRP Bridge", *Serviceability and Durability of Construction Materials; Proceedings of the First Materials Engineering Congress*, pp.1006-1015
- Bakis, C. E., Bank, L. C., Brown, V. L., Cosenza, E., Davalos, J. F., Lesko, J. J., Machida, A., Rizkalla, S. H. and Triantafillou, T. C. (2002). "Fiber-Reinforced Polymer Composites for Construction – State-of-the-Art Review", *Journal of Composites for Construction*, vol. 6, No. 2, pp 73-87
- Ballinger, C. A. (1992). "Advanced Composites in the Construction Industry", *International SAMPE Symposium and Exhibition: [Proceedings] I*, vol. 37, pp 1-14
- Barbero, E. J. (1999). "Introduction to Composite Materials Design", *Taylor & Francis, Inc.*, Philadelphia, U.S.A
- Barker, R. M. and Pucket, J. A. (1997). "Design of Highway Bridges: Based on AASHTO LRFD Bridge Design Specifications", *John Willey and Sons Publishing Company*, New York, U.S.A
- Bradford, N., Sen, R. and Mosallam, A. (2001). "Development of a New Modular Composite Panel System", *International SAMPE Symposium and Exhibition: [Proceedings]*, vol.46 I, pp 931-942
- Bussel, J. P. (2002). "Engineered FRP Bridge Decks – Solutions for the Future", *SAMPE Journal*, vol. 38, No.5, pp 46-48
- Calvo, L. and Meyers, M. (1991). "Overlay Materials for Bridge Decks", *Concrete International; Design and Construction* /, vol.13, no.7, pp 46-47
- Cassity, P, Richards, D. and Gillespie, J (2002). "Compositely Acting FRP Deck and Girder System", *Structural Engineering International: Journal of the International Association for Bridge and Structural Engineering (IABSE)*, vol.12, no.2, pp 71-75

Chamis, C. C. (1984). "Simplified Composite Micromechanics Equations for Strength, Fracture Toughness and Environmental Effects", *Technical sessions of the Thirty-ninth Annual Conference, Reinforced Plastics/Composites Institute : January 16-19, 1984*, pp 1-16

Chen, A. and Davalos, J.F. (2004). "Behavior of FRP Sandwich Sinusoidal Core Panels with Skin Effect", *Engineering, Construction, and Operations in Challenging Environments : Earth and Space 2004 : Proceedings of the Ninth Biennial ASCE Aerospace Division International Conference on Engineering, Construction, and Operations in Challenging Environment*, pp 625-632

Davalos, J. F. et. al. (2001). "Modeling and Characterization of Fiber-Reinforced Plastic Honeycomb Sandwich Panels", *Composite Structures*, vol. 52, No. 3-4, pp 441-452

Ehlen, M. A. (1999). "Life-Cycle Costs of Fiber-Reinforced-Polymer Bridge Decks", *Journal of Material in Civil Engineering*, vol. 11, No. 3, pp 224-230

Flaga, K. (2000). "Advances in Materials Applied in Civil Engineering", *Journal of Materials Processing Technology*, vol 106, no 1-3, pp173-183

Foster, D. C., Richards, D. and Bogner, B. R. (2000). "Design and Installation of Fiber-Reinforced Polymer Composite Bridge", *Journal of Composites for Construction*, vol.4, No.1, pp 33-37

GangaRao, H.V.S. and Laosiriphone, K. (2001). "Design and Construction of Market Street Bridge – WV", *International SAMPE Symposium and Exhibition: [Proceedings]*, vol.46 II, pp 1321-1330

Gutierrez, J. (2002). "Repair of a Damaged Fiber-Reinforced Polymer Composite Bridge Deck", *International SAMPE Symposium and Exhibition: [Proceedings]*, vol.47 I, pp 645-654

Hayes, M. D. (1998). "Characterization and Modeling of a FRP Hybrid Structural Beam and Bridge Structure for use in Tom's Creek Rehabilitation Project", *MS Thesis, Virginia Polytechnic Institute and State University, Blacksburg, Virginia* (<http://www.thesis.org/vt.htm>)

Hayes, M. D., Lesko, J. J., Haramis, J., Cousins, T.E. and Gomez, J. (2000). "Laboratory and Field Testing of Composite Bridge Superstructure", *Journal of Composites for Construction*, vol.4, no.3, pp 120-128

He, Y and Aref, A. J. (2003). "An Optimization Design Procedure for Fiber Reinforced Polymer Web-Core Sandwich bridge Deck Systems", *Composite Structures*, vol. 60, No. 2, pp 183-195

Hicks, R.G., Dussek, I.J. and Seim, C. (2000). "Asphalt Surfaces on Steel Bridge Decks", *Transportation Research Record*, no.1740, pp 135-142

Hooks, J. M. (2001). "Innovative Materials for Bridges of the 21st Century", *International SAMPE Symposium and Exhibition: [Proceedings] /*, vol. 46, pp 1352-1363

Howard, J.D. (1988). "Marquam Bridge Repair. Latex-Modified-Concrete Overlay and Joint Replacement", *Transportation Research Record*, no 1204, pp 59-70

Hulsey, J.L., Raad, L. and Connor, B. (2002). "Deck Wearing Surfaces for the Yukon River Bridge", *Cold Regions Engineering; Cold Regions Impacts on Transportation and Infrastructure; Proceedings of the Eleventh International Conference*, pp 400-411

Hulsey, J.L., Yang, L. and Raad, L. (1999). "Wearing Surfaces for Orthotropic Steel Bridge Decks", *Transportation Research Record*, no.1654, pp 141-150

Kalny, O. (2003). "Structural Performance of Fiber-Reinforced Polymer Honeycomb Sandwich Panels for Bridge Applications", *MS Thesis, Kansas State University, Manhattan, Kansas*

Keller, T. (2002). "Fiber Reinforced Polymers in Bridge Construction: An Introduction", *Structural Engineering International; Journal of the International Association for Bridge and Structural Engineering (IABSE)*, vol. 12, No. 2, pp 66-68

Khalifa, M.A., Kaska, S.S.B. and Krieger, J. (1993). "Bridges Constructed Using Fiber Reinforced Plastics", *Concrete International: Design and Construction*, vol.15, no.6, pp 43-47

Klaiber, F., Dunker, K., Wipt, T. and Sanders, W. (1987). "Methods of Strengthening Highway Bridges", *Transportation Research Board, NCHRP Research Report. 293*

Lamanna, A. J. (2001). "Flexural Strengthening of Reinforced Concrete Beams using Fasteners and Fiber-Reinforced Polyer Strips", *ACI Structural Journal*, vol. 98, No. 3, pp 368-376

Meggers, D. (2005). Personal communication, Kansas Department of Transportation, Topeka, Kansas.

Meier, U. (2000). "Composite Materials in Bridge Repair", *Applied Composite Materials*, vol. 7, No. 2-3, pp 75-94

Mufti, A. A., Labossiere, P. and Neale, K. W. (2002). "Recent Bridge Applications of FRPs in Canada", *Structural Engineering International: Journal of the International Association for Bridge and Structural Engineering (IABSE)*, vol.12, no.2, pp 96-98

- Munley, E. (1994). "Federal Highway Administration Research Program: Fiber Reinforced Polymer Composite Materials", *10th ASM/ESD Advanced Composites Conference*, Dearborn, MI
- Murton, M. C. (2001). "Commercialization of FRP Bridge Decks: Lessons and Challenges for Ohio's 'Project 100'", *International SAMPE Symposium and Exhibition: [Proceedings]*, vol.46 I, pp 943-951
- Nearle, K. W. (1997). "Advanced Composites and Integrated Sensing for Rehabilitation", *ISIS Canada Annual Report*, p. 6
- Plunkett, J. D. (1997). 'Fiber-Reinforced Polymer Honeycomb Short Span Bridge for Rapid Installation', *IDEA Project Final Report, Contract NCHRP-96-IDO30, IDEA Program, Transportation Research Board, National Research Council*
- Qiao, P., Wang, J and Hu, G. (2003). "On the Mechanics of Composite Sinusoidal Honeycomb Cores", *A Collection of Technical papers /*, pp 2397-2405
- Saito, M. (2002). "Carbon Fiber Composites in the Japanese Civil Engineering Market – Conventional Uses and Developing Products", *SAMPE Journal*, vol. 38, No. 5, pp 20-25
- Scott, I. and Wheeler, K. (2001). "Application of Fibre Reinforced Polymer Composites in Bridge Construction", *The Second IPWEA Conference*, October 28 2001, Port Macquarie, NSW, Australia
- Shekar, V., Petro, S. H. and GangaRao, H. V. S. (2002). "Construction of Fiber-Reinforced Plastic Modular Decks for Highway Bridges", *Transportation Research Record*, no 1813, pp 203-209
- Stenko, M. S. and Chawalwala, A. J. (2001). "Thin Polysulfide Epoxy Bridge Deck Overlays", *Transportation Research Record*, no.1749, pp 64-67
- Vinson, J. R. and Sierakowski, R. L. (1986). "The Behavior of Structures Composed of Composite Materials", *Mechanics of Structural Systems*, Martinus Nijhoff Publishers, Dordrecht, The Netherlands
- Whitney, J. M., Daniel, I. M. and Pipes, R. B. (1982). "Experimental Mechanics of Fiber Reinforced Composite Materials", *published by The Society for Experimental Stress Analysis*, Brookfield Center, Connecticut, U.S.A
- Zureick, A., Shih, B and Munley, E (1995). "Fiber-Reinforced Polymeric Bridge Decks", *Structural Engineering Review*, vol.7, no.3, pp 257-266

APPENDIX A: MICROSOFT C++ PROGRAM FOR GENERATION OF MACRO FILES

Source File (meshit.cpp)

```
#include "slab.h"
#include "node.h"
#include "time.h"
void main(int argc, char** argv) {
if (!argv[1]) {argv[1] = new char[7]; argv[1]="in.txt";}
if (!argv[2]) {argv[2] = new char[12]; argv[2]="in-grid.txt";}
okHoneyCombSlab slab(argv[1]);
slab.ReadGrid("in-grid.txt");
slab.PrintInfo("grid-info.txt");
slab.AllocateNodeArrays();
slab.AddRibs();
//slab.PrintCoreToFile("core-info0.txt");
//slab.PrintFlangeToFile("flange-info0.txt");
slab.MergeNodes();
//slab.PrintCoreToFile("core-info1.txt");
//slab.PrintFlangeToFile("flange-info1.txt");
slab.PrintNodeFile("nodes.mac");
slab.PrintElementFile("elements.mac");
slab.Select();
cout << "\nConsumed time: " << " ???";
cout << "\n\nMeshIt, OK (c) 2001\n";
}
```

Header File (slab.h)

```
//slab.h
#include <iostream.h>
#include <math.h>
#include <fstream.h>
#include <iomanip.h> //for matrix output formatting
#include "util_ok1.h"
#include "node.h"
#if !defined(_SLAB_H)
#define _SLAB_H
inline double ABS(double x) {if (x>=0) return x; else return -x;};
//Borland's abs is piece of junk (in some cases also rounds)!!!
#define M_PI 3.14159265358979323846
//as defined in Borland math.h file to ensure compiler independence
#define SMALL_NO 0.00001 //1e-5
//to cope with numerical instability
//function added to set up breakpoint for gdb debugging
void gdbdebug() {};
class okHoneyCombSlab {
public:
//following are 2D and 3D arrays of pointers
okNode*** bottom_fl; //coordinates of nodes at the bottom flange
```

```

okNode**** web_nodes; //coordinates of nodes in the web (1st and last row are duplication of
    //data from bottom_fl & top_fl; very useful for easier creation
    //of web elements, but I will not print them as duplicate nodes
    //into input macro file for ANSYS
okNode*** top_fl; //coordinates of nodes at the top flange
okHoneyCombSlab() {};
//function for wave shape calculation
double f(okRib r, double x);
okHoneyCombSlab(const char* filename);
int ReadGrid(const char* filename);
void AllocateNodeArrays(); //allocate BF, W_N and TF arrays
int AddRib(int index); //adds one rib
void AddRibs(); //adds all ribs
void MergeNodes();
void ImproveMesh();
//not necessary
void PrintNodeFile(char* filename); //prints nodes into input macro file for ANSYS
void PrintElementFile(char* filename);
void Select(char* filename="sel-default.mac");
void SelectAll();
void PrintInfo (const char* filename);
void PrintCoreToFile(char* filename);
void PrintFlangeToFile(char* filename);
private:
//whether to generate mesh template of refined mesh
int option;
double depth; //distance between the middle of top and bottom flange
double fl_x, fl_y, fl_X, fl_Y; //"corner" coordinates of flanges
double co_x, co_y, co_X, co_Y; //"corner" coordinates of core
//number of overhanging nodes
int fl_x_nodes_over, fl_y_nodes_over, fl_X_nodes_over, fl_Y_nodes_over;
//to be calculated
int fl_x_nodes, fl_y_nodes; //total nodes per width and length of flange
int co_x_nodes, co_y_nodes; //total nodes per width and length of core
//number of flutes and flats
int flute_no;
int flat_no;
//default values
double def_quarterwavelength;
/*
if other value than default is used than we need to recalculate number of
nodes per wavelength to maintain consistent grid
*/
double def_flutewidth;
//following entries include boundary nodes
int def_nodes_per_quarterwavelength;
int def_nodes_per_flutewidth;
int nodes_per_depth;
//x, y and z coordinates of the 3D grid
double* x_grid;
double* y_grid;
double** z_grid;
/*
to have different increments but same number of nodes in z direction,
this will be possible just for non-touching elements
*/

```

```

//pattern of flats and flutes
okRib* pattern;
//number of selections
int sel_no;
okSelection* s;
}; //class okHoneyCombSlab
#endif

okHoneyCombSlab::okHoneyCombSlab(const char* filename) {
    int i,j,k;
    Comments_Leave(filename);
    ifstream file(filename);
    file >> option;
    //slab properties
    file >> fl_x; file >> fl_y; file >> fl_X; file >> fl_Y;
    file >> co_x; file >> co_y; file >> co_X; file >> co_Y;
    file >> depth;
    file >> def_quarterwavelength;
    file >> def_flutewidth;
    file >> flute_no;
    file >> flat_no;
    //mesh properties
    file >> fl_x_nodes_over; file >> fl_y_nodes_over;
    file >> fl_X_nodes_over; file >> fl_Y_nodes_over;
    file >> def_nodes_per_quarterwavelength;
    file >> nodes_per_depth;
    file >> def_nodes_per_flutewidth;
    //refined slab properties
    /*
    if certain rib is invisible, than it will not included in AddRib() function
    */
    pattern=new okRib[flute_no+flat_no];
    int no; //auxiliary variable
    for (i=0; i<=flute_no+flat_no-1; i++) {
        file >> no;
        switch (no) {
            case 0: pattern[i].t=flat; break;
            case 1: pattern[i].t=flute_sin0; break;
            case 2: pattern[i].t=flute_sin90; break;
            case 3: pattern[i].t=flute_sin180; break;
            case 4: pattern[i].t=flute_sin270; break;
            default: break;
        } //switch
        file >> pattern[i].x;
        file >> pattern[i].y;
        file >> pattern[i].X;
        file >> pattern[i].flutewidth;
        file >> pattern[i].nodes_per_flutewidth;
        file >> pattern[i].quarterwavelength;
        //if different from default, def_nodes_per_quarterwavelength must be changed
        file >> pattern[i].invisible;
    }
    //determination of last flute
    int flute_index=0;
    for (i=0; i<flat_no+flute_no; i++) {
        pattern[i].lastflute=0;
    }
}

```

```

if (pattern[i].t!=0) {
    flute_index++;
    if (flute_index==flute_no) pattern[i].lastflute=1;
}
}
//selections input
file >> sel_no;
s = new okSelection[sel_no];
for (i=0; i<sel_no; i++) {
    file >> s[i].output;
    s[i].no=i;
    file >> s[i].n0_e1;
    int cislo;
    file >> cislo;
    switch (cislo) {
        case 0: s[i].part=BF; break;
        case 1: s[i].part=TF; break;
        case 2: s[i].part=WEB; break;
        default: break;
    }
    file >> s[i].web_no;
    file >> s[i].input_type;
    switch (s[i].input_type) {
        case 0: file >> s[i].x; file >> s[i].y;
            file >> s[i].X; file >> s[i].Y;
            break;
        case 1: file >> s[i].xa; file >> s[i].ya;
            file >> s[i].Xa; file >> s[i].Ya;
            break;
        default: break;
    } //switch
} //selections

Comments_Add(filename);
//insert default widths and lengths, etc; beg & end must be calculated
cout << "\n";
for (i=0; i<flute_no+flat_no; i++) {
    if (pattern[i].flutewidth==-1)
        {pattern[i].flutewidth=def_flutewidth;}
    if (pattern[i].nodes_per_flutewidth==-1)
        {pattern[i].nodes_per_flutewidth=def_nodes_per_flutewidth;}
    if (pattern[i].quarterwavelength==-1)
        {pattern[i].quarterwavelength=def_quarterwavelength;}
    else {
        //change nodes_per_quarterwavelength; for future modification
    };
} //for
//calculation of co_x(y)_nodes and fl_x(y)_nodes
co_x_nodes=(co_X-co_x)/def_quarterwavelength*(def_nodes_per_quarterwavelength-1)+1;
co_y_nodes=0;
for (i=0; i<flute_no+flat_no; i++) {
    if (pattern[i].t!=0) co_y_nodes=co_y_nodes+pattern[i].nodes_per_flutewidth-1;
}
co_y_nodes++; //to add last row of boundary nodes
fl_x_nodes=co_x_nodes+(fl_x_nodes_over-1)+(fl_X_nodes_over-1);
fl_y_nodes=co_y_nodes+(fl_y_nodes_over-1)+(fl_Y_nodes_over-1);

```

```

//memory allocation for x_,y_,z_grid
x_grid = new double[fl_x_nodes];
y_grid = new double[fl_y_nodes];
z_grid = new double*[flat_no+flute_no];
for (i=0; i<flute_no+flat_no; i++) {
  z_grid[i] = new double[nodes_per_depth];
}
//calculation of x_grid
if (fl_x_nodes_over==1) {x_grid[0]=0;}
else {for (i=0; i<fl_x_nodes_over; i++) {x_grid[i]=i*(co_x-fl_x)/(fl_x_nodes_over-1);}}
for (i=fl_x_nodes_over; i<fl_x_nodes_over+co_x_nodes-2; i++) {
  x_grid[i]=co_x+(i-fl_x_nodes_over+1)*def_quarterwavelength/(def_nodes_per_quarterwavelength-1);
}
if (fl_X_nodes_over==1) {x_grid[fl_x_nodes-1]=fl_X;}
else {for (i=fl_x_nodes_over+co_x_nodes-2; i<fl_x_nodes; i++) {
  x_grid[i]=co_X+(i-(fl_x_nodes_over+co_x_nodes-2))*(fl_X-co_X)/(fl_X_nodes_over-1);
} //for
} //else
//calculation of y_grid
//"overhanging" y flange
if (fl_y_nodes_over==1) {y_grid[0]=0;}
else {for (i=0; i<fl_y_nodes_over; i++) {y_grid[i]=i*(co_y-fl_y)/(fl_y_nodes_over-1);}}
//core: we have to go flute by flute
i=fl_y_nodes_over;
for (j=0; j<flat_no+flute_no; j++) {
  if (pattern[j].t!=0 & pattern[j].lastflute==0) {
    pattern[j].low=i-1;
    for (k=1; k<pattern[j].nodes_per_flutewidth; k++) {
      y_grid[i]=y_grid[i-1]+pattern[j].flutewidth/(pattern[j].nodes_per_flutewidth-1);
      i++;
    }
    pattern[j].top=i-1;
  }
  if (pattern[j].t!=0 & pattern[j].lastflute==1) {
    pattern[j].low=i-1;
    for (k=1; k<pattern[j].nodes_per_flutewidth-1; k++) {
      y_grid[i]=y_grid[i-1]+pattern[j].flutewidth/(pattern[j].nodes_per_flutewidth-1);
      i++;
    }
    pattern[j].top=i;
  }
  if (pattern[j].t==0) {
    if (fl_x_nodes_over==1 & i==1) {pattern[j].low=0; pattern[j].top=0;}
    else if (j==flat_no+flute_no-1) {pattern[j].low=i; pattern[j].top=i;}
    else {pattern[j].low=i-1; pattern[j].top=i-1;}
  }
}
//"overhanging" Y flange
if (fl_Y_nodes_over==1) {y_grid[fl_y_nodes-1]=fl_Y;}
else {for (i=fl_y_nodes_over+co_y_nodes-2; i<fl_y_nodes; i++) {
  y_grid[i]=co_Y+(i-(fl_y_nodes_over+co_y_nodes-2))*(fl_Y-co_Y)/(fl_Y_nodes_over-1);
} //for
} //else
//calculation of z_grid
for (i=0; i<flat_no+flute_no; i++) {
  for (j=0; j<nodes_per_depth; j++) {

```

```

    z_grid[i][j]=j*depth/(nodes_per_depth-1);
  }
}
//determination of pattern[i].beg(end)
for (i=0; i<flute_no+flat_no; i++) {
  for (j=0; j<fl_x_nodes; j++) {
    if (ABS(pattern[i].x-x_grid[j])<SMALL_NO) {pattern[i].beg=j;}
    if (ABS(pattern[i].X-x_grid[j])<SMALL_NO) {pattern[i].end=j;}
  }
}
} //okHoneyCombSlab::okHoneyCombSlab(char* filename)
void okHoneyCombSlab::PrintInfo(const char* filename) {
  int i, j;
  ofstream file(filename); //for output of grid information
  cout << "\n\n***okHoneyCombSlab::PrintInfo()***";
  cout << "\nOption for mesh definition: " << option;
  cout << "\n\nCorner coord. (x,y,X,Y) - flange: ";
  cout << fl_x << "; " << fl_y << "; " << fl_X << "; " << fl_Y;
  cout << "\n          - core(x,y,X,Y): ";
  cout << co_x << "; " << co_y << "; " << co_X << "; " << co_Y;
  cout << "\nDepth: " << depth;
  cout << "\nDefault - quarterwavelength: " << def_quarterwavelength;
  cout << "\n          - flutewidth: " << def_flutewidth;
  cout << "\n\nTotal (length x width) nodes - flange: ";
  cout << fl_x_nodes << "; " << fl_y_nodes;
  cout << "\n          - core: ";
  cout << co_x_nodes << "; " << co_y_nodes;
  cout << "\nOverhanging nodes (in direction of x,y,X,Y): ";
  cout << fl_x_nodes_over << "; " << fl_y_nodes_over << "; ";
  cout << fl_X_nodes_over << "; " << fl_Y_nodes_over;
  cout << "\nNodes per - quarterwavelength (default): " << def_nodes_per_quarterwavelength;
  cout << "\n          - flutewidth (default): " << def_nodes_per_flutewidth;
  cout << "\n          - depth: " << nodes_per_depth;
  cout << "\n\n-----";
  cout << "\n| Individual web info |";
  cout << "\n-----";
  cout << "\n[ i] type|  x |  y |  X | width | n. | 1/4L | in.| beg | end ";
  cout << "\n-----";
  for (i=0; i<flute_no+flat_no; i++) {
    cout << "\n[" << setw(2) << i << "]" ";
    cout << setw(3) << pattern[i].t << " | ";
    cout << setw(5) << pattern[i].x << " | ";
    cout << setw(6) << pattern[i].y << " | ";
    cout << setw(6) << pattern[i].X << " | ";
    cout << setw(5) << pattern[i].flutewidth << " | ";
    cout << setw(2) << pattern[i].nodes_per_flutewidth << " | ";
    cout << setw(5) << pattern[i].quarterwavelength << " | ";
    cout << setw(2) << pattern[i].invisible << " | ";
    cout << setw(3) << pattern[i].beg << " | ";
    cout << setw(3) << pattern[i].end << " | ";
    cout << pattern[i].lastflute << "|";
    cout << pattern[i].low << "*" << pattern[i].top;
  }
  cout << "\n";
  cout << "\nlast flute | pattern low | pattern top";
}

```

```

//output of x_,y_,z_grid into the file
file << "*** X grid:\n";
for (i=0; i<fl_x_nodes; i++) {
    file << setw(10) << x_grid[i] << " * [" << setw(3) << i << "]\n";
}
file << "\n*** Y grid:\n";
for (i=0; i<fl_y_nodes; i++) {
    file << setw(10) << y_grid[i] << " * [" << setw(3) << i << "]\n";
}
file << "\n*** Z grid:\n";
for (i=0; i<flat_no+flute_no; i++) {
    file << "rib number " << i << "\n";
    for (j=0; j<nodes_per_depth; j++) {
        file << setw(10) << z_grid[i][j] << " * [" << setw(3) << j << "]\n";
    }
}
} //okHoneyCombSlab::PrintInfo()

void okHoneyCombSlab::AllocateNodeArrays() {
    int i,j,k;
    //memory allocation
    bottom_fl = new okNode**[fl_x_nodes];
    top_fl = new okNode**[fl_x_nodes];
    for (i=0; i<fl_x_nodes; i++) {
        bottom_fl[i] = new okNode*[fl_y_nodes];
        top_fl[i] = new okNode*[fl_y_nodes];
        for (j=0; j<fl_y_nodes; j++) {
            bottom_fl[i][j] = new okNode;
            top_fl[i][j] = new okNode;
        }
    }
    web_nodes = new okNode***[co_x_nodes];
    for (i=0; i<co_x_nodes; i++) {
        web_nodes[i] = new okNode**[flute_no+flat_no];
        for (j=0; j<flute_no+flat_no; j++) {
            web_nodes[i][j] = new okNode*[nodes_per_depth];
            for (k=0; k<nodes_per_depth; k++) {web_nodes[i][j][k] = new okNode;}
        }
    }
    //coordinates assignment to TF and BF
    for (i=0; i<fl_x_nodes; i++) {
        for (j=0; j<fl_y_nodes; j++) {
            //BF
            bottom_fl[i][j]->x=x_grid[i];
            bottom_fl[i][j]->y=y_grid[j];
            bottom_fl[i][j]->z=0;
            bottom_fl[i][j]->toprint=1;
            //TF
            top_fl[i][j]->x=x_grid[i];
            top_fl[i][j]->y=y_grid[j];
            top_fl[i][j]->z=depth;
            top_fl[i][j]->toprint=1;
        }
    }
} //okHoneyCombSlab::AllocateNodeArrays()
//functions describing different shapes of waves

```

```

double okHoneyCombSlab::f(okRib r, double x) {
    switch (r.t) {
        case 0: return 0;
        //value goes from the "lower edge" of the flute
        case 1: return (0.5*r.flutewidth*(1+sin(M_PI*x/(2*r.quarterwavelength))));
        case 2: return (0.5*r.flutewidth*(1+sin(M_PI/2+M_PI*x/(2*r.quarterwavelength))));
        case 3: return (0.5*r.flutewidth*(1+sin(M_PI+M_PI*x/(2*r.quarterwavelength))));
        case 4: return (0.5*r.flutewidth*(1+sin(M_PI*1.5+M_PI*x/(2*r.quarterwavelength))));
        default: return 211;
    }
}
//okHoneyCombSlab::f(web shape, double x)
int okHoneyCombSlab::AddRib(int index) {
    int i,j;
    //node shift in x direction
    int ns=fl_x_nodes_over-1;
    if (pattern[index].invisible==1) {return index;}
    for (i=pattern[index].beg-ns; i<=pattern[index].end-ns; i++) {
        for (j=0; j<nodes_per_depth; j++) {
            web_nodes[i][index][j]->x=x_grid[i+ns];
            //add ofset using low
            web_nodes[i][index][j]->y=y_grid[pattern[index].low]+f(pattern[index],x_grid[i+ns]-co_x);
            web_nodes[i][index][j]->z=z_grid[index][j];
            web_nodes[i][index][j]->toprint=1;
        }
    }
    return 0;
}
//okHoneyCombSlab::AddRib(int index)
void okHoneyCombSlab::AddRibs() {
    int i; for (i=0; i<flat_no+flute_no; i++) {AddRib(i);}
}
//prints cut through the core to the file
/*
unfortunately (due to the regular rectangular character of array)
works only for ribs running from beginning to the end
*/
void okHoneyCombSlab::PrintCoreToFile(char* filename) {
    int i,j;
    ofstream file(filename);
    file << "Columns follows the x axis of the slab!\n";
    file << "1st column is x coordinate for all nodes, followed by y coordinates for each row!\n";
    for (i=0; i<co_x_nodes; i++) {
        file << setw(8) << setprecision(3) << web_nodes[i][0][0]->x;
        for (j=0; j<flute_no+flat_no; j++) {
            file.flags(ios::fixed);
            file << setw(8) << setprecision(3) << web_nodes[i][j][0]->y;
        }
        file << "\n";
    }
}
//okHoneyCombSlab::PrintCoreToFile(char* filename)
void okHoneyCombSlab::MergeNodes() {
    int i,j,k,l,merge,CritNode;
    //nsx, nsy: node shift of flange nodes indexing to core nodes indexing
    int nsy=fl_y_nodes_over-1;
    int nsx=fl_x_nodes_over-1;
    double dist;
    //-----

```

```

//merge web nodes first
for (i=0; i<co_x_nodes; i++) {
  for (j=0; j<nodes_per_depth; j++) {
    for (merge=0; merge<flat_no+flute_no; merge++) {

      //there can be only following or "next 2" following ribs to merge
      if (merge+1<flat_no+flute_no) {
        if (ABS(web_nodes[i][merge][j]->y-web_nodes[i][merge+1][j]->y)<SMALL_NO) {
          if (web_nodes[i][merge][j]->toprint) {
            web_nodes[i][merge+1][j]=web_nodes[i][merge][j];
          }
          if (web_nodes[i][merge+1][j]->toprint) {
            web_nodes[i][merge][j]=web_nodes[i][merge+1][j];
          }
        } //if
      } //if
      if (merge+2<flat_no+flute_no) {
        if (ABS(web_nodes[i][merge][j]->y-web_nodes[i][merge+2][j]->y)<SMALL_NO) {
          if (web_nodes[i][merge][j]->toprint) {
            web_nodes[i][merge+2][j]=web_nodes[i][merge][j];
          }
          if (web_nodes[i][merge+2][j]->toprint) {
            web_nodes[i][merge][j]=web_nodes[i][merge+2][j];
          }
        } //if
      } //if

    } //for merge=
  } //for j=
} //for i=
//-----
//flats nodes are taken care of in here
for (i=0; i<co_x_nodes; i++) {
  for (merge=0; merge<flat_no+flute_no; merge++) {
    if (pattern[merge].t!=0) continue;
    for (j=0; j<co_y_nodes; j++) {
      if (ABS(web_nodes[i][merge][0]->y-bottom_fl[i+nsx][j+nsy]->y)<SMALL_NO &
        (web_nodes[i][merge][0]->toprint)) {
        bottom_fl[i+nsx][j+nsy]=web_nodes[i][merge][0];
        bottom_fl[i+nsx][j+nsy]->fixed=true;
        top_fl[i+nsx][j+nsy]=web_nodes[i][merge][nodes_per_depth-1];
        top_fl[i+nsx][j+nsy]->fixed=true;
        break;
      } // if
    } //for j=
  } //for merge=
} //for i=
//-----
//flute nodes are taken care of in here
for (i=0; i<co_x_nodes; i++) {
  for (merge=0; merge<flat_no+flute_no; merge++) {
    if (pattern[merge].t==0) continue;
    //to get some initial starting distance
    dist=y_grid[co_y_nodes-1+nsy]-y_grid[nsy];
    CritNode=-1; //for !...->toprint cases
    for (j=0; j<co_y_nodes; j++) {
      if ((ABS(web_nodes[i][merge][0]->y-bottom_fl[i+nsx][j+nsy]->y)<SMALL_NO) &
        (web_nodes[i][merge][0]->toprint)) {
        CritNode=j;
        break;
      }
    }
  }
}

```

```

} //if
if ((dist>ABS(web_nodes[i][merge][0]->y-bottom_fl[i+nsx][j+nsy]->y))&
    (!bottom_fl[i+nsx][j+nsy]->fixed) &
    (web_nodes[i][merge][0]->toprint)) {
    CritNode=j;
    dist=ABS(web_nodes[i][merge][0]->y-bottom_fl[i+nsx][j+nsy]->y);
} //if
} //for j=
if (CritNode!=-1) {
    bottom_fl[i+nsx][CritNode+nsy]=web_nodes[i][merge][0];
    bottom_fl[i+nsx][CritNode+nsy]->fixed=true;
    top_fl[i+nsx][CritNode+nsy]=web_nodes[i][merge][nodes_per_depth-1];
    top_fl[i+nsx][CritNode+nsy]->fixed=true;
} //if
} //for merge=
} //for j=
//-----
//make all fop_fl and bottom_fl nodes ->toprint
for (i=0; i<fl_x_nodes; i++) {
    for (j=0; j<fl_y_nodes; j++) {
        top_fl[i][j]->toprint=1;
        bottom_fl[i][j]->toprint=1;
    } //for j=
} //for i=
//-----
//label (number) nodes
int actual=1;
//label first all by -1
for (i=0; i<fl_x_nodes; i++) {
    for (j=0; j<fl_y_nodes; j++) {
        bottom_fl[i][j]->no=-1;
        top_fl[i][j]->no=-1;
    } //for j=
} //for i=
for (i=0; i<co_x_nodes; i++) {
    for (j=0; j<flat_no+flute_no; j++) {
        //k=1 to nodes_per_depth-1 is why some nodes have number 0
        for (k=1; k<nodes_per_depth-1; k++) {web_nodes[i][j][k]->no=-1;}
    } //for j=
} //for i=

//label in ascending order
for (i=0; i<fl_x_nodes; i++) {
    for (j=0; j<fl_y_nodes; j++) {
        if (bottom_fl[i][j]->no==-1) {bottom_fl[i][j]->no=actual++;}
        if (top_fl[i][j]->no==-1) {top_fl[i][j]->no=fl_x_nodes*fl_y_nodes+actual-1;}
    } //for j=
} //for i=
actual=actual*2;
for (i=0; i<co_x_nodes; i++) {
    for (j=0; j<flat_no+flute_no; j++) {
        for (k=0; k<nodes_per_depth; k++) {
            //nodes with no=-1 are those that won't be printed
            if ((web_nodes[i][j][k]->no==-1) & web_nodes[i][j][k]->toprint)
                {web_nodes[i][j][k]->no=actual++;}
        } //for k=

```

```

    } //for j=
  } //for i=
  cout << "\nTotal nodes generated: " << actual;
} //okHoneyCombSlab::MergeNodes()
void okHoneyCombSlab::PrintFlangeToFile(char* filename) {
  int i,j;
  ofstream file(filename);
  file << "Columns follows the x axis of the slab!\n";
  file << "1st column is x coordinate for all nodes, followed by y coordinates for each row!\n";
  for (i=0;i<fl_x_nodes;i++) {
    file << setw(8) << setprecision(3) << top_fl[i][0]->x;
    for (j=0;j<fl_y_nodes;j++) {
      file.flags(ios::fixed);
      file << setw(8) << setprecision(3) << top_fl[i][j]->y;
    } //for j=
    file << "\n";
  } //for i=
} //okHoneyCombSlab::PrintFlangeToFile(char* filename)
void okHoneyCombSlab::PrintNodeFile(char* filename) {
  int i,j,k;
  ofstream file(filename);
  //set printed=false for all nodes
  for (i=0; i<fl_x_nodes; i++) {
    for (j=0; j<fl_y_nodes; j++) {
      bottom_fl[i][j]->printed=false;
      top_fl[i][j]->printed=false;
    } //for
  } //for
  for (i=0; i<co_x_nodes; i++) {
    for (j=0; j<flat_no+flute_no; j++) {
      for (k=0; k<nodes_per_depth; k++) {web_nodes[i][j][k]->printed=false;}
    } //for
  } //for

  //print in ascending order
  file << "!\n";
  file << "!*Nodes of bottom flange:\n";
  file << "!\n";
  for (j=0; j<fl_y_nodes; j++) {
    file << "!BF row #" << j << "\n";
    for (i=0; i<fl_x_nodes; i++) {
      //if (!bottom_fl[i][j]->toprint) {file << "!";}
      if (bottom_fl[i][j]->printed) {file << "!N,";}
      if (!bottom_fl[i][j]->printed) {file << " N,";}
      file << setw(10) << bottom_fl[i][j]->no << ",";
      file << setw(10) /* << setprecision(2)*/ << bottom_fl[i][j]->x << ",";
      file << setw(10) /* << setprecision(2)*/ << bottom_fl[i][j]->y << ",";
      file << setw(10) /* << setprecision(2)*/ << bottom_fl[i][j]->z << "\n";
      bottom_fl[i][j]->printed=true;
    } //for i=
  } //for j=
  file << "!\n";
  file << "!*Nodes of top flange:\n";
  file << "!\n";
  for (j=0; j<fl_y_nodes; j++) {
    file << "!TF row #" << j << "\n";

```

```

for (i=0; i<fl_x_nodes; i++) {
  //if (!top_fl[i][j]->toprint) {file << "!";}
  if (top_fl[i][j]->printed) {file << "!N,";}
  if (!top_fl[i][j]->printed) {file << " N,";}
  file << setw(10) << top_fl[i][j]->no << ",";
  file << setw(10) /*<< setprecision(2)*/ << top_fl[i][j]->x << ",";
  file << setw(10) /*<< setprecision(2)*/ << top_fl[i][j]->y << ",";
  file << setw(10) /*<< setprecision(2)*/ << top_fl[i][j]->z << "\n";
  top_fl[i][j]->printed=true;
} //for i=
} //for j=
file << "!\n";
file << "!\nNodes of web:\n";
file << "!\n";
for (j=0; j<flat_no+flute_no; j++) {
  for (k=0; k<nodes_per_depth; k++) {
    file << "!Flute #" << j;
    file << "; row #" << k << "\n";
    for (i=0; i<co_x_nodes; i++) {
      if (!web_nodes[i][j][k]->toprint) {
        file << "!N,";
        file << setw(10) << web_nodes[i][j][k]->no << ",";
        file << setw(10) /*<< setprecision(2)*/ << web_nodes[i][j][k]->x << ",";
        file << setw(10) /*<< setprecision(2)*/ << web_nodes[i][j][k]->y << ",";
        file << setw(10) /*<< setprecision(2)*/ << web_nodes[i][j][k]->z << ",invisible\n";
      } //if
    } else {
      if (web_nodes[i][j][k]->printed) {file << "!N,";}
      if (!web_nodes[i][j][k]->printed) {file << " N,";}
      file << setw(10) << web_nodes[i][j][k]->no << ",";
      file << setw(10) /*<< setprecision(2)*/ << web_nodes[i][j][k]->x << ",";
      file << setw(10) /*<< setprecision(2)*/ << web_nodes[i][j][k]->y << ",";
      file << setw(10) /*<< setprecision(2)*/ << web_nodes[i][j][k]->z << "\n";
      web_nodes[i][j][k]->printed=true;
    } //else
  } //for i=
} //for k=
} //for j=
} //okHoneyCombSlab::PrintNodeFile(char* filename)
void okHoneyCombSlab::PrintElementFile(char* filename) {
  int i,j,k;
  ofstream file(filename);
  int v[4]; //whether to print rib elements
  int repeat; //0,1,2,3
  int actual=1;
  file << "!\n";
  file << "!\nElements of bottom flange:\n";
  file << "!\n";
  file << "TYPE,1" << "\n";
  for (j=0; j<fl_y_nodes-1; j++) {
    file << "!BF row #" << j << "\n";
    for (i=0; i<fl_x_nodes-1; i++) {
      file << "EN,";
      file << setw(5) << actual++ << ",";
      file << setw(5) << bottom_fl[i][j]->no << ",";
      file << setw(5) << bottom_fl[i+1][j]->no << ",";
    }
  }
}

```

```

    file << setw(5) << bottom_fl[i+1][j+1]->no << ", ";
    file << setw(5) << bottom_fl[i][j+1]->no << "\n";
}
}
file << "!*****\n";
file << "!*Elements of top flange:* \n";
file << "!*****\n";
for (j=0; j<fl_y_nodes-1; j++) {
    file << "!TF row #" << j << "\n";
    for (i=0; i<fl_x_nodes-1; i++) {
        file << "EN,";
        file << setw(5) << actual++ << ", ";
        file << setw(5) << top_fl[i][j]->no << ", ";
        file << setw(5) << top_fl[i+1][j]->no << ", ";
        file << setw(5) << top_fl[i+1][j+1]->no << ", ";
        file << setw(5) << top_fl[i][j+1]->no << "\n";
    }
}
file << "!*****\n";
file << "!*Elements of web:* \n";
file << "!*****\n";
for (j=0; j<flat_no+flute_no; j++) {
    for (k=0; k<nodes_per_depth-1; k++) {
        file << "!Flute #" << j;
        file << "; row #" << k << "\n";
        v[0]=0; v[1]=0; v[2]=0; v[3]=0;
        for (i=0; i<co_x_nodes-1; i++) {
            v[0]=web_nodes[i][j][k]->toprint;
            v[1]=web_nodes[i+1][j][k]->toprint;
            v[2]=web_nodes[i+1][j][k+1]->toprint;
            v[3]=web_nodes[i][j][k+1]->toprint;
            if (v[0]+v[1]+v[2]+v[3]==4) {
                file << " EN,";
                file << setw(5) << actual++ << ", ";
                file << setw(5) << web_nodes[i][j][k]->no << ", ";
                file << setw(5) << web_nodes[i+1][j][k]->no << ", ";
                file << setw(5) << web_nodes[i+1][j][k+1]->no << ", ";
                file << setw(5) << web_nodes[i][j][k+1]->no << "\n";
            } //if
            else {
                file << "!EN,";
                file << setw(5) << actual++ << ", ";
                file << setw(5) << web_nodes[i][j][k]->no << ", ";
                file << setw(5) << web_nodes[i+1][j][k]->no << ", ";
                file << setw(5) << web_nodes[i+1][j][k+1]->no << ", ";
                file << setw(5) << web_nodes[i][j][k+1]->no << ",invisible\n";
            } //else
        } //for i=
    } //for k=
} //for j=
cout << "\nTotal elements generated: " << actual;
} //okHoneyCombSlab::PrintElementFile(char* filename)
int okHoneyCombSlab::ReadGrid(const char* filename) {
    int i,j;
    if (option==0) {return 0;}
    else {

```

```

Comments_Leave(filename);
ifstream file(filename);
for (i=0; i<fl_x_nodes; i++) {file >> x_grid[i];}
for (i=0; i<fl_y_nodes; i++) {file >> y_grid[i];}
for (i=0; i<flat_no+flute_no; i++) {
    for (j=0; j<nodes_per_depth; j++) {file >> z_grid[i][j];}
} //for i=
Comments_Add(filename);
} //else
return(0);
} //void ReadGrid(const char* filename)
void okHoneyCombSlab::Select(char* filename) {
    int i,j,index;
    //write for writing selection information
    char* write1;
    char* write2;
    //width of output stream for setw
    int w=30;
    ofstream file(filename);
    file << "!\n";
    file << "!*Selection input macro file for ANSYS*\n";
    file << "!\n";
    for (index=0; index<sel_no; index++) {
        file << setw(w) << "\n!Selection number: " << s[index].no;
        file << setw(w) << "\n!Selection output: " << s[index].output;
        file << setw(w) << "\n!Nodes (0) or elements (1): " << s[index].n0_e1;
        file << setw(w) << "\n!BF (0), TF (1), WEB (2): " << s[index].part;
        file << setw(w) << "\n!Web no (starting 0; -1 for BF or TF): " << s[index].web_no;
        file << setw(w) << "\n!Input type (0: value coord.; 1: 'array' coord.): ";
        file << s[index].input_type;
        file << setw(w) << "\n!Coordinates (x,y,X,Y or xa,ya,Xa,Ya): ";
        switch (s[index].input_type) {
            case 0: file << s[index].x << "; ";
                    file << s[index].y << "; ";
                    file << s[index].X << "; ";
                    file << s[index].Y; break;
            case 1: file << s[index].xa << "; ";
                    file << s[index].ya << "; ";
                    file << s[index].Xa << "; ";
                    file << s[index].Ya; break;
            default: break;
        } //switch
    }
    file << "\n";
    switch (s[index].output) {
        case 0: write1=new char[3]; write1="D,\0";
                write2=new char[5]; write2="ALL\0"; break;
        case 1: write1=new char[14]; write1="nset,a,node,,\0";
                write2=new char[2]; write2=" \0"; break;
        case 2: write1=new char[14]; write1="esel,a,elem,,\0";
                write2=new char[2]; write2=" \0"; break;
        case 3: write1=new char[3]; write1="D,\0";
                write2=new char[14]; write2="UX,,,,UY,UZ\0"; break;
        case 4: write1=new char[3]; write1="D,\0";
                write2=new char[11]; write2="UY,,,,UZ\0"; break;
        case 5: write1=new char[3]; write1="D,\0";
                write2=new char[13]; write2="UX,,,,ROTY\0"; break;
    }
}

```

```

case 6: write1=new char[3]; write1="D,\0";
       write2=new char[23]; write2="UX,,,,,ROTX,ROTY,ROTZ\0"; break;
default: break;
} //switch

//core nodes shift related to flange
int nsx=fl_x_nodes_over-1;
int nsy=fl_y_nodes_over-1;
gdbdebug();
//creation of array coordinates, if not available
if (s[index].input_type==0) {
//longitudinal coordinates for both flanges and web
if (s[index].part<2) {
//bottom or top flange xa and Xa
for (i=0; i<fl_x_nodes; i++) {
if (s[index].x<x_grid[i]) {s[index].xa=i-1; break;}
}
for (i=fl_x_nodes-1; i>=0; i--) {
if (s[index].X>x_grid[i]) {s[index].Xa=i+1; break;}
}
//bottom or top flange ya and Ya
for (i=0; i<fl_y_nodes; i++) {
if (s[index].y<y_grid[i]) {s[index].ya=i-1; break;}
}
for (i=fl_y_nodes-1; i>=0; i--) {
if (s[index].Y>y_grid[i]) {s[index].Ya=i+1; break;}
}
} //if
else {
//web xa and Xa
for (i=0; i<co_x_nodes; i++) {
if (s[index].x<x_grid[i+nsx]) {s[index].xa=i-1; break;}
} //for
for (i=co_x_nodes-1; i>=0; i--) {
if (s[index].X>x_grid[i+nsx]) {s[index].Xa=i+1; break;}
}
//web ya and Ya (or za and Za)
for (i=0; i<nodes_per_depth; i++) {
if (s[index].y<z_grid[index][i]) {s[index].ya=i-1; break;}
} //for
for (i=nodes_per_depth-1; i>=0; i--) {
if (s[index].Y>z_grid[index][i]) {s[index].Ya=i+1; break;}
}
} //else
} //if "array coordinates" need to be calculated

//node selection
if (s[index].n0_e1==0) {
switch (s[index].part) {
case 0: //BF
for (i=s[index].xa; i<=s[index].Xa; i++) {
file << "!Whatever(x direction) #: " << i << "\n";
for (j=s[index].ya; j<=s[index].Ya; j++) {
file << write1;
file << bottom_fl[i][j]->no;
file << write2 << "\n";
}
}
}
}
}

```

```

    } //for
  } //for
break;
case 1: //TF
  for (i=s[index].xa; i<=s[index].Xa; i++) {
    file << "!Whatever(x direction) #: " << i << "\n";
    for (j=s[index].ya; j<=s[index].Ya; j++) {
      file << write1;
      file << top_fl[i][j]->no;
      file << write2 << "\n";
    } //for
  } //for
break;
case 2: //WEB
  for (i=s[index].xa; i<=s[index].Xa; i++) {
    file << "!Whatever(x direction) #: " << i << "\n";
    for (j=s[index].ya; j<=s[index].Ya; j++) {
      file << write1;
      file << web_nodes[i][s[index].web_no][j]->no;
      file << write2 << "\n";
    } //for
  } //for
break;
default: break;
} //switch
} //if node selection
//element selection
int number=0;
if (s[index].n0_e1==1) {
  switch (s[index].part) {
    case 0: //BF
      for (i=s[index].xa; i<=s[index].Xa; i++) {
        file << "!Whatever(x direction) #: " << i << "\n";
        for (j=s[index].ya; j<=s[index].Ya; j++) {
          file << write1;
          number = 1+(fl_x_nodes-1)*j+i; //just bottom flange
          file << number;
          file << write2 << "\n";
        } //for
      } //for
break;
case 1: //TF
  for (i=s[index].xa; i<=s[index].Xa; i++) {
    file << "!Whatever(x direction) #: " << i << "\n";
    for (j=s[index].ya; j<=s[index].Ya; j++) {
      file << write1;
      number = 1+(fl_x_nodes-1)*(fl_y_nodes-1); //bottom flange
      number = number+(fl_x_nodes-1)*j+i; //addition from top flange
      file << number;
      file << write2 << "\n";
    } //for
  } //for
break;
case 2: //WEB
  for (i=s[index].xa; i<=s[index].Xa; i++) {
    file << "!Whatever(x direction) #: " << i << "\n";

```

```

    for (j=s[index].ya; j<=s[index].Ya; j++) {
        file << write1;
        number = 1+2*(fl_x_nodes-1)*(fl_y_nodes-1); //flanges
        number = number+s[index].web_no*(co_x_nodes-1)*(nodes_per_depth-1); //preceding webs
        number = number+(co_x_nodes-1)*j+i;
        file << number;
        file << write2 << "\n";
    } //for
} //for
break;
default: break;
} //switch
} //if element selection
} //for (index=0; index<sel_no; index++)
} //okHoneyCombSlab::Select(char* filename)
void SelectAll() {
} //okHoneyCombSlab::SelectAll()
//node.h
#ifndef _NODE_H
#define _NODE_H
class okNode {
public:
    okNode() {no=0; x=0; y=0; z=0; fixed=0; toprint=0; printed=0;}
    double x,y,z; //node coordinates
    int no; //node number (important for ANSYS)
    //int users; //number of "users" (eg. 3 for bottom flange, flat and flute)
    int printed; //for printing into the file finds out whether the node was already printed
    int fixed; //nodes of bottom flange that cannot be shifted
    int toprint; //where the core doesn't continue
    //okNode* master; //"master node" in the case the case that several nodes are overlapping
}; //class okNode
enum subpart {BF,TF,WEB};
enum web {flat, flute_sin0, flute_sin90, flute_sin180, flute_sin270};
//type of single web (self-explanatory)
class okSelection {
public:
    int output; //0 for D,
                //1 for NSEL,
                //2 for ESEL,
    int no; //selection number
    int n0_e1; //0 for node selection, 1 for element selection
    subpart part; //enum type {BF, TF, WEB}
    int web_no; //starting zero, -1 for BF or TF
    int input_type; //0 for value coordinates, 1 for "array coordinates"
    int xa, ya, Xa, Ya; //"array coordinates"
    double x, y, X, Y; //value coordinates
}; //class okNodeSelection
class okRib {
public:
    web t;
    double x, y, X;
    double flutewidth;
    int nodes_per_flutewidth;
    double quarterwavelength;
    int nodes_per_quarterwavelength;
    int invisible;

```

```

int lastflute;
int beg, end;
int low, top;
/*
if the rib does not run through the whole length of the core,
this says where is beginning and end in array coordinates
*/
}; //class okRib
#endif

```

Header File (node.h)

```

//node.h
#ifndef _NODE_H
#define _NODE_H
class okNode {
public:
    okNode() {no=0; x=0; y=0; z=0; fixed=0; toprint=0; printed=0;}
    double x,y,z; //node coordinates
    int no; //node number (important for ANSYS)
    //int users; //number of "users" (eg. 3 for bottom flange, flat and flute)
    int printed; //for printing into the file finds out whether the node was already printed
    int fixed; //nodes of bottom flange that cannot be shifted
    int toprint; //where the core doesn't continue
    //okNode* master; //"master node" in the case the case that several nodes are overlapping
}; //class okNode
enum subpart {BF,TF,WEB};
enum web {flat, flute_sin0, flute_sin90, flute_sin180, flute_sin270};
//type of single web (self-explanatory)
class okSelection {
public:
    int output; //0 for D,
                //1 for NSEL,
                //2 for ESEL,
    int no; //selection number
    int n0_e1; //0 for node selection, 1 for element selection
    subpart part; //enum type {BF, TF, WEB}
    int web_no; //starting zero, -1 for BF or TF
    int input_type; //0 for value coordinates, 1 for "array coordinates"
    int xa, ya, Xa, Ya; //"array coordinates"
    double x, y, X, Y; //value coordinates
}; //class okNodeSelection
class okRib {
public:
    web t;
    double x, y, X;
    double flutewidth;
    int nodes_per_flutewidth;
    double quarterwavelength;
    int nodes_per_quarterwavelength;
    int invisible;
    int lastflute;
    int beg, end;
    int low, top;
/*

```

```

if the rib does not run through the whole length of the core,
this says where is beginning and end in array coordinates
*/
}; //class okRib
#endif

```

Header File (util_ok1.h)

```

#include <fstream.h>
#include <stdio.h>
#include <string.h>
/*Nasledujici funkce vypusti ze souboru, jehož jmeno je ji predano jako
parametr vsechny komentare - pricemz za komentar je povazovan libovolny
text od znaku * ("hvezdicka") az do konce radky. Namisto komentaru jsou do
puvodniho souboru vlozeny mezera. Tento tedy zabira stale stejnou pamet.
Komentare nejsou vymazany, ale jsou ulozeny do stejne pojmenovaneho souboru
s priponou .lcf (Left Comments File - vzdy je vytvoren prazdny soubor),
ktery se vyuziva pri rekonstrukci
puvodniho souboru - viz dalsi funkce Comments_Add. Obe funkce se musi pozivat
synchronizovane!!! Kazdemu komentari navic predchazi pozice jeho prvniho znaku
v puvodnim souboru - toto je dulezite pro rekonstrukci.*/
void Comments_Leave(const char* file_name) {
    //musime otevrit pro zapis i pro cteni
    fstream input_file(file_name, ios::in | ios::out /*| ios::nocreate*/);
    //cout << file_name << " " << strlen(file_name);
    //musime vytvorit nahradni jmeno pro soubor s komentari
    int DelkaJmena,i;
    DelkaJmena=strlen(file_name);
    for (i=0; i<DelkaJmena; i++) {
        if (file_name[i]=='.') {DelkaJmena=i; break;}
    }
    char* left_comments_file_name = new char[DelkaJmena+5];
    for (i=0; i<DelkaJmena; i++) {
        left_comments_file_name[i]=file_name[i];
    }
    //vytvarime soubor s priponou .lcf
    left_comments_file_name[DelkaJmena]='.';
    left_comments_file_name[DelkaJmena+1]='l';
    left_comments_file_name[DelkaJmena+2]='c';
    left_comments_file_name[DelkaJmena+3]='f';
    left_comments_file_name[DelkaJmena+4]='\0';
    //cout << " " << left_comments_file_name << "\n";
    //cout << "vstupni proud * vystupni proud\n";
    //dale ulozi komentare do vytvoreneho souboru
    fstream output_file(left_comments_file_name, ios::out | ios::trunc /*| ios::noreplace*/);
    char c;
    bool Komentar=false;
    bool PisCisloPozice=true; //zda ma psat do vystupniho souboru cislo pozice
    bool Zvetsil=false; //kvuli tomu, ze \n zabira 2bajty (ale je to jeden znak)
    int PocetZnakuVSouboru;
    //zjistime velikost vstupniho souboru
    input_file.seekg(0, ios::end);
    PocetZnakuVSouboru=input_file.tellg();
    input_file.seekg(0);
    /*i se modifikuje i uvnitr cyklu, pokud je nacten znak konce radky \n,

```

```

ktery se uklada jako dva znaky - viz promenna Zvetsil*/
for (i=0; i<PocetZnakuVSouboru; i++) {
    if (Zvetsil) {i++; Zvetsil=false;}
    input_file.seekg(i); //musime nastavit na aktualni pozici pro cteni (jde zlepsit!)
    input_file.get(c);
    if (c=='\n') {PisCisloPozice=true; Zvetsil=true;}
    //neni komentar
    if (!Komentar && (c!='*')) {
        continue;
    }
    //jsme uvnitr komentare
    if (Komentar && (c!='\n')) {
        output_file.put(c);
        input_file.seekp(i);
        input_file.put(' '); //ve vstupnim souboru prepisujeme komentar mezerou
        continue;
    }
    //konec komentare
    if (Komentar && (c=='\n')) {
        Komentar=false;
        output_file.put('\n');
        continue;
    }
    //zacatek komentare
    if (!Komentar && (c=='*')) {
        if (PisCisloPozice) {
            output_file << input_file.tellg()-1 << " ";
            PisCisloPozice=false;
        }
        output_file.put(c);
        input_file.seekp(i);
        if (c=='\n') {input_file.put('\n');}
        else input_file.put(' ');
        Komentar=true;
        continue;
    }
} //while
} //Comments_Leave
/*Nasledujici funkce zajisti rekonstrukci souboru, ze kterych byly odstraneny
komentare funkci Comments_Leave. Na mista specifikovana v souboru s priponou
.lcf jsou opet vlozeny komentare a soubor s priponou .lcf je smazan, aby
zbytecne nezabiral pamet.*/
void Comments_Add(const char* file_name) {
    /*musime otevrit pro zapis (ale i pro vystup, protoze jinak po otevreni obsahuje
    pouze mezery*/
    fstream output_file(file_name, ios::out | ios::in /*| ios::nocreate*/);
    //cout << file_name << " " << strlen(file_name);
    //musime vytvorit nahradni jmeno pro soubor s komentari
    int DelkaJmena,i;
    DelkaJmena=strlen(file_name);
    for (i=0; i<DelkaJmena; i++) {
        if (file_name[i]!='.') {DelkaJmena=i; break;}
    }
    char* left_comments_file_name = new char[DelkaJmena+5];
    for (i=0; i<DelkaJmena; i++) {
        left_comments_file_name[i]=file_name[i];

```

```

}
left_comments_file_name[DelkaJmena]='.';
left_comments_file_name[DelkaJmena+1]='I';
left_comments_file_name[DelkaJmena+2]='c';
left_comments_file_name[DelkaJmena+3]='f';
left_comments_file_name[DelkaJmena+4]='\0';
//cout << " " << left_comments_file_name << "\n";
//cout << "vstupni proud * vystupni proud\n";
//dale vlozime komentare zpět do původního souboru
fstream input_file(left_comments_file_name, ios::in /*| ios::nocreate*/);
char c;
int NaPozici;
int PocetZnakuSouboru;
//zjistime pocet znaku ve vstupním souboru
input_file.seekg(0, ios::end);
PocetZnakuSouboru=input_file.tellg();
input_file.seekg(0);
while ((PocetZnakuSouboru-1)>input_file.tellg()) {
    input_file >> NaPozici; //přeteme na jakou pozici máme vložit
    //cout << NaPozici << " ";
    output_file.seekp(NaPozici); //nastavíme kam budeme kopírovat
    input_file.get(c); //preskocime mezeru a dale uz jen kopirujeme
    while(c!='\n') {
        input_file.get(c);
        output_file.put(c);
    }
    //na konci musime preskocit znak noveho radku \n
    input_file.seekg(input_file.tellg());
} //while
//nakonec zbyva vymazat nepotrebný pomocný soubor
input_file.close();
//cout << "remove:" << remove(left_comments_file_name) << "\n";
remove(left_comments_file_name);
} //Comments_Add

```

APPENDIX B: MATLAB PROGRAM SCRIPT FOR GENERATION OF INPUT FILE

```

A=zeros(12,1); B=zeros(1,9);
Option = input('option: '); A(1,1)=Option;
xFlangcoord = input('Enter x coordinate of flange: '); A(2,1)=xFlangcoord;
yFlangcoord = input('Enter y coordinate of flange: '); A(3,1)=yFlangcoord;
XFlangcoord = input('Enter X coordinate of flange: '); A(4,1)=XFlangcoord;
YFlangcoord = input('Enter Y coordinate of flange: '); A(5,1)=YFlangcoord;
xCorecoord = input('Enter x coordinate of core: '); A(6,1)=xCorecoord;
yCorecoord = input('Enter y coordinate of core: '); A(7,1)=yCorecoord;
XCorecoord = input('Enter X coordinate of core: '); A(8,1)=XCorecoord;
YCorecoord = input('Enter Y coordinate of core: '); A(9,1)=YCorecoord;
Depth = input('Enter depth of slab: '); A(10,1)=Depth;
Defquartwave = input('Enter default quarterwavelength: '); A(11,1)=Defquartwave;
Deflutewidth = input('Enter default flutewidth: '); A(12,1)=Deflutewidth;
Nflutes = input('Enter number of flutes: '); B(1,1)=Nflutes;
Nflats = input('Enter number of flats: '); B(1,2)=Nflats;
xnodeover = input('Enter number of nodes per "overhang" for x: '); B(1,3)=xnodeover;
ynodeover = input('Enter number of nodes per "overhang" for y: '); B(1,4)=ynodeover;
Xnodeover = input('Enter number of nodes per "overhang" for X: '); B(1,5)=Xnodeover;
Ynodeover = input('Enter number of nodes per "overhang" for Y: '); B(1,6)=Ynodeover;
nodquartwave = input('Enter default nodes per quarterwavelength: '); B(1,7)=nodquartwave;
noddepth = input('Enter number of nodes per depth: '); B(1,8)=noddepth;
nodflut = input('Enter default nodes per flutewidth: '); B(1,9)=nodflut;
Type = input('Enter core configuration: 1 for "204", 2 for "0204", 3 for "402", 4 for "0402": ');
Core_width = YCorecoord-yCorecoord;
N=(Core_width-2*Deflutewidth)/(2*Deflutewidth);
k=Nflutes + Nflats;
C=zeros(k+1,8);
k=1;
if Type ~= 1
    y=yCorecoord;
    C(k,3)=y;
    if Type == 4
        k=k+1;
        C(k,3)=y; C(1,1)=0; C(2,1)=4;
    end
    k=k+1;
    if Type ~= 2
        y=y+Deflutewidth;
        if ((Type==3) | (Type==4))
            C(k,3)=y;
            y=y+Deflutewidth;
            k=k+1;
            if Type==3
                C(1,1)=4; C(2,1)=0;
            end
        end
    end
end
end
if ((Type==1) | (Type==2))

```

```

    y=yCorecoord+Deflutewidth;
end
    C(k,3)=y; C(k,1)=2;
    k=k+1;
for a=1:N
    for b=1:2
        C(k,3)=y;
        b=(k/2); c=round(k/2);
        if Type==1;
            if b==c
                C(k,1)=0;
            else
                x=k+2;
                C(k,1)=3+(round(sin(x*pi/2)));
            end
        end
    end
    if Type==2
        if b ~= c
            C(k,1)=0;
        else
            x=k+1;
            C(k,1)=3+(round(sin(x*pi/2)));
        end
    end
end
    if Type==3
        if b == c
            C(k,1)=0;
        else
            C(k,1)=3+(round(sin(k*pi/2)));
        end
    end
end
    if Type==4
        if b ~= c
            C(k,1)=0;
        else
            x=k-1;
            C(k,1)=3+(round(sin(x*pi/2)));
        end
    end
end
    k=k+1;
    continue
end
for c=1:2
    y=y+Deflutewidth;
    C(k,3)=y;
    b=(k/2); c=round(k/2);
    if Type==1
        if b==c
            C(k,1)=0;
        else
            x=k+2;
            C(k,1)=3+(round(sin(x*pi/2)));
        end
    end
end
    if Type==2
        if b ~= c

```

```

        C(k,1)=0;
        else
            x=k+1;
            C(k,1)=3+(round(sin(x*pi/2)));
        end
    end
end
if Type==3
    if b == c
        C(k,1)=0;
        else
            C(k,1)=3+(round(sin(k*pi/2)));
        end
    end
end
if Type==4
    if b ~= c
        C(k,1)=0;
        else
            x=k-1;
            C(k,1)=3+(round(sin(x*pi/2)));
        end
    end
end
    k=k+1;
    continue
end
continue
end
if Type ~=3
    C(k,3)=y;
    C(k,1)=C(k-4,1);
    if Type ~=4; k=k+1;
    C(k,3)=y; C(k,1)=C(k-4,1);
    if Type==2; k=k+1; y=y+Deflutewidth;
    C(k,3)=y; C(k,1)=C(k-4,1);
    end
end
end
end
m=Nflutes+Nflats;
for a=1:m
    C(a,2)=xCorecoord; C(a,4)=XCorecoord;
    C(a,7)=-1; C(a,8)=0;
    if C(a,1)~=0
        C(a,5)= -1; C(a,6)= -1;
    else
        C(a,5)=0; C(a,6)=1;
    end
    continue
end
end

```

APPENDIX C: THERMAL COEFFICIENT OF EXPANSION COMPUTATION

Ply Name	k	$\alpha_1^k * 10^{-6} (/^{\circ}\text{C})$	$\alpha_2^k * 10^{-6} (/^{\circ}\text{C})$	$Q_{11}^k \alpha_1^k$	$Q_{12}^k \alpha_2^k$	$Q_{12}^k \alpha_1^k$	$Q_{22}^k \alpha_2^k$	$(N_x^T / \Delta T)^k$	$(N_y^T / \Delta T)^k$
Bond Layer	1	22.5588	22.5588	259.5649	102.2686	102.2686	259.5649	29.6703	29.6703
CM3205	2	8.1114	25.4062	230.6420	61.5033	19.6362	208.4858	7.1576	5.5890
CM3205	3	25.4062	8.1114	208.4858	19.6362	61.5033	230.6420	5.5890	7.1576
CM3205	4	20.7706	20.7706	292.0877	117.4193	117.4193	292.0877	4.0951	4.0951
UM1810	5	7.7253	24.4050	238.0348	62.6685	19.8374	213.8856	7.5176	5.8431
UM1810	6	17.8798	17.8798	342.0415	139.8950	139.8950	342.0415	6.3616	6.3616
UM1810	7	7.7253	24.4050	238.0348	62.6685	19.8374	213.8856	7.5176	5.8431
UM1810	8	17.8798	17.8798	342.0415	139.8950	139.8950	342.0415	6.3616	6.3616
UM1810	9	7.7253	24.4050	238.0348	62.6685	19.8374	213.8856	7.5176	5.8431
UM1810	10	17.8798	17.8798	342.0415	139.8950	139.8950	342.0415	6.3616	6.3616
UM1810	11	17.8798	17.8798	342.0415	139.8950	139.8950	342.0415	6.3616	6.3616
UM1810	12	7.7253	24.4050	238.0348	62.6685	19.8374	213.8856	7.5176	5.8431
UM1810	13	17.8798	17.8798	342.0415	139.8950	139.8950	342.0415	6.3616	6.3616
UM1810	14	7.7253	24.4050	238.0348	62.6685	19.8374	213.8856	7.5176	5.8431
UM1810	15	17.8798	17.8798	342.0415	139.8950	139.8950	342.0415	6.3616	6.3616
UM1810	16	7.7253	24.4050	238.0348	62.6685	19.8374	213.8856	7.5176	5.8431
CM3205	17	20.7706	20.7706	292.0877	117.4193	117.4193	292.0877	4.0951	4.0951
CM3205	18	25.4062	8.1114	208.4858	19.6362	61.5033	230.6420	5.5890	7.1576
CM3205	19	8.1114	25.4062	230.6420	61.5033	19.6362	208.4858	7.1576	5.5890
Summation =								146.6284	136.5814

